

## Dendritic MRI contrast agents : synthetic strategies for targeting and multivalency

**Citation for published version (APA):**

Langereis, S. (2005). *Dendritic MRI contrast agents : synthetic strategies for targeting and multivalency*. [Phd Thesis 1 (Research TU/e / Graduation TU/e), Chemical Engineering and Chemistry]. Technische Universiteit Eindhoven. <https://doi.org/10.6100/IR591435>

**DOI:**

[10.6100/IR591435](https://doi.org/10.6100/IR591435)

**Document status and date:**

Published: 01/01/2005

**Document Version:**

Publisher's PDF, also known as Version of Record (includes final page, issue and volume numbers)

**Please check the document version of this publication:**

- A submitted manuscript is the version of the article upon submission and before peer-review. There can be important differences between the submitted version and the official published version of record. People interested in the research are advised to contact the author for the final version of the publication, or visit the DOI to the publisher's website.
- The final author version and the galley proof are versions of the publication after peer review.
- The final published version features the final layout of the paper including the volume, issue and page numbers.

[Link to publication](#)

**General rights**

Copyright and moral rights for the publications made accessible in the public portal are retained by the authors and/or other copyright owners and it is a condition of accessing publications that users recognise and abide by the legal requirements associated with these rights.

- Users may download and print one copy of any publication from the public portal for the purpose of private study or research.
- You may not further distribute the material or use it for any profit-making activity or commercial gain
- You may freely distribute the URL identifying the publication in the public portal.

If the publication is distributed under the terms of Article 25fa of the Dutch Copyright Act, indicated by the "Taverne" license above, please follow below link for the End User Agreement:

[www.tue.nl/taverne](http://www.tue.nl/taverne)

**Take down policy**

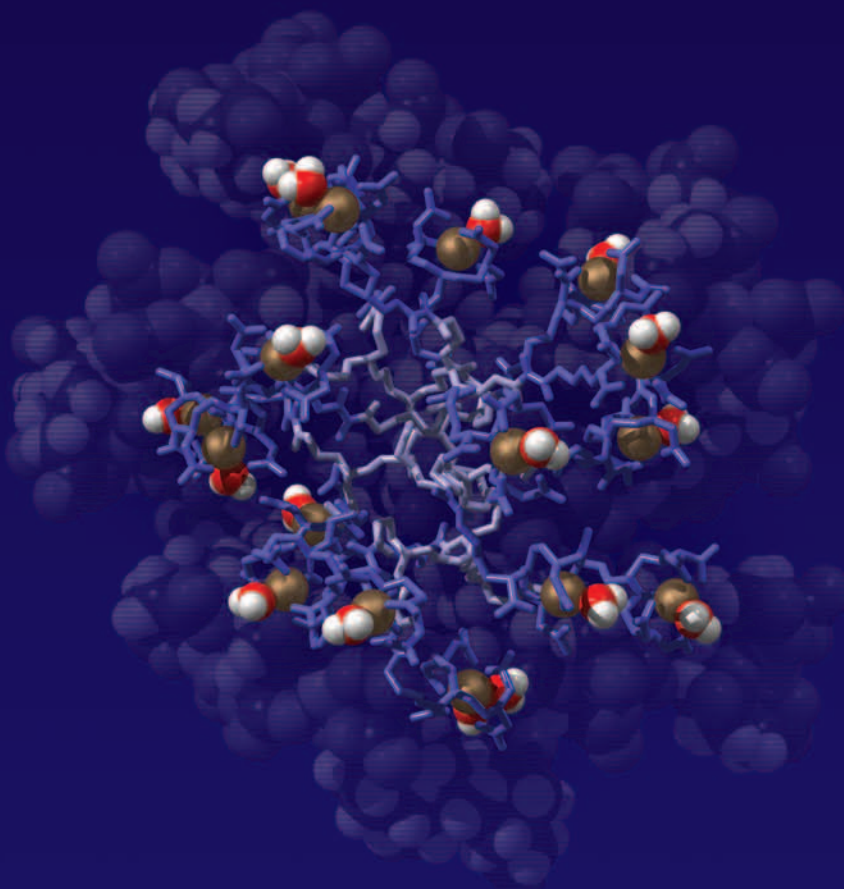
If you believe that this document breaches copyright please contact us at:

[openaccess@tue.nl](mailto:openaccess@tue.nl)

providing details and we will investigate your claim.

# Dendritic MRI Contrast Agents

*Synthetic strategies for targeting and multivalency*



Sander Langereis



# **Dendritic MRI contrast agents**

**Synthetic strategies for targeting and multivalency**



# **Dendritic MRI contrast agents**

## **Synthetic strategies for targeting and multivalency**

PROEFSCHRIFT

ter verkrijging van de graad van doctor aan de Technische Universiteit Eindhoven, op gezag van de Rector Magnificus, prof.dr.ir. C.J. van Duijn, voor een commissie aangewezen door het College voor Promoties in het openbaar te verdedigen op woensdag 15 juni 2005 om 16.00 uur

door

**Sander Langereis**

geboren te Geldrop

Dit proefschrift is goedgekeurd door de promotor:

prof.dr. E.W. Meijer

Copromotor:

dr.ir. M.H.P. van Genderen

This research has been financially supported by the Council for Chemical Sciences of the Netherlands Organization for Scientific Research (NWO-CW).

Omslagontwerp: Koen Pieterse, Sander Langereis en Jan-Willem Luiten (JWL Producties)

Druk: Universiteitsdrukkerij, Technische Universiteit Eindhoven

CIP-DATA LIBRARY TECHNISCHE UNIVERSITEIT EINDHOVEN

Langereis, Sander

Dendritic MRI contrast agents : synthetic strategies for targeting and multivalency / by Sander Langereis. – Eindhoven : Technische Universiteit Eindhoven, 2005.

Proefschrift. – ISBN 90-386-2577-4

NUR 913

Trefwoorden: dendrimeren / magnetische resonantie ; MRI / beeldverwerking ; contrastmiddelen / gadolinium / angiogenese / peptiden ; NGR

Subject headings: dendrimers / Magnetic Resonance Imaging ; MRI / imaging ; contrast agents / imaging agents ; gadolinium / angiogenesis / peptides ; NGR

“In de wetenschap gelijken wij op kinderen, die aan de oever der kennis hier en daar een steentje oprapen, terwijl de wijde oceaan van het onbekende zich voor onze ogen uitstrekt.”

John Newton

Voor Muriël





# Contents

<b>Chapter 1: Dendrimers for biomedical imaging</b>	<b>1</b>
1.1 Introduction .....	1
1.2 Synthesis and conformational characteristics of dendrimers .....	3
1.3 Biocompatibility .....	7
1.4 Multivalency .....	7
1.5 Dendrimers for MR imaging .....	8
1.6 Aim and outline of the thesis .....	12
1.7 References .....	14
<b>Chapter 2: Novel methodologies for the synthesis of functionalized Gd(III)DTPA complexes</b>	<b>19</b>
2.1 Introduction .....	20
2.2 Synthesis .....	21
2.2.1 Amine-functionalized DTPA pentaester .....	21
2.2.2 General strategies for the synthesis of functionalized Gd(III)DTPA complexes .....	22
2.2.3 Isocyanate-functionalized DTPA synthon: strategy A .....	22
2.2.4 Synthesis of glycinyurea-functionalized Gd(III)DTPA complex: strategy B .....	26
2.2.5 Introduction of ureidopyrimidinone units to Gd(III)DTPA complexes: strategy C .....	29
2.3 Relaxivities of functionalized Gd(III)DTPA complexes .....	30
2.3.1 Nuclear magnetic resonance: an introduction .....	30
2.3.2 Relaxivity measurements .....	33
2.4 Conclusions .....	35
2.5 Experimental .....	36
2.6 References .....	43
<b>Chapter 3: Multivalent Gd(III)DTPA-terminated poly(propylene imine) dendrimers</b>	<b>45</b>
3.1 Introduction .....	46
3.2 Gd(III)DTPA-terminated poly(propylene imine) dendrimers .....	48
3.2.1 Synthesis .....	48
3.2.2 Cryo-TEM and AFM studies .....	51
3.2.3 Molecular modeling .....	53
3.2.4 Longitudinal and transverse relaxivities .....	54
3.3 Combined Y(III)DTPA- and Gd(III)DTPA-based dendritic contrast agents .....	56
3.4 Partially functionalized Gd(III)DTPA-based dendritic contrast agents .....	58
3.5 Conclusions .....	60
3.6 Experimental .....	61
3.7 References .....	66

<b>Chapter 4: Evaluation of dendritic contrast agents for MR imaging</b>	<b>69</b>
4.1 Introduction .....	70
4.2 <i>In vitro</i> MR Imaging .....	72
4.2.1 Relaxivities in mouse plasma .....	72
4.2.2 Concentration detection limits of MRI contrast agents <i>in vitro</i> .....	74
4.3 Pharmacokinetics of dendritic MRI contrast agents .....	76
4.3.1 Serial CE-MRI .....	77
4.3.2 Dynamic CE-MRI .....	78
4.4 MR Imaging of tumor angiogenesis .....	79
4.5 Conclusions .....	82
4.6 Materials and Methods .....	83
4.6.1 Synthesis of Gd(III)DTPA-terminated poly(propylene imine) dendrimers .....	83
4.6.2 <i>In vitro</i> MR imaging .....	83
4.6.3 <i>In vivo</i> MR imaging .....	83
4.7 References .....	85
<b>Chapter 5: Probing the interaction of the biotin–avidin complex with the relaxivity of biotinylated MRI contrast agents</b>	<b>87</b>
5.1 Introduction .....	88
5.2 Biotinylated Gd(III)DTPA .....	89
5.2.1 Synthesis and characterization .....	89
5.2.2 Binding studies .....	91
5.3 Biotinylated Gd(III)DO3A .....	94
5.3.1 Synthesis and characterization .....	94
5.3.2 Binding studies .....	96
5.4 Gd(III)DTPA-based complexes in supramolecular structures .....	98
5.4.1 Dendritic host-guest systems .....	98
5.4.2 Mixed polymeric micelles as MRI contrast agents .....	101
5.5 Overall conclusions .....	103
5.6 Experimental .....	104
5.7 Appendix .....	108
5.7.1 Fitting the E-titration data .....	108
5.7.2 Fitting the M-titration data .....	109
5.8 References .....	110
<b>Chapter 6: Synthetic strategies for targeting and bimodality</b>	<b>113</b>
6.1 Introduction .....	114
6.2 Cyclic NGR-functionalized Gd(III)DTPA .....	115
6.2.1 Solid phase peptide synthesis .....	115
6.2.2 Serial contrast-enhanced MRI .....	118
6.3 Fluorescently labeled Gd(III)DTPA complex: a bimodal contrast agent .....	119

6.4 General strategy for the double labeling of oligopeptides .....	122
6.4.1 Introduction.....	123
6.4.2 Synthesis of bimodal target-specific MRI contrast agents.....	124
6.5 Overall conclusions.....	129
6.6 Experimental .....	130
6.7 References.....	135

**Chapter 7: Design and synthesis of multivalent target-specific MRI contrast agents**

<b>agents</b> .....	<b>137</b>
7.1 Introduction.....	138
7.2 A supramolecular approach to multivalent target-specific MRI contrast agents .....	140
7.2.1 Synthesis .....	140
7.2.2 Binding studies.....	142
7.3 Multivalent target-specific dendritic MRI contrast agents.....	144
7.4 Overall conclusions.....	147
7.5 Experimental .....	148
7.6 References.....	149

<b>Summary</b> .....	<b>151</b>
<b>Samenvatting</b> .....	<b>153</b>
<b>Curriculum Vitae</b> .....	<b>155</b>
<b>List of publications</b> .....	<b>156</b>
<b>Dankwoord</b> .....	<b>157</b>



---

# Chapter 1

## Dendrimers for biomedical imaging

---

### 1.1 INTRODUCTION

The multivalent character of dendrimers has positioned these well-defined, highly branched macromolecules at the forefront in the development of new contrast agents for biomedical imaging. By modifying the periphery of the dendrimer with gadolinium(III) chelates, the relaxivity of the MRI contrast agent is increased considerably. The monodisperse character of dendrimers creates a unique opportunity to introduce dendritic MRI contrast agents into the clinic. In addition, a prolonged vascular retention time is obtained, due to their larger size. Furthermore, the multivalent character of dendrimers is often used to enhance ligand-marker interactions. At present, research for the next generation of MRI contrast agents is focused on the combination of multivalent targeting with an enhanced relaxivity. This Chapter describes the current status of dendrimers in biomedical imaging.

In the beginning of the twentieth century, the field of biomedical imaging emerged from Röntgen's discovery of X-rays in 1895. With the sophisticated imaging tools of today, such as magnetic resonance imaging (MRI), computed tomography (CT), positron emission tomography (PET), and ultrasonography (US), the diagnosis and recognition of disease has evolved tremendously. Traditionally, diagnostic imaging has focused on the detection and visualization of the ultimate effects of a disease. The rapidly emerging discipline of molecular imaging aims to probe fundamental molecular processes at the origin of the disease for early diagnosis and efficient therapy.<sup>1-5</sup> Through early diagnosis the need for exploratory surgery would also be decreased, if not completely eliminated, thereby improving patient care. Molecular imaging uses molecular probes *in vivo*. The attachment of various labels to a target-specific ligand permits *in vivo* diagnosis based on a combination of existing imaging tools, giving an increasing understanding of a disease on a molecular level.<sup>4,6,7</sup> MRI is anticipated to become one of the prominent non-invasive imaging techniques for disease diagnosis. Its advantages include a high spatial resolution, a non-ionizing radiation source, and the ability to extract simultaneously physiological and anatomical information of soft tissue. A major limitation of MRI, however, remains its inherently low sensitivity.

To address the problem of low sensitivity, scientists have developed non-toxic contrast agents for MRI over the previous decades. So far, the Federal Drug Agency (FDA) and the European Medicines Agency (EMA) have approved only low molecular weight (MW) Gd(III) complexes

with a precise structure as MRI contrast agents. Unfortunately, the non-specificity, low contrast efficiency, and fast renal excretion of these low MW contrast agents require a high dosage. These aspects severely limit the utility of these materials for molecular MR imaging (See Figure 1.1a). One method to increase the contrast and to reduce the required dosage is to attach multiple MRI labels to a single scaffold as shown in Figure 1.1b. This concept led to research in the area of functional polymers bearing multiple contrast agent moieties. The large MW distribution in synthetic linear polymers prevented their *in vivo* administration by the aforementioned agencies. Whereas several polymers bearing multiple Gd(III)-based MRI contrast agent moieties have been evaluated experimentally, none of them has entered clinical trials for reasons including toxicity or incomplete renal excretion. In a similar fashion MRI labels can be tagged to hyperbranched polymers, but also here the polydispersity of the synthetic scaffold may hamper its *in vivo* application. An alternative synthetic scaffold capable of carrying multiple contrast agent functionalities within its structure is a dendrimer.<sup>8</sup> These highly branched macromolecules, with nanoscopic dimensions and tunable sizes, have been successfully employed as multivalent MRI contrast agents as will be outlined in this Chapter.

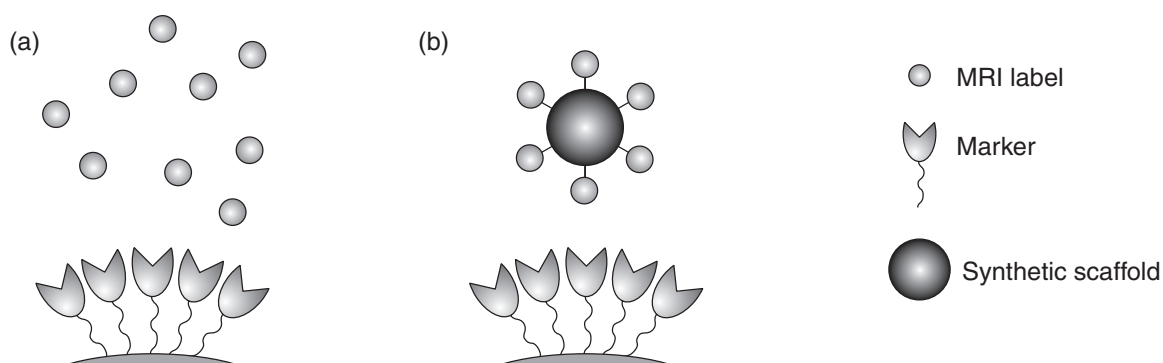


**Figure 1.1** (a) The non-specificity and low contrast efficiency of monovalent MRI contrast agents requires the usage of a high dosage; (b) multiple MRI labels attached to a synthetic scaffold will give more contrast while at the same time the required dosage is reduced.

Besides its inherently low sensitivity, MRI also lacks specificity, which is required for molecular MR imaging. Specificity is introduced by tagging an MRI label to a ligand, which recognizes a marker specific for a certain disease. Binding of this ligand to its marker results in the accumulation of the MRI contrast agent at the region of interest (Figure 1.2a). A second advantage of a multivalent scaffold containing multiple ligands is that the binding to its marker may increase due to cooperative binding (Figure 1.2b) (*vide infra*).<sup>9</sup>

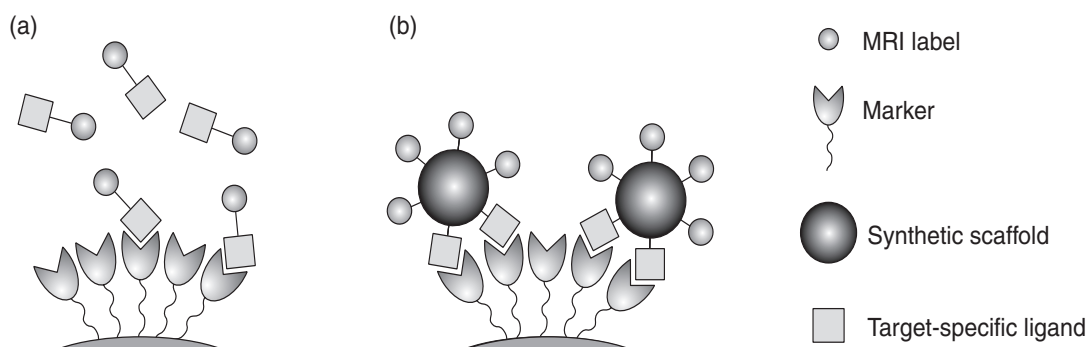


**Figure 1.2** (a) Monovalent target-specific MRI contrast agents; (b) multivalent target-specific MRI contrast agents for the specific accumulation of MRI contrast agent at regions of interest.

Consequently, the next generation of MRI contrast agents can be rationally designed to possess both high contrast efficiency and target specificity. Dendrimers are uniquely qualified to address all of these points. Moreover, the chemistry, characterization, and physicochemical behavior of dendritic structures have been studied in detail.<sup>8,10-13</sup> The desired combination of size and orthogonal peripheral functionality can be obtained *via* a general modular synthetic approach enabling the optimization of MR imaging contrast and binding affinity.

In the following sections, the synthesis and intriguing properties of dendritic structures will be briefly addressed and their potential for applications in biomedical imaging will be highlighted.

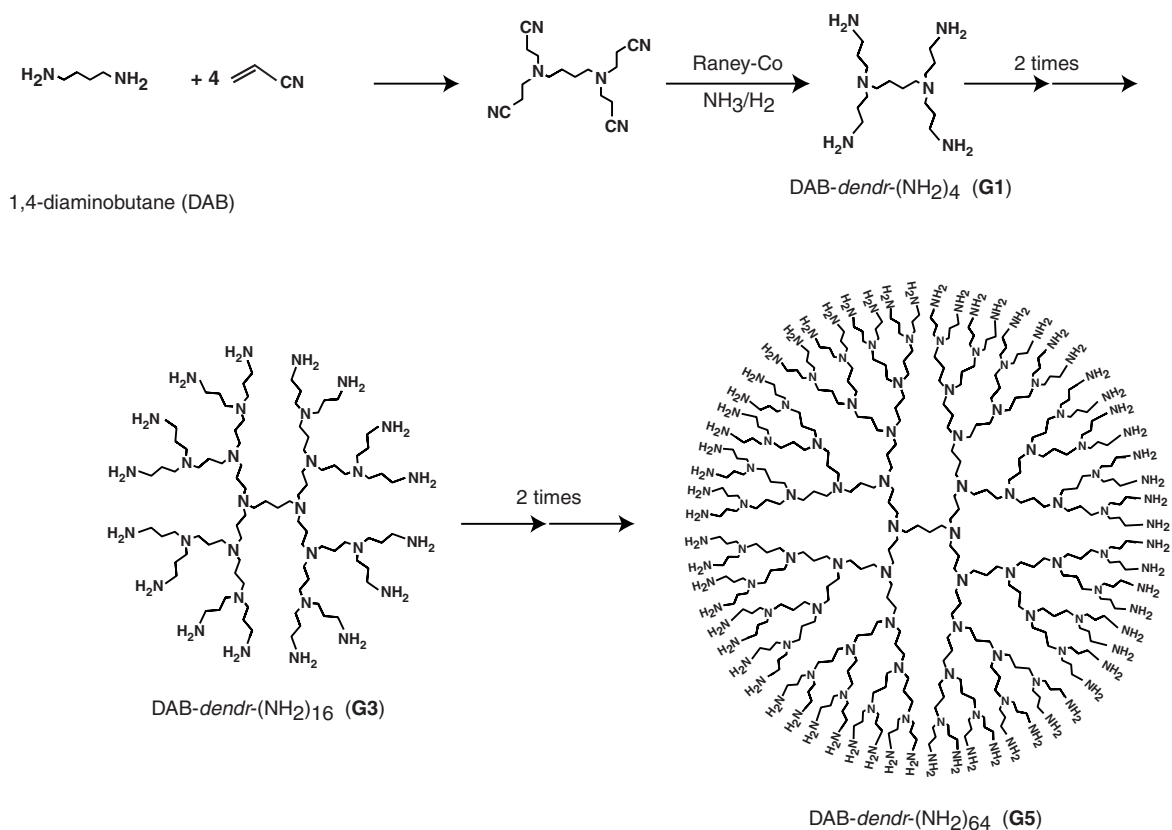
## 1.2 SYNTHESIS AND CONFORMATIONAL CHARACTERISTICS OF DENDRIMERS

Dendrimers are multivalent macromolecules with a regular, highly branched structure and dimensions resembling those of small proteins. These structures are synthesized *via* a “cascade” synthesis using an iterative sequence of reaction steps. There are two conceptually different synthetic routes towards dendritic structures: the divergent approach and the convergent approach.

In the divergent approach, the synthesis starts at the core of the molecule and elaborates to the periphery. In this synthetic methodology, the number of functional end groups increases exponentially upon going to higher generations, implying that numerous reactions have to be performed on a single molecule. In the early 1980's Denkewalter *et al.* patented the synthesis of L-lysine-based dendrimers.<sup>14-16</sup> However, despite size exclusion chromatography data, no detailed information concerning the structural characteristics of these dendrimers was given. The first dendritic structures that have been thoroughly investigated and that have received widespread attention are Tomalia's poly(amidoamino) (PAMAM) dendrimers<sup>17,18</sup> and Newkome's “arborols”.<sup>19</sup> Both dendrimers are constructed *via* a divergent approach. In 1993, in continuation of the original work of Vögtle,<sup>20</sup> Mülhaupt *et al.*<sup>21</sup> and Meijer *et al.*<sup>22</sup> independently reported on the divergent



approach for the synthesis of poly(propylene imine) (PPI) dendrimers. The synthetic methodology towards poly(propylene imine) dendrimers is depicted in Scheme 1.1. The synthesis of poly(propylene imine) dendrimers starts with a double Michael addition of acrylonitrile with the primary amines of 1,4-diaminobutane (DAB), the bifunctional core molecule. Subsequently, the nitriles are hydrogenated to the amines using Raney-Co as a catalyst to give the first generation amine-terminated poly(propylene imine) dendrimer (DAB-dendr-(NH<sub>2</sub>)<sub>4</sub>).<sup>22</sup> Repetition of this sequence of reactions leads to poly(propylene imine) dendrimers with 8, 16, 32, or 64 functional end groups for the 2<sup>nd</sup>, 3<sup>rd</sup>, 4<sup>th</sup> and 5<sup>th</sup> generation, respectively. The poly(propylene imine) dendrimers have been characterized in detail by a wide range of analytical techniques, including NMR spectroscopy,<sup>23</sup> IR spectroscopy, high pressure liquid chromatography (HPLC), and electrospray ionization mass spectrometry (ESI-MS).<sup>24</sup>



**Scheme 1.1** Divergent synthesis of the commercially available poly(propylene imine) dendrimers utilizing an iterative sequence of reaction steps, illustrating the exponential growth of functional end groups upon going to higher generations of the poly(propylene imine) dendrimer.<sup>22</sup>

In the convergent approach, first the dendritic wedges are synthesized and subsequently attached to a multifunctional core. An example of convergently constructed dendrimers are Fréchet's aromatic polyether dendrimers<sup>25,26</sup> and Moore's phenylacetylene dendrimers.<sup>27-29</sup> Although the yields obtained using the convergent synthesis are in general lower than for the divergent approach, the purity of these dendrimers is high. Thus, the convergent approach can be regarded as the "organic chemistry approach", whereas the divergent approach is considered as the "polymer chemistry" equivalent.<sup>8</sup> Following the divergent and convergent approach, many other types of aesthetically appealing dendritic structures have been developed. The preparation of these structures has been described in excellent books and reviews.<sup>8,30-38</sup>

The developed synthetic strategies to dendrimers allow the introduction of a precise number of functional groups in the core, within the branches, and/or along the periphery. Such modifications in the dendritic framework can have a great impact on the physiochemical properties of the dendrimer. Although dendrimers are often depicted as perfect spheres, they do not behave as such. In excellent work, Percec *et al.* reported on the self-assembly of dendritic wedges in a wide range of highly organized architectures, such as helical porous columns and spherical supermolecular dendrimers.<sup>39,40</sup> Most dendrimers display a high degree of flexibility: depending on the external conditions these structures can adopt conformations that are far from globular. The size and shape of dendritic structures on an air–solid interface, an air–water interface, and in solution have been described in several studies.<sup>41-43</sup> AFM studies on PAMAM dendrimers deposited on a mica surface have shown that the observed diameter was much larger than the height of the dendrimer, implying that the dendrimers were no longer globular, but flattened on the surface. This results in a compressed structure as depicted in Figure 1.3a.<sup>41,42</sup> Studies with PPI and PAMAM dendrimers modified with long hydrophobic chains have shown that these amphiphilic structures form stable monolayers at the air–water interface. The polar interior of the dendrimer associates with the water, whereas the hydrophobic tails extend upwards, away from the water surface (Figure 1.3b).<sup>44,45</sup> In contrast, adamantyl-functionalized poly(propylene imine) dendrimers adopt a shape persistent globular conformation at the air–water surface, most likely due to steric constraints of the bulky adamantyl functionalities along the periphery.<sup>45</sup> Baars *et al.* functionalized PPI dendrimers with cyanobiphenyl mesogenic moieties to study the effect of the molecular structure on the self-assembly of the dendritic mesogens in the liquid-crystalline mesophase.<sup>46</sup> It was found that the spontaneous orientations of the mesogenic units force the dendrimer in a highly distorted conformation with the cyanobiphenyl units oriented in an anti-parallel fashion (Figure 1.3c). Each of these examples demonstrate that dendrimers can adopt various conformations depending on the functionalities introduced.

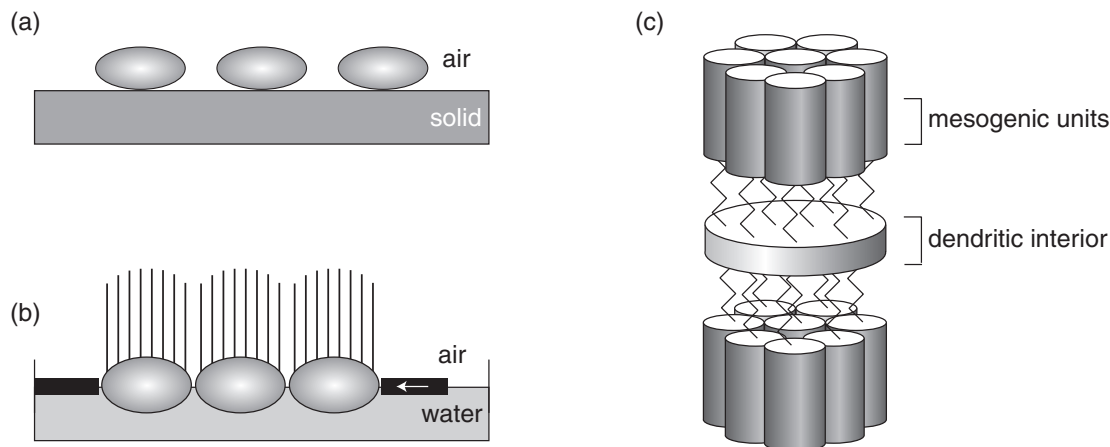


**Figure 1.3** (a) Strong interactions between the polar interior of the dendrimer on a polar surface resulting in a flattening of the dendritic structure;<sup>41,42</sup> (b) self-assembled dendrimers with hydrophobic end groups on an air–water interface;<sup>44,45</sup> (c) self-assembled cyanobisphenyl-terminated PPI dendrimers in a liquid-crystalline mesophase.<sup>46</sup>

In aqueous solution, amino-terminated PAMAM dendrimers and PPI dendrimers are polyelectrolytes and as a consequence the conformation of these dendrimers depends on the pH and the ionic strength of the solution.<sup>47–49</sup> Molecular dynamics studies showed that in acidic conditions ( $\text{pH} < 4$ ), amine-terminated PAMAM dendrimers adopt an extended conformation (*i.e.* dense-shell structure), whereas at  $\text{pH} > 9$  backfolding of the end groups occurs, leading to a dense-core structure.<sup>47,50,51</sup> Monte Carlo simulations of dendritic polyelectrolytes showed a pronounced change in the dendritic structures depending on the ionic strength.<sup>52</sup> At low ionic strength, repulsive forces between the protonated tertiary amines force the PPI dendrimer branches apart and a dense-shell structure is created (Figure 1.4a). At high ionic strength, backfolding of the end groups takes place and a dense-core structure is formed (Figure 1.4b)

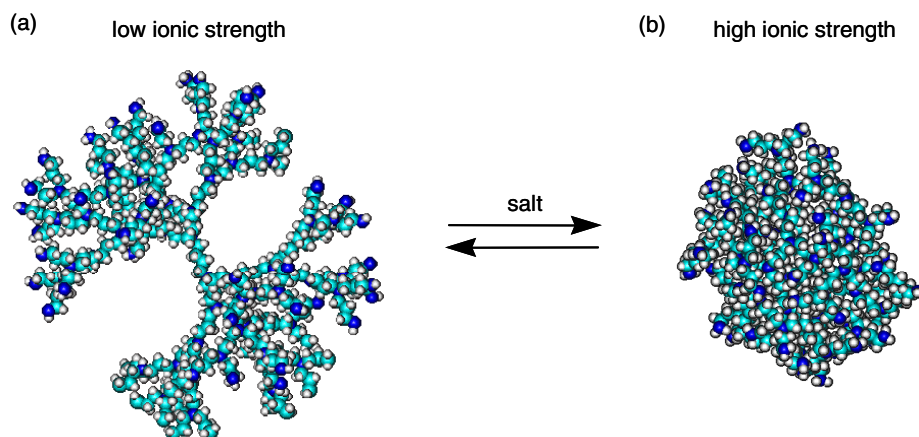


**Figure 1.4** Conformations of amine-functionalized poly(propylene imine) dendrimers at different ionic strengths. (a) A dense-shell structure at low ionic strength; (b) a dense-core structure at high ionic strength (picture kindly provided by B. Coussens, DSM Research, the Netherlands).

The different synthetic strategies discussed in this paragraph can be utilized for the synthesis of both dendritic MRI contrast agents and target-specific dendrimers. However, the introduction of functional groups within the dendritic framework may have a great influence on the conformation of the dendrimers and thus on its properties. This aspect should be taken into account when studying the properties of functionalized dendrimers, in particular when targeting units are introduced and their binding to markers is investigated.

### 1.3 BIOCOMPATIBILITY

The biocompatibility of dendrimers is an important issue when *in vivo* applications are considered.<sup>53</sup> Recently, *in vitro* studies have shown that amine-terminated PPI and PAMAM dendrimers are cytotoxic, with higher generations of the cationic dendrimers being most cytotoxic ( $IC_{50}$  for DAB-*dendr*-(NH<sub>2</sub>)<sub>64</sub> < 5 μg·mL<sup>-1</sup>).<sup>54</sup> These results are in agreement with the haematotoxicity studies by Malik *et al.*<sup>55</sup> They concluded that the haemolytic effect of PAMAM and PPI dendrimers on rat blood cells increases considerably as a function of generation dendrimer.<sup>55</sup> These effects may be attributed to favorable interactions between positively charged dendrimers and the negatively charged cell membranes.<sup>56</sup> PPI and PAMAM dendrimers with carboxylate end groups, however, are neither cytotoxic nor haemolytic up to a concentration of 2 mg·mL<sup>-1</sup>. This suggests that the overall toxicity of dendritic structures is strongly determined by the functionalities along the periphery. To date, only a few systematic studies on the *in vivo* toxicity of dendrimers have been reported. Remarkably, the general trend is that PAMAM dendrimers (up to G5), either unmodified or modified with chemically inert surface moieties, do not appear to be toxic in mice.<sup>57</sup> Another class of dendrimers that are biocompatible are peptide-functionalized poly(lysine) dendrimers.<sup>58</sup>

### 1.4 MULTIVALENCY

Multivalency plays an essential role in various biological processes, however, the underlying mechanisms of multivalency are still under discussion.<sup>9,59-62</sup> Although dendrimers are multivalent structures, this does not directly lead to multivalency, since the concept of multivalency describes the stronger effects arising from the interactions between multivalent ligands and multivalent markers. In the case of multivalent binding events, multiple ligands on one entity interact simultaneously with multiple markers on a complementary entity, known as the chelate effect (Figure 1.5a).<sup>60</sup> This may be enhanced by a process called receptor-clustering, where multivalent binding brings the markers together leading to a biological signal.<sup>63</sup> In the case of monovalent binding, a multivalent ligand can have an enhanced affinity due to a statistical effect (Figure 1.5b).<sup>60</sup>

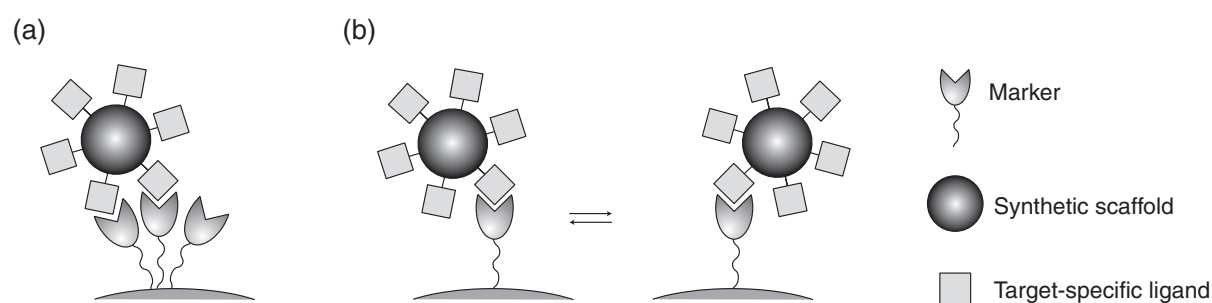


**Figure 1.5** Mechanisms involved in multivalent ligand binding. (a) Interactions between the multivalent ligand and multiple markers increase the overall affinity (chelate effect); (b) rebinding of the multivalent ligand is favored because of a high local concentration of ligand (statistical effect).<sup>59,60</sup>

The idea of using a dendritic multifunctional platform for the amplification of binding has been explored. A wide range of carbohydrate-functionalized dendrimers (“glycodendrimers”) has been synthesized to investigate multivalent carbohydrate–protein interactions.<sup>64–73</sup> Cloninger *et al.* studied the lectin binding properties of mannose-functionalized PAMAM dendrimers.<sup>71,74</sup> Compared to monovalent methyl mannose a strong enhancement in binding was observed for the sixth generation of the mannose dendrimer to concanavalin A (Con A), due to cooperative binding.<sup>71</sup> Okasada *et al.* have investigated glycodendrimers based on PAMAM dendrimers with both lactose and maltose residues at the exterior. These “sugar balls” showed strong interactions with Con A, which was confirmed by quantitative predictions.<sup>75</sup> Dissociation of the maltose-functionalized dendrimer from the aggregate was only observed when a 1200 molar excess of D-glucose was added.<sup>75</sup> Furthermore, oligopeptide-functionalized poly(lysine) dendrimers have been used to study multivalent binding events. The increased binding affinity of these dendrimers compared to monovalent peptides is becoming an important factor in the design of peptides aimed at inhibiting metastasis of various types of cancer cells.<sup>58,76,77</sup> Nowadays, there are many examples of multivalent structures reported in literature. However, more systematic studies are required to fully understand the concept of multivalency and to fully profit from its benefits in biomedical applications.

## 1.5 DENDRIMERS FOR MR IMAGING

The well-defined nature of dendritic architectures and their multivalent properties have intrigued researchers to use dendrimers in the biomedical arena. Dendritic structures have been actively investigated for diagnostic and therapeutic purposes,<sup>78–84</sup> as well as drug-delivery vehicles,<sup>53,83,85</sup> and other appealing applications, such as tissue engineering,<sup>86,87</sup> molecular encapsulation,<sup>36,88–93</sup> and light harvesting.<sup>94–97</sup> In recent years, a number of research groups have explored the use of dendrimers as a new class of macromolecular MRI contrast agents.<sup>10,98–127</sup> In

seminal work, Wiener *et al.*<sup>10</sup> reported on the synthesis of different generations of Gd(III)DTPA-based PAMAM dendrimers (DTPA = diethylenetriaminepentaacetic acid) (Figure 1.6). The sixth generation of the dendritic MRI contrast agent (MW = 139 kg·mol<sup>-1</sup>), containing 170 Gd(III) ions, showed a six-fold increase in the longitudinal ionic relaxivity (ionic  $r_1$ ), *i.e.* the contrast efficiency per Gd(III), compared to the monovalent Gd(III)DTPA complex.<sup>10</sup> This strong increase in the ionic  $r_1$  was ascribed to the lower molecular tumbling rate of the Gd(III)DTPA complex as evidenced from the increase in the rotational correlation times.<sup>118</sup> Interestingly, no increase in ionic  $r_1$  was observed for flexible macromolecular polymers with comparable molecular weights,<sup>128,129</sup> indicating that segmental motions dominate the rotational correlation time. Bryant *et al.* investigated the relationship between the ionic  $r_1$  and the molecular weight of the dendritic MRI contrast agent using different generations of the Gd(III)DOTA-based PAMAM dendrimers (DOTA = 1,4,7,10-tetraazacyclododecane-1,4,7,10-tetraacetic acid).<sup>119</sup> In that case, a plateau value for the ionic  $r_1$  of 36 mM<sup>-1</sup>s<sup>-1</sup> (0.47 T, 20 °C) was reached for the seventh generation of the Gd(III)DOTA-based dendrimer (MW = 375 kg·mol<sup>-1</sup>).<sup>10,119</sup> Moreover, the authors demonstrated that the ionic  $r_1$  of the seventh generation dendrimer increases with increasing temperature, indicating that a slow water-exchange limits the relaxivity.<sup>119,120</sup> Although a plateau value was reached for the ionic  $r_1$ , an increase in the molecular  $r_1$ , defined as the longitudinal relaxivity per single dendrimer, was observed for higher generations of the dendrimer.

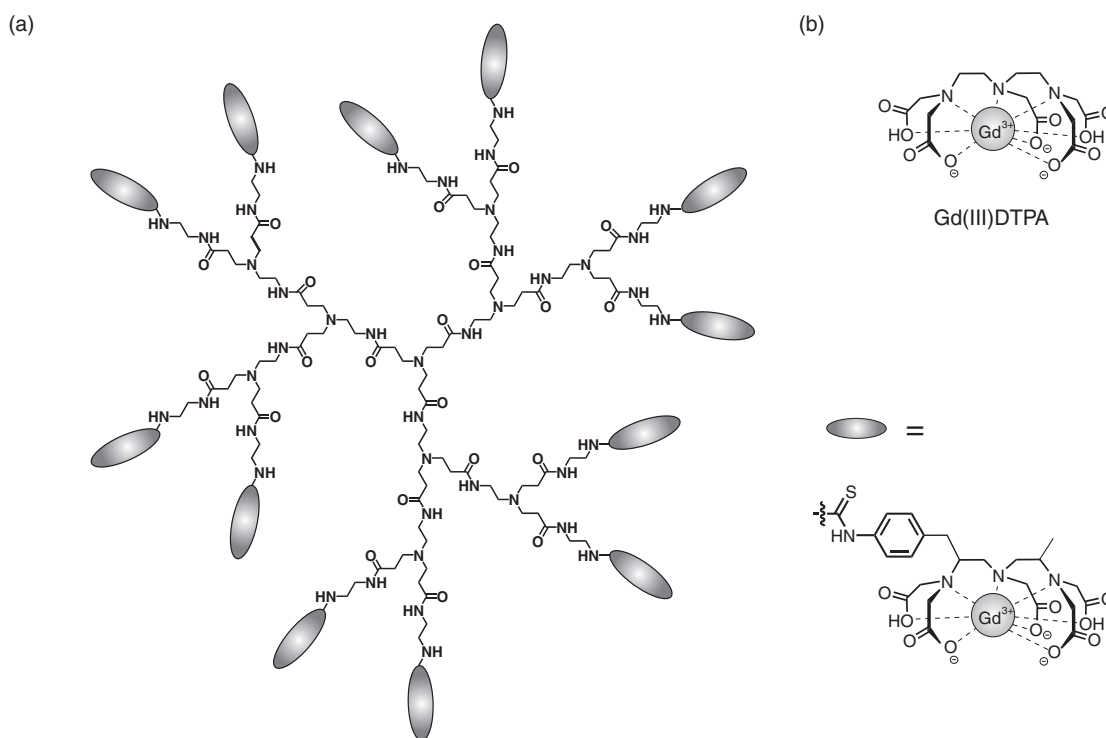


**Figure 1.6** Gd(III)DTPA-based MRI contrast agents. (a) A second generation of the Gd(III)DTPA-based PAMAM dendrimer;<sup>10</sup> (b) Gd(III)DTPA complex.

A series of Gd(III)DTPA-functionalized PPI dendrimers was reported by Kobayashi *et al.*<sup>101</sup> The authors demonstrated that the ionic  $r_1$  almost linearly increases with the molecular weight of the Gd(III)DTPA-based PPI dendrimer, eventually resulting in an ionic  $r_1$  of  $29 \text{ mM}^{-1}\text{s}^{-1}$  (1.5 T, 20 °C) for the fifth generation dendrimer.<sup>101</sup> Researchers at Schering AG (Berlin, Germany) developed another class of dendritic contrast agents: Gadomer-17<sup>®</sup> and Gd(III)DTPA-24-cascade-polymer.<sup>114-127</sup> These macromolecular MRI contrast agents are built from a trimesoyltriamide central core to which 18 lysine amino acid residues are introduced. Gadomer-17<sup>®</sup> consist of 24 *N*-monosubstituted Gd(III)DO3A moieties (DO3A = 1,4,7,10-tetraazacyclododecane-1,4,7-triacetic acid) (Figure 1.7), whereas Gd(III)DTPA-24-cascade-polymer contains 24 Gd(III)DTPA complexes.

The aforementioned dendritic MRI contrast agents have been evaluated in animal models for high resolution MR imaging.<sup>10,101-117,121</sup> *In vivo* MR imaging studies in several animal models with the higher generations of dendritic MRI contrast agents have shown prolonged vascular retention times of the MRI contrast agent and an improved visualization of vascular structures compared to low molecular Gd(III) chelates. Moreover, Kobayashi *et al.* demonstrated that Gd(III)DTPA-terminated PPI dendrimers are suitable for *in vivo* MR angiography, lymphography, and evaluation of MRI contrast agent distribution and clearance.<sup>101,110-113</sup> Gadomer-17<sup>®</sup> is currently in clinical development for blood pool imaging.<sup>114-117,121</sup>

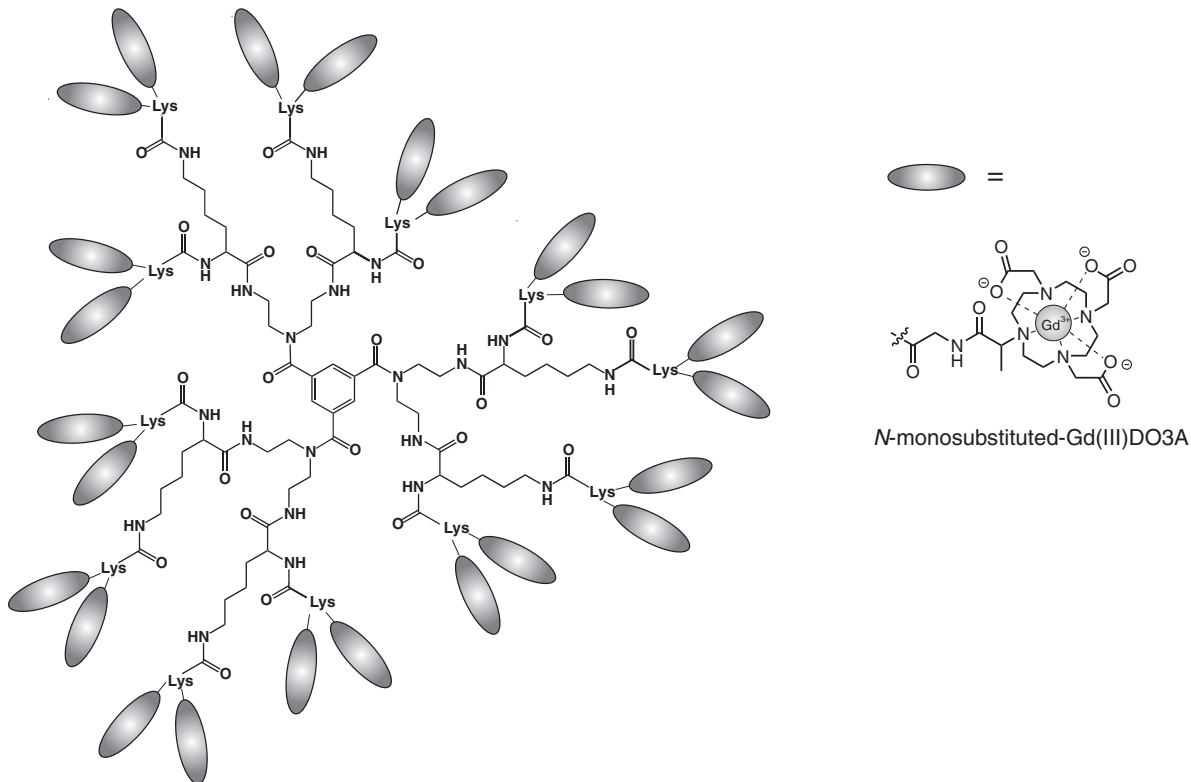


**Figure 1.7** Schematic representation of Gadomer-17<sup>®</sup>.

In the previous examples, dendrimers have shown to be suitable synthetic scaffolds for the incorporation of multiple Gd(III) moieties leading to an improved sensitivity of MRI as well as a prolonged blood circulation time of the MRI contrast agent. However, these highly efficient MRI contrast agents lack specificity, which is required for molecular MR imaging.<sup>130</sup> The development of target-specific dendritic MRI contrast agents directed to defined molecular markers could dramatically improve the imaging of a specific disease, due to an accumulation of MRI contrast agent at the region of interest, thereby generating a detectable MR signal. So far, only a few examples of target-specific dendritic MRI contrast agents are known. Konda *et al.* reported on the functionalization of the fourth generation Gd(III)DTPA-based PAMAM dendrimer with on average one or two folate moieties.<sup>131</sup> *In vivo* MR imaging in mice with ovarian tumors expressing the folate receptor resulted in a significant signal enhancement using the folate-dendrimer Gd(III) chelate, while no enhancement was observed for mice with folate-receptor negative tumors.<sup>131-134</sup> A conceptually different approach to Gd(III)DTPA-based dendrimers by immobilizing Gd(III) at the interior of the dendritic framework has been described by Takahashi *et al.* (Figure 1.8).<sup>135</sup> Dendritic wedges composed of one DTPA unit at the focal point and eight carbohydrates at the periphery, where associated through complexation with Gd(III). The authors speculated that the high local concentration of carbohydrates might further improve the binding affinity, due to multivalency.

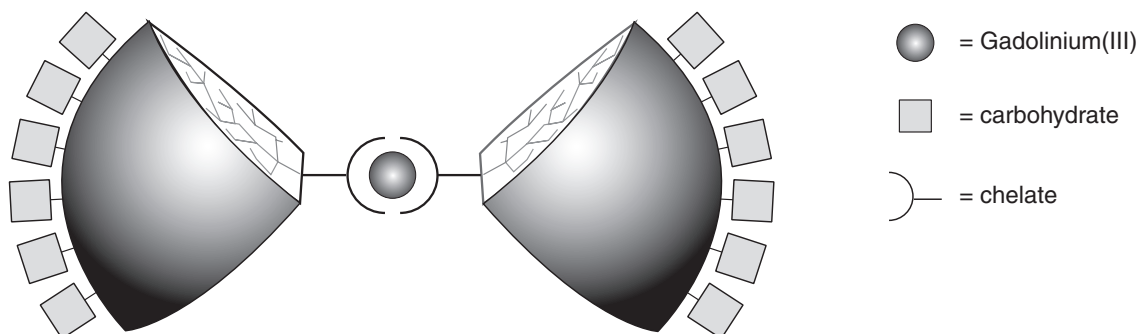


**Figure 1.8** Schematic representation of a dendritic structure with Gd(III) at the interior and multiple carbohydrates at the periphery.<sup>135</sup>



## 1.6 AIM AND OUTLINE OF THE THESIS

Future challenges in the field of MRI contrast agents involve the rational design and synthesis of multivalent target-specific MRI contrast agents. The combination of target-specific ligands and multiple MRI labels to a single scaffold is anticipated to be beneficial for the accumulation of MRI labels at regions of interest as well as for the generation of a detectable MR signal. Moreover, the combination of MRI labels and fluorescent labels on a single scaffold would allow for bimodality in imaging, thereby integrating the advantages of MRI (a non-invasive technique with a high spatial resolution) and optical imaging (a high sensitivity). Ultimately, by tuning the ratio between MRI labels and targeting units the efficacy of target-specific dendritic contrast agents may be optimized.

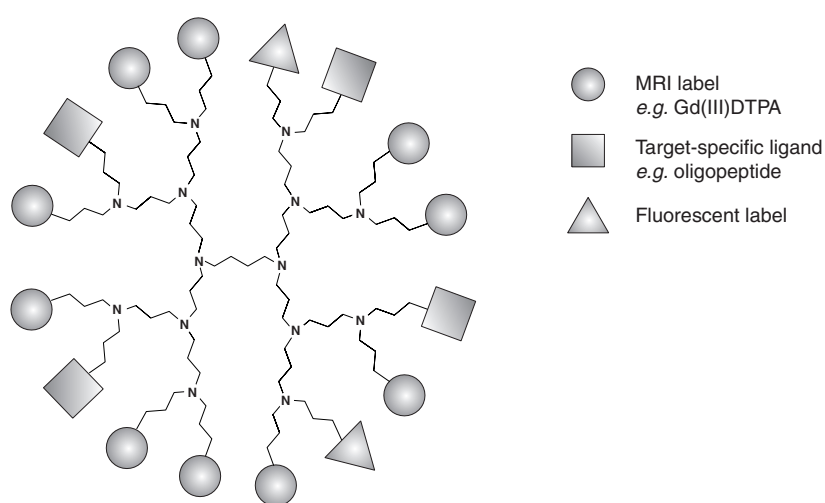


**Figure 1.9** A schematic representation of a target-specific dendritic MRI contrast agent for bimodality in imaging.

In this thesis, novel synthetic strategies for the construction of multivalent MRI contrast agents are presented. In **Chapter 2**, a modular approach for the synthesis of several functional Gd(III)DTPA-based MRI contrast agents is introduced, which employs an amine-functionalized lysine-based DTPA building block. A brief introduction is given into the basic principles underlying the use of MRI contrast agents. Moreover, relaxivity measurements for a series of low molecular weight functional Gd(III)DTPA complexes are presented. **Chapter 3** deals with the synthesis of different generations of Gd(III)DTPA-terminated poly(propylene imine) dendrimers employing an isocyanate-functionalized DTPA synthon.<sup>136</sup> The intrinsic properties of this novel series of dendritic MRI contrast agents are presented. In **Chapter 4**, an *in vitro* study of Gd(III)DTPA-terminated poly(propylene imine) dendrimers in blood plasma is described. Also, the biodistribution and pharmacokinetics of different generations of dendritic MRI contrast agents are studied in detail with *in vivo* contrast-enhanced MR imaging.<sup>137</sup> Furthermore, an interesting application of dendritic MRI contrast agents for the *in vivo* characterization of tumor angiogenesis is

described.<sup>138</sup> In **Chapter 5**, the longitudinal relaxivity of biotinylated Gd(III)-based complexes is used to probe the strong and specific binding of biotin to avidin in a quantitative fashion.<sup>139</sup> This model demonstrates that the longitudinal relaxivity can be utilized as a probe to study the formation of supramolecular assemblies in water. This principle is investigated for two additional supramolecular systems, namely dendritic host–guest systems and mixed polymeric micelles. In **Chapter 6**, synthetic strategies for the preparation of Gd(III)DTPA complexes equipped with either a fluorescent label and/or a targets-specific oligopeptides are discussed.<sup>140-142</sup> The potential of bimodal imaging is shown for fluorescently labeled Gd(III)DTPA employing the chick chorioallantoic membrane (CAM) model. In a pilot study, the efficacy of MRI contrast agents equipped with cyclic NGR as a target-specific ligand is studied for MR imaging of angiogenesis. Finally, in **Chapter 7** two approaches for the synthesis of multivalent target-specific MRI contrast agents are developed: (i) a supramolecular approach based on the self-assembly of biotinylated target-specific MRI contrast agents, containing the cyclic oligopeptide cNGR and Gd(III)DTPA, and avidin,<sup>143</sup> (ii) a covalent approach, whereby multiple oligopeptides are introduced at the periphery of poly(propylene imine) dendrimers using native chemical ligation, followed by the labeling of the sulfhydryl moiety with maleimide-functionalized DTPA.

## 1.7 REFERENCES

- (1) Weissleder, R.; Mahmood, U. *Radiology* **2001**, *219*, 316-333.
- (2) Wagenaar, D. J.; Weissleder, R.; Hengerer, A. *Acad. Radiol.* **2001**, *8*, 409-420.
- (3) Herschman, H. R. *Science* **2003**, *302*, 605-608.
- (4) Massoud, T. F.; Gambhir, S. S. *Genes & Development* **2003**, *17*, 545-580.
- (5) Weissleder, R.; Ntziachristos, V. *Nature Med.* **2003**, *9*, 123-128.
- (6) Louie, A. Y.; Huber, M. M.; Ahrens, E. T.; Rothbacher, U.; Moats, R.; Jacobs, R. E.; Fraser, S. E.; Meade, T. J. *Nature Biotechnol.* **2000**, *18*, 321-325.
- (7) Weissleder, R. *Nat. Rev. Cancer* **2002**, *2*, 11-19.
- (8) Bosman, A. W.; Janssen, H. M.; Meijer, E. W. *Chem. Rev.* **1999**, *99*, 1665-1688.
- (9) Mammen, M.; Chio, S.-K.; Whitesides, G. M. *Angew. Chem. Int. Ed.* **1998**, *37*, 2755-2794.
- (10) Wiener, E. C.; Brechbiel, M. W.; Brothers, H.; Magin, R. L.; Gansow, O. A.; Tomalia, D. A.; Lauterbur, P. C. *Magn. Reson. Med.* **1994**, *31*, 1-8.
- (11) Tomalia, D. A.; Kaplan, D. A.; Kruper, W. J., Jr.; Cheng, R. C.; Tomlinson, I. A.; Fazio, M. J.; Hedstrand, D. M.; Wilson, L. R.; U.S. Pat. 5,338,532, Aug. 16, 1994.
- (12) Tomalia, D. A.; Wilson, L. R.; Hedstrand, D. M.; Tomlinson, I. A.; Fazio, M. J.; Kruper, W. J., Jr.; Kaplan, D. A.; Cheng, R. C.; Edwards, D. S.; Jung, C. W. In *U.S.*; U.S. Pat. 5,527,524, Jun. 18, 1996.
- (13) Tomalia, D. A.; Baker, J. R.; Cheng, R. C.; Bielinska, A. U.; Fazio, M. J.; Hedstrand, D. M.; Johnson, J. A.; Kaplan, D. A.; Klakamp, S. L.; et al.; U.S. Pat. 5,714,166, Feb. 3, 1998.
- (14) Denkwalter, R. G.; Kolc, J.; Lukasavage, W. J.; U.S. Pat. 4,289,872, Sept. 15, 1981.
- (15) Denkwalter, R. G.; Kolc, J. F.; Lukasavage, W. J.; U.S. Pat. 4,360,646, Nov. 23, 1982.
- (16) Denkwalter, R. G.; Kolc, J.; Lukasavage, W. J.; U.S. Pat. 4,410,688, Oct. 18, 1983.
- (17) Tomalia, D. A.; Baker, H.; Dewald, J.; Hall, M.; Kallos, G.; Martin, S.; Roeck, J.; Ryder, J.; Smith, P. *Polymer J. (Tokyo, Japan)* **1985**, *17*, 117-132.
- (18) Tomalia, D. A.; Baker, H.; Dewald, J.; Hall, M.; Kallos, G.; Martin, S.; Roeck, J.; Ryder, J.; Smith, P. *Macromolecules* **1986**, *19*, 2466-2468.
- (19) Newkome, G. R.; Yao, Z.; Baker, G. R.; Gupta, V. K. *J. Org. Chem.* **1985**, *50*, 2003-2004.
- (20) Buhleier, E.; Wehner, W.; Vögtle, F. *Synthesis* **1978**, 155-158.
- (21) Wörner, C.; Mühlaupt, R. *Angew. Chem., Int. Ed. Engl.* **1993**, 1306-1308.
- (22) de Brabander-van den Berg, E. M. M.; Meijer, E. W. *Angew. Chem., Int. Ed. Engl.* **1993**, *32*, 1308-1311.
- (23) Koper, G. J. M.; van Genderen, M. H. P.; Elissen-Roman, C.; Baars, M. W. P. L.; Meijer, E. W.; Borkovec, M. *J. Am. Chem. Soc.* **1997**, *119*, 6512-6521.
- (24) Hummelen, J. C.; Van Dongen, J. L. J.; Meijer, E. W. *Chem. Eur. J.* **1997**, *3*, 1489-1493.
- (25) Hawker, C. J.; Fréchet, J. M. J. *J. Am. Chem. Soc.* **1990**, *112*, 7638-7647.
- (26) Hawker, C. J.; Fréchet, J. M. J. *Chem. Comm.* **1990**, 1010-1013.
- (27) Moore, J. S.; Xu, Z. *Macromolecules* **1991**, *24*, 5893-5894.
- (28) Xu, Z.; Moore, J. S. *Angew. Chem., Int. Ed. Engl.* **1993**, *32*, 246-248.
- (29) Kawaguchi, T.; Walker, K. L.; Wilkins, C. L.; Moore, J. S. *J. Am. Chem. Soc.* **1995**, *117*, 2159-2165.
- (30) Newkome, G. R.; Moorefield, C. N.; Vögtle, F. *Dendritic Molecules: Concepts, Syntheses, Perspectives*; Wiley-VCH: New York, 1996.
- (31) Zeng, F.; Zimmerman, S. C. *Chem. Rev.* **1997**, *97*, 1681-1712.
- (32) Grayson, S. M.; Fréchet, J. J. M. *Chem. Rev.* **2001**, *101*, 3819-3868.
- (33) Janssen, H. M.; Meijer, E. W. *Materials Science and Technology* **1999**, *20*, 403-458.
- (34) Newkome, G. R.; He, E.; Moorefield, C. N. *Chem. Rev.* **1999**, *99*, 1689-1746.

- (35) Newkome, G. R.; Moorefield, C. N.; Vögtle, F. *Dendrimers and Dendrons*; Wiley-VCH: New York, 2001.
- (36) Hecht, S.; Fréchet, J. M. J. *Angew. Chem. Int. Ed.* **2001**, *40*, 74-91.
- (37) Turnbull, W. B.; Kalovidouris, S. A.; Stoddart, J. F. *Chem. Eur. J.* **2002**, *8*, 2988-3000.
- (38) Tomalia, D. A. *Materials Today* **2005**, *8*, 34-46.
- (39) Percec, V.; Ahn, C. H.; Ungar, G.; Yeardley, D. J. P.; Moller, M.; Sheiko, S. S. *Nature* **1998**, *391*, 161-164.
- (40) Percec, V.; Dulcey, A. E.; Balagurusamy, V. S. K.; Miura, Y.; Smidrkal, J.; Peterca, M.; Nummelin, S.; Edlund, U.; Hudson, S. D.; Heiney, P. A.; Duan, H.; Magonov, S. N.; Vinogradov, S. A. *Nature (London, United Kingdom)* **2004**, *430*, 764-768.
- (41) Li, J.; Piehler, L. T.; Qin, D.; Baker, J. R., Jr.; Tomalia, D. A.; Meier, D. J. *Langmuir* **2000**, *16*, 5613-5616.
- (42) Tsukruk, V. V.; Rinderspacher, F.; Bliznyuk, V. N. *Langmuir* **1997**, *13*, 2171-2176.
- (43) Zhang, H.; Grim, P. C. M.; Foubert, P.; Vosch, T.; Vanoppen, P.; Wiesler, U. M.; Berresheim, A. J.; Müllen, K.; De Schryver, F. C. *Langmuir* **2000**, *16*, 9009-9014.
- (44) Sayed-Sweet, Y.; Hedstrand, D. M.; Spinder, R.; Tomalia, D. A. *J. Mater. Chem.* **1997**, *7*, 1199-1205.
- (45) Schenning, A. P. H. J.; Elissen-Roman, C.; Weener, J.-W.; Baars, M. W. P. L.; van der Gaast, S. J.; Meijer, E. W. *J. Am. Chem. Soc.* **1998**, *120*, 8199-8208.
- (46) Baars, M. W. P. L.; Söntjens, S. H. M.; Fischer, H. M.; Peerlings, H. W.; Meijer, E. W. *Chem. Eur. J.* **1998**, *4*, 2456-2466.
- (47) Lee, I.; Athey, B. D.; Wetzell, A. W.; Meixner, W.; Baker, J. R., Jr. *Macromolecules* **2002**, *35*, 4510-4520.
- (48) Chen, W.; Tomalia, D. A.; Thomas, J. L. *Macromolecules* **2000**, *33*, 9169-9172.
- (49) Maiti, P. K.; Cagin, T.; Lin, S.-T.; Goddard, W. A., III. *Macromolecules* **2005**, *38*, 979-991.
- (50) Young, J. K.; Baker, G. R.; Newkome, G. R.; Morris, K. F.; Johnson Jr., C. S. *Macromolecules* **1994**, *27*, 3464-3471.
- (51) Ramzi, A.; Scherrenberg, R.; Brackman, J.; Joosten, J.; Mortensen, K. *Macromolecules* **1998**, *31*, 1621-1626.
- (52) Welch, P.; Muthukumar, M. *Macromolecules* **1998**, *31*, 5892-5897.
- (53) Boas, U.; Heegaard, P. M. H. *Chem. Soc. Rev.* **2004**, *33*, 43-63.
- (54) Zinselmeyer, B. H.; Mackay, S. P.; Schatzlein, A. G.; Uchegbu, I. F. *Pharmaceutical Research* **2002**, *19*, 960-967.
- (55) Malik, N.; Wiwattanapatapee, R.; Klopsch, R.; Lorenz, K.; Frey, H.; Weener, J. W.; Meijer, E. W.; Paulus, W.; Duncan, R. *Journal of Controlled Release* **2000**, *68*, 299-302.
- (56) Rittner, K.; Benavente, A.; Bompard-Sorlet, A.; Heitz, F.; Divita, G.; Brasseur, R.; Jacobs, E. *Mol. Therapy* **2002**, *5*, 104-114.
- (57) Roberts, J. C.; Bhalgat, M. K.; Zera, R. T. *Journal of Biomedical Materials Research* **1996**, *30*, 53-65.
- (58) Sadler, K.; Tam James, P. *J. Biotechnol.* **2002**, *90*, 195-229.
- (59) Kiessling, L. L.; Strong, L. E.; Gestwicki, J. E. *Annual Reports in Medicinal Chemistry* **2000**, *35*, 321-330.
- (60) Gestwicki, J. E.; Cairo, C. W.; Strong, L. E.; Oetjen, K. A.; Kiessling, L. L. *J. Am. Chem. Soc.* **2002**, *124*, 14922-14933.
- (61) Mulder, A.; Huskens, J.; Reinhoudt, D. N. *Org. Biomol. Chem.* **2004**, *2*, 3409-3424.

- (62) Huskens, J.; Mulder, A.; Auletta, T.; Nijhuis, C. A.; Ludden, M. J. W.; Reinhoudt, D. N. *J. Am. Chem. Soc.* **2004**, *126*, 6784-6797.
- (63) Cairo, C. W.; Gestwicki, J. E.; Kanai, M.; Kiessling, L. L. *J. Am. Chem. Soc.* **2002**, *124*, 1615-1619.
- (64) Roy, R. in *Dendrimers and Other Dendritic Polymers*, edited by J. M. J. Fréchet and D.A. Tomalia, Wiley-VCH: New York, 2001, 361-385.
- (65) Page, D.; Zanini, D.; Roy, R. *Bioorganic & Medicinal Chemistry* **1996**, *4*, 1949-1961.
- (66) Ashton, P. R.; Boyd, S. E.; Brown, C. L.; Jayaraman, N.; Stoddart, J. F. *Angew. Chem. Int. Ed.* **1997**, *36*, 732-735.
- (67) Zanini, D.; Roy, R. *J. Am. Chem. Soc.* **1997**, *119*, 2088-2095.
- (68) Zanini, D.; Roy, R. *J. Org. Chem.* **1998**, *63*, 3486-3491.
- (69) Peerlings, H. W. I.; Nepogodiev, S. A.; Stoddart, J. F.; Meijer, E. W. *Eur. J. Org. Chem.* **1998**, 1879-1886.
- (70) Colonna, B.; Harding, V. D.; Nepogodiev, S. A.; Raymo, F. M.; Spencer, N.; Stoddart, J. F. *Chem. Eur. J.* **1998**, *4*, 1244-1254.
- (71) Woller, E. K.; Cloninger, M. J. *Org. Lett.* **2002**, *4*, 7-10.
- (72) Vrasidas, I.; De Mol, N. J.; Liskamp, R. M. J.; Pieters, R. J. *Eur. J. Org. Chem.* **2001**, 4685-4692.
- (73) Lundquist, J. J.; Toone, E. J. *Chem. Rev.* **2002**, *102*, 555-578.
- (74) Woller, E. K.; Walter, E. D.; Morgan, J. R.; Singel, D. J.; Cloninger, M. J. *J. Am. Chem. Soc.* **2003**, *125*, 8820-8826.
- (75) Aoi, K.; Itoh, K.; Okada, M. *Macromolecules* **1995**, *28*, 5391-5393.
- (76) Nomizu, M.; Yamamura, K.; Kleinman, H. K.; Yamada, Y. *Cancer Res.* **1993**, *53*, 3459-3461.
- (77) Thumshirn, G.; Hersel, U.; Goodman, S. L.; Kessler, H. *Chem. Eur. J.* **2003**, *9*, 2717-2725.
- (78) Hawthorne, M. F. *Angew. Chem., Int. Ed. Engl.*, **1993**, *32*, 950-984.
- (79) Soloway, A. H.; Tjarks, W.; Barnum, B. A.; Rong, F.-G.; Barth, R. F.; Codogni, I. M.; Wilson, J. G. *Chem. Rev.* **1998**, *98*, 1515-1562.
- (80) Fischer, M.; Vögtle, F. *Angew. Chem. Int. Ed.* **1999**, *38*, 885-905.
- (81) Stiriba, S.-E.; Frey, H.; Haag, R. *Angew. Chem. Int. Ed.* **2002**, *41*, 1329-1334.
- (82) Fischer-Durand, N.; Salmain, M.; Rudolf, B.; Vessieres, A.; Zakrzewski, J.; Jaouen, G. *ChemBioChem* **2004**, *5*, 519-525.
- (83) Gillies, E. R.; Fréchet, J. M. J. *Drug Discovery Today* **2005**, *10*, 35-43.
- (84) Maliakal, A. J.; Turro, N. J.; Bosman, A. W.; Cornel, J.; Meijer, E. W. *J. Phys. Chem. A* **2003**, *107*, 8467-8475.
- (85) Esfand, R.; Tomalia, D. A. *Drug Discovery Today* **2001**, *6*, 427-436.
- (86) Grinstaff, M. W. *Chem. Eur. J.* **2002**, *8*, 2838-2846.
- (87) Carnahan, M. A.; Middleton, C.; Kim, J.; Kim, T.; Grinstaff, M. W. *J. Am. Chem. Soc.* **2002**, *124*, 5291-5293.
- (88) Naylor, A. M.; Goddard, W. A., III; Kiefer, G. E.; Tomalia, D. A. *J. Am. Chem. Soc.* **1989**, *111*, 2339-2341.
- (89) Tomalia, D. A.; Naylor, A. M.; Goddard, W. A., III. *Angew. Chem.* **1990**, *102*, 119-157.
- (90) Hawker, C. J.; Wooley, K. L.; Fréchet, J. M. J. *J. Am. Chem. Soc.* **1993**, *115*, 4375-4376.
- (91) Crooks, R. M.; Zhao, M.; Sun, L.; Chechik, V.; Yeung, L. K. *Acc. Chem. Res.* **2001**, *34*, 181-190.
- (92) Jiang, D.-L.; Aida, T. *Nature* **1997**, *388*, 454-456.
- (93) Lemon, B. I.; Crooks, R. M. *J. Am. Chem. Soc.* **2000**, *122*, 12886-12887.
- (94) Hofkens, J.; Maus, M.; Gensch, T.; Vosch, T.; Cotlet, M.; Koehn, F.; Herrmann, A.; Muellen, K.; De Schryver, F. *J. Am. Chem. Soc.* **2000**, *122*, 9278-9288.

- (95) Schultze, X.; Serin, J.; Adronov, A.; Fréchet, J. M. J. *Chem. Commun.* **2001**, 1160-1161.
- (96) Gilat, S. L.; Adronov, A.; Fréchet, J. M. J. *Angew. Chem. Int. Ed.* **1999**, *38*, 1422-1427.
- (97) Balzani, V.; Campagna, S.; Denti, G.; Juris, A.; Serroni, S.; Venturi, M. *Acc. Chem. Res.* **1998**, *31*, 26-34.
- (98) Merbach, A. E.; Tóth, E. *The Chemistry of Contrast Agents in Medical Magnetic Resonance Imaging*; John Wiley & Sons: New York, 2001.
- (99) Caravan, P.; Ellison, J. J.; McMurry, T. J.; Lauffer, R. B. *Chem. Rev.* **1999**, *99*, 2293-2352.
- (100) Clarkson, R. B. *Top. Curr. Chem.* **2002**, *221*, 201-235.
- (101) Kobayashi, H.; Kawamoto, S.; Jo, S.-K.; Bryant, H. L., Jr.; Brechbiel, M. W.; Star, R. A. *Bioconjugate Chem.* **2003**, *14*, 388-394.
- (102) Kobayashi, H.; Sato, N.; Kawamoto, S.; Saga, T.; Hiraga, A.; Haque, T. L.; Ishimori, T.; Konishi, J.; Togashi, K.; Brechbiel, M. W. *Bioconjugate Chem.* **2001**, *12*, 100-107.
- (103) Sato, N.; Kobayashi, H.; Hiraga, A.; Saga, T.; Togashi, K.; Konishi, J.; Brechbiel, M. W. *Magn. Reson. Med.* **2001**, *46*, 1169-1173.
- (104) Kobayashi, H.; Shirakawa, K.; Kawamoto, S.; Saga, T.; Sato, N.; Hiraga, A.; Watanabe, I.; Heike, Y.; Togashi, K.; Konishi, J.; Brechbiel, M. W.; Wakasugi, H. *Cancer Res.* **2002**, *62*, 860-866.
- (105) Kobayashi, H.; Sato, N.; Kawamoto, S.; Saga, T.; Hiraga, A.; Ishimori, T.; Konishi, J.; Togashi, K.; Brechbiel, M. W. *Magn. Reson. Med.* **2001**, *46*, 579-585.
- (106) Kobayashi, H.; Sato, N.; Hiraga, A.; Saga, T.; Nakamoto, Y.; Ueda, H.; Konishi, J.; Togashi, K.; Brechbiel, M. W. *Magn. Reson. Med.* **2001**, *45*, 454-460.
- (107) Kobayashi, H.; Kawamoto, S.; Saga, T.; Sato, N.; Hiraga, A.; Ishimori, T.; Konishi, J.; Togashi, K.; Brechbiel, M. W. *Magn. Reson. Med.* **2001**, *46*, 781-788.
- (108) Kobayashi, H.; Kawamoto, S.; Saga, T.; Sato, N.; Hiraga, A.; Konishi, J.; Togashi, K.; Brechbiel, M. W. *J. Magn. Res. Imaging* **2001**, *14*, 705-713.
- (109) Kobayashi, H.; Kawamoto, S.; Star, R. A.; Waldmann, T. A.; Tagaya, Y.; Brechbiel, M. W. *Cancer Res.* **2003**, *63*, 271-276.
- (110) Kobayashi, H.; Kawamoto, S.; Saga, T.; Sato, N.; Hiraga, A.; Ishimori, T.; Akita, Y.; Mamede, M. H.; Konishi, J.; Togashi, K.; Brechbiel, M. W. *Magn. Reson. Med.* **2001**, *46*, 795-802.
- (111) Kobayashi, H.; Saga, T.; Kawamoto, S.; Sato, N.; Hiraga, A.; Ishimori, T.; Konishi, J.; Togashi, K.; Brechbiel, M. W. *Cancer Res.* **2001**, *61*, 4966-4970.
- (112) Kobayashi, H.; Brechbiel, M. W. *Molecular Imaging* **2003**, *2*, 1-10.
- (113) Kobayashi, H.; Kawamoto, S.; Choyke, P. L.; Sato, N.; Knopp, M. V.; Star, R. A.; Waldmann, T. A.; Tagaya, Y.; Brechbiel, M. W. *Magn. Reson. Med.* **2003**, *50*, 758-766.
- (114) Dong, Q.; Hurst, D. R.; Weinmann, H. J.; Chenevert, T. L.; Londy, F. J.; Prince, M. R. *Invest. Radiol.* **1998**, *33*, 699-708.
- (115) Link, H. E. D.; Shames, D. M.; Wendland, M.; Muhler, A.; Gossman, A.; Rosenau, W.; Brasch, R. C. *Acad. Radiol.* **2000**, *7*, 934-944.
- (116) Misselwitz, B.; Schmitt-Willich, H.; Ebert, W.; Frenzel, T.; Weinmann, H. J. *MAGMA* **2001**, *12*, 128-134.
- (117) Misselwitz, B.; Schmitt-Willich, H.; Michaelis, M.; Oellinger, J. J. *Invest. Radiol.* **2002**, *37*, 146-151.
- (118) Wiener, E. C.; Auteri, F. P.; Chen, J. W.; Brechbiel, M. W.; Gansow, O. A.; Schneider, D. S.; Belford, R. L.; Clarkson, R. B.; Lauterbur, P. C. *J. Am. Chem. Soc.* **1996**, *118*, 7774-7782.
- (119) Bryant Jr., L. H.; Brechbiel, M. W.; Wu, C.; Bulte, J. W.; Herynek, V.; Frank, J. A. *J. Magn. Res. Imaging* **1999**, *9*, 348-352.
- (120) Tóth, E.; Pubanz, D.; Vauthey, S.; Helm, L.; Merbach, A. E. *Chem. Eur. J.* **1996**, *2*, 1607-1615.

- (121) Fink, C.; Kiessling, F.; Bock, M.; Lichy Matthias, P.; Misselwitz, B.; Peschke, P.; Fusenig, N. E.; Grobholz, R.; Delorme, S. *J. Magn. Res. Imaging* **2003**, *18*, 59-65.
- (122) Nicolle, G. M.; Tóth, E.; Schmitt-Willich, H.; Raduchel, B.; Merbach, A. E. *Chem. Eur. J.* **2002**, *8*, 1040-1048.
- (123) Adam, G.; Neuerburg, J.; Spuntrup, E.; Muhler, A.; Scherer, K.; Gunther, R. W. *J. Magn. Res. Imaging* **1994**, *4*, 462-466.
- (124) Adam, G.; Neuerburg, J.; Spuntrup, E.; Muhler, A.; Scherer, K.; Gunther, R. W. *Magn. Reson. Med.* **1994**, *32*, 622-628.
- (125) Schwickert, H. C.; Roberts, T. P.; Muhler, A.; Stiskal, M.; Demsar, F.; Brasch, R. C. *European Journal of Radiology* **1995**, *20*, 144-150.
- (126) Roberts, H. C.; Saeed, M.; Roberts, T. P.; Muhler, A.; Shames, D. M.; Mann, J. S.; Stiskal, M.; Demsar, F.; Brasch, R. C. *J. Magn. Res. Imaging* **1997**, *7*, 331-338.
- (127) Roberts, H. C.; Saeed, M.; Roberts, T. P.; Muhler, A.; Brasch, R. C. *J. Magn. Res. Imaging* **1999**, *9*, 204-208.
- (128) Vexler, V. S.; Clement, O.; Schmitt-Willich, H.; Brasch, R. C. *J. Magn. Res. Imaging* **1994**, *4*, 381-388.
- (129) Desser, T. S.; Rubin, D. L.; Muller, H. H.; Qing, F.; Khodor, S.; Zanazzi, G.; Young, S. W.; Ladd, D. L.; Wellons, J. A.; Kellar, K. E. *J. Magn. Res. Imaging* **1994**, *4*, 467-472.
- (130) Artemov, D. *Journal of Cellular Biochemistry* **2003**, *90*, 518-524.
- (131) Konda, S. D.; Aref, M.; Wang, S.; Brechbiel, M.; Wiener, E. C. *MAGMA* **2001**, *12*, 104-113.
- (132) Wiener, E. C.; Konda, S.; Shadron, A.; Brechbiel, M.; Gansow, O. *Invest. Radiol.* **1997**, *32*, 748-754.
- (133) Konda, S. D.; Aref, M.; Brechbiel, M.; Wiener, E. C. *Invest. Radiol.* **2000**, *35*, 50-57.
- (134) Konda, S. D.; Wang, S.; Brechbiel, M.; Wiener, E. C. *Invest. Radiol.* **2002**, *37*, 199-204.
- (135) Takahashi, M.; Hara, Y.; Aoshima, K.; Kurihara, H.; Oshikawa, T.; Yamashita, M. *Tetrahedron Letters* **2000**, *41*, 8485-8488.
- (136) Langereis, S.; de Lussanet, Q. G.; van Genderen, M. H. P.; Backes, W. H.; Meijer, E. W. *Macromolecules* **2004**, *37*, 3084-3091.
- (137) Langereis, S.; Lussanet, Q. G.; van Genderen Marcel, H. P.; Meijer, E. W.; Beets-Tan, R. G. H.; Griffioen, A. W.; van Engelshoven, J. M. A.; Backes, W. H. *NMR in Biomedicine* **2005**, submitted for publication.
- (138) Lussanet, Q. G.; Langereis, S.; Beets-Tan, R. G. H.; van Genderen, M. H. P.; Griffioen, A. W.; van Engelshoven, J. M. A.; Backes, W. H. *Radiology* **2005**, *235*, 65-72.
- (139) Langereis, S.; Kooistra, H. A. T.; van Genderen, M. H. P.; Backes, W. H.; Meijer, E. W. *Org. Biomol. Chem.* **2004**, *2*, 1271-1273.
- (140) Langereis, S.; de Lussanet, Q. G.; van Genderen, M. H. P.; Backes, W. H.; Hackeng, T. M.; van Engelshoven, J. M. A.; Meijer, E. W. *Polym. Mater. Sci. Eng.* **2004**, *91*, 56-57.
- (141) Dirksen, A.; Langereis, S.; de Waal, B. F. M.; van Genderen, M. H. P.; Meijer, E. W.; de Lussanet, Q. G.; Hackeng, T. M. *Org. Lett.* **2004**, *6*, 4857-4860.
- (142) Langereis, S.; Dirksen, A.; de Waal, B. F. M.; van Genderen, M. H. P.; de Lussanet, Q. G.; Hackeng, T. M.; Meijer, E. W. *Eur. J. Org. Chem.* **2005**, accepted for publication.
- (143) Dirksen, A.; Langereis, S.; de Waal, B. F. M.; van Genderen, M. H. P.; Hackeng, T. M.; Meijer, E. W. *Chem. Commun.* **2005**, accepted for publication.

---

## Chapter 2

### Novel methodologies for the synthesis of functionalized

### Gd(III)DTPA complexes

---

**ABSTRACT:** *A modular approach for the synthesis of MRI contrast agents based on an amine-functionalized DTPA pentaester has been developed. Through the use of orthogonal chemistries, novel methodologies have been developed in order to arrive at a series of functionalized Gd(III)DTPA complexes. The first approach deals with the conversion of the primary amine of the DTPA pentaester into the corresponding isocyanate using di-tert-butyltricarboxylate under mild conditions. This procedure has been applied to prepare a reference Gd(III)DTPA complex and DTPA-functionalized poly(ethylene butylene). Alternative approaches utilizing either activated carbamates or blocked isocytosine isocyanates have been employed to prepare Gd(III)DTPA-based complexes bearing a glycinyurea entity or a ureidopyrimidinone hydrogen-bonding motif, respectively. All Gd(III)DTPA-based complexes have been characterized with IR spectroscopy, ESI-MS and ICP-AES. The longitudinal ( $r_1$ ) and transverse ( $r_2$ ) relaxivities of these Gd(III)DTPA-based complexes are in the range of 8–8.5  $\text{mM}^{-1}\text{s}^{-1}$  and 9–9.6  $\text{mM}^{-1}\text{s}^{-1}$ , respectively. These values are significantly higher in comparison with the relaxivities of parent Gd(III)DTPA.*



## 2.1 INTRODUCTION

Magnetic Resonance Imaging (MRI) contrast agents based on gadolinium(III) complexes are generally applied as diagnostics in medical imaging.<sup>1</sup> The Gd(III) ion is by far the most frequently chosen metal ion for MRI contrast agents, due to its very high magnetic moment (seven unpaired electrons) and relatively slow electronic relaxation.<sup>2</sup> The high toxicity of  $[\text{Gd(III)(H}_2\text{O)}_8]^{3+}$ , LD<sub>50</sub> values are in the range of 0.2–0.5 mmol·kg<sup>-1</sup>, requires the metal ion to be strongly complexed by a chelating agent.<sup>1,2</sup> Diethylenetriaminepentaacetic acid (DTPA **1**) is a very efficient chelating agent for the complexation of the Gd(III) ion. The corresponding Gd(III)DTPA complex has been safely used as an MRI contrast agent over the past decades.<sup>3-6</sup>

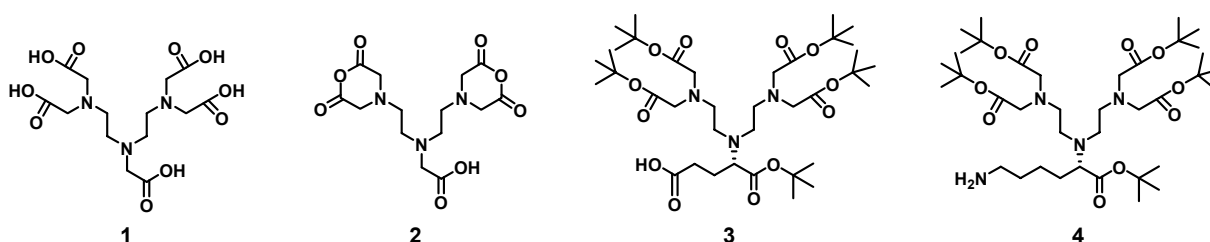


**Figure 2.1** Chemical structures of DTPA (**1**), cyclic dianhydride of DTPA (**2**), glutamic acid-based DTPA pentaester (**3**), and lysine-based DTPA pentaester (**4**).<sup>7,8</sup>

In recent years, the DTPA moiety has been covalently coupled to a wide variety of molecules including oligopeptides,<sup>9</sup> proteins,<sup>10,11</sup> and polysaccharides<sup>12</sup> by using the cyclic dianhydride of DTPA (**2**). The non-selective reaction of the cyclic dianhydride of DTPA with the amine functionalities of the molecule of interest, results in a mixture of monoamide-DTPA and bisamide-DTPA conjugates, which is an inherent disadvantage of this methodology.<sup>13</sup> Moreover, Sherry *et al.* reported that a significant decrease in the thermodynamic stability of the Gd(III)DTPA complex occurs upon conversion of only one of the five carboxylic acids of DTPA into an amide.<sup>14</sup> When designing synthetic approaches to thermodynamically and kinetically stable Gd(III)DTPA complexes, it is important that all five carboxylic acids remain available for Gd(III) complexation in order to reduce toxicity both *in vitro* and *in vivo*.<sup>8,15,16</sup> Alternative DTPA pentaesters based on glutamic acid (**3**, carboxylic acid terminated) or lysine (**4**, amine terminated) were reported by Williams *et al.*<sup>7</sup> and Anelli *et al.*<sup>8</sup> Upon deprotection of the *tert*-butyl esters, these DTPA compounds retain a reactive functional group handle as well as all five carboxylic acids for Gd(III) complexation.

This Chapter outlines a modular approach for the synthesis of several MRI contrast agents based on lysine-based DTPA pentaester **4**. Through the use of orthogonal chemistries, novel methodologies have been developed in order to arrive at a series of functionalized Gd(III)DTPA complexes. In Section 2.3, a brief introduction is given into the basic principles underlying the use

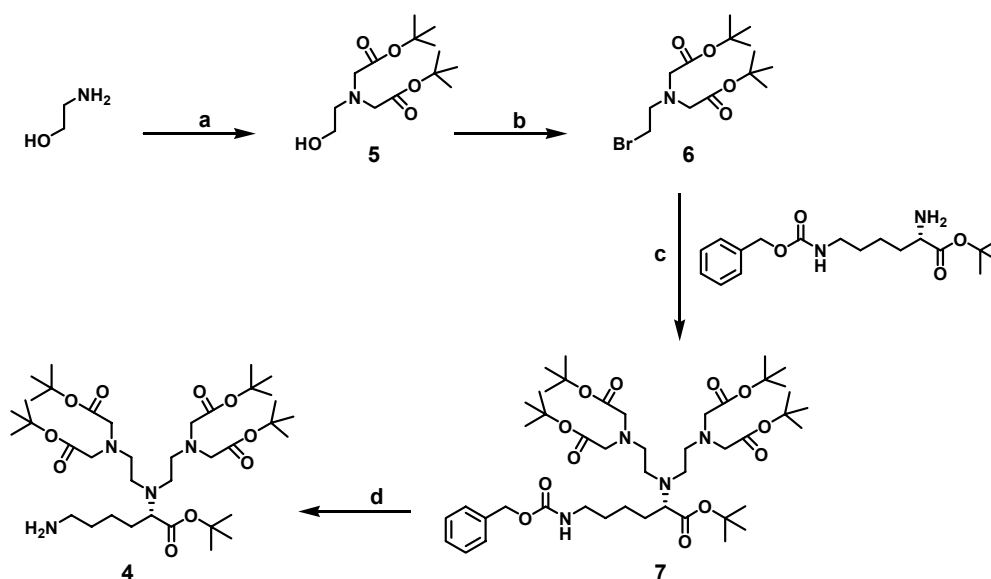
of MRI contrast agents. Finally the contrast efficiency, expressed in terms of longitudinal and transverse relaxivities, for a series of functionalized Gd(III)DTPA complexes is presented.

## 2.2 SYNTHESIS

In this section, an amine-functionalized DTPA-based building block is introduced as a versatile synthon. The primary amine functionality of the DTPA synthon will be used as a synthetic handle for further coupling.

### 2.2.1 Amine-functionalized DTPA pentaester

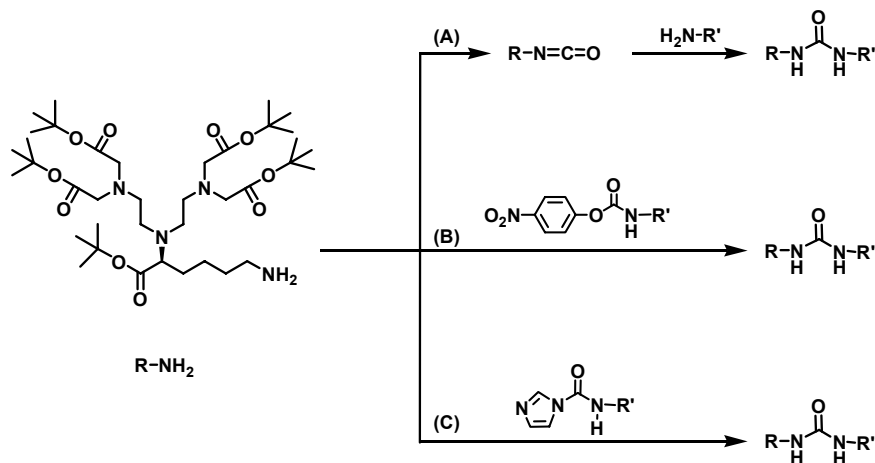
The synthetic route to (L)-lysine-based DTPA analogue **4**, of which the five carboxylic acids are protected with acid removable *tert*-butyl esters, is shown in Scheme 2.1. Bis-*N*-alkylated alcohol **5** was synthesized *via* a nucleophilic substitution reaction of *tert*-butyl bromoacetate with aminoethanol, according to the previously described literature procedure of Williams *et al.*<sup>7</sup> The reaction was carried out in DMF using 2.2 equivalents of K<sub>2</sub>CO<sub>3</sub> as a base. Recrystallization from pentane provided compound **5** in 75% yield. Alcohol **5** was reacted with tetrabromomethane and triphenylphosphine in dichloromethane (DCM) to give bromide **6** in 72% yield. The dialkylation reaction of H-Lys(Z)-OtBu with bromide **6** was performed in DMF with KHCO<sub>3</sub> as a base. Compound **7** was isolated in 48% yield. Catalytic hydrogenation of **7** with hydrogen and 10% Pd/C in a solution of MeOH/H<sub>2</sub>O (40:1 v/v) in the presence of acetic acid resulted in the formation of lysine-based DTPA building block **4** in an overall yield of 23%. All compounds were characterized with <sup>1</sup>H-NMR and <sup>13</sup>C-NMR spectroscopy, IR spectroscopy, and MALDI-TOF spectrometry.



**Scheme 2.1** Synthetic route towards amine-functionalized DTPA synthon (**4**). (a) *tert*-Butyl-bromoacetate, KHCO<sub>3</sub>, DMF; (b) CBr<sub>4</sub>, Ph<sub>3</sub>P, DCM; (c) H-Lys(Z)OtBu, KHCO<sub>3</sub>, DMF; (d) H<sub>2</sub>, 10% Pd/C, 1:9:40 v/v/v H<sub>2</sub>O/CH<sub>3</sub>COOH/MeOH.<sup>7,8</sup>

### 2.2.2 General strategies for the synthesis of functionalized Gd(III)DTPA complexes

To enable coupling of the amine-functionalized DTPA pentaester **4** to any primary amine containing functionality, different synthetic strategies were developed (Scheme 2.2).



**Scheme 2.2** Synthetic strategies to DTPA-functionalized structures.

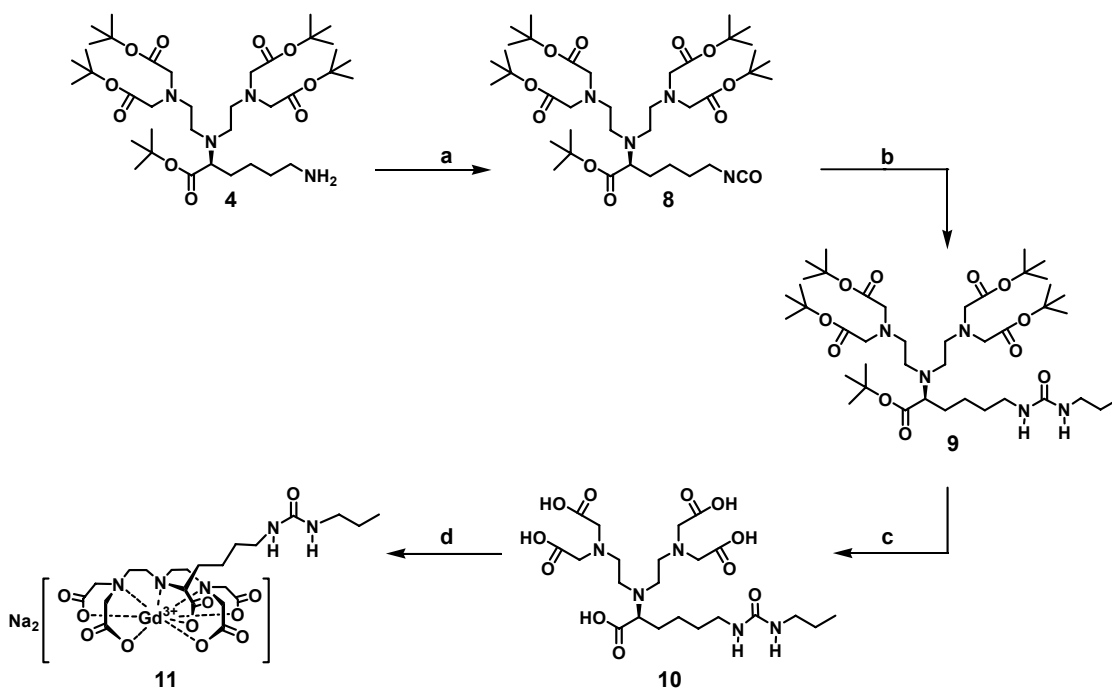
The first methodology (strategy A) deals with the conversion of the primary amine of **4** into the corresponding isocyanate using di-*tert*-butyl-tricarbonate, which is a very versatile procedure for the conversion of primary amines into isocyanates under mild reaction conditions.<sup>17,18</sup> The reaction of the isocyanate-functionalized DTPA analogue with the primary amine was employed to synthesize a reference Gd(III) complex and DTPA functionalized poly(ethylene butylene) (*vide infra*) as well as dendritic MRI contrast agents (Chapter 3) and oligopeptide-functionalized MRI contrast agents (Chapter 6). Alternative methodologies utilizing either activated carbamates (strategy B) or blocked isocytosine isocyanates (strategy C) were employed to prepare Gd(III)DTPA complexes modified with a glycylurea entity or a ureidopyrimidinone hydrogen-bonding motif, respectively.

### 2.2.3 Isocyanate-functionalized DTPA synthon: strategy A

#### *Synthesis of reference Gd(III)DTPA complex*

The reaction of isocyanate-functionalized DTPA building blocks with primary amines is illustrated by the addition of propylamine in DCM to obtain urea **9** (Scheme 2.3). Subsequent deprotection and complexation with GdCl<sub>3</sub> yields Gd(III) complex **11**. The reaction of amine-functionalized DTPA building block **4** with 1.1 equivalents of di-*tert*-butyl-tricarbonate was carried out in freshly distilled DCM under an atmosphere of argon. This reaction is accompanied by the formation of two moles of both carbon dioxide and *tert*-butanol. It is important to note that the solution of amine **4** was injected under the surface of a solution of di-*tert*-butyl-tricarbonate to prevent the side-reaction between the primary amine of **4** and carbon dioxide into carbamic acid.<sup>19</sup>

The course of the reaction between **4** and di-*tert*-butyl-tricarbonate was monitored with IR spectroscopy. In the IR spectrum, a strong absorption corresponding to the N=C=O stretch vibration was observed at  $2272\text{ cm}^{-1}$  and the reaction was completed within 1 h. A few drops of pyridine were added to quench the excess of di-*tert*-butyl-tricarbonate. The reaction of **8** with propyl amine was completed within 10 minutes as deduced from the disappearance of the isocyanate vibration in the IR spectrum and the simultaneous formation of the urea carbonyl stretch vibrations at  $1639\text{ cm}^{-1}$  and  $1567\text{ cm}^{-1}$ .



**Scheme 2.3** Synthesis of Gd(III) complex **11**. (a) Di-*tert*-butyl-tricarbonate, DCM; (b) propylamine, DCM; (c) 1:2 v/v TFA/DCM; (d)  $\text{GdCl}_3 \cdot 6\text{H}_2\text{O}$ , NaOH,  $\text{H}_2\text{O}$ , pH 7.

Structural characterization of urea **9** was performed with a combination of analytical techniques including electrospray ionization mass spectrometry (ESI-MS),  $^1\text{H}$ - and  $^{13}\text{C}$ -NMR spectroscopy, and IR spectroscopy. The  $^1\text{H}$ -NMR spectrum of compound **9** is shown in Figure 2.2a. The urea protons of **9** could be observed at 4.8 and 4.9 ppm and the signals of the methylene protons adjacent to the urea ( $\text{H}_3$  and  $\text{H}_6$ ) appeared between 3.0–3.3 ppm together with proton  $\text{H}_9$ . The assignment of the resonances in the  $^1\text{H}$ -NMR spectrum of **9** was based on the peak assignment that could be deduced from  $^1\text{H}$ ,  $^1\text{H}$ -homonuclear correlation spectroscopy (COSY) (as shown in Figure 2.2b) and  $^1\text{H}$ ,  $^{13}\text{C}$ -heteronuclear correlation spectroscopy (HETCOR).

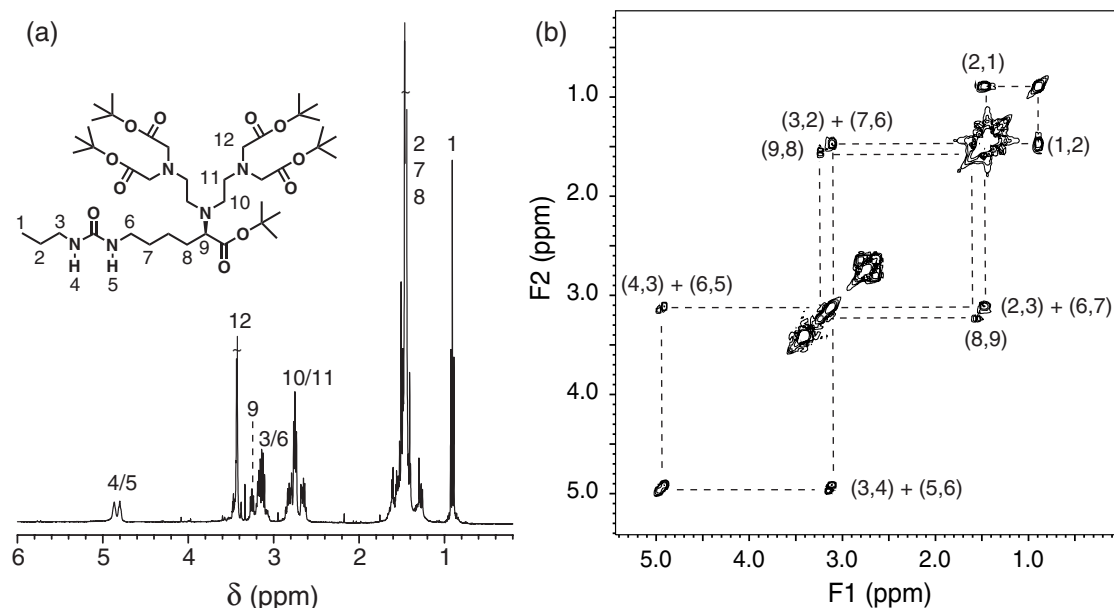


**Figure 2.2**  $^1\text{H-NMR}$  and  $^1\text{H},^1\text{H-COSY}$  spectra of **9** in  $\text{CDCl}_3$ .

Cleavage of the *tert*-butyl esters of **9** was accomplished with trifluoroacetic acid (TFA) in DCM, affording the water-soluble chelate **10**. TFA was successfully removed *via* extensive dialysis and the absence of TFA was confirmed with  $^{19}\text{F-NMR}$ . Gd(III) complex **11** was obtained by adding a stoichiometric amount of  $\text{GdCl}_3$  to an aqueous solution of **10**. The pH was maintained at 7 by adding 0.1 N NaOH solution ensuring a fast reaction of Gd(III) with the DTPA moiety.<sup>20</sup> The solution of **11** was purified with dialysis in order to remove traces of residual (toxic) Gd(III). After freeze-drying Gd(III) complex **11** was obtained in a quantitative yield.

Characterization of the Gd(III) complex was performed with IR spectroscopy and ESI-MS, while the Gd(III) content was determined with inductively coupled plasma atomic emission spectroscopy (ICP-AES) analysis. ICP-AES is a multi-elemental analytical technique, which is commonly used for the quantitative trace analysis of lanthanides in aqueous solutions.<sup>21,22</sup> The value for the observed Gd(III) content was found to be 91% of the theoretical value. IR spectroscopy demonstrated that more than 90% of **10** was complexated with Gd(III), by the disappearance of the C–O stretching vibration at  $1217\text{ cm}^{-1}$  and the shifts of the carbonyl stretches to  $1586\text{ cm}^{-1}$  (Figure 2.3a). ESI-MS is a soft spectrometric technique, which allows pre-existing ions in solution to be transferred to the gas phase with minimum fragmentation.<sup>23</sup> This technique proved to be very suitable for the characterization of Gd(III) complexes. ESI-MS spectra of Gd(III) complexes under neutral and basic conditions are recorded in the negative mode, since deprotonation of the carboxylic acid moieties results in an overall negative charge the Gd(III)DTPA complex. In the ESI-MS spectrum the molecular ion  $[\text{M} - \text{H}]^-$  of the desired Gd(III) complex could be observed at  $m/z = 703.2$  (Figure 2.3b). The signal at  $m/z = 1407.3$  is assigned to a noncovalent dimeric species, whereas the signal at 1055.3 corresponds to a noncovalent doubly charged trimeric species.

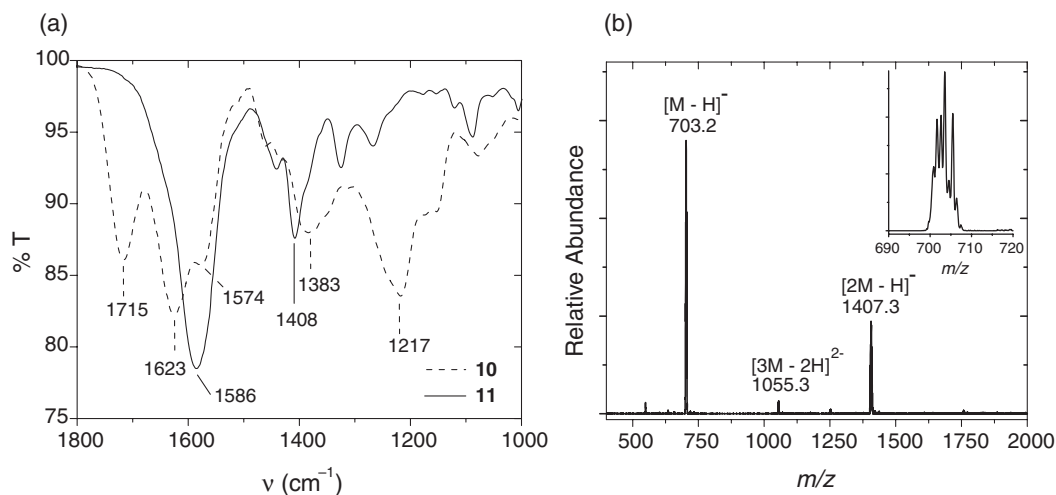
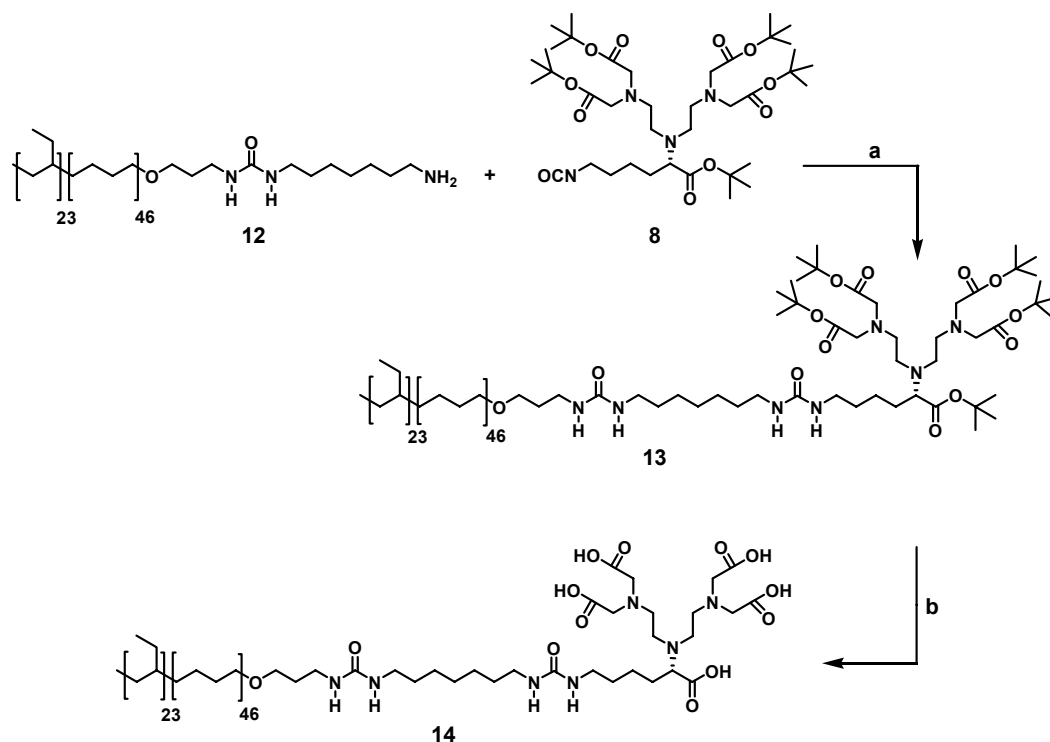


**Figure 2.3** (a) FT-IR spectra of **10** and **11**; (b) negative mode ESI-MS spectrum of Gd(III) complex **11**, inset: Gd(III) isotope pattern of the molecular anion.

### Synthesis of DTPA-functionalized poly(ethylene butylene)

In an attempt to broaden the scope of our synthetic approach to high molecular weight species, isocyanate-functionalized DTPA analogue (**8**) was reacted with amine-terminated poly(ethylene butylene) (**12**,  $M_n = 3.8 \text{ kg}\cdot\text{mol}^{-1}$ ). The latter compound was kindly provided by dr. N. Chebotareva of our laboratories. The synthesis of **13** is analogous to that described for **9**, with the difference that the reaction time required for the coupling with the polymer is much longer.



**Scheme 2.4** Synthesis of DTPA-functionalized polymer **14**. (a) DCM; (b) 1:2 v/v TFA/DCM.

Purification with column chromatography yielded **13**. Deprotection with TFA resulted in the formation of **14**. MALDI-TOF mass spectrometry proved to be an excellent analytical tool to monitor the chemical modifications carried out on amine-functionalized poly(ethylene butylene). The mass difference between the signals of 56 amu exactly corresponds to the molecular weight of the repeating unit. Figure 2.4 shows the shifts occurring in the MALDI-TOF spectrum upon modification of polymer **12** with DTPA followed by the cleavage of the *tert*-butyl ester groups.

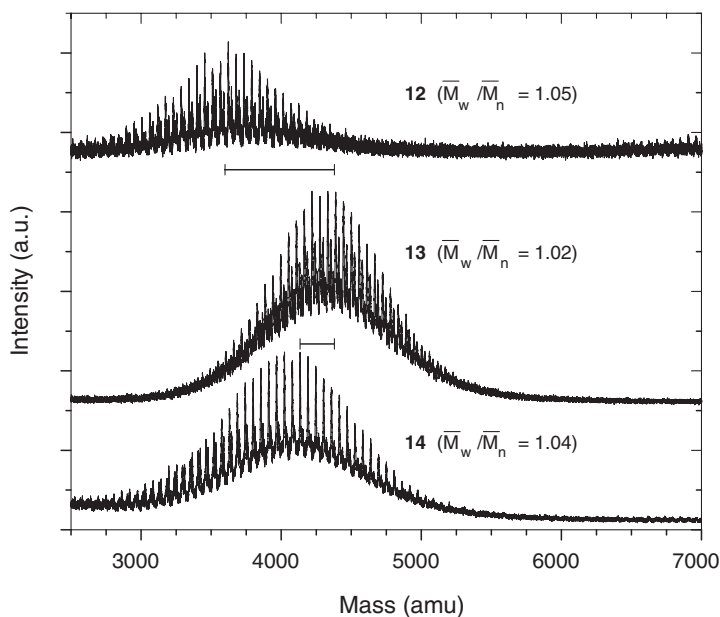


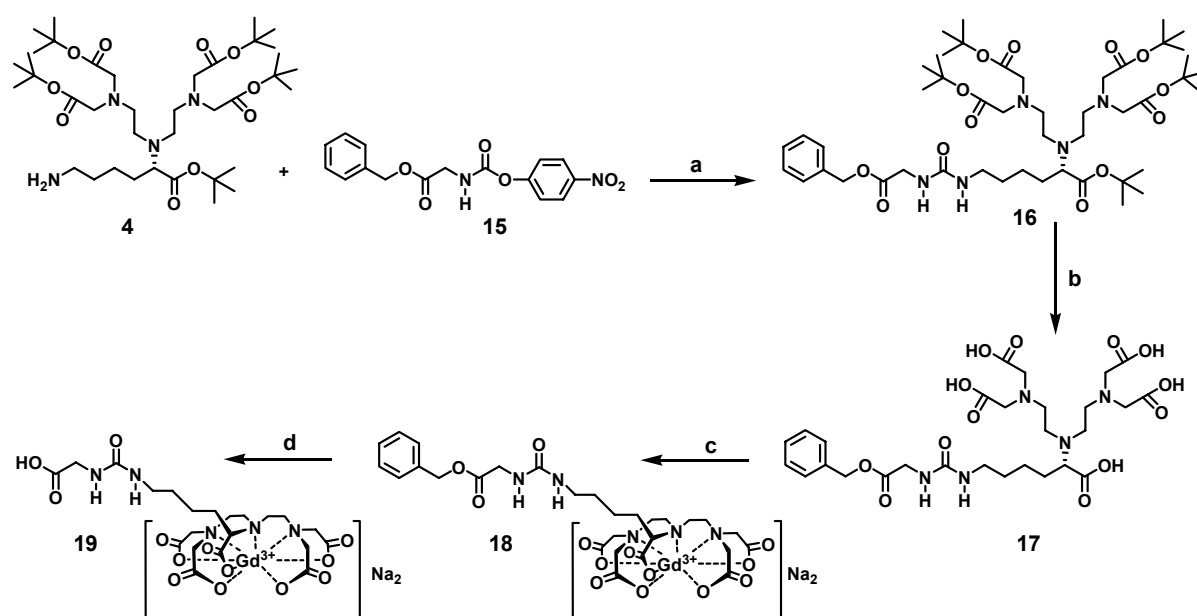
**Figure 2.4** MALDI-TOF spectra of **12** (top), **13** (middle), and **14** (bottom).

Attempts to prepare the Gd(III) complex of **14** in aqueous medium and 0.3 M citric acid buffer at pH 5.8 were unsuccessful, due to the insolubility of **14** in aqueous media. If one of the compounds is not molecularly dissolved, the corresponding reaction centers will not be accessible for the reaction, and hence no complexation will take place. A strategy to solubilize the DTPA-functionalized poly(ethylene butylene) to allow complexation with Gd(III) is to make use of polymeric micelles as will be demonstrated in Chapter 5 (Section 5.4.2).

#### 2.2.4 Synthesis of glycylurea-functionalized Gd(III)DTPA complex: strategy B

One chemical moiety that can be incorporated into the Gd(III)DTPA complex is the glycylurea functionality. This group has been shown to have a strong non-covalent interaction with the periphery of adamantyl-urea functionalized poly(propylene imine) dendrimers.<sup>24-26</sup> The mixing of an adamantyl-urea functionalized dendrimer with a glycylurea-functionalized Gd(III) complex should result in a highly loaded dendrimer bearing Gd(III) ions. The synthesis of the glycylurea-functionalized Gd(III) complex is outlined in Scheme 2.5. Benzyl glycinate was

reacted with bis(4-nitrophenyl)-carbonate in chloroform, yielding *N*-(4-nitrophenyloxy-carbonyl)benzyl glycinate **15**. This carbamate was then reacted with DTPA synthon **4** to provide intermediate **16**. The APT  $^{13}\text{C}$ -NMR (Attached Proton Test) spectrum of **16** in  $\text{CDCl}_3$  is depicted in Figure 2.5. In the APT  $^{13}\text{C}$ -NMR spectrum, a positive signal is produced for carbons with zero or an even number of protons attached to it, whereas a negative signal is generated for carbons with an odd number of protons attached to it. The APT  $^{13}\text{C}$ -NMR spectrum of **16** showed a set of well-resolved signals, which could all be assigned. The carbonyl resonance of the urea bond was observed at  $\delta = 157$  ppm. The *tert*-butyl ester groups were present as three sets of signals located around  $\delta = 28.2$  ppm,  $\delta = 79.9$  ppm and in the region of 160–180 ppm. The signals in the range of  $\delta = 120$ –140 ppm were ascribed to the aromatic carbons of the benzyloxycarbonyl protective group.



**Scheme 2.5** Synthetic route towards carboxymethyl-3-ureido-functionalized Gd(III) complex **19**. (a) DCM; (b) 1:1 v/v TFA/DCM; (c)  $\text{GdCl}_3 \cdot 6\text{H}_2\text{O}$ , NaOH,  $\text{H}_2\text{O}$ , pH 7; (d)  $\text{H}_2$ , 10% Pd/C, *tert*-BuOH,  $\text{H}_2\text{O}$ .

Removal of the *tert*-butyl ester groups with TFA in DCM proceeded smoothly with no evidence of side reactions, to provide **17**. Subsequently, DTPA analogue **17** was reacted with  $\text{GdCl}_3$  in water under neutral conditions, to afford Gd(III) complex **18**. The benzyloxycarbonyl protective group of **18** was removed by hydrogenation using 10% Pd/C as a catalyst to give glyciny lurea-functionalized Gd(III)DTPA complex **19**.



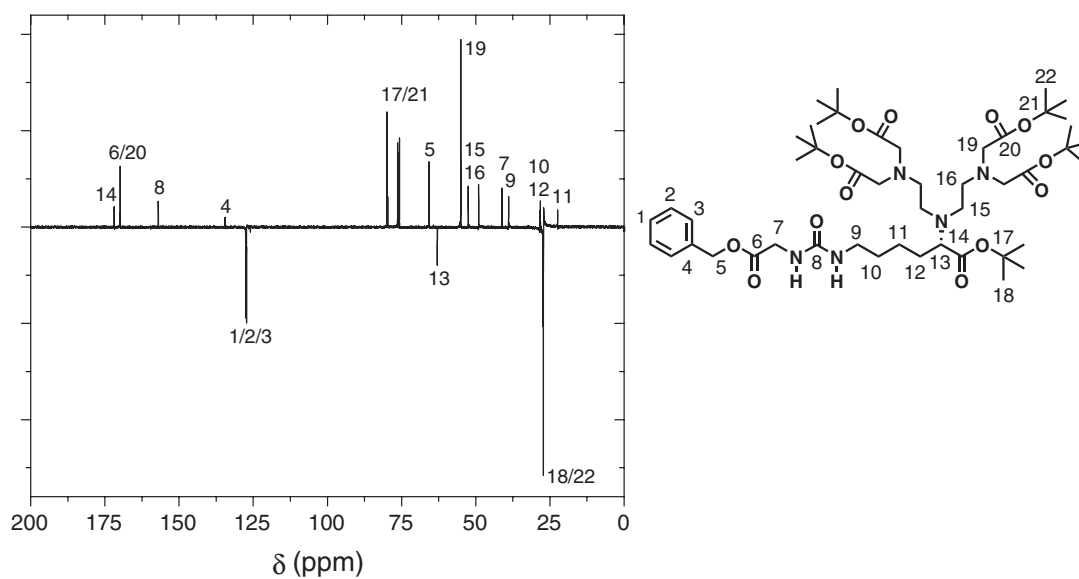


**Figure 2.5** APT  $^{13}\text{C}$ -NMR spectrum of **16** in  $\text{CDCl}_3$ .

Gd(III) complexes **18** and **19** displayed an excellent solubility in water at pH 7 and were characterized in detail with FT-IR spectroscopy, ESI-MS spectrometry and ICP-AES. The cleavage of the benzyloxycarbonyl protective group ( $\Delta m = 89.9$ ) was confirmed by ESI-MS. Moreover, no decomplexation of Gd(III) was observed.

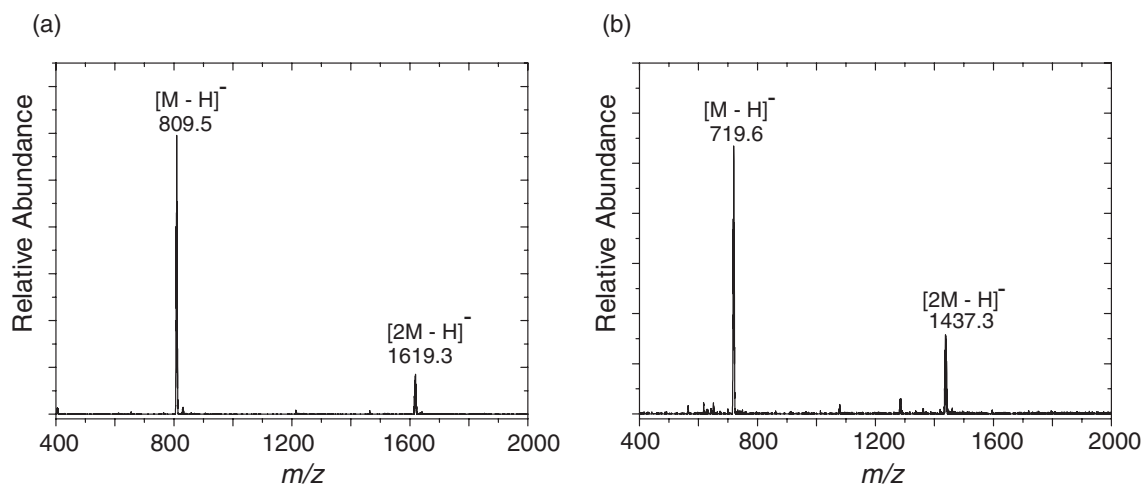
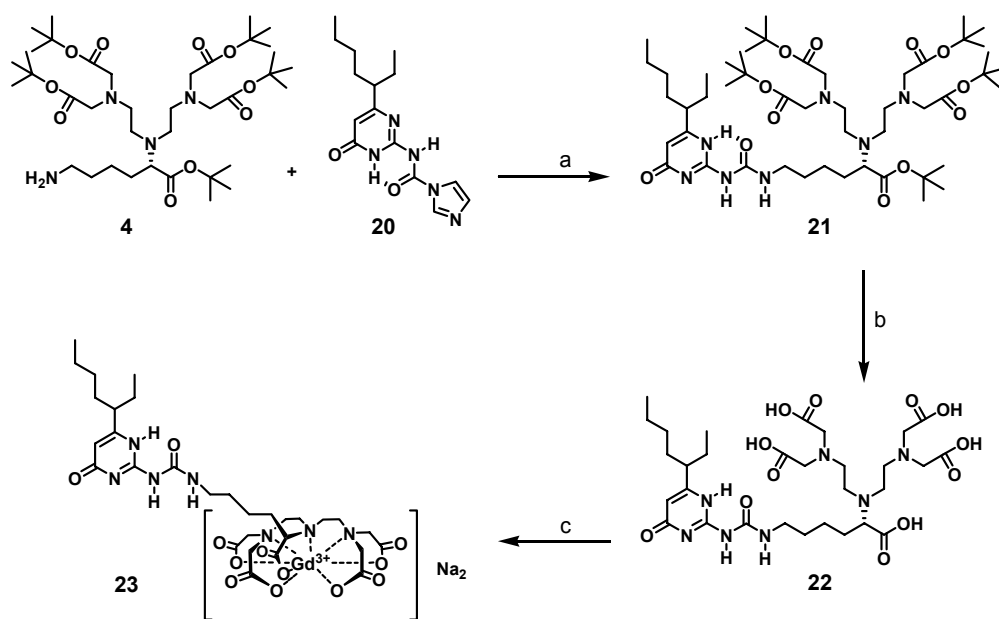


**Figure 2.6** (a) ESI-MS spectrum of Gd(III) complex **18** (before hydrogenation); (b) ESI-MS spectrum of Gd(III) complex **19** (after hydrogenation).

Gd(III) complex **19** possesses a unique binding motif, *i.e.* the glycylurea moiety, which binds specifically to a dendritic host with a complementary binding site. Preliminary results will be presented in Chapter 5 (Section 5.4.1).

### 2.2.5 Introduction of ureidopyrimidinone units to Gd(III)DTPA complexes: strategy C

Another orthogonal chemical moiety that can be incorporated into the Gd(III)DTPA complex is the ureidopyrimidinone moiety. This unit has been applied successfully for the construction of supramolecular polymers using quadruple hydrogen bonding.<sup>27-30</sup> Ureidopyrimidinone-functionalized DTPA analogue (**21**) was synthesized by reacting the amine-functionalized DTPA analogue **4** with 1.3 equivalents of imidazolide **20** in DCM (Scheme 2.6). Compound **21** was characterized by <sup>1</sup>H- and <sup>13</sup>C-NMR, IR spectroscopy and ESI-QTOF mass spectrometry. Cleavage of the *tert*-butyl esters was accomplished by treatment with TFA in DCM as evidenced with IR and NMR analysis, to obtain **22**. Complexation experiments with **22** and GdCl<sub>3</sub> in water, while maintaining the pH at 7 through the addition of NaOH (aq) solution, resulted in undesired precipitation of material that was not further studied, since the complexation of **22** with GdCl<sub>3</sub> in 0.3 M citrate buffer was more successful. Exhaustive dialysis of the solution of **23** with a 0.1 kDa MWCO membrane in deionized water, followed by freeze drying yielded the desired Gd(III) complex as a white fluffy powder. The Gd(III) complex was characterized with IR spectroscopy and ESI-MS.



**Scheme 2.6** Synthesis of ureido-pyrimidinone-functionalized Gd(III) complex **23**. (a) DCM; (b) 1:4 v/v TFA/DCM; (c) GdCl<sub>3</sub>·6 H<sub>2</sub>O, 0.3 M citrate buffer, pH 5.8.

The ureidopyrimidinone entity is commonly used for the construction of supramolecular polymers.<sup>31</sup> Through the use of Gd(III) complex **23** MRI labels can be implemented in supramolecular polymers. Future research will focus on the probing of the formation and degradation of these supramolecular polymers in aqueous medium using MRI.

## 2.3 RELAXIVITIES OF FUNCTIONALIZED Gd(III)DTPA COMPLEXES

MRI contrast arises from the difference in relaxation times exhibited by the water protons in different kinds of tissue. Higher contrast between tissues can be accomplished through the use of Gd(III)DTPA-based MRI contrast agents. The efficiency of these MRI contrast agents to lower the relaxation times is often expressed in terms of relaxivities. As the relaxivity of Gd(III)-based MRI contrast agents depends on many factors (*vide infra*), there is no *a priori* knowledge of how a slight change in the structure of the contrast agent alters its function. However, the longitudinal and transverse relaxivities are intrinsic properties of MRI contrast agents. In this section, a brief introduction into the physical principles of Nuclear Magnetic Resonance is given, followed by the principles underlying the use of MRI contrast agents. In Section 2.3.2, the measurement of the longitudinal and transverse relaxivities is illustrated for the series of Gd(III)DTPA complexes **11**, **19**, and **23**.

### 2.3.1 Nuclear magnetic resonance: an introduction

#### *Nuclear spin relaxation processes*

The nuclear spins of an ensemble of water molecules will spontaneously align when they are exposed to an external magnetic field ( $B_0$ ). Moreover, this alignment is either parallel or anti-parallel to the direction of  $B_0$ . At thermal equilibrium, the nuclear spins will be distributed *via* a Boltzmann distribution into low (parallel) and high (anti-parallel) energy states. Although this process has to be treated in a quantum mechanical fashion, it can be illustrated in a qualitative way as shown in Figure 2.7.<sup>32</sup>

A small surplus of parallel, low-energy spins results in a net magnetization vector ( $M_0$ ) in the direction of the external field (Figure 2.7a).<sup>32</sup> Application of a 90° radio frequency-pulse (RF-pulse) at the Larmor frequency of protons leads to a rotation of the magnetization into the  $x,y$ -plane ( $M_{x,y}$ ), which is perpendicular to the direction of  $B_0$  (Figure 2.7b). This involves both a redistribution of nuclear spins over the high and low energy levels and the phase coherence of spins. After excitation, the magnetization will relax back to its original orientation.

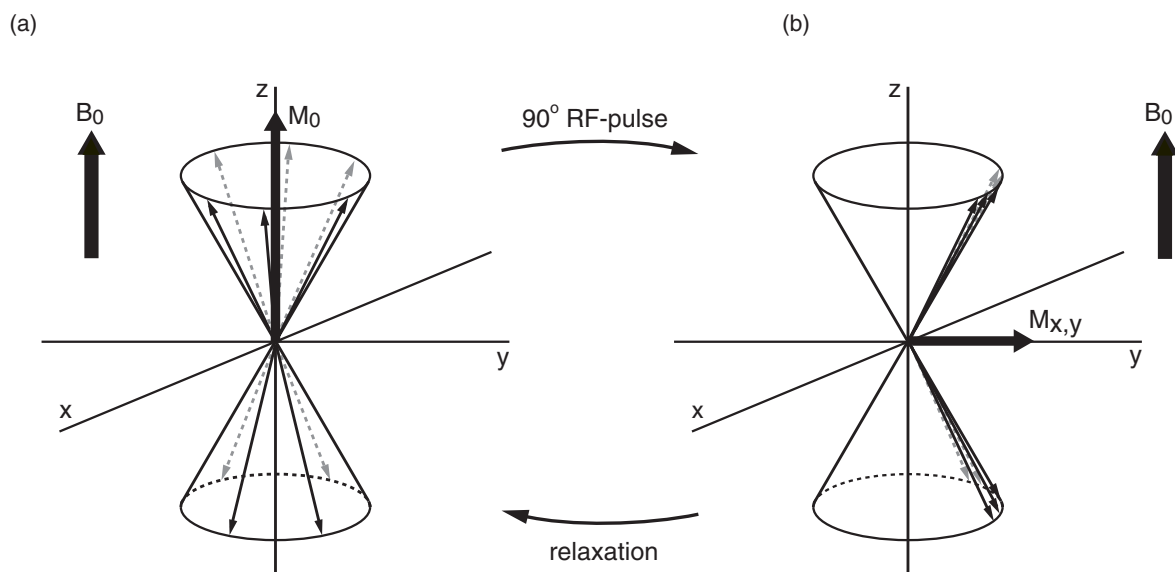


**Figure 2.7** Qualitative picture of spins during excitation and relaxation. (a) Nuclear spin system in thermal equilibrium, showing the net magnetization vector ( $M_0$ ) along the direction of the static external magnetic field ( $B_0$ ). Since the individual spins have no phase coherence, there is no net magnetization in the  $x,y$ -plane. (b) Spin system after excitation with a  $90^\circ$  RF-pulse, illustrating the phase coherence of spins resulting in the magnetization vector in the  $x,y$ -plane ( $M_{x,y}$ ). Additionally, no magnetization remains along the  $z$ -axis, due to a redistribution of nuclear spins over the high and low energy levels.

There are two basic modes of relaxation available: spin-lattice relaxation and spin-spin relaxation. Spin-lattice relaxation is related to the  $z$ -component of the magnetization vector and is an enthalpic process. The  $z$ -component of the magnetization returns to its original orientation while the absorbed energy is transferred from the nuclei to the rotational and translational modes of the surrounding molecules (lattice). The spin-lattice relaxation is characterized by a time constant  $T_1$ , also known as the longitudinal relaxation time (Figure 2.8a).

In contrast to  $T_1$  relaxation, the transverse relaxation is an entropic process and describes the magnetization decay in the  $x,y$ -plane. The nuclear spins will lose their phase coherence, *i.e.* show dephasing, due to spin-spin interactions (Figure 2.7). As a result the transverse magnetization decays to zero. The spin-spin relaxation is characterized by a time constant  $T_2$ , also known as the transverse relaxation time (Figure 2.8b). Both  $T_1$  and  $T_2$  are strongly affected by the temperature and the magnetic field.

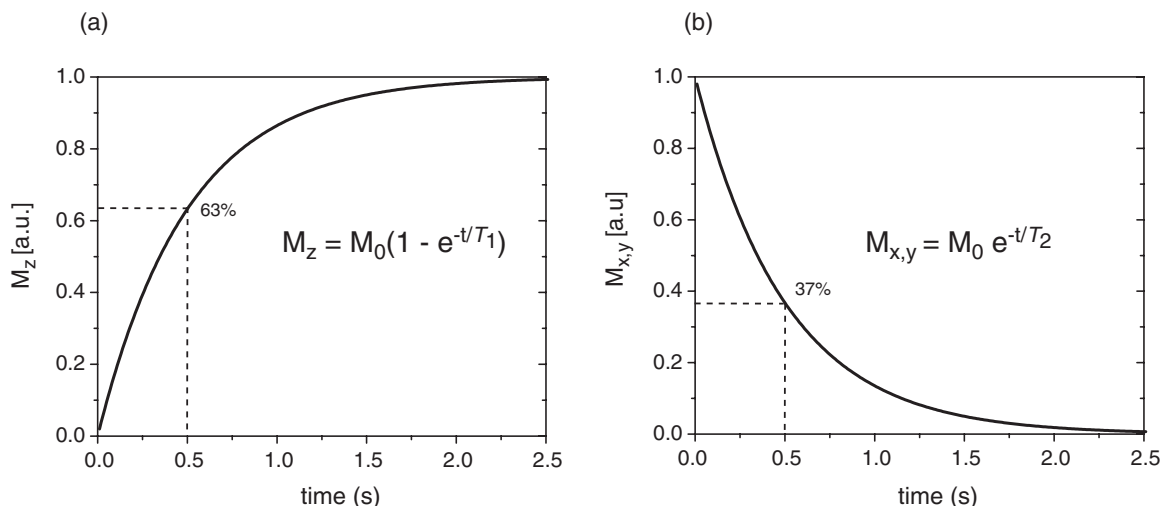


**Figure 2.8** Return of the longitudinal (a) and transverse (b) relaxation to its equilibrium value.

### ***Relaxation in the presence of paramagnetic MRI contrast agents***

Paramagnetic ions, such as Gd(III), decrease both the  $T_1$  and  $T_2$  of the water protons dramatically. The effect originates from dipole-dipole interactions between the nuclear spins of water molecules and the fluctuating local magnetic field caused by the spins of the unpaired electrons in the metal ion.<sup>33,34</sup> The high magnetic moment (seven unpaired electrons) of Gd(III), coupled with its slow electronic relaxation makes it a very efficient relaxation agent; therefore, trace amounts of Gd(III) are sufficient to decrease the relaxation times of bulk water significantly.

The ability of MRI contrast agents to lower the  $T_1$  and  $T_2$  is often expressed in terms of longitudinal ( $r_1$ ) and transverse ( $r_2$ ) relaxivities. In equation 3.1,  $(1/T_{1,2})_{\text{observed}}$  is the observed relaxation rate in the presence of contrast agent,  $[\text{Gd(III)}]$  is the concentration of Gd(III), and  $(1/T_{1,2})_{\text{diamagnetic}}$  is the diamagnetic relaxation rate (in the absence of paramagnetic species).

$$(1/T_{1,2})_{\text{observed}} = (1/T_{1,2})_{\text{diamagnetic}} + r_{1,2}[\text{Gd(III)}] \quad (3.1)$$

### ***Inner sphere and outer sphere relaxation***

In this section, the most relevant parameters that contribute to the relaxivity will be addressed for Gd(III)DTPA. Coordination of Gd(III) to DTPA occurs in an octadentate fashion, leaving one site available for coordination of water to the paramagnetic centre, *i.e.* inner sphere water molecule, as illustrated in Figure 2.9. This inner-sphere water molecule exchanges rapidly with the bulk water. The contribution of the inner-sphere relaxation mechanism to the relaxivity of Gd(III)DTPA is approximately 60%.<sup>5,35</sup> The remaining 40% arises from outer sphere relaxation referring to

relaxation enhancement of water molecules in the second coordination sphere (hydrogen-bonded water molecules to the carboxylate moieties of DTPA) and from bulk water molecules diffusing in the proximity of the Gd(III) complex.<sup>35,36</sup> The inner sphere effect can be modulated relatively easy, whereas outer sphere effects are difficult to address.<sup>5</sup>

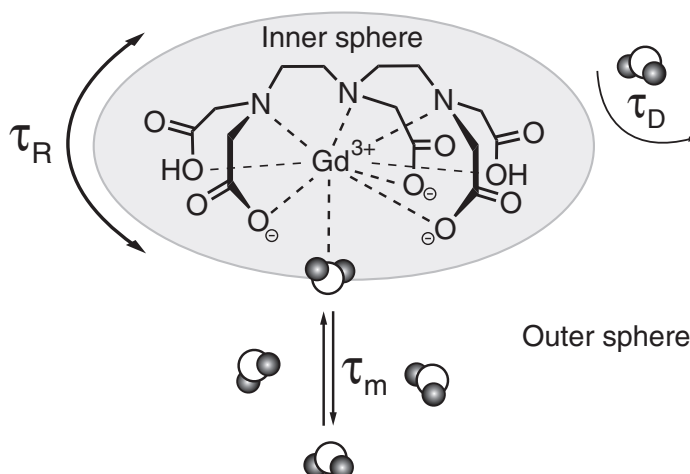


**Figure 2.9** Schematic representation of the most relevant parameters that influence the relaxation of Gd(III)DTPA-based complexes in aqueous solution; the rotational correlation time ( $\tau_R$ ), the mean residence time of the water molecules at the inner sphere ( $\tau_m$ ) and the diffusion correlation time ( $\tau_D$ ).<sup>5,35,37</sup>

The inner sphere contribution to the relaxivity can be described by the Solomon–Bloembergen–Morgan equation.<sup>1,36-42</sup> The relaxivities of Gd(III)-based MRI contrast agents are strongly affected by the chemical structure of the Gd(III) complex. Two relevant parameters are the rotational correlation time ( $\tau_R$ ), which describes the molecular tumbling rate of the Gd(III) complex, and the mean residence time of water coordinated to the metal center ( $\tau_m$  is defined as the reciprocal of the water exchange rate) as shown in Figure 2.9. Other parameters that can also influence the relaxivity are the viscosity and the ionic strength of the solute, the temperature, and the magnetic field. In this thesis, the relaxivities of Gd(III)-based complexes will be compared within a series of related Gd(III)DTPA complexes or otherwise with Gd(III)DTPA and will be discussed in terms of molecular structure.

### 2.3.2 Relaxivity measurements

Longitudinal ( $r_1$ ) and transverse relaxivities ( $r_2$ ) were determined for Gd(III)DTPA complexes **11**, **19**, and **23** as well as for Gd(III)DTPA by concentration-dependent measurements of the relaxation times in water at pH 6.5–7 at 1.5 T (Figure 2.10). The  $T_1$  and  $T_2$  values were determined from a set of images acquired with a single slice 2D mixed MRI protocol, consisting of dual-echo spin echo sequence interleaved with a dual-echo inversion recovery sequence.<sup>43</sup> This sequence is suitable for the accurate measurement of relaxation times in the range of 100–2000 ms.

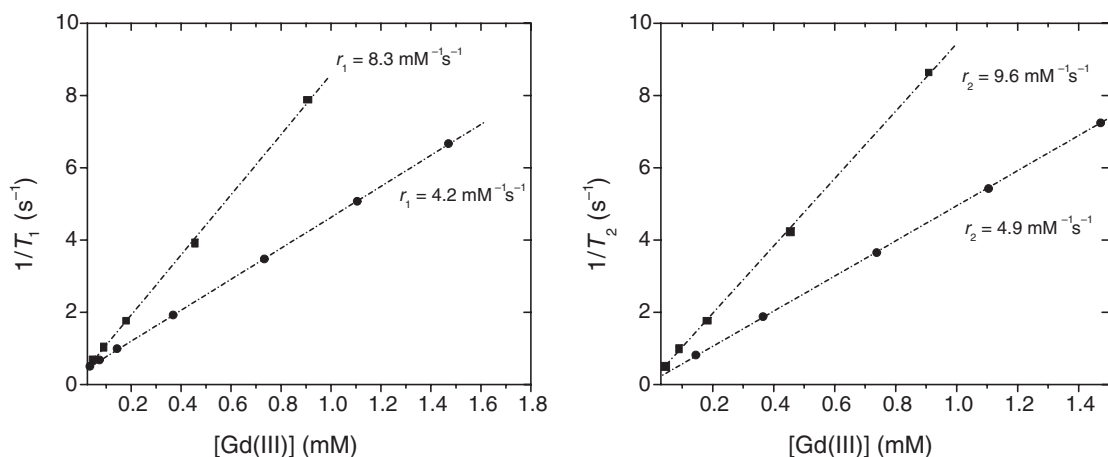


**Figure 2.10** The longitudinal and transverse relaxation rate ( $1/T_1$  and  $1/T_2$ ) versus the concentration of Gd(III) at 1.5 T and 20°C. Reference Gd(III) complex **11** (squares) and Gd(III)DTPA (circles).

The data gave good linear fits ( $R^2 > 0.999$ ) to the equation  $(1/T_{1,2})_{\text{observed}} = (1/T_{1,2})_{\text{diamagnetic}} + r_{1,2}[\text{Gd(III)}]$ . The standard deviation in the relaxivities from the fitting procedure did not exceed 2%. The Gd(III) concentrations used for the relaxivity measurements were determined by ICP-AES. Detection limits for Gd(III) are typically at the 80  $\mu\text{g/L}$  level and analytical errors are commonly in the range of 0.5–2%. The values for the observed Gd(III) content for all Gd(III) complexes were very close to the theoretical values, typically between 90% and 100%, except for Gd(III) complex **23** for which a Gd(III) content of only 68% of the theoretical value was found. This may be attributed to the presence of residual salts originating from the citrate buffer. The normalized longitudinal and transverse relaxivities of the series of Gd(III) complexes and Gd(III)DTPA are shown in Figure 2.11. For a fair comparison of the relaxivities of Gd(III)DTPA, **11**, **19**, and **23**, identical conditions are used during data acquisition.

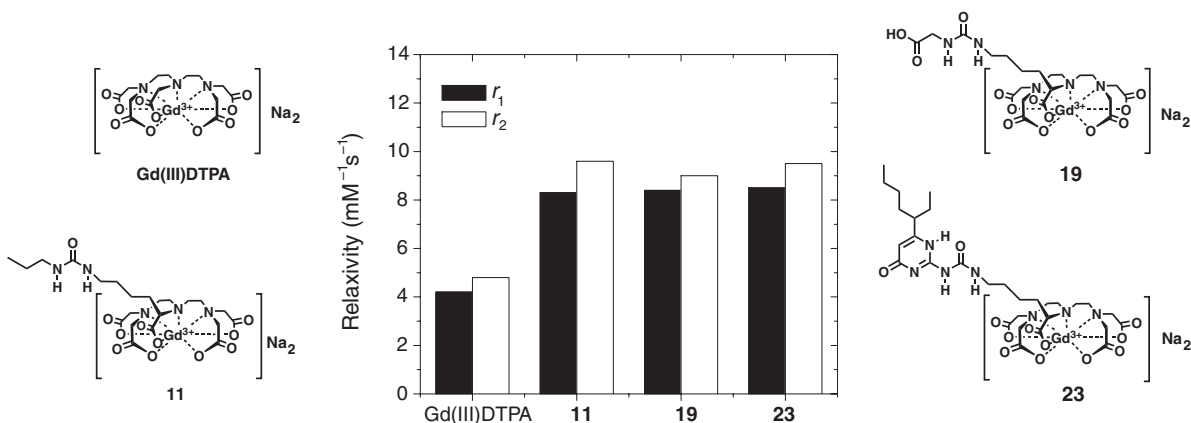


**Figure 2.11** Longitudinal and transverse relaxivities of a series of Gd(III)DTPA-based complexes in aqueous solution at 1.5 T and 20°C.

The  $r_1$  and  $r_2$  values of Gd(III)DTPA of  $4.2 \text{ mM}^{-1}\text{s}^{-1}$  and  $4.9 \text{ mM}^{-1}\text{s}^{-1}$ , respectively, are in full agreement with the previously reported values in the literature.<sup>44</sup> Gd(III) complexes **11**, **19** and **23** display  $r_1$  and  $r_2$  values in the range of  $8\text{--}8.5 \text{ mM}^{-1}\text{s}^{-1}$  and  $9\text{--}9.6 \text{ mM}^{-1}\text{s}^{-1}$ , respectively. These relaxivities are significantly higher than the  $r_1$  and  $r_2$  values of the parent Gd(III)DTPA complex. This is presumably due to the slower molecular tumbling of the Gd(III) complex as a result of the higher molecular weight ( $0.75$ ,  $0.76$ , and  $0.90 \text{ kg}\cdot\text{mol}^{-1}$  for **11**, **19**, and **23**, respectively, *versus*  $0.59 \text{ kg}\cdot\text{mol}^{-1}$  for Gd(III)DTPA). Moreover, these Gd(III)DTPA-based MRI contrast agents exhibit  $r_2/r_1$  ratios ranging between  $1.1\text{--}1.2$ . The observed  $r_2/r_1$  ratios are in excellent agreement with  $r_2/r_1$  ratios on low molecular weight Gd(III)DTPA-based complexes as reported by Reichenbach *et al.*<sup>44</sup>

## 2.4 CONCLUSIONS

A modular approach for the synthesis of functional Gd(III)DTPA complexes has been developed, which employs an amine-functionalized DTPA synthon. Through the use of orthogonal chemistries, novel synthetic methodologies have been developed in order to arrive at a series of low molecular weight Gd(III)DTPA-based complexes. The longitudinal ( $r_1$ ) and transverse ( $r_2$ ) relaxivities of these MRI contrast agents are in the range of  $8\text{--}8.5 \text{ mM}^{-1}\text{s}^{-1}$  and  $9\text{--}9.6 \text{ mM}^{-1}\text{s}^{-1}$ , respectively. These values are significantly higher in comparison with parent Gd(III)DTPA. The implementation of MRI contrast agents **19** and **23** in supramolecular constructs is anticipated to give an increase in the relaxivity. This can be utilized as a tool to study the formation of supramolecular assemblies.



## 2.5 EXPERIMENTAL

### General

Unless stated otherwise, all reagents and chemicals were obtained from commercial sources and used without further purification. Water was demineralized prior to use. Dichloromethane was obtained by distillation from P<sub>2</sub>O<sub>5</sub>. <sup>1</sup>H-NMR, <sup>13</sup>C-NMR and <sup>19</sup>F-NMR spectra were recorded on a Varian Gemini-2000 300 MHz spectrometer, a Varian Mercury Vx 400 MHz spectrometer and a Varian Unity Inova 500 MHz spectrometer at 298 K. Chemical shifts are given in ppm ( $\delta$ ) values. Infrared spectra were recorded at 298 K on a Perkin-Elmer 1605 FT-IR spectrometer. MALDI-TOF spectra were obtained at a Perspective Biosystems Voyager DE-Pro MALDI-TOF spectrometer using  $\alpha$ -cyano-4-hydroxycinnamic acid as matrix (University of California, Berkeley, USA). ESI-QTOF-MS experiments were recorded on a Q-TOF Ultima GLOBAL mass spectrometer (Micromass, Manchester, UK). ESI-MS experiments were obtained at a Finnigan LCQ Deca XP Max mass spectrometer (Thermo Electron Corporation, San Jose, USA).  $T_1$ -measurements were performed using a clinical head coil and a 1.5 T MRI system (Philips Intera, Release 9, Philips Medical Systems, Best, the Netherlands). Five glass tubes containing different concentrations of MRI contrast agent ([Gd(III)] = 0.05–2.0 mM) were prepared (volume, 2 mL). To determine  $T_1$ -relaxation times, a 2D-mixed (single slice TSE, TR<sub>SE</sub> 1000 ms, TR<sub>IR</sub> 2260 ms, IR delay 500 ms, TE<sub>1</sub> 15 ms, TE<sub>2</sub> 100 ms) dual-echo sequence was performed, matrix dimensions 256 × 256 and voxel size 10 × 10 × 8 mm<sup>3</sup>. All relaxation measurements were performed for circular regions of interest of (area, 150 ± 10 mm<sup>2</sup>) positioned centrally each sample. The longitudinal relaxivity was calculated from the slope of 1/ $T_1$  versus the Gd(III) concentration. Gd(III) concentrations of the aqueous solutions used for the  $T_1$ -relaxivity measurements were determined by means of inductively coupled plasma atomic emission spectroscopy (ICP-AES) at 342.247 nm (Leeman Labs Echelle Unicam701 emission spectrometer, TNO, Eindhoven, the Netherlands).

### *tert*-Butyl 6-amino-2-*{bis-[2-[bis-(*tert*-butoxycarbonylmethyl)amino]-ethyl]-amino}* hexanoate (**4**)

To a solution of **7** (4.65 g, 5.33 mmol) in methanol (40 mL) was added acetic acid (9 mL) and water (1 mL). The solution was purged with argon for 15 min. Subsequently, palladium, 10 wt% on activated carbon (0.33 g) was added and the heterogeneous mixture was shaken in a parr reactor for 5 h under an atmosphere of hydrogen (70 psi). The catalyst was removed by filtration and the filtrate was concentrated under reduced pressure at 30 °C. The obtained colorless oil was dissolved in diethyl ether (300 mL) and washed with 2 N NaOH (2 × 100 mL). The combined water phase was extracted with diethyl ether (100 mL). The combined organic layers were washed with brine (2 × 100 mL) and dried over anhydrous Na<sub>2</sub>SO<sub>4</sub>. The solvent was removed under reduced pressure, giving the title compound **4** (3.50 g, 4.70 mmol, 88%) as a colorless oil. The purity of **4** was confirmed by thin layer chromatography ( $R_f$  = 0.5, Et<sub>3</sub>N/MeOH/CH<sub>2</sub>Cl<sub>2</sub> 5:5:90 v/v/v). <sup>1</sup>H-NMR (CDCl<sub>3</sub>):  $\delta$  = 3.43 (s, 8H, NCH<sub>2</sub>COOC(CH<sub>3</sub>)<sub>3</sub>), 3.23 (m, 1H, H<sub>2</sub>N(CH<sub>2</sub>)<sub>4</sub>CHN), 2.83–2.60 (m, 10H, NCH<sub>2</sub>CH<sub>2</sub>N {4H} + NCH<sub>2</sub>CH<sub>2</sub>N {4H} + H<sub>2</sub>NCH<sub>2</sub>(CH<sub>2</sub>)<sub>3</sub> {2H}), 1.74–1.23 (m, 6H, CONHCH<sub>2</sub>CH<sub>2</sub>(CH<sub>2</sub>)<sub>2</sub>CHN; s, 45H, COOC(CH<sub>3</sub>)<sub>3</sub>). The assignment of the <sup>1</sup>H-NMR spectrum was confirmed by <sup>1</sup>H,<sup>1</sup>H-COSY. APT <sup>13</sup>C-NMR (CDCl<sub>3</sub>):  $\delta$  = 173.0 (1C, C=O), 170.8 (4C, C=O), 80.9 (4C, C(CH<sub>3</sub>)<sub>3</sub>), 80.8 (1C, C(CH<sub>3</sub>)<sub>3</sub>), 64.7 (1C, H<sub>2</sub>N(CH<sub>2</sub>)<sub>4</sub>CHN), 56.2 (4C, NCH<sub>2</sub>COOC(CH<sub>3</sub>)<sub>3</sub>), 54.1 (2C, NCH<sub>2</sub>CH<sub>2</sub>N), 50.7 (2C, NCH<sub>2</sub>CH<sub>2</sub>N), 42.3 (1C, H<sub>2</sub>NCH<sub>2</sub>(CH<sub>2</sub>)<sub>3</sub>CHN), 33.7 (1C, NH<sub>2</sub>CH<sub>2</sub>CH<sub>2</sub>(CH<sub>2</sub>)<sub>2</sub>), 30.1 (1C, H<sub>2</sub>N(CH<sub>2</sub>)<sub>3</sub>CH<sub>2</sub>CHN), 28.4–28.2 (15C, C(CH<sub>3</sub>)<sub>3</sub>), 23.9 (H<sub>2</sub>N(CH<sub>2</sub>)<sub>2</sub>CH<sub>2</sub>CH<sub>2</sub>). The assignment of the APT <sup>13</sup>C-NMR was confirmed by HETCOR NMR spectroscopy. FT-IR (ATR):  $\nu$  (cm<sup>-1</sup>) 3418 (-NH<sub>2</sub> stretch), 2977, 2933, 1724 (C=O stretch), 1457, 1367, 1249, 1220, and 1146 (C–O stretch). Elemental analysis: Calcd. for C<sub>38</sub>H<sub>72</sub>N<sub>4</sub>O<sub>10</sub>: 61.26% C, 9.74% H, 7.52% N; Obsd. 61.29% C, 9.53% H, 7.30% N. MALDI-TOF:  $m/z$  [M + H]<sup>+</sup> Calcd. 746.01 Da, Obsd. 745.79 Da; [M + Na]<sup>+</sup> Calcd. 767.51 Da, Obsd. 767.77 Da.

***N,N*-Bis[(*tert*-butoxycarbonyl)methyl]-2-hydroxyethylamine (5)**

To a solution of *tert*-butylbromoacetate (66.0 g, 0.338 mol) in dry DMF (150 mL) was added  $\text{KHCO}_3$  (36 g, 0.36 mol). The heterogeneous reaction mixture was cooled with an ice bath to 0 °C. A solution of ethanolamine (9.85 g, 0.161 mol) in DMF (50 mL) was added under vigorous stirring under an atmosphere of argon. After 3 h the ice bath was removed and the reaction mixture was allowed to attain room temperature overnight. The heterogeneous reaction mixture was poured into a saturated  $\text{NaHCO}_3$  (aq) (200 mL) and was extracted with diethyl ether (300 mL). The organic phase was washed with saturated  $\text{NaHCO}_3$  (aq) solution (100 mL). The combined water phase was extracted with diethyl ether (2 × 150 mL). The combined organic phase was washed with saturated KCl (aq) solution (2 × 200 mL), dried with anhydrous  $\text{Na}_2\text{SO}_4$ , filtered, and concentrated under reduced pressure. Pentane (200 mL) was added to the crude product and the suspension was stirred for 2 h and stored overnight in the freezer to facilitate the crystallization of the product as a white solid. The product was collected by filtration and washed with cold pentane (−20 °C). Analytically pure alcohol **5** (34.95 g, 0.121 mol) was obtained as a white solid in 75% yield.  $^1\text{H-NMR}$  ( $\text{CDCl}_3$ ):  $\delta$  = 3.81 (br s, 1H,  $\text{HOCH}_2\text{CH}_2\text{N}$ ), 3.69 (t, 2H,  $J$  = 4.9 Hz,  $\text{HOCH}_2\text{CH}_2\text{N}$ ), 3.51 (s, 4H,  $\text{NCH}_2\text{COOC}(\text{CH}_3)_3$ ), 2.94 (t, 2H,  $J$  = 4.9 Hz,  $\text{HOCH}_2\text{CH}_2\text{N}$ ), and 1.52 (s, 18H,  $\text{COOC}(\text{CH}_3)_3$ ).  $^{13}\text{C-NMR}$  ( $\text{CDCl}_3$ ):  $\delta$  = 171.4 (2C,  $\text{C}=\text{O}$ ), 81.4 (2C,  $\text{C}(\text{CH}_3)_3$ ), 59.3 (1C,  $\text{HOCH}_2\text{CH}_2\text{N}$ ), 57.0 (1C,  $\text{HOCH}_2\text{CH}_2\text{N}$ ), 56.6 (2C,  $\text{NCH}_2\text{COOC}(\text{CH}_3)_3$ ), 28.0 (6C,  $\text{C}(\text{CH}_3)_3$ ). FT-IR (ATR):  $\nu$  ( $\text{cm}^{-1}$ ) 3488 (−OH stretch), 2977, 1726 (C=O stretch), 1457, 1416, 1366, 1225, 1154, 1140 (C−O stretch), 1061  $\text{cm}^{-1}$ . Melting point 57–58 °C. Elemental analysis: Calcd. for  $\text{C}_{14}\text{H}_{27}\text{NO}_5$ : 58.11% C, 9.40% H, 4.84% N; Obsd. 58.16% C, 9.70% H, 4.78% N.

***N,N*-Bis[(*tert*-butoxycarbonyl)methyl]-2-bromoethylamine (6)**

Alcohol **5** (15.42 g, 53.3 mmol) was dissolved in freshly distilled DCM (70 mL) and tetrabromomethane (17.65 g, 53.2 mmol) was added under an atmosphere of argon. The solution was cooled with an ice bath to 0 °C. The solution was vigorously stirred and triphenylphosphine (15.39 g, 53.2 mmol) was slowly added under an atmosphere of argon. The reaction was continued overnight at room temperature and concentrated *in vacuo*. Triphenylphosphine oxide was removed by precipitation in hexane. The filtrate was concentrated under reduced pressure. The crude product was purified by column chromatography (silica,  $\text{Et}_2\text{O}$ /hexane 1:5 v/v) yielding **6** (13.61 g, 38.6 mmol, 72%) as a viscous oil. Upon standing at room temperature for extended periods of time, bromide **6** was found to convert slowly to a mixture of products including the corresponding aziridinium salt.<sup>7</sup> Therefore, compound **6** needs to be stored in the fridge prior to use.  $^1\text{H-NMR}$  ( $\text{CDCl}_3$ ):  $\delta$  = 3.45 (s, 4H,  $\text{NCH}_2\text{COOC}(\text{CH}_3)_3$ ), 3.41 (t, 2H,  $J$  = 7.4 Hz,  $\text{BrCH}_2$ ), 3.11 (t, 2H,  $J$  = 7.4 Hz,  $\text{BrCH}_2\text{CH}_2\text{N}$ ) and 1.44 (s, 18H,  $\text{COOC}(\text{CH}_3)_3$ ).  $^{13}\text{C-NMR}$  ( $\text{CDCl}_3$ ):  $\delta$  = 170.7 (1C,  $\text{C}=\text{O}$ ), 80.7 (2C,  $\text{C}(\text{CH}_3)_3$ ), 56.8 (1C,  $\text{BrCH}_2\text{CH}_2$ ), 56.7 (2C,  $\text{NCH}_2\text{COOC}(\text{CH}_3)_3$ ), 30.4 (1C,  $\text{BrCH}_2\text{CH}_2\text{N}$ ), 28.4 (6C,  $\text{C}(\text{CH}_3)_3$ ). FT-IR (ATR):  $\nu$  ( $\text{cm}^{-1}$ ) 2977, 2933, 1730 (C=O stretch), 1367, 1220, 1147 (C−O stretch), 1122. MALDI-TOF:  $m/z$  [ $\text{C}_{14}\text{H}_{26}\text{BrNO}_4 + \text{Na}$ ]<sup>+</sup> Calcd. 374.09 Da, Obsd. 374.1 Da.

***tert*-Butyl 6-benzyloxycarbonylamino-2-[[bis-{2-[bis-(*tert*-butoxycarbonylmethyl)amino]-ethyl}-amino]] hexanoate (7)**

H-Lys(Z)OtBu.HCl (4.96 g, 13.3 mmol) was dissolved in 1 N NaOH (100 mL) and extracted with diethyl ether (2 × 100 mL). The combined organic phase was dried over anhydrous  $\text{Na}_2\text{SO}_4$  and evaporated to provide H-Lys(Z)OtBu (4.45 g, 13.23 mmol, 99.5%) as a colorless oil. To a solution of H-Lys(Z)OtBu (4.43 g, 13.16 mmol) in dry DMF (10 mL) was added  $\text{KHCO}_3$  (3.43 g, 34.3 mmol) under an atmosphere of argon. A solution of bromide **6** (9.60 g, 27.3 mmol, 2.1 equivalents) in DMF (50 mL) was added dropwise under vigorous stirring under an atmosphere of argon. The mixture was stirred for 52 h at 55 °C. After cooling, the mixture was poured into 2.5 N NaOH (50 mL) and extracted with diethyl ether (2 × 100 mL). The combined organic

layer was washed with saturated KCl (aq) solution (3 × 200 mL), dried with anhydrous NaSO<sub>4</sub>, filtered, and concentrated *in vacuo* at 40 °C. The crude product was purified by column chromatography (silica, EtOAc/hexane 1:4 *v/v*, followed by EtOAc/hexane 1:2 *v/v*). The pure title compound (5.59 g, 6.36 mmol, 48.1%) was obtained as a viscous oil. <sup>1</sup>H-NMR (CDCl<sub>3</sub>): δ = 7.36–7.27 (m, 5H, ArH), 5.12 (br, 1H, CONH(CH<sub>2</sub>)<sub>4</sub>N), 5.09 (s, 2H, CH<sub>2</sub>Ph), 3.42 (s, 8H, NCH<sub>2</sub>COOC(CH<sub>3</sub>)<sub>3</sub>), 3.26 (m, 1H, CONH(CH<sub>2</sub>)<sub>4</sub>CHN), 3.18 (m, 2H, CONHCH<sub>2</sub>(CH<sub>2</sub>)<sub>3</sub>CHN), 2.83–2.60 (m, 8H, NCH<sub>2</sub>CH<sub>2</sub>N {4H} + NCH<sub>2</sub>CH<sub>2</sub>N {4H}), 1.74–1.23 (m, 6H, CONHCH<sub>2</sub>(CH<sub>2</sub>)<sub>3</sub>CHN ; s, 45H, COOC(CH<sub>3</sub>)<sub>3</sub>). The assignment of the <sup>1</sup>H-NMR spectrum is confirmed by <sup>1</sup>H,<sup>1</sup>H-COSY. <sup>13</sup>C-NMR (CDCl<sub>3</sub>): δ = 172.8 (1C, C=O), 170.7 (4C, C=O), 156.5 (1C, C=O), 136.9 (1C, aromatic carbon), 128.5–128.0 (5C, aromatic carbons), 80.8 (4C, C(CH<sub>3</sub>)<sub>3</sub>), 80.7 (1C, C(CH<sub>3</sub>)<sub>3</sub>), 66.5 (CH<sub>2</sub>Ph), 64.0 (1C, OCONH(CH<sub>2</sub>)<sub>3</sub>CHN), 56.0 (4C, NCH<sub>2</sub>COOC(CH<sub>3</sub>)<sub>3</sub>), 53.7 (2C, NCH<sub>2</sub>CH<sub>2</sub>N), 50.3 (2C, NCH<sub>2</sub>CH<sub>2</sub>N), 40.9 (1C, OCONHCH<sub>2</sub>(CH<sub>2</sub>)<sub>3</sub>), 29.5 (1C, OCONHCH<sub>2</sub>CH<sub>2</sub>(CH<sub>2</sub>)<sub>2</sub>), 28.4 (1C, OCONH(CH<sub>2</sub>)<sub>3</sub>CH<sub>2</sub>CHN), 28.3–28.2 (16C, C(CH<sub>3</sub>)<sub>3</sub> + CONH(CH<sub>2</sub>)<sub>3</sub>CHCHN), 23.4 (OCONH(CH<sub>2</sub>)<sub>2</sub>CH<sub>2</sub>CH<sub>2</sub>). FT-IR (ATR): ν (cm<sup>-1</sup>) 3385 (–NH stretch), 2977, 2934, 1721 (C=O stretch), 1525 (aromatic C=C stretch), 1456, 1367, 1247, 1219, 1144 (C–O stretch). Elemental analysis: Calcd. for C<sub>46</sub>H<sub>77</sub>N<sub>4</sub>O<sub>12</sub>: 62.92% C, 8.84% H, 6.38% N; Obsd. 62.67% C, 8.86% H, 6.21% N. MALDI-TOF *m/z* [M + H]<sup>+</sup> Calcd. 879.56 Da. Obsd. 879.4 Da.

***tert*-Butyl 2-{{Bis-2-[bis-(*tert*-butoxycarbonylmethyl)amino]-ethyl}-amino}}-6-(3-propylaminocarbonyl-amino)-hexanoate (9)**

A solution of **4** (0.32 g, 0.43 mmol) in dry DCM (2 mL) was injected into a stirred solution of di-*tert*-butyl tricarbonate<sup>18</sup> (0.124 g, 0.47 mmol) in freshly distilled DCM (2.5 mL) was injected under an atmosphere of argon. The colorless solution was vigorously stirred for 1 h at room temperature, and IR spectroscopy revealed the presence of the characteristic isocyanate absorption at 2272 cm<sup>-1</sup>. The excess of di-*tert*-butyl tricarbonate was reacted by the addition of two droplets of dry pyridine. Subsequently, a solution of propylamine (77 mg, 1.30 mmol) in DCM (2 mL) was added to a solution of compound **8**, and the solution was stirred for another 10 min. The reaction was monitored with IR spectroscopy and revealed the complete disappearance of the isocyanate signal. The solvent was evaporated to give in 90% yield monofunctional model compound **9** as a colorless oil (0.32 g, 0.39 mmol). <sup>1</sup>H-NMR (CDCl<sub>3</sub>): δ = 4.87 (br t, 1H, NH), 4.80 (br t, 1H, NH), 3.43 (s, 8H, NCH<sub>2</sub>COOC(CH<sub>3</sub>)<sub>3</sub>), 3.26 (m, 1H, CONH(CH<sub>2</sub>)<sub>4</sub>CHN), 3.14–3.06 (m, 4H, CONHCH<sub>2</sub>(CH<sub>2</sub>)<sub>3</sub> {2H} + CH<sub>3</sub>CH<sub>2</sub>CH<sub>2</sub>NHCO {2H}), 2.86–2.62 (m, 8H, NCH<sub>2</sub>CH<sub>2</sub>N {4H} + NCH<sub>2</sub>CH<sub>2</sub>N {4H}), 1.66–1.23 (m, 8H, CONHCH<sub>2</sub>CH<sub>2</sub>(CH<sub>2</sub>)<sub>2</sub>CHN {6H} + CH<sub>3</sub>CH<sub>2</sub>CH<sub>2</sub>NHCO {2H} ; s, 45H, COOC(CH<sub>3</sub>)<sub>3</sub>), 0.84 (t, 3H, CH<sub>3</sub>CH<sub>2</sub>). <sup>13</sup>C-NMR (CDCl<sub>3</sub>) : δ = 173.0 (1C, C=O), 171.0 (4C, C=O), 158.7 (1C, NHCONH), 81.1 (4C, C(CH<sub>3</sub>)<sub>3</sub>), 80.9 (1C, C(CH<sub>3</sub>)<sub>3</sub>), 64.3 (1C, CONH(CH<sub>2</sub>)<sub>4</sub>CHN), 56.2 (4C, NCH<sub>2</sub>COOC(CH<sub>3</sub>)<sub>3</sub>), 53.8 (2C, NCH<sub>2</sub>CH<sub>2</sub>N), 50.4 (2C, NCH<sub>2</sub>CH<sub>2</sub>N), 42.3 (1C, CH<sub>3</sub>CH<sub>2</sub>CH<sub>2</sub>NHCO), 40.2 (1C, CONHCH<sub>2</sub>(CH<sub>2</sub>)<sub>3</sub>), 29.7 (1C, CONHCH<sub>2</sub>CH<sub>2</sub>), 28.5–28.3 (16C, C(CH<sub>3</sub>)<sub>3</sub> {15C} + CONH(CH<sub>2</sub>)<sub>3</sub>CH<sub>2</sub>CHN {1C}), 23.8–23.7 (2C, CH<sub>3</sub>CH<sub>2</sub>CH<sub>2</sub>NHCO {1C} + CONH(CH<sub>2</sub>)<sub>2</sub>CH<sub>2</sub> {1C}), 11.6 (CH<sub>3</sub>CH<sub>2</sub>). The assignment of the peaks was confirmed by <sup>1</sup>H,<sup>1</sup>H-COSY and HETCOR spectroscopy. FT-IR (ATR): ν (cm<sup>-1</sup>) 3364 (NH stretch), 2977, 2933, 1724 (C=O stretch), 1639 (C=O amide I stretch), 1567 (C=O amide II stretch), 1457, 1367, 1249, 1220, 1144 (C–O stretch). MALDI-TOF: *m/z* [C<sub>42</sub>H<sub>79</sub>N<sub>5</sub>O<sub>11</sub> + H]<sup>+</sup> Calcd. 830.58 Da, Obsd. 830.60 Da; [C<sub>42</sub>H<sub>79</sub>N<sub>5</sub>O<sub>11</sub> + Na]<sup>+</sup> Calcd. 852.57 Da, Obsd. 852.58 Da.

***2-{{Bis-2-[bis-(carboxymethyl)amino]-ethyl}-amino}}-6-(3-propylamino-carbonyl-amino)-hexanoic acid (10)***

To a stirred solution of **9** (0.19 g, 0.23 mmol) in DCM (4 mL) was added TFA (2 mL), and the reaction mixture was stirred overnight at room temperature. After evaporation of the solvent a second portion of TFA

(2 mL) and dry DCM (4 mL) were added, and stirring was continued overnight. The solution was concentrated *in vacuo* resulting in a brownish salt. The crude product was dissolved in demineralized water and was extensively dialyzed with a 100 Da MWCO membrane. The solution was lyophilized and a white solid, **10** (58.5 mg, 0.107 mmol) was obtained in 46% yield.  $^{19}\text{F}$ -NMR spectroscopy confirmed the successful removal of TFA by the absence of a signal at  $-75.6$  ppm.  $^1\text{H}$ -NMR ( $\text{D}_2\text{O}$ ):  $\delta = 4.20$  (s, 8H,  $\text{NCH}_2\text{COOH}$ ), 3.65–3.40 (m, 5H,  $\text{CONH}(\text{CH}_2)_4\text{CHN}$  {1H} +  $\text{NCH}_2\text{CH}_2\text{NCH}_2\text{COOH}$  {4H}), 3.21 (t, 4H,  $\text{NCH}_2\text{CH}_2\text{N}$ ), 3.10 (t, 2H,  $\text{CONHCH}_2(\text{CH}_2)_3$ ), 3.03 (t, 2H,  $\text{CH}_2\text{NHCO}$ ), 1.80–1.60 (m, 8H,  $\text{CONH}(\text{CH}_2)_3\text{CH}_2$  {2H} +  $\text{CONHCH}_2(\text{CH}_2)_2$  {4H} +  $\text{CH}_3\text{CH}_2$  {2H}), 0.85 (t, 3H,  $\text{CH}_3\text{CH}_2$ ).  $^{13}\text{C}$ -NMR ( $\text{D}_2\text{O}$ ):  $\delta = 174.9$  (1C, C=O), 169.1 (4C, C=O), 160.6 (1C,  $\text{NHCONH}$ ), 63.4 (1C,  $\text{CONH}(\text{CH}_2)_4\text{CHN}$ ), 55.2 (4C,  $\text{NCH}_2\text{COOH}$ ), 53.2 (2C,  $\text{NCH}_2\text{CH}_2\text{NCH}_2\text{COOH}$ ), 46.7 (2C,  $\text{NCH}_2\text{CH}_2\text{N}$ ), 42.0 (1C,  $\text{CH}_3\text{CH}_2\text{CH}_2\text{NHCO}$ ), 39.7 (1C,  $\text{CONHCH}_2(\text{CH}_2)_3$ ), 29.0 (1C,  $\text{CONHCH}_2\text{CH}_2$ ), 27.7 (1C,  $\text{CONH}(\text{CH}_2)_3\text{CH}_2\text{CHN}$ ), 23.4 (1C,  $\text{CH}_3\text{CH}_2\text{CH}_2\text{NHCO}$ ), 22.6 (1C,  $\text{CONH}(\text{CH}_2)_2\text{CH}_2$ ), 10.6 (1C,  $\text{CH}_3\text{CH}_2$ ). FT-IR (ATR):  $\nu$  ( $\text{cm}^{-1}$ ) 3334 (NH stretch), 2963, 2521 (COOH stretch), 1715 (C=O stretch), 1623 (C=O stretch), 1574 (C=O stretch), 1383, 1217 (C–O stretch), and 1148. MALDI-TOF:  $m/z$  [ $\text{C}_{22}\text{H}_{39}\text{N}_5\text{O}_{11} + \text{H}$ ] $^+$  Calcd. 550.26 Da, Obsd. 550.32 Da; [ $\text{C}_{22}\text{H}_{39}\text{N}_5\text{O}_{11} + \text{Na}$ ] $^+$  Calcd. 572.25 Da, Obsd. 572.30 Da.

### Gd(III) complex 11

Compound **10** (50.4 mg, 0.092 mmol) was dissolved in water (7 mL) and the pH was adjusted to 6.5–7.0 by adding aliquots of 0.1 N NaOH. The Gd(III) complex of **10** was prepared by adding a stoichiometric amount of  $\text{Gd(III)Cl}_3 \cdot 6 \text{H}_2\text{O}$  (34.2 mg, 0.092 mmol). The solution was vigorously stirred for 3 h at room temperature. The pH was continuously monitored and maintained at pH 7 with a 0.1 N NaOH solution. The formation of the complex was monitored with ESI-MS. The Gd(III) complex **11** was dialyzed with a 0.1 kDa MWCO membrane and lyophilized, resulting in a hygroscopic white powder (quantitative yield). FT-IR (ATR):  $\nu$  ( $\text{cm}^{-1}$ ) 3350 (NH stretch), 2977, 2933, 1585 (C=O stretch), 1440, 1407, 1324, and 1267. ESI-QTOF-MS (positive mode, direct injection):  $m/z$  [ $\text{C}_{22}\text{H}_{36}\text{N}_5\text{O}_{11}\text{Gd} + \text{H}$ ] $^+$  Calcd. 705.17 Da.; Obsd. 705.17 Da., isotope pattern of Gd(III); [ $\text{C}_{22}\text{H}_{36}\text{N}_5\text{O}_{11}\text{Gd} + \text{Na}$ ] $^+$  Calcd. 727.17 Da.; Obsd. 727.17 Da., [ $\text{C}_{22}\text{H}_{35}\text{N}_5\text{O}_{11}\text{NaGd} + \text{Na}$ ] $^+$  calcd. 749.17 Da.; Obsd. 749.16 Da. ESI-MS (negative mode):  $m/z$  [ $\text{C}_{22}\text{H}_{36}\text{N}_5\text{O}_{11}\text{Gd} - \text{H}$ ] $^-$  Calcd. 703.16 Da, Obsd. 703.25 Da. ICP-AES (Gd(III)): aqueous solution of **11** Calcd. 50.0  $\mu\text{M}$ , Obsd. 45.4  $\mu\text{M}$ .

### Amine-functionalized poly(ethylene butylene) (12)

Amine-functionalized poly(ethylene butylene) (**12**) was kindly provided by dr. N. Chebotareva. The synthesis started from commercially available hydroxy-terminated poly(ethylenebutylene) (Kraton).

### DTPA-functionalized poly(ethylene butylene) (tert-butyl ester protected) (13)

Into a stirred solution of di-tert-butyl tricarbonate<sup>18</sup> (0.088 g, 0.34 mmol) in freshly distilled dichloromethane (1 mL) was injected a solution of **4** (0.23 g, 0.31 mmol) in dry dichloromethane (2 mL) under an atmosphere of argon. The colorless solution was vigorously stirred for 50 min at room temperature, and IR spectroscopy revealed the presence of the characteristic isocyanate absorption at  $2271 \text{ cm}^{-1}$ . The excess of di-tert-butyl tricarbonate was quenched by the addition of two droplets of dry pyridine. Subsequently, a solution of amine-functionalized poly(ethylene butylene) **12** (1.0 g, 0.256 mmol of  $\text{NH}_2$  end groups) in DCM (2 mL) was added to a solution containing the isocyanate-functionalized DTPA pentaester **8**, and the solution was stirred overnight under an atmosphere of argon. The solvent was concentrated under reduced pressure. The crude product was purified using column chromatography (silica, DCM/MeOH 95:5 *v/v*) to give **13** (0.2 g, 0.04 mmol) in 14% yield.  $^1\text{H}$ -NMR ( $\text{CDCl}_3$ ):  $\delta = 4.93$  (br t, 1H,  $\text{NH}$ ), 4.86 (br t, 1H,  $\text{NH}$ ), 4.78 (br t, 1H,  $\text{NH}$ ), 4.61 (br t, 1H,  $\text{NH}$ ), 3.50 (t, 2H,  $\text{CH}_2\text{OCH}_2(\text{CH}_2)_2\text{NHCONH}$ ), 3.43–3.39 (m, 10H,  $\text{NCH}_2\text{COOC}(\text{CH}_3)_3$  {8H} +

(CH<sub>2</sub>)<sub>2</sub>CH<sub>2</sub>OCH<sub>2</sub>{2H}); 3.29–3.12 (m, 9H, CONHCH<sub>2</sub>(CH<sub>2</sub>)<sub>3</sub> {2H} + CH<sub>2</sub>NHCONH {6H} + CONH(CH<sub>2</sub>)<sub>4</sub>CHN {1H}), 2.86–2.62 (m, 8H, NCH<sub>2</sub>CH<sub>2</sub>N {4H} + NCH<sub>2</sub>CH<sub>2</sub>N {4H}), 1.75 (m, 2H, OCH<sub>2</sub>CH<sub>2</sub>CH<sub>2</sub>NHCONH), 1.7–0.6 (br m, polymer + NHCONHCH<sub>2</sub>(CH<sub>2</sub>)<sub>5</sub>CH<sub>2</sub>NHCONH + CONHCH<sub>2</sub>CH<sub>2</sub>(CH<sub>2</sub>)<sub>2</sub>CHN + COOC(CH<sub>3</sub>)<sub>3</sub>). The MALDI-TOF spectrum of **13** is depicted in Figure 2.4. FT-IR (ATR):  $\nu$  (cm<sup>-1</sup>) 3334 (NH stretch), 2959, 1729 (C=O stretch), 1636 (C=O stretch), 1573 (C=O stretch), 1461, 1367, and 1148.

#### **DTPA-functionalized poly(ethylene butylene) (14)**

To a stirred solution of **13** (0.15 g) in DCM (4 mL) was added TFA (2 mL), and the reaction mixture was stirred overnight at room temperature. After evaporation of the solvent a second portion of TFA (2 mL) and dry DCM (4 mL) were added, and stirring was continued overnight. The solution was concentrated *in vacuo* resulting in a yellowish solid. The crude product was dissolved in DCM (20 mL), washed with 1 N NaOH (aq) (3 × 15 mL) and the precipitated white solid was collected. The crude product was washed with water and lyophilization yielded polymer **14** (0.06 g). <sup>1</sup>H-NMR (CDCl<sub>3</sub> + TFA):  $\delta$  = 4.2 (br s, 8H, NCH<sub>2</sub>COOH) 3.92 (m, CONH(CH<sub>2</sub>)<sub>4</sub>CHN), 3.7–3.0 (br m, NCH<sub>2</sub>CH<sub>2</sub>NCH<sub>2</sub>COOH + CH<sub>2</sub>CH<sub>2</sub>OCH<sub>2</sub>CH<sub>2</sub> + CH<sub>2</sub>NHCONHCH<sub>2</sub>), 2.0–0.6 (polymer + NHCONHCH<sub>2</sub>(CH<sub>2</sub>)<sub>5</sub>CH<sub>2</sub>NHCONH + CONHCH<sub>2</sub>CH<sub>2</sub>(CH<sub>2</sub>)<sub>2</sub>CHN). The MALDI-TOF spectrum of **14** is depicted in Figure 2.4. FT-IR (ATR):  $\nu$  (cm<sup>-1</sup>) 3334 (NH stretch), 2959, 1672, 1626, 1587, 1460, and 1119.

#### **N-(4-Nitrophenyloxycarbonyl)benzyl glycinate (15)**

A solution of glycine benzyl ester *p*-toluenesulfonate salt (17.05 g, 50.53 mmol) in DCM was washed with 0.5 N NaOH (100 mL). The organic layer was washed with brine (3 × 100 mL), dried over Na<sub>2</sub>SO<sub>4</sub>, filtered and the solvent was removed under reduced pressure, to give pure benzyl glycinate (7.45 g, 45.67 mmol, 90%). Bis(4-nitrophenyl)carbonate (13.9 g, 45.7 mmol) was dissolved in chloroform (150 mL) and quickly added to a solution of benzyl glycinate (7.45 g, 45.7 mmol) in chloroform (100 mL) under vigorous stirring. The solution was stirred for 70 h at room temperature. The solvent was removed under reduced pressure. The crude product was precipitated in diethyl ether (300 mL). The reaction mixture was refluxed for 1 h, after which it was cooled to room temperature and stored in the fridge at -4°C. The precipitate was washed with cold ether (2 × 50 mL), dried *in vacuo* at 40 °C. The pure product **15** (10.87 g, 32.91 mmol, 72%) was obtained as a white powder. R<sub>f</sub> = 0.24 (hexane/EtOAc 1:1 v/v). <sup>1</sup>H-NMR (CDCl<sub>3</sub>):  $\delta$  = 8.31–8.28 (m, 2H), 7.44–7.31 (m, 7H), 5.78–5.74 (t, 1H, *J* = 5.7 Hz), 5.29 (s, 2H), 4.18–4.16 (d, 2H, *J* = 5.7 Hz). <sup>13</sup>C-NMR (CDCl<sub>3</sub>):  $\delta$  = 169.2, 155.5, 153.0, 144.8, 134.8, 128.6, 128.6, 128.38, 125.0, 121.9, 67.4, and 42.8. FT-IR (ATR):  $\nu$  (cm<sup>-1</sup>) 3325, 1758 (C=O stretch), 1721 (C=O stretch), 1517, 1487, 1345, 1192 (C–O stretch), and 946.

#### **tert-Butyl 6-(benzyloxycarbonylmethyl-3-ureido) 2-{{bis-{{2-[bis-(tert-butoxycarbonylmethyl)amino]-ethyl}-amino}} hexanoate (16)**

Amine-terminated DTPA pentaester **4** (3.86 g, 5.18 mmol) was dissolved in freshly distilled DCM (30 mL) and *N*-(4-nitrophenyloxycarbonyl)benzyl glycinate **15** (1.71 g, 5.18 mmol) was added. The solution was stirred at room temperature overnight under an argon atmosphere, diluted with DCM (100 mL), washed with saturated Na<sub>2</sub>CO<sub>3</sub> (5 × 200 mL), and brine (200 mL). The organic phase was dried with anhydrous Na<sub>2</sub>SO<sub>4</sub>, filtered, and concentrated under reduced pressure. The crude product was purified by column chromatography (silica, EtOAc/hexane 1:1 v/v, followed by EtOAc/hexane 2:1 v/v), to yield pure **16** (4.54 g, 4.85 mmol, 93.4%) as a colorless oil. R<sub>f</sub> = 0.25 (EtOAc/hexane 2:1 v/v). <sup>1</sup>H-NMR (CDCl<sub>3</sub>):  $\delta$  = 7.36–7.27 (m, 5H, ArH), 5.20 (t, 1H, *J* = 5.5 Hz, COOCH<sub>2</sub>NHCONH), 5.14–5.02 (m, 3H, CH<sub>2</sub>Ph {2H} + NHCONH {1H}), 3.97–3.96

(d, 2H,  $J = 5.5$  Hz, COOCH<sub>2</sub>NHCONH), 3.36 (s, 8H, NCH<sub>2</sub>COOC(CH<sub>3</sub>)<sub>3</sub>), 3.19 (m, 1H, CONH(CH<sub>2</sub>)<sub>4</sub>CHN), 3.15 (m, 2H, NHCONHCH<sub>2</sub>CH<sub>2</sub>), 2.77–2.57 (m, 8H, NCH<sub>2</sub>CH<sub>2</sub>N {4H} + NCH<sub>2</sub>CH<sub>2</sub>N {4H}), 1.62–1.19 (m, 6H, NHCONHCH<sub>2</sub>(CH<sub>2</sub>)<sub>3</sub>CHN ; s, 45H, COOC(CH<sub>3</sub>)<sub>3</sub>). The assignment of the <sup>1</sup>H-NMR spectrum is confirmed by <sup>1</sup>H,<sup>1</sup>H-COSY. <sup>13</sup>C-NMR (CDCl<sub>3</sub>):  $\delta = 171.9$  (1C, C=O), 170.0 (1C, C=O), 169.8 (4C, C=O), 157.0 (1C, NHCONH), 134.5 (1C, aromatic carbon), 127.5–127.3 (5C, aromatic carbons), 79.9 (4C, C(CH<sub>3</sub>)<sub>3</sub>), 79.8 (1C, C(CH<sub>3</sub>)<sub>3</sub>), 65.7 (2C, CH<sub>2</sub>Ph), 62.9 (1C, NHCONH(CH<sub>2</sub>)<sub>3</sub>CHN), 55.0 (4C, NCH<sub>2</sub>COOC(CH<sub>3</sub>)<sub>3</sub>), 52.6 (2C, NCH<sub>2</sub>CH<sub>2</sub>N), 49.0 (2C, NCH<sub>2</sub>CH<sub>2</sub>N), 41.2 (1C, OCOCH<sub>2</sub>NHCONH), 39.0 (1C, NHCONHCH<sub>2</sub>(CH<sub>2</sub>)<sub>3</sub>), 28.4 (1C, NHCONHCH<sub>2</sub>CH<sub>2</sub>(CH<sub>2</sub>)<sub>2</sub>), 28.3–28.2 (16C, C(CH<sub>3</sub>)<sub>3</sub> + CONH(CH<sub>2</sub>)<sub>3</sub>CHCHN), 22.4 (1C, NHCONH(CH<sub>2</sub>)<sub>2</sub>CH<sub>2</sub>CH<sub>2</sub>). FT-IR (ATR):  $\nu$  (cm<sup>-1</sup>) 3374 (-NH stretch), 2977, 2934, 1725 (C=O stretch), 1644 (C=O amide I stretch), 1560 (C=O amide II stretch), 1366, 1244, and 1143 (C–O stretch). ESI-MS:  $m/z$  [C<sub>48</sub>H<sub>81</sub>N<sub>5</sub>O<sub>13</sub> + H]<sup>+</sup> Calcd. 936.59 Da, Obsd. 936.55 Da; [C<sub>48</sub>H<sub>81</sub>N<sub>5</sub>O<sub>13</sub> + Na]<sup>+</sup> Calcd. 958.57 Da, Obsd. 958.52 Da.

**6-(Benzyloxycarbonylmethyl-3-ureido) 2-{{bis-2-[bis-(carboxymethyl)amino]}-ethyl}}-amino-hexanoic acid (17)**

To a stirred solution of **16** (2.30 g, 2.46 mmol) in DCM (20 mL) was added TFA (20 mL) and the reaction mixture was stirred overnight at room temperature under a nitrogen atmosphere. After evaporation of the solvent a second portion of TFA (20 mL) and dry DCM (20 mL) was added and stirring was continued overnight. The solution was concentrated *in vacuo* resulting in the TFA salt of **17**. Additional purification by dialysis (100 Da MWCO membrane) and freeze-drying yielded compound **17** (0.80 g, 1.22 mmol, 49%) as a white powder. <sup>1</sup>H-NMR (D<sub>2</sub>O):  $\delta = 7.38$ –7.33 (m, 5H, ArH), 5.13 (s, 2H, CH<sub>2</sub>Ph), 3.91–3.80 (m, 10H, NCH<sub>2</sub>COOH {8H} + COOCH<sub>2</sub>NHCONH {2H}), 3.44–3.32 (m, 5H, 1H, NHCONH(CH<sub>2</sub>)<sub>4</sub>CHN {1H} + NCH<sub>2</sub>CH<sub>2</sub>NCH<sub>2</sub>COO {4H}), 3.12–2.99 (m, 6H, NCH<sub>2</sub>CH<sub>2</sub>N {4H} + NHCONHCH<sub>2</sub> {2H}), 1.74–1.46 (m, 2H, (CH<sub>2</sub>)<sub>3</sub>CH<sub>2</sub>CHN), 1.43–1.22 (m, 4H, NHCONH CH<sub>2</sub>(CH<sub>2</sub>)<sub>2</sub>CH<sub>2</sub>CHN). The assignment of the <sup>1</sup>H-NMR spectrum is fully confirmed by <sup>1</sup>H,<sup>1</sup>H-COSY. <sup>13</sup>C-NMR (D<sub>2</sub>O):  $\delta$  175.3 (C=O), 173.0 (C=O), 169.7 (C=O), 160.4 (NHCONH), 135.4 (aromatic carbon), 128.8–128.0 (aromatic carbons), 67.3 (CH<sub>2</sub>Ph), 63.2 (NHCONH(CH<sub>2</sub>)<sub>4</sub>CHN), 56.2 (NCH<sub>2</sub>COOH), 52.9 (NCH<sub>2</sub>CH<sub>2</sub>N), 46.1 (NCH<sub>2</sub>CH<sub>2</sub>N), 42.1 (CH<sub>2</sub>NHCONH(CH<sub>2</sub>)<sub>2</sub>), 39.4 (NHCONHCH<sub>2</sub>(CH<sub>2</sub>)<sub>3</sub>), 28.8 (NHCONHCH<sub>2</sub>CH<sub>2</sub>), 27.9 (NHCONH(CH<sub>2</sub>)<sub>2</sub>CH<sub>2</sub>), 23.1 (NHCONH(CH<sub>2</sub>)<sub>2</sub>CH<sub>2</sub>). FT-IR (ATR):  $\nu$  (cm<sup>-1</sup>) 3369 (NH stretch), 2962, 2500 (COOH stretch), 1724 (C=O stretch), 1623 (C=O stretch), 1571, 1389, 1356, 1204 (C–O stretch). MALDI-TOF:  $m/z$  [C<sub>28</sub>H<sub>41</sub>N<sub>5</sub>O<sub>13</sub> + H]<sup>+</sup> Calcd. 656.28 Da, Obsd. 656.18 Da; [C<sub>28</sub>H<sub>41</sub>N<sub>5</sub>O<sub>13</sub> + Na]<sup>+</sup> Calcd. 678.26 Da, Obsd. 678.17 Da.

**Gd(III) complex 18**

DTPA derivative **17** (195.4 mg, 0.298 mmol) was dissolved in demineralized water (20 mL). The pH was adjusted to 7 by adding aliquots of 0.1 N NaOH. Subsequently, an aqueous solution of Gd(III)Cl<sub>3</sub>·6 H<sub>2</sub>O (122 mg, 0.328 mmol) in water (10 mL) was added and the solution was vigorously stirred for 2 h at room temperature. The pH was continuously monitored and maintained at pH 7.2 by adding aliquots of 0.1 N NaOH. The aqueous solution was extensively dialysed (100 Da MWCO membrane) and lyophilized. The corresponding Gd(III) complex **18** was obtained in 54% yield (137 mg, 0.160 mmol) as a fluffy white powder. FT-IR (ATR):  $\nu$  (cm<sup>-1</sup>) 3349, 2933, 1575 (antisym. COO stretch), 1442, 1404 (sym. COO stretch), 1265, 1188, 1087, 929. ESI-QTOF-MS:  $m/z$  [C<sub>28</sub>H<sub>36</sub>N<sub>5</sub>O<sub>13</sub>Na<sub>2</sub>Gd + Na]<sup>+</sup> Calcd. 877.13 Da, Obsd. 877.32 Da. ESI-MS (negative mode):  $m/z$  [C<sub>28</sub>H<sub>38</sub>N<sub>5</sub>O<sub>13</sub>Gd – H]<sup>-</sup> Calcd. 809.2 Da, Obsd. 809.5 Da. ICP-AES (Gd(III)): Calcd. 50.0  $\mu$ M, Obsd. 44.5  $\mu$ M.

**Carboxymethyl-3-ureido functionalized Gd(III) complex (19)**

In a Parr apparatus was hydrogenated **18** (31.3 mg, 36.6  $\mu\text{mol}$ ) in the presence of *tert*-BuOH (0.5 mL), water (3 mL) and 10% palladium on activated carbon (10 mg). The reaction was continued overnight and the mixture was filtered over Celite, washed with water, and concentrated under reduced pressure. The colorless solution was lyophilized and Gd(III) complex **19** (23.6 mg, 30.9  $\mu\text{mol}$ ) was obtained in 84% yield. FT-IR (ATR):  $\nu$  ( $\text{cm}^{-1}$ ) 3341, 2933, 1575 (antisym. COO stretch), 1440, 1403 (sym. COO stretch), 1323, 1266, 1087, 932. ESI-QTOF-MS  $m/z$  [ $\text{C}_{21}\text{H}_{30}\text{N}_5\text{O}_{13}\text{Na}_2\text{Gd} + \text{Na}$ ]<sup>+</sup> Calcd. 787.08 Da, Obsd. 787.07 Da. ESI-MS (negative mode):  $m/z$  [ $\text{C}_{21}\text{H}_{32}\text{N}_5\text{O}_{13}\text{Gd} - \text{H}$ ]<sup>-</sup> Calcd. 719.2 Da, Obsd. 719.6 Da. ICP-AES (Gd(III)): Calcd. 50.0  $\mu\text{M}$ , Obsd. 50.0  $\mu\text{M}$ .

**Carbonylimidazole-activated 6-(heptan-3-yl)-isocytosine (20)**

Compound **20** was kindly provided by Michel Fransen (SyMO-Chem BV, Eindhoven, the Netherlands). Details on the synthetic procedure are given in the literature.<sup>45</sup>

**2-Ureido-6-(heptan-3-yl)-4[1H]-pyrimidinone functionalized DTPA (tert-butyl protected) (21)**

To a colorless solution of imidazolide **20** (0.376 g, 1.24 mmol) in DCM (5 mL) was slowly added a solution DTPA synthon **4** (0.713 g, 0.96 mmol). The solution was vigorously stirred for 12 h at 20 °C. The yellowish solution was washed with 1 M  $\text{KHSO}_3$  (aq) pH 1.95 ( $2 \times 10$  mL). Subsequently, the organic layer was washed with 1 M  $\text{K}_2\text{CO}_3$  (aq) pH 10 ( $3 \times 10$  mL) and brine ( $3 \times 10$  mL). The combined water layer was extracted with DCM ( $2 \times 10$  mL) and the organic layer was dried over  $\text{MgSO}_4$ . The reaction mixture was concentrated under reduced pressure, yielding a yellowish liquid (0.84 g). The crude product (0.730 g) was purified by column chromatography using EtOAc, to give pure **21** (0.51 g, 0.52 mmol) in 62% yield.  $R_f = 0.5$  (EtOAc). <sup>1</sup>H-NMR ( $\text{CDCl}_3$ ):  $\delta = 13.30$  (s, 1H, N(1)H), 11.87 (s, 1H, C(2)NH), 10.18 (s, 1H, NCONHCH<sub>2</sub>), 5.84 (s, 1H, C(5)H), 3.46 (s, 8H, NCH<sub>2</sub>COOC(CH<sub>3</sub>)<sub>3</sub>), 3.3–3.2 (m, 3H, CONH(CH<sub>2</sub>)<sub>4</sub>CHN) {1H} + CONHCH<sub>2</sub>(CH<sub>2</sub>)<sub>3</sub> {2H}, 3.0–2.6 (m, 8H, NCH<sub>2</sub>CH<sub>2</sub>N {4H} + NCH<sub>2</sub>CH<sub>2</sub>N {4H}), 2.33 (m, 1H, CH<sub>3</sub>CH<sub>2</sub>CH<sub>2</sub>CH<sub>2</sub>), 2.0–1.2 (m, 14H, CONHCH<sub>2</sub>CH<sub>2</sub>(CH<sub>2</sub>)<sub>2</sub>CHN {6H} + CH<sub>3</sub>CH<sub>2</sub>CH(CH<sub>2</sub>)<sub>3</sub>CH<sub>3</sub> {8H} ; s, 45H, COOC(CH<sub>3</sub>)<sub>3</sub>), 0.94 (m, 6H, CH<sub>3</sub>CH<sub>2</sub>CH(CH<sub>2</sub>)<sub>3</sub>CH<sub>3</sub>). <sup>13</sup>C-NMR ( $\text{CDCl}_3$ ):  $\delta = 173.1$  (C=O), 172.7 (C(5)H), 170.7 (C=O), 159.6 (C(2)), 155.3 (NHCONH), 154.9 (C(6)), 106.3 (C(5)), 80.7 (C(CH<sub>3</sub>)<sub>3</sub>), 80.5 (C(CH<sub>3</sub>)<sub>3</sub>), 64.8 (CONH(CH<sub>2</sub>)<sub>4</sub>CHN), 56.1 (NCH<sub>2</sub>COOC(CH<sub>3</sub>)<sub>3</sub>), 54.0 (NCH<sub>2</sub>CH<sub>2</sub>N), 50.5 (NCH<sub>2</sub>CH<sub>2</sub>N), 45.4 (CH<sub>3</sub>(CH<sub>2</sub>)<sub>3</sub>CHCH<sub>2</sub>CH<sub>3</sub>), 40.1 (CONHCH<sub>2</sub>(CH<sub>2</sub>)<sub>3</sub>), 32.9 (CH<sub>3</sub>(CH<sub>2</sub>)<sub>2</sub>CH<sub>2</sub>), 29.9 (CH<sub>3</sub>CH<sub>2</sub>CH<sub>2</sub>), 29.4 (CONHCH<sub>2</sub>CH<sub>2</sub>), 28.3 (C(CH<sub>3</sub>)<sub>3</sub> + CONH(CH<sub>2</sub>)<sub>3</sub>CH<sub>2</sub>CHN), 26.6 (CH<sub>3</sub>(CH<sub>2</sub>)<sub>3</sub>CHCH<sub>2</sub>CH<sub>3</sub>), 24.1 (CH<sub>3</sub>CH<sub>2</sub>(CH<sub>2</sub>)<sub>2</sub>CH), 22.5 (CONH(CH<sub>2</sub>)<sub>2</sub>CH<sub>2</sub>), 13.9 (CH<sub>3</sub>(CH<sub>2</sub>)<sub>3</sub>CHCH<sub>2</sub>CH<sub>3</sub>), 11.7 (CH<sub>3</sub>(CH<sub>2</sub>)<sub>3</sub>CHCH<sub>2</sub>CH<sub>3</sub>). FT-IR (ATR):  $\nu$  ( $\text{cm}^{-1}$ ) 2975, 2932, 1724 (C=O ester stretch), 1698 (C=O), 1658, 1646, 1586, 1526, 1367, 1253, 1219, 1148 (C–O stretch). ESI-QTOF-MS:  $m/z$  [ $\text{C}_{50}\text{H}_{89}\text{N}_7\text{O}_{12} + \text{H}$ ]<sup>+</sup> Calcd. 980.67 Da, Obsd. 980.71 Da; [ $\text{C}_{50}\text{H}_{89}\text{N}_7\text{O}_{12} + \text{Na}$ ]<sup>+</sup> Calcd. 1002.65 Da, Obsd. 1002.65 Da.

**2-Ureido-6-(heptan-3-yl)-4[1H]-pyrimidinone functionalized DTPA (22)**

To a stirred solution of **21** (0.388 g, 0.396 mmol) in DCM (8 mL) was added TFA (2 mL) and the reaction mixture was stirred overnight at room temperature. After evaporation of the solvent a second portion of TFA (2 mL) and dry DCM (5 mL) was added and stirring was continued overnight. The solution was concentrated *in vacuo* resulting in the TFA salt of **22**. Additional purification by dialysis at 60 °C (100 Da MWCO membrane) and freeze-drying yielded compound **22** (0.266 g, 0.385 mmol, 97%) as a white hygroscopic powder. <sup>1</sup>H-NMR ( $\text{D}_2\text{O}$ , 348 K):  $\delta = 6.20$  (s, 1H, C(5)H), 4.06 (s, 8H, NCH<sub>2</sub>COOH), 3.58 (t, 1H, CONH(CH<sub>2</sub>)<sub>4</sub>CHN), 3.42 (t, 4H, NCH<sub>2</sub>CH<sub>2</sub>NCH<sub>2</sub>COOH), 3.25–3.08 (m, 6H, NCH<sub>2</sub>CH<sub>2</sub>N {4H} +

NHCONHCH<sub>2</sub> {2H}), 2.56 (m, 1H, CH<sub>3</sub>CH<sub>2</sub>CH<sub>2</sub>CH<sub>2</sub>), 2.0–1.2 (m, 14H, CONHCH<sub>2</sub>CH<sub>2</sub>(CH<sub>2</sub>)<sub>2</sub>CHN {6H} + CH<sub>3</sub>CH<sub>2</sub>CH(CH<sub>2</sub>)<sub>3</sub>CH<sub>3</sub> {8H}), 0.79 (m, 6H, CH<sub>3</sub>CH<sub>2</sub>CH(CH<sub>2</sub>)<sub>3</sub>CH<sub>3</sub>). The assignment of the <sup>1</sup>H-NMR spectrum was confirmed by <sup>1</sup>H,<sup>1</sup>H-COSY. <sup>19</sup>F-NMR spectroscopy confirmed the successful removal of TFA by the absence of a signal at –75.6 ppm. FT-IR (ATR): ν (cm<sup>-1</sup>) 3215, 2933, 2531 (COOH stretch), 1700 (C=O stretch), 1630 (C=O stretch), 1551, 1431, 1389, 1333, 1202 (C–O stretch). ESI-QTOF-MS: m/z [C<sub>30</sub>H<sub>49</sub>N<sub>7</sub>O<sub>12</sub> + H]<sup>+</sup> Calcd. 700.35 Da, Obsd. 700.40 Da; [C<sub>30</sub>H<sub>49</sub>N<sub>7</sub>O<sub>12</sub> + Na]<sup>+</sup> Calcd. 722.33 Da, Obsd. 722.40 Da.

### Gd(III) complex of 2-Ureido-6-(heptan-3-yl)-4[1H]-pyrimidinone functionalized DTPA (23)

The desired Gd(III) complex **23** was prepared by adding a stoichiometric amount of GdCl<sub>3</sub>·6 H<sub>2</sub>O (4.97 mg, 13.1 μmol) in demineralized water (3 mL) to a solution of **22** (9.16 mg, 13.1 μmol) in 0.3 M citrate buffer at pH 5.8. The buffered solution was vigorously stirred for 2 h at room temperature. The aqueous solution was extensively dialysed (100 Da MWCO membrane) and lyophilized. The corresponding Gd(III) complex **23** was obtained in 96% yield (10.7 mg, 12.5 μmol) as a white hygroscopic powder. FT-IR (ATR): ν (cm<sup>-1</sup>) 3384, 2932, 1696, 1579, 1407, 1183, 1135, 1083. ESI-MS: m/z [C<sub>30</sub>H<sub>46</sub>N<sub>7</sub>O<sub>12</sub>Gd + H]<sup>+</sup> Calcd. 855.25 Da, Obsd. 855.27 Da; [C<sub>30</sub>H<sub>45</sub>N<sub>7</sub>O<sub>12</sub>NaGd + H]<sup>+</sup> Calcd. 877.23 Da, Obsd. 877.27 Da. [C<sub>30</sub>H<sub>44</sub>N<sub>7</sub>O<sub>12</sub>Na<sub>2</sub>Gd + H]<sup>+</sup> Calcd. 899.22 Da, Obsd. 899.27 Da. ICP-AES (Gd(III)): Calcd. 50.0 μM, Obsd. 33.9 μM.

## 2.6 REFERENCES

- (1) Caravan, P.; Ellison, J. J.; McMurry, T. J.; Lauffer, R. B. *Chem. Rev.* **1999**, *99*, 2293-2352.
- (2) Lauffer, R. B. *Chem. Rev.* **1987**, *87*, 901-927.
- (3) Frost, A. E. *Nature* **1956**, *178*, 322.
- (4) Moeller, T.; Thompson, L. C. *Inorg. Nucl. Chem.* **1962**, *24*, 499-510.
- (5) Merbach, A. E.; Tóth, E. *The Chemistry of Contrast Agents in Medical Magnetic Resonance Imaging*; John Wiley & Sons: New York, 2001.
- (6) Gries, H. *Top. Curr. Chem.* **2002**, *221*, 1-24.
- (7) Williams, M. A.; Rapoport, H. *J. Org. Chem.* **1993**, *58*, 1151-1158.
- (8) Anelli, P. L.; Fedeli, F.; Gazzotti, O.; Lattuada, L.; Lux, G.; Rebasti, F. *Bioconjugate Chem.* **1999**, *10*, 137-140.
- (9) Edwards, W. B.; Fields, C. G.; Anderson, C. J.; Pajean, T. S.; Welch, M. J.; Fields, G. B. *J. Med. Chem.* **1994**, *37*, 3749-3757.
- (10) Hnatowich, D. J.; Layne, W. W.; Childs, R. L.; Lanteigne, D.; Davis, M. A.; Griffin, T. W.; Doherty, P. W. *Science* **1983**, *220*, 613-615.
- (11) Lauffer, R. B.; Brady, T. J. *Magn. Res. Imaging* **1985**, *3*, 11-16.
- (12) Armitage, F. E.; Richardson, D. E.; Li, K. C. P. *Bioconjugate Chem.* **1990**, *1*, 365-374.
- (13) Maisano, F.; Gozzini, L.; De Haen, C. *Bioconjugate Chem.* **1992**, *3*, 212-217.
- (14) Sherry, A. D.; Cacheris, W. P.; Kuan, K. T. *Magn. Reson. Med.* **1988**, *8*, 180-190.
- (15) Fossheim, R.; Dugstad, H.; Dahl, S. G. *J. Med. Chem.* **1991**, *34*, 819-826.
- (16) Brechbiel, M. W.; Gansow, O. A. *Bioconjugate Chem.* **1991**, *2*, 187-194.
- (17) Pope, B. M.; Yamamoto, Y.; Tarbell, D. S. *Organic Syntheses* **1973**, *53*, 1851.
- (18) Peerlings, H. W. I.; Meijer, E. W. *Tetrahedron Letters* **1999**, *40*, 1021-1024.
- (19) Versteegen, R. *PhD thesis*; Eindhoven University of Technology, 2003.
- (20) Buezli, J. C. G.; Choppin, G. R.; Editors. *Lanthanide Probes in Life, Chemical and Earth Sciences: Theory and Practice*, 1989.



- (21) Fassel, V. A. *Science* **1978**, *202*, 183-191.
- (22) Boumans, P. W. J. M. *Chemical Analysis* **1987**, *90*, 69-99.
- (23) Cole, R. B. *Electrospray Ionization Mass Spectrometry: Fundamentals, Instrumentation, and Applications*; John Wiley & Sons, 1997.
- (24) Baars, M. W. P. L.; Karlsson, A. J.; Sorokin, V.; De Waal, B. F. M.; Meijer, E. W. *Angew. Chem. Int. Ed.* **2000**, *39*, 4262-4265.
- (25) Broeren, M. A. C.; van Dongen, J. L. J.; Pittelkow, M.; Christensen, J. B.; van Genderen, M. H. P.; Meijer, E. W. *Angew. Chem. Int. Ed.* **2004**, *43*, 3557-3562.
- (26) Banerjee, D.; Broeren, M. A. C.; Van Genderen, M. H. P.; Meijer, E. W.; Rinaldi, P. L. *Macromolecules* **2004**, *37*, 8313-8318.
- (27) Sijbesma, R. P.; Beijer, F. H.; Brunsveld, L.; Folmer, B. J. B.; Hirschberg, J. H. K. K.; Lange, R. F. M.; Lowe, J. K. L.; Meijer, E. W. *Science* **1997**, *278*, 1601-1604.
- (28) Beijer, F. H.; Sijbesma, R. P.; Kooijman, H.; Spek, A. L.; Meijer, E. W. *J. Am. Chem. Soc.* **1998**, *120*, 6761-6769.
- (29) Beijer, F. H.; Kooijman, H.; Spek, A. L.; Sijbesma, R. P.; Meijer, E. W. *Angew. Chem. Int. Ed.* **1998**, *37*, 75-78.
- (30) Hirschberg, J. H. K.; Beijer, F. H.; van Aert, H. A.; Magusin, P. C. M. M.; Sijbesma, R. P.; Meijer, E. W. *Macromolecules* **1999**, *32*, 2696-2705.
- (31) Folmer, B. J. B.; Sijbesma, R. P.; Versteegen, R. M.; van der Rijt, J. A. J.; Meijer, E. W. *Adv. Mater.* **2000**, *12*, 874-878.
- (32) Claridge, T. D. W. *High-Resolution NMR Techniques in Organic Chemistry*; Elsevier Science: Amsterdam, 1999; Vol. 19.
- (33) Dwek, R. A. *Nuclear Magnetic Resonance in Biochemistry. Applications to Enzyme Systems*; Clarendon Press: Oxford, 1973.
- (34) Burton, D. R.; Forsen, S.; Karlstrom, G.; Dwek, R. A. *Prog. Nucl. Magn. Reson. Spectrosc.* **1979**, *13*, 1-45.
- (35) Botta, M. *Eur. J. Inorg. Chem.* **2000**, 399-407.
- (36) Peters, J. A.; Huskens, J.; Raber, D. J. *Prog. Nucl. Magn. Reson. Spectrosc.* **1996**, *28*, 283-350.
- (37) Comblin, V.; Gilsoul, D.; Hermann, M.; Humblet, V.; Jacques, V.; Mesbahi, M.; Sauvage, C.; Desreux, J. F. *Coordination Chemistry Reviews* **1999**, *185-186*, 451-470.
- (38) Bloembergen, N.; Purcell, E. M.; Pound, R. V. *Physical Review* **1948**, *73*, 679-712.
- (39) Solomon, I. *Physical Review* **1955**, *99*, 559-565.
- (40) Bloembergen, N.; Morgan, L. O. *J. Chem. Phys.* **1961**, *34*, 842-850.
- (41) Kowalewski, J.; Nordenskiöld, L.; Benetis, N.; Westlund, P. O. *Prog. Nucl. Magn. Reson. Spectrosc.* **1985**, *17*, 141-185.
- (42) Banci, L.; Bertini, I.; Luchinat, C. *Nuclear and Electronic Relaxation*; VCH: Weinheim, 1991.
- (43) In den Kleef, J. J. E.; Cuppen, J. J. M. *Magn. Reson. Med.* **1987**, *5*, 513-524.
- (44) Reichenbach, J. R.; Hacklander, T.; Harth, T.; Hofer, M.; Rassek, M.; Modder, U. *Eur. Radiol.* **1997**, *7*, 264-274.
- (45) Keizer, H. M.; Sijbesma, R. P.; Meijer, E. W. *Eur. J. Org. Chem.* **2004**, 2553-2555.

---

## Chapter 3

# Multivalent Gd(III)DTPA-terminated poly(propylene imine) dendrimers\*

---

### ABSTRACT:

*A convenient methodology has been developed for the synthesis of Gd(III)DTPA-terminated poly(propylene imine) dendrimers as contrast agents for magnetic resonance imaging (MRI). In our strategy, isocyanate-activated, tert-butyl-protected DTPA analogues were coupled to different generations of poly(propylene imine) dendrimers. Deprotection of the tert-butyl esters with trifluoroacetic acid in dichloromethane and extensive dialysis afforded DTPA-terminated poly(propylene imine) dendrimers. The corresponding dendritic MRI contrast agents were prepared from GdCl<sub>3</sub> in either water or citrate buffer. Cryogenic Transmission Electron Microscopy (cryo-TEM) experiments on the fifth generation Gd(III)DTPA-terminated dendritic MRI contrast agent in citrate buffer at pH 5.8 demonstrated the presence of well-defined spherical particles with nanoscopic dimensions (5–6 nm); no aggregation of dendrimers was observed. The  $r_1$  and  $r_2$  values increase considerably with increasing generation of the Gd(III)DTPA-terminated dendrimer. The fifth generation dendritic MRI contrast agent displays the highest ionic relaxivities (per Gd(III)),  $r_1 = 19.5 \text{ mM}^{-1}\text{s}^{-1}$  and  $r_2 = 27.7 \text{ mM}^{-1}\text{s}^{-1}$ , and these values are substantially higher than the ionic relaxivities of the parent Gd(III)DTPA complex ( $r_1 = 5.9 \text{ mM}^{-1}\text{s}^{-1}$  and  $r_2 = 6.5 \text{ mM}^{-1}\text{s}^{-1}$ ). Moreover, a series of combined Gd(III) and Y(III) complexes of the fifth generation DTPA-terminated dendrimer has been prepared, resulting in dendritic MR contrast agents with tunable molecular relaxivities.*

---

\* Part of this work has been published: Langereis, S.; de Lussanet, Q.G.; van Genderen, M.H.P.; Backes, W.H.; Meijer E.W. *Macromolecules* **2004**, 37, 3084-3091.

### 3.1 INTRODUCTION

Among paramagnetic contrast agents, water-soluble gadolinium(III) chelates, *e.g.* Gd(III) diethylenetriaminepentaacetic acid (Gd(III)DTPA) complexes, display intriguing properties in terms of high thermodynamic stability and kinetic inertness.<sup>1</sup> Gd(III)DTPA complexes reduce the longitudinal and transverse relaxation times ( $T_1$  and  $T_2$ , respectively) of the protons of the water molecules, resulting in a pronounced contrast enhancement in an MR image.<sup>2</sup> The ability of an MRI contrast agent to reduce the relaxation times is often expressed in terms of relaxivity ( $r_{i=1,2}$ ), *i.e.* the change of the relaxation rate ( $1/T_{i=1,2}$ ) divided by the concentration of MRI contrast agent. Drawbacks of low molecular weight MRI contrast agents, such as Gd(III)DTPA (MW =  $0.6 \text{ kg}\cdot\text{mol}^{-1}$ ), however, are their non-specificity, their rapid renal excretion, and their relatively low relaxivity.<sup>3</sup>

In recent years, various encouraging strategies have been explored to improve the relaxivities of MRI contrast agents.<sup>3,4</sup> It was recognized early that the proton relaxivity of low molecular weight MRI contrast agents is primarily limited by the fast rotation of the Gd(III) complex.<sup>1</sup> Consequently, low molecular weight MRI contrast agents were attached to various macromolecules, either covalently<sup>5-9</sup> or non-covalently,<sup>10,11</sup> to reduce the molecular tumbling rate of the complex and to increase the proton relaxivity. However, the gain in proton relaxivity was often much lower than anticipated. This was presumed to be due to a high conformational flexibility of the polymer backbone. For instance, relaxivities of macromolecular contrast agents composed of linear flexible polymers, such as poly(lysine)<sup>12</sup> and poly(ethylene glycol)<sup>13</sup>, were reported to be independent of their molecular weight and only slightly higher than the relaxivity of the parent Gd(III) complex.

Lately, several studies have shown that dendrimers are excellent multivalent scaffolds for attaching MRI labels.<sup>14</sup> These highly branched macromolecular architectures have well-defined molecular weights and a precise number of end groups, which reside in virtually identical environments.<sup>15</sup> Wiener, Tomalia and Lauterbur *et al.* were the first to demonstrate the use of dendrimers scaffolding for presentation of Gd(III) chelates to produce MRI contrast agents with high relaxivities.<sup>16</sup> Wiener *et al.*<sup>16</sup> and others<sup>17,18</sup> reported on the conjugation of isothiocyanate-activated, Gd(III)-chelating groups to different generations of poly(amidoamine) (PAMAM) dendrimers. Their sixth-generation Gd(III)DTPA-terminated PAMAM dendrimer<sup>16</sup> displays a strong increase in molecular relaxivity, which was attributed not only to the large number of Gd(III)DTPA complexes attached to a single molecule, but also to a higher longitudinal ionic relaxivity (ionic  $r_1$ , defined as the longitudinal relaxivity per Gd(III)). This strong relative increase in ionic  $r_1$  (up to  $36 \text{ mM}^{-1}\text{s}^{-1}$  at 0.47 T, 23 °C) with increasing generation of the dendrimer (higher molecular weights) was ascribed to the slower molecular tumbling of the Gd(III) complex, *i.e.* higher rotational correlation times.<sup>19</sup> However, it was demonstrated that the ionic  $r_1$  reaches a plateau value for the higher generations of the dendrimer as a result of a limited water exchange rate.<sup>17,20</sup> Researchers at

Schering AG (Berlin, Germany) developed another class of dendritic contrast agents: Gadomer-17<sup>®</sup>, a polylysine-terminated contrast agent (MW = 17.5 kg·mol<sup>-1</sup>) with 24 *N*-monosubstituted Gd(III)DO3A complexes (DO3A = 1,4,7,10-tetraazacyclododecane-1,4,7-triacetic acid).<sup>21,22</sup> Gadomer-17<sup>®</sup> has an ionic relaxivity of 17.3 mM<sup>-1</sup>s<sup>-1</sup> (0.47 T, 39 °C). Recently, Kobayashi and co-workers<sup>18,23</sup> reported on the synthesis of dendritic MRI contrast agents composed of poly(propylene imine) dendrimers. In their work, the primary amines of the dendrimer have been conjugated to the chelator 2-(4-isothiocyanatobenzyl)-6-methyl-diethylenetriaminepentaacetic acid. Remarkably, their results showed no “saturation” of the ionic relaxivity upon increasing generation of the Gd(III)DTPA-terminated dendrimer. These literature data prompted us to investigate the relaxivities of different generations of Gd(III)DTPA-terminated poly(propylene imine) dendrimers in detail.

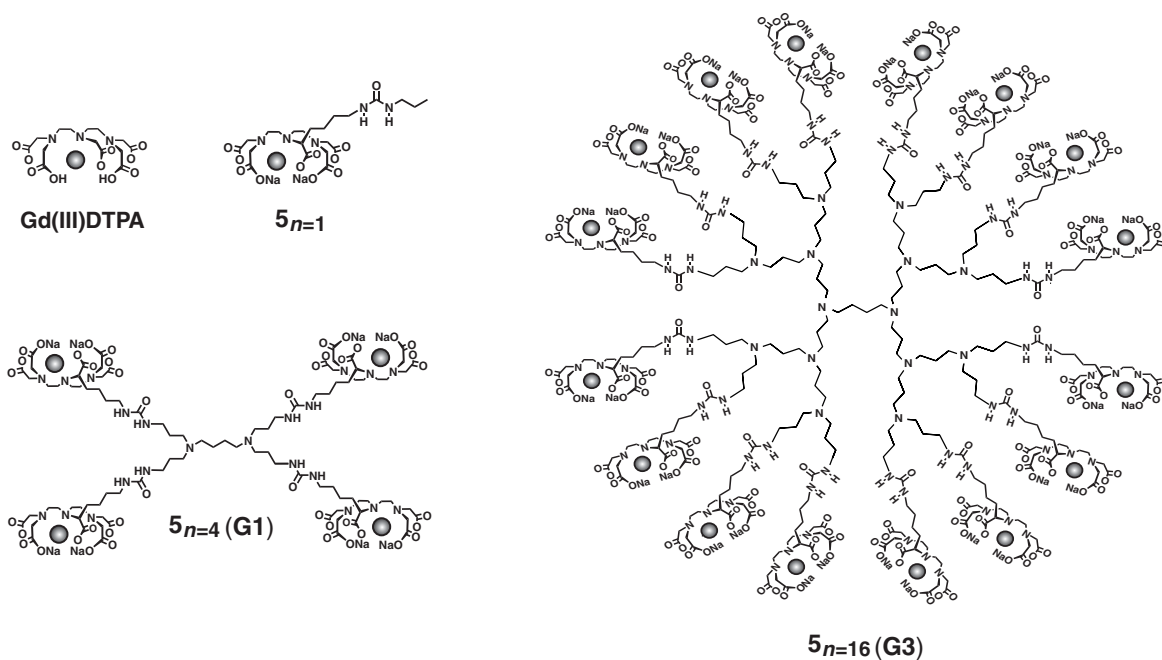


**Figure 3.1** Schematic representations of Gd(III)DTPA, Gd(III)DTPA-based complex  $5_{n=1}$ , and Gd(III)DTPA-terminated poly(propylene imine) dendrimers  $5_{n=4,16}$ .  $n$  denotes the number of Gd(III)DTPA moieties per single dendrimer and  $G$  represents the generation of the dendrimer.

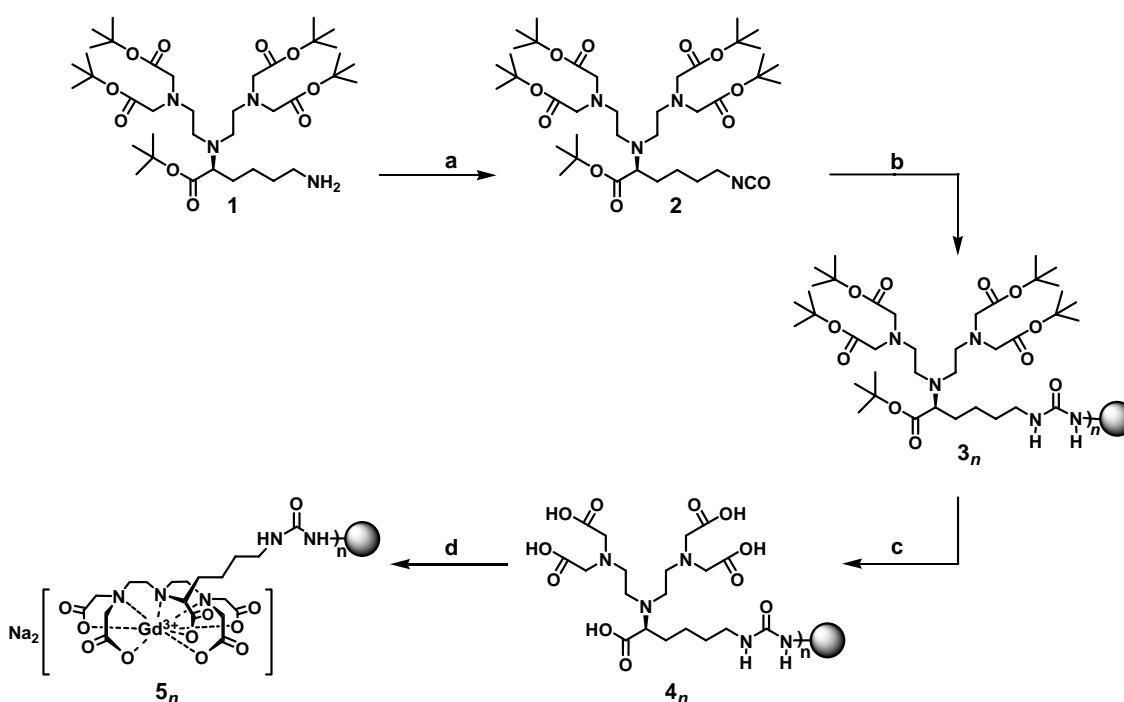
In this Chapter, a convenient and versatile methodology for the synthesis of Gd(III)DTPA-terminated poly(propylene imine) dendrimers as MRI contrast agents is presented. Additionally, a series of combined Gd(III) and yttrium(III) complexes of the fifth generation DTPA-terminated poly(propylene imine) dendrimer is prepared and the influence of the loading Gd(III) on the corresponding longitudinal ionic relaxivity is investigated. From our experience with highly charged, multivalent architectures it is known that aggregation of the dendrimers can occur

easily under certain conditions.<sup>24,25</sup> Since aggregation of the MRI contrast agent can have profound implications on its effective molecular weight, and hence on its behavior as a contrast agent, its behavior in solution is studied using cryogenic transmission electron microscopy (cryo-TEM).

### 3.2 Gd(III)DTPA-TERMINATED POLY(PROPYLENE IMINE) DENDRIMERS

#### 3.2.1 Synthesis

Gd(III)-chelating poly(propylene imine) dendrimers of the first, the third and the fifth generation (with, respectively, 4, 16 and 64 end groups) were synthesized using isocyanate-functionalized DTPA synthon **2** (Scheme 3.1).<sup>26</sup>



**Scheme 3.1** Synthesis of Gd(III)DTPA-terminated poly(propylene imine) dendrimers **5<sub>n</sub>**. *n* denotes the number of end groups and *G* represents the generation of the dendrimer: *n*=4 (**G1**), 16 (**G3**) and 64 (**G5**). (a) Di-*tert*-butyl-tricarbonate, DCM; (b) DAB-dendr-(NH<sub>2</sub>)<sub>*n*</sub>, DCM; (c) 1:2 v/v TFA/DCM; (d) GdCl<sub>3</sub>·6 H<sub>2</sub>O, water or 0.3 M citrate buffer pH 5.8.

Therefore, the amine-functionalized DTPA building block **1** (See Chapter 2, Section 2.2.1) was conveniently reacted with di-*tert*-butyl-tricarbonate in freshly distilled dichloromethane (DCM), affording isocyanate-activated DTPA building block **2**. The reaction of the *tert*-butyl ester-protected DTPA synthon **2** with one of the generations of poly(propylene imine) dendrimers was conducted in DCM. Purification with size-exclusion chromatography yielded the corresponding *tert*-butyl ester-protected DTPA-terminated poly(propylene imine) dendrimers **3<sub>n</sub>**. Structural characterization of **3<sub>n=4</sub>** with <sup>1</sup>H-NMR, <sup>13</sup>C-NMR, and IR spectroscopy and ESI-QTOF spectrometry showed complete

modification of the primary amines of the poly(propylene imine) dendrimer. The inverse-gated decoupled  $^{13}\text{C}$ -NMR spectrum of the first generation DTPA-functionalized poly(propylene imine) dendrimer (*tert*-butyl ester protected)  $\mathbf{3}_{n=4}$  is depicted in Figure 3.2.

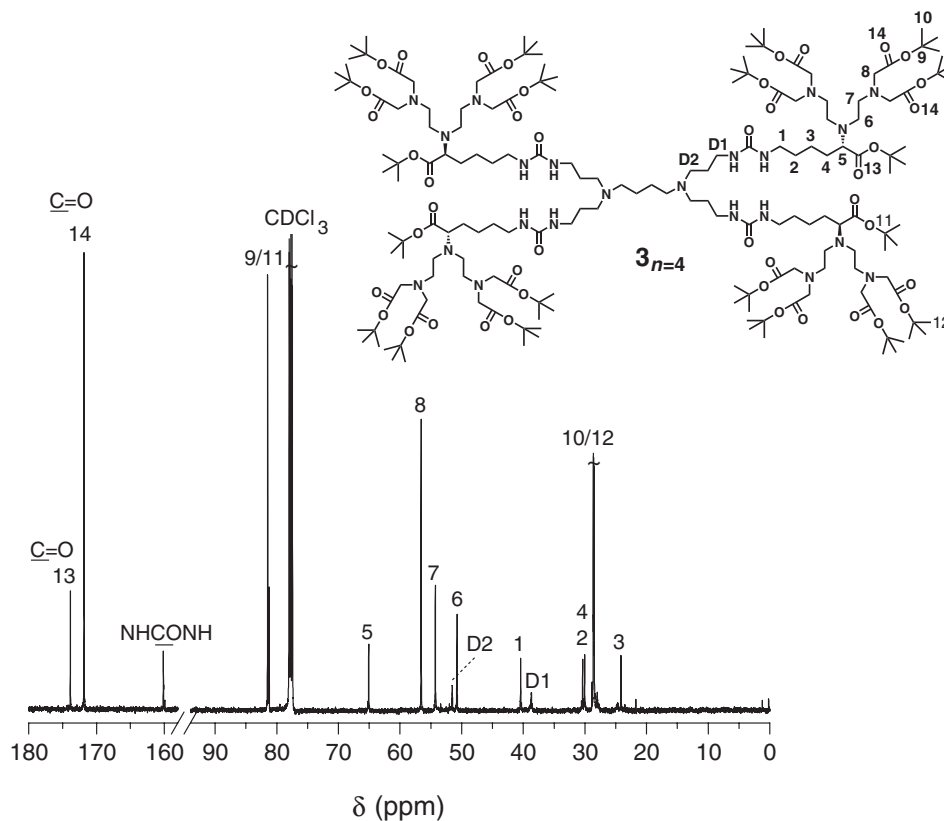


**Figure 3.2** Inverse-gated decoupled  $^{13}\text{C}$ -NMR spectrum of  $\mathbf{3}_{n=4}$  in  $\text{CDCl}_3$ .

The inverse-gated decoupled  $^{13}\text{C}$ -NMR spectrum revealed the presence of three distinct carbonyl carbons. The signals at 173 and 171 ppm were ascribed to the two different carbonyl ester groups in the DTPA part of the molecules. The resonance at 159 ppm belonged to the urea carbonyl atom and confirmed the successful coupling reaction between isocyanate-functionalized DTPA building block  $\mathbf{2}$  and the primary amines of the first generation of the poly(propylene imine) dendrimer. The higher generation dendrimers  $\mathbf{3}_{n=16,64}$  were solely characterized by means of  $^1\text{H}$ -NMR and IR spectroscopy. Mass spectrometry was not successful for  $\mathbf{3}_{n=16,64}$ , probably due to the low degree of ionization of these high molecular weight materials. Cleavage of the *tert*-butyl esters with trifluoroacetic acid (TFA) in DCM afforded water-soluble Gd(III)-chelating dendrimers  $\mathbf{4}_n$ . TFA was successfully removed *via* extensive dialysis and the absence of TFA salts was confirmed with  $^{19}\text{F}$ -NMR. The  $^1\text{H}$ -NMR spectra of  $\mathbf{3}_{n=4}$  and  $\mathbf{4}_{n=4}$  recorded in  $\text{CDCl}_3$  and  $\text{D}_2\text{O}$ , respectively, are shown in Figure 3.3.

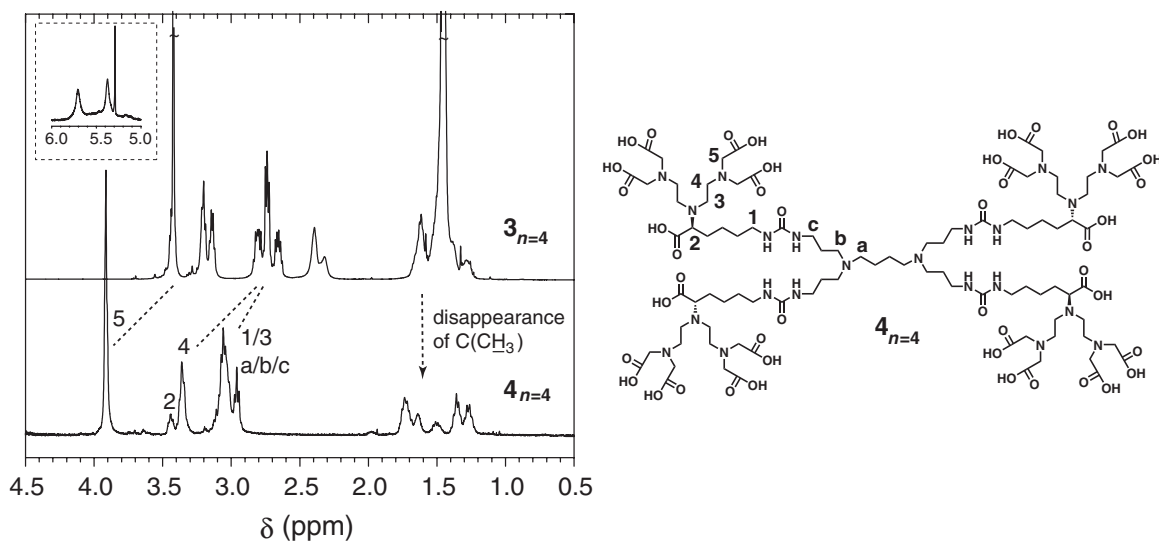


**Figure 3.3**  $^1\text{H-NMR}$  spectra recorded at 500 MHz of  $3_{n=4}$  ( $\text{CDCl}_3$ ) and  $4_{n=4}$  ( $\text{D}_2\text{O}$ ). The inset shows the  $-\text{NH}$  protons of the urea of  $3_{n=4}$ .

The synthesis of the corresponding Gd(III) complexes  $5_n$  was performed either in demineralized water or in a 0.3 M citrate buffer. Excess of (toxic)  $\text{GdCl}_3$  was removed via exhaustive dialysis. Structure elucidation of the Gd(III) complexes by means of  $^1\text{H}$ - and  $^{13}\text{C}$ -NMR spectroscopy was complicated due to the paramagnetic nature of Gd(III). Nevertheless, the formation of the corresponding Gd(III) complexes could be confirmed with IR spectroscopy. The IR spectrum demonstrated that more than 90% of the DTPA chelates were complexated with Gd(III), by the disappearance of the C–O stretching vibration at  $1200\text{ cm}^{-1}$  and the shift of the carbonyl stretch from  $1622\text{ cm}^{-1}$  to  $1586\text{ cm}^{-1}$  (Figure 3.4).

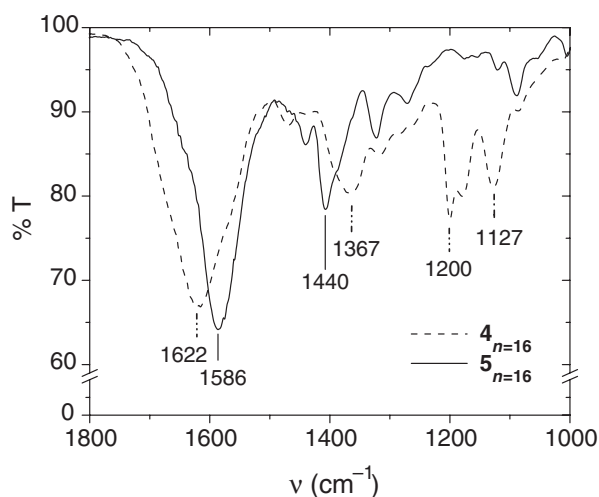


**Figure 3.4** IR spectra of DTPA-terminated dendrimer  $4_{n=16}$  and Gd(III)DTPA-terminated dendrimer  $5_{n=16}$ .

In addition, the Gd(III) content was determined with inductively coupled plasma atomic emission spectroscopy (ICP-AES) analysis. The values for the observed Gd(III) content for  $\mathbf{5}_{n=1,4,16,64}$  were lower than the theoretical values, typically between 70% and 90%. Since IR spectroscopy showed that more than 90% of the DTPA moieties were complexated, and since the ESI-MS data of the amine-terminated poly(propylene imine) dendrimers, used as the starting material, showed very few defects,<sup>27</sup> the deviations in the value for the Gd(III) content were attributed to the presence of water or residual salts. Therefore, we used in our analysis the ideal structure for the dendrimers; *i.e.* the number of end groups equals 4, 16, and 64 for the first, third, and fifth generation of the poly(propylene imine) dendrimer, respectively.

<sup>1</sup>H-NMR spectra of the third and the fifth generation of the DTPA-terminated dendrimer ( $\mathbf{4}_{n=16, 64}$ ) in D<sub>2</sub>O showed a considerable broadening of signals, due to the aggregation of dendrimers. This was attributed to their multiple zwitterionic character, since both acidic groups and basic tertiary amines are present. This aggregation was strongly pH-dependent;  $\mathbf{4}_{n=16}$  was only soluble below pH 2 and above pH 5.5, indicating the presence of an isoelectric point. Complexation of the dendritic ligands with GdCl<sub>3</sub> could lead to aggregation as well, depending on the generation of the dendrimer and the medium. The first-generation dendrimer  $\mathbf{4}_{n=4}$  could be complexed with GdCl<sub>3</sub> in water, whereas  $\mathbf{4}_{n=16}$  and  $\mathbf{4}_{n=64}$  could only be successfully complexed in buffered solutions, *e.g.* 0.3 M citrate buffer at pH 5.8.

### 3.2.2 Cryo-TEM and AFM studies

To exclude self-aggregation of the fifth generation Gd(III)DTPA-terminated dendrimer ( $\mathbf{5}_{n=64}$ ) under the experimental conditions used for the relaxivity measurements, cryo-TEM and AFM experiments were performed in 0.3 M citrate buffer. Cryo-TEM is a powerful technique for the elucidation of structures in their natural hydrated state. Cryo-TEM studies on  $\mathbf{5}_{n=64}$  in 0.3 M citrate buffer at pH 5.8 confirmed the presence of well-defined isolated dendrimers with an approximate diameter of 5–6 nm, and, equally important, no aggregation of the dendrimer  $\mathbf{5}_{n=64}$  was observed (Figure 3.5). The value for the observed diameter is consistent with the calculated value and supported by other literature studies on dendrimers.<sup>28</sup> The contrast of the cryo-TEM image was high (without staining), due to the presence of Gd(III). Topographic AFM images of  $\mathbf{5}_{n=64}$  on a silicon wafer are depicted in Figure 3.6 (*vide infra*). The Gd(III)-loaded dendrimer  $\mathbf{5}_{n=64}$  forms spherical structures on a silicon substrate. Although a constant width of about  $32 \pm 1$  nm for the dendritic structures was found, the measured lateral dimensions are easily overestimated due to tip-convolution effects. Therefore, the values of the measured heights of the structures are a more accurate way to determine the diameter of the structures, especially since soft tapping conditions



were applied. The height of these dendritic structures was deduced from the topographic image and was found to be  $1.3 \pm 0.2$  nm, implying flattening of individual dendrimers on a silicon surface.<sup>29-31</sup>

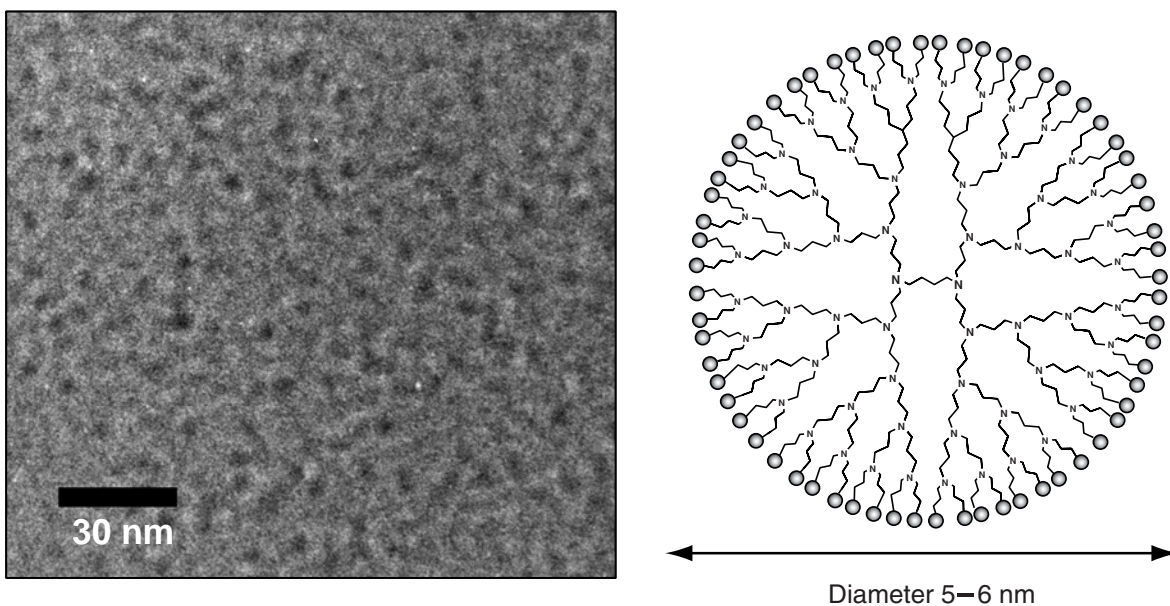


**Figure 3.5** Cryo-TEM image of a  $10^{-4}$  M solution of Gd(III)DTPA-terminated poly(propylene imine) dendrimer  $5_{n=64}$  in 0.3 M citrate buffer, pH 5.8 (magnification of 329,000 $\times$ , without staining).

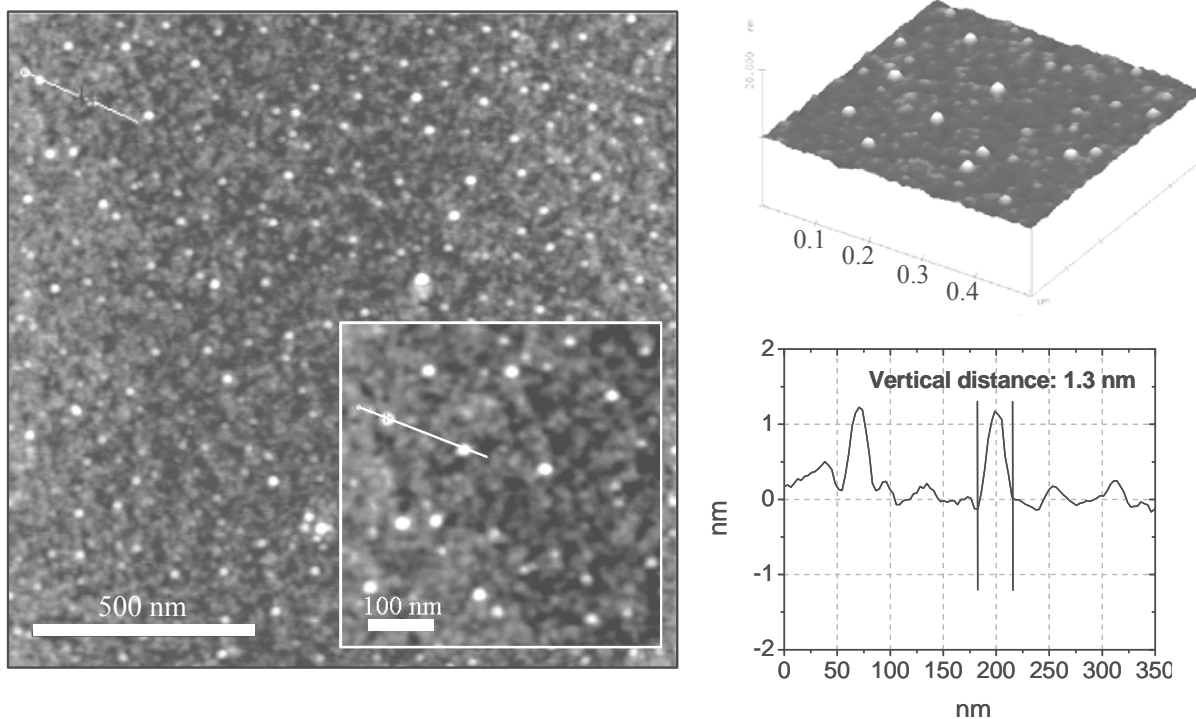


**Figure 3.6** Topographic AFM images of Gd(III)DTPA-terminated poly(propylene imine) dendrimer  $5_{n=64}$  on a silicon wafer.

### 3.2.3 Molecular modeling

Molecular dynamics (MD) simulations for Gd(III)DTPA and different generations of the Gd(III)DTPA-terminated dendrimer in water were carried out to illustrate the effect of varying generation of the dendrimer on the molecular shape. The 3D space filling representation and stick diagram of the different generations of the Gd(III)DTPA-terminated dendrimer are shown in Figure 3.7. The first generation of the dendrimer shows a relatively open structure with a high local degree of flexibility. Higher generations of the dendrimer, however, adopt a globular three-dimensional structure, which results in a more restricted conformation and a higher local concentration of Gd(III) species.

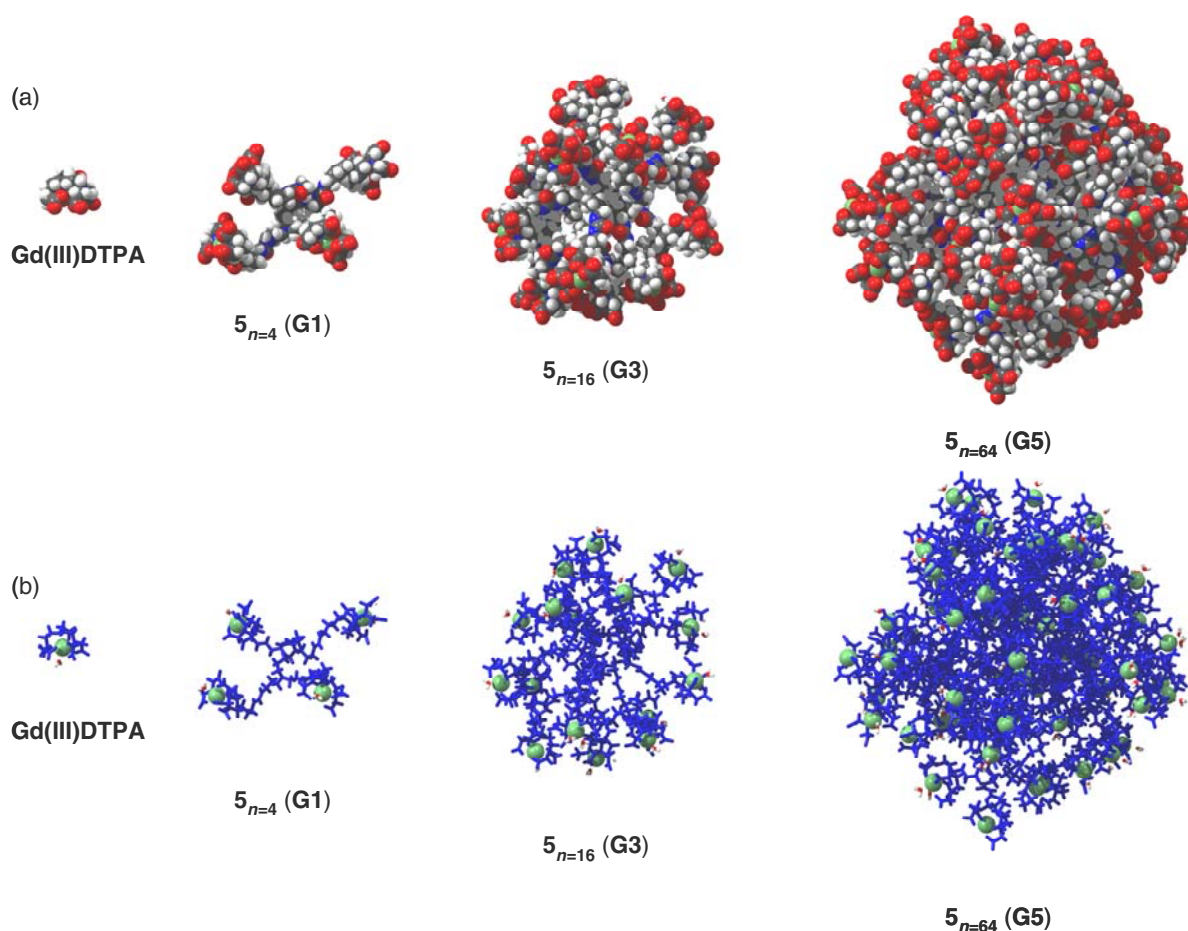


**Figure 3.7** MD simulations of Gd(III)DTPA and different generations of the Gd(III)DTPA-terminated poly(propylene imine) dendrimer in aqueous solution. (a) The 3D-space filling representations illustrate the effect of varying dendrimer generation on the molecular shape (the water molecules are omitted for clarity); (b) the stick diagram representations of the Gd(III)DTPA-terminated poly(propylene imine) dendrimers with the Gd(III) ions depicted as green VanderWaals spheres and the inner-sphere water molecules (the water molecules of the bulk are omitted for clarity).

### 3.2.4 Longitudinal and transverse relaxivities

Longitudinal ( $r_1$ ) and transverse ( $r_2$ ) relaxivities were determined for Gd(III)DTPA-terminated poly(propylene imine) dendrimers by concentration-dependent measurements of the relaxation times in either 0.3 M citrate buffer at pH 5.8 or in water at pH 6.5–7. The data gave good linear fits ( $R^2 > 0.999$ ) to the equation  $(1/T_{1,2})_{\text{observed}} = (1/T_{1,2})_{\text{diamagnetic}} + r_{1,2}[\text{Gd(III)}]$ . Both the  $r_1$  and  $r_2$  were calculated in terms of the actual Gd(III) content as determined by inductively coupled plasma atomic emission spectroscopy (ICP-AES) measurements. The transverse and longitudinal relaxivities of Gd(III)DTPA, Gd(III)DTPA-based complex  $\mathbf{5}_{n=1}$ , and Gd(III)DTPA-terminated poly(propylene imine) dendrimers  $\mathbf{5}_{n=4,16,64}$  are shown in Table 3.1 and Figure 3.8.

**Table 3.1** Ionic and molecular relaxivities of Gd(III)DTPA, Gd(III)DTPA-based complex  $\mathbf{5}_{n=1}$ , and Gd(III)DTPA-terminated poly(propylene imine) dendrimers  $\mathbf{5}_{n=4,16,64}$  in 0.3 M citrate buffer at pH 5.8. <sup>a</sup>

	Ionic $r_1^b$ ( $\text{mM}^{-1}\text{s}^{-1}$ )	Ionic $r_2^b$ ( $\text{mM}^{-1}\text{s}^{-1}$ )	Ratio $r_2/r_1$	Theoretical no. Gd ions	Mol. $r_1$ ( $\text{mM}^{-1}\text{s}^{-1}$ ) <sup>c</sup>	Mol. $r_2$ ( $\text{mM}^{-1}\text{s}^{-1}$ ) <sup>c</sup>	MW ( $\text{kg}\cdot\text{mol}^{-1}$ )
Gd(III)DTPA	$5.9 \pm 0.1$	$6.5 \pm 0.1$	1.1	1	$5.9 \pm 0.1$	$6.5 \pm 0.1$	0.6
$\mathbf{5}_{n=1}$	$11.2 \pm 0.2$	$11.9 \pm 0.2$	1.1	1	$11.2 \pm 0.2$	$11.9 \pm 0.2$	0.7
$\mathbf{5}_{n=4}$ ( <b>G1</b> )	$13.2 \pm 0.2$	$13.9 \pm 0.2$	1.1	4	$52.8 \pm 0.8$	$55.6 \pm 0.8$	3.1
$\mathbf{5}_{n=16}$ ( <b>G3</b> )	$16.1 \pm 0.2$	$19.7 \pm 0.5$	1.2	16	$258 \pm 4$	$315 \pm 8.0$	12.7
$\mathbf{5}_{n=64}$ ( <b>G5</b> )	$19.5 \pm 0.3$	$27.7 \pm 0.8$	1.4	64	$1248 \pm 20$	$1772 \pm 52$	51.2

<sup>a</sup> Measured with MR spectroscopy at 1.5 T and 20°C (inversion recovery pulse sequence).<sup>32</sup>

<sup>b</sup> The ionic relaxivity is defined as the relaxivity per Gd(III).

<sup>c</sup> The maximum molecular relaxivity (mol.  $r_{i=1,2}$ ) is defined as the ionic relaxivity multiplied with the theoretical number of Gd(III) moieties attached to a single dendrimer.

The observed values for the ionic  $r_1$  in water for Gd(III)DTPA,  $\mathbf{5}_{n=1}$ , and  $\mathbf{5}_{n=4}$  (**G1**), were 4.2, 8.3, and 11.7  $\text{mM}^{-1}\text{s}^{-1}$ , respectively. These values were significantly lower than the corresponding relaxivities measured in 0.3 M citric acid buffer at pH 5.8, which might be attributed to differences in the ionic strength or the viscosity of the solution. Higher generations of Gd(III)DTPA-terminated poly(propylene imine) dendrimers displayed strongly increased relaxivities (both  $r_1$  and  $r_2$ ) compared to Gd(III)DTPA, even when expressed per Gd(III) (Figure 3.8). The fifth generation of the dendritic MRI contrast agent displayed the highest ionic relaxivities, ionic  $r_1 = 19.5 \text{ mM}^{-1}\text{s}^{-1}$  and ionic  $r_2 = 27.7 \text{ mM}^{-1}\text{s}^{-1}$ . These values were substantially higher than the relaxivities of parent Gd(III)DTPA (Table 3.1 and Figure 3.8).

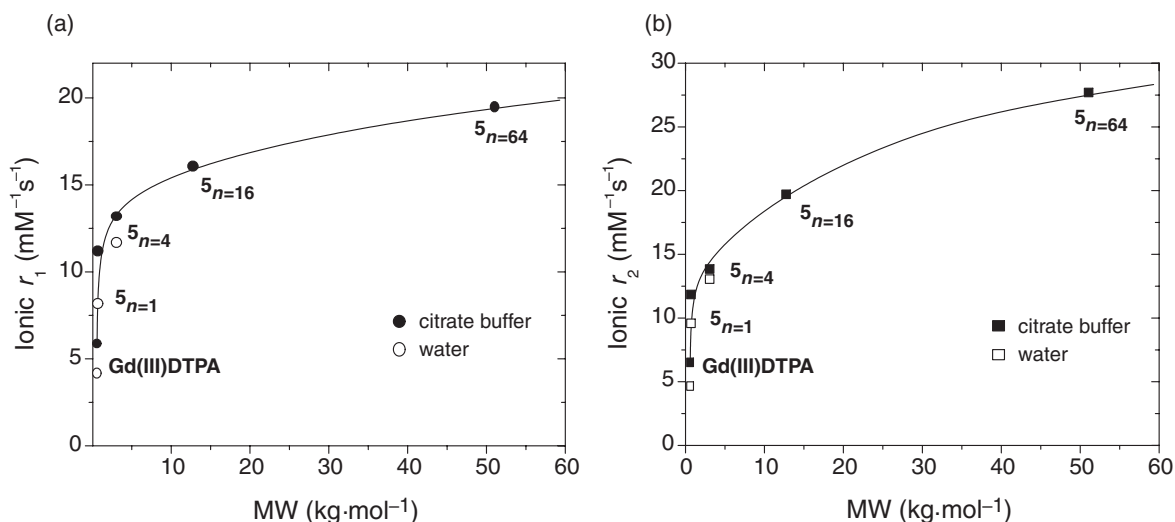


**Figure 3.8** Ionic relaxivities of Gd(III)DTPA, Gd(III)DTPA-based complex  $5_{n=1}$ , and different generations of Gd(III)DTPA-based dendrimers ( $5_{n=4,16,64}$ ) in water or 0.3 M citric acid buffer at pH 5.8 (1.5 T and 20°C). (a) Ionic  $r_1$  versus theoretical molecular weight; (b) ionic  $r_2$  versus theoretical molecular weight. A solid line is drawn to guide the eye.

In addition, the  $r_2/r_1$  ratio increased from 1.1 to 1.4 on going to higher generations of the dendrimer. The molecular relaxivity, defined as the ionic relaxivity multiplied by the theoretical number of Gd(III) moieties attached to a single dendrimer, increased exponentially upon going to higher generation of the dendrimer (Table 3.1 and Figure 3.9).

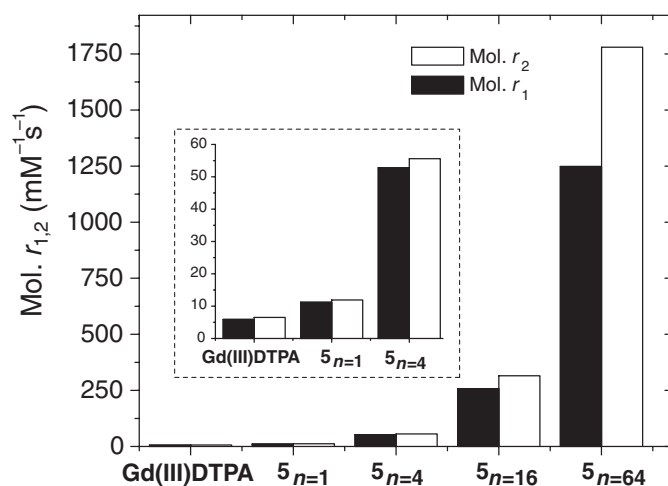


**Figure 3.9** Molecular relaxivities of different generations of the Gd(III)DTPA-terminated dendrimer in citrate buffer at pH 5.8. The maximum molecular relaxivity is defined as the ionic relaxivity multiplied by the theoretical number of Gd(III) moieties attached to a single dendrimer. The inset shows the expansion of the molecular relaxivity for Gd(III)DTPA, Gd(III)DTPA-based complex  $5_{n=1}$  and the first generation Gd(III)DTPA-based dendrimer  $5_{n=4}$ .

The relaxivities and effective loading of Gd(III) of the fifth generation dendritic contrast agent  $\mathbf{5}_{n=64}$  were considerably higher compared with those of linear macromolecular analogues.<sup>12</sup> The observed gain of the ionic relaxivity for the higher generations of dendrimers was in agreement with reported literature data,<sup>16,21</sup> implying there is an influence of the molecular weight and/or the local mobility of the Gd(III) complexes. Furthermore, “saturation” of the ionic relaxivity upon increasing generation of the Gd(III)DTPA-terminated poly(propylene imine) dendrimer was observed in contrast to the reported study of Kobayashi *et al.*<sup>18</sup> In their work, the Gd(III)DTPA-chelating moiety is attached to the dendrimer through a short, rigid linker. The longitudinal ionic relaxivity of their fifth generation dendritic contrast agent (ionic  $r_1 = 29 \text{ mM}^{-1}\text{s}^{-1}$  at 1.5 T) is higher than the longitudinal ionic relaxivity for  $\mathbf{5}_{n=64}$  found in this study (ionic  $r_1 = 19.5 \text{ mM}^{-1}\text{s}^{-1}$ ). In the system presented here, the Gd(III)DTPA complex is covalently linked to the poly(propylene imine) dendrimer through a more flexible linker. Consequently, the local mobility of the Gd(III) complex is relatively high and segmental motions of the flexible linker might dominate the rotational correlation time, thereby limiting a further gain in relaxivity.<sup>19</sup>

### 3.3 COMBINED Y(III)DTPA- AND Gd(III)DTPA-BASED DENDRITIC CONTRAST AGENTS

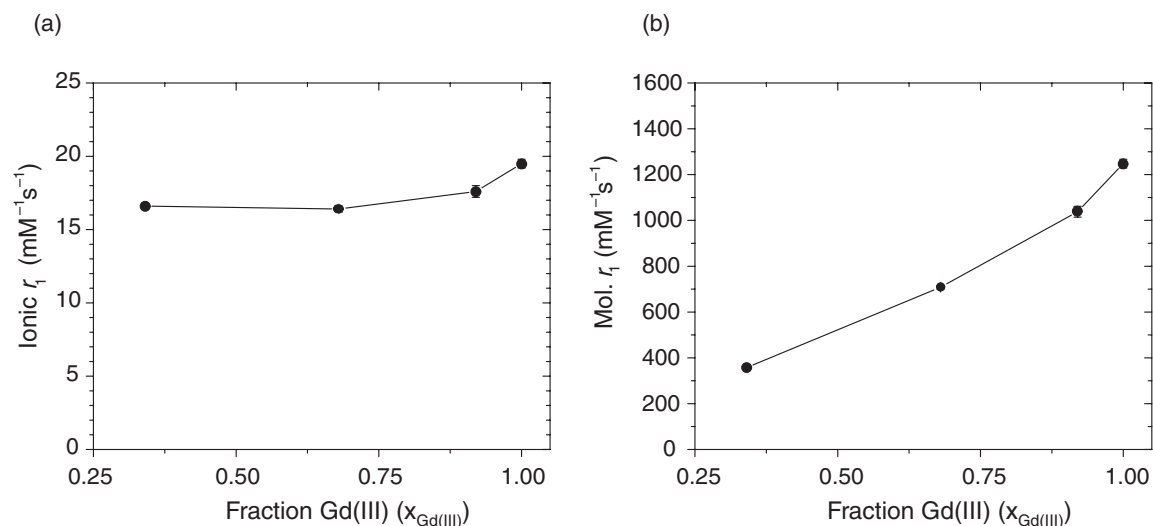
An additional contribution to the longitudinal relaxivity may arise from paramagnetic interactions between Gd(III) moieties, due to the high local concentration of paramagnetic species at the periphery. Recently, Merbach *et al.* have seen an enhanced electronic relaxation for Gd(III) in a binuclear complex, which may prevent the increase of the longitudinal relaxivity for macromolecular systems with a fast water exchange.<sup>33</sup> Therefore, a series of combined Gd(III) and yttrium(III) complexes of the fifth generation DTPA-terminated poly(propylene imine) dendrimer was prepared, varying the ratio between Y(III)DTPA- and Gd(III)DTPA-based complexes along the periphery. Y(III) was used as a diamagnetic probe with a size similar to that of Gd(III), thus keeping the packing density and the molecular weight comparable. IR spectroscopy data confirmed the formation of the corresponding complexes based on the diagnostic shift of the carbonyl stretches to  $1582\text{--}1583 \text{ cm}^{-1}$ . The Gd(III) and Y(III) contents were independently determined by means of ICP-AES analysis. From these values, the fraction of Gd(III) ( $x_{Gd}$ ) was calculated. It was found that Gd(III) was preferentially incorporated. The ionic  $r_1$  was calculated in terms of Gd(III) concentration.

**Table 3.2** Longitudinal relaxivities ( $r_1$ ) of combined Y(III)DTPA- and Gd(III)DTPA-based dendritic contrast agents of the fifth generation dendrimer (G5-mixed).<sup>a,b</sup>

	Fraction of Gd(III) ( $x_{Gd}$ )	Ionic $r_1$ ( $\text{mM}^{-1}\text{s}^{-1}$ )	Average no. of Gd(III) ions <sup>b</sup>	Average no. of Y(III) ions <sup>b</sup>	Mol. $r_1$ <sup>b</sup> ( $\text{mM}^{-1}\text{s}^{-1}$ )	MW ( $\text{kg}\cdot\text{mol}^{-1}$ )
G5-mixed-A	0.34	$16.6 \pm 0.2$	21.8	42.2	$362 \pm 5$	48.3
G5-mixed-B	0.68	$16.4 \pm 0.2$	43.5	20.5	$713 \pm 9$	49.8
G5-mixed-C	0.92	$17.7 \pm 0.4$	58.9	5.0	$1043 \pm 24$	50.9
<b><math>5_n=64</math> (G5)</b>	1.00	$19.5 \pm 0.3$	64.0	0	$1248 \pm 20$	51.2

<sup>a</sup> Measured in 0.3 M citrate buffer at pH 5.8 (MR spectroscopy, inversion-recovery sequence at 1.5 T, 20°C).

<sup>b</sup> From the fraction of Gd(III) ( $x_{Gd}$ ) and the theoretical number of end groups for the fifth generation DTPA-terminated dendrimer ( $n=64$ ), the average number of Gd(III) moieties per dendrimer and the average number of Y(III) moieties per dendrimer were calculated. Multiplication of the average number of Gd(III) moieties by the longitudinal ionic relaxivity (ionic  $r_1$ ) gives the maximum molecular relaxivity (mol.  $r_1$ ).

**Figure 3.10** Longitudinal relaxivities of combined Y(III)DTPA- and Gd(III)DTPA-based dendritic MRI contrast agents of the fifth generation poly(propylene imine) dendrimer. (a) Ionic  $r_1$  versus the fraction of Gd(III); (b) molecular  $r_1$  against the fraction of Gd(III).

As shown in Table 3.2 and Figure 3.10, the ionic  $r_1$  increases with increasing fraction of Gd(III) ( $x_{Gd}$ ), accompanied by a minor increase in the molecular weight. Furthermore, the molecular  $r_1$  increases from  $362 \text{ mM}^{-1}\text{s}^{-1}$  to  $1248 \text{ mM}^{-1}\text{s}^{-1}$ . The observed gain in ionic  $r_1$  is more distinct at higher loadings of Gd(III) and can be explained neither in terms of differences molecular weight nor in terms of packing density. This effect is attributed to magnetic interactions between Gd(III) moieties and is a direct result of the high local concentration of Gd(III)DTPA end groups on a single dendrimer, giving rise to a *dendritic effect*.

### 3.4 PARTIALLY FUNCTIONALIZED Gd(III)DTPA-BASED DENDRITIC CONTRAST AGENTS

In Section 3.3, the effect of the Gd(III) density on the ionic  $r_1$  was investigated by varying the Gd(III) to Y(III) ratio at the periphery of the dendrimer, while keeping the molecular weight nearly constant. An alternative approach to study the effect of the Gd(III) density on the ionic  $r_1$  involves the synthesis of partially functionalized Gd(III)DTPA-based dendrimers possessing a statistical distribution of MRI labels at the periphery. Therefore, amine-terminated poly(propylene imine) dendrimers were functionalized with on average two Gd(III)DTPA complexes per dendrimer, while the residual amines were acetylated. The synthesis of Gd(III)DTPA-terminated dendrimer **9** started with the reaction of isocyanate **2** with an 8-fold excess of the third generation amine-terminated poly(propylene imine) dendrimer (Figure 3.11). Subsequently, the residual amine-functionalities of dendrimer **6** were acetylated with acetic anhydride. Purification of the crude mixture with an ion-exchange column yielded dendrimer **7**. The average number of DTPA units per dendrimer of  $2.2 \pm 0.7$  was deduced from the  $^1\text{H-NMR}$  spectrum. Cleavage of the *tert*-butyl esters was accomplished with TFA in DCM. The quantitative removal of the *tert*-butyl ester groups was verified with  $^1\text{H-NMR}$  spectroscopy in  $\text{D}_2\text{O}$ .

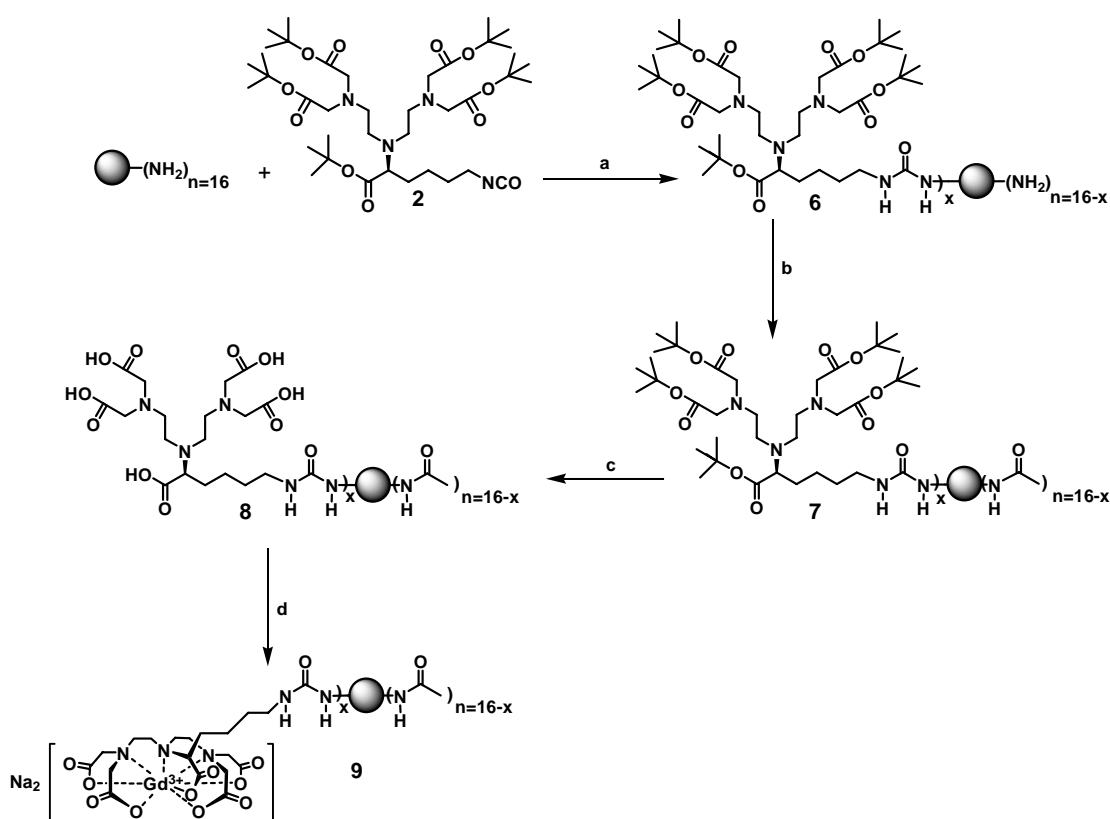


**Figure 3.11** Synthesis of Gd(III)DTPA-terminated dendrimer **9** (randomly functionalized).  $x$  denotes the average number of Gd(III)DTPA moieties per dendrimer, where  $n=16-x$  equals the average number of acetyl moieties per dendrimer. (a) DCM; (b) acetic anhydride,  $\text{NEt}_3$ , MeOH; (c) 1:2 v/v TFA/DCM; (d)  $\text{GdCl}_3 \cdot 6 \text{H}_2\text{O}$ , water, pH 7.

The corresponding Gd(III) complex **9** was obtained by adding GdCl<sub>3</sub> to an aqueous solution of dendrimer **8**, while maintaining the pH at 7. Additional purification by dialysis (0.5 kDa MWCO membrane) in demineralized water and freeze-drying yielded Gd(III) complex **9**. The ionic  $r_1$  of dendrimer **9** was  $14.2 \pm 0.2 \text{ mM}^{-1}\text{s}^{-1}$  in citrate buffer at pH 5.8 (Figure 3.12a), and was slightly higher in comparison with the ionic  $r_1$  of the first generation of the Gd(III)DTPA-terminated dendrimer  $5_{n=4}$  (Figure 3.12b)

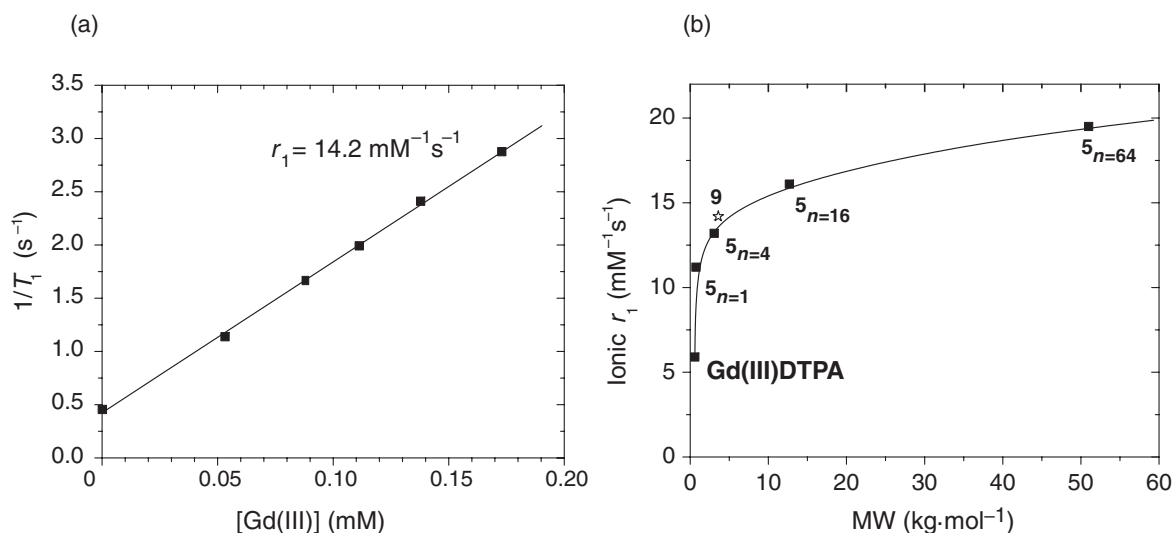


**Figure 3.12** (a) Longitudinal relaxation rate ( $1/T_1$ ) versus the Gd(III) concentration of dendrimer **9** in citrate buffer at pH 5.8. (b) Longitudinal ionic relaxivities of Gd(III)DTPA-based complexes versus the theoretical molecular weight.

The ionic  $r_1$  of **9** lies in between  $5_{n=4}$  and  $5_{n=16}$ , while the molecular weight of **9** is slightly higher than  $5_{n=4}$  its Gd(III) density at the periphery of the dendrimer is less than that of  $5_{n=16}$ . It seems that the Gd(III) density along the periphery of dendrimer **9** has a negligible effect on the ionic  $r_1$ , but that the ionic  $r_1$  of **9** is predominantly determined by the molecular weight of the MRI contrast agent.



### 3.5 CONCLUSIONS

A convenient methodology has been presented for the synthesis of Gd(III)DTPA-terminated poly(propylene imine) dendrimers as contrast agents for MR imaging. AFM and cryo-TEM images of the fifth generation Gd(III)DTPA-terminated dendrimer in citrate buffer showed the presence of spherical particles with nanoscopic dimensions. Both the longitudinal ( $r_1$ ) and the transverse ( $r_2$ ) relaxivities increases considerably on going to higher generations of the Gd(III)DTPA-terminated dendrimer. Additionally, a series of combined Gd(III) and Y(III) complexes of the fifth generation DTPA-terminated dendrimer showed a significant increase of the longitudinal ionic relaxivity on going to higher fractions of Gd(III). This effect is attributed to magnetic interactions between Gd(III) moieties and is a direct result of the high local concentration of Gd(III)DTPA end groups on a single dendrimer, giving rise to a *dendritic effect*.

### 3.6 EXPERIMENTAL

#### *General procedures*

Unless stated otherwise, all reagents and chemicals were obtained from commercial sources and used without further purification. Water was demineralized prior to use. DCM was obtained by distillation from P<sub>2</sub>O<sub>5</sub>. Amine-terminated poly(propylene imine) dendrimers (DAB-*dendr*-(NH<sub>2</sub>)<sub>n</sub>, n=4, 16, and 64) were obtained from SyMO-Chem BV (Eindhoven, the Netherlands) and dried prior to use. Di-*tert*-butyl tricarbonate was prepared according to the procedure described by Peerlings *et al.*<sup>34</sup> Preparative size exclusion chromatography was performed on BIORAD Bio-Beads S-X1 swollen in DCM. <sup>1</sup>H-NMR, <sup>13</sup>C-NMR and <sup>19</sup>F-NMR spectra were recorded on a Varian Gemini-2000 300 MHz spectrometer, a Varian Mercury Vx 400 MHz spectrometer and a Varian Unity Inova 500 MHz spectrometer at 298 K. Chemical shifts are given in parts per million ( $\delta$ ) values. Infrared spectra were recorded at 298 K on a Perkin-Elmer 1605 FT-IR spectrophotometer. MALDI-TOF spectra were obtained on a Perspective Biosystems Voyager DE-Pro MALDI-TOF spectrometer using  $\alpha$ -cyano-4-hydroxycinnamic acid as matrix (University of California, Berkeley, USA). ESI-QTOF-MS experiments were recorded on a Q-TOF Ultima GLOBAL mass spectrometer (Micromass, Manchester, U.K.).

#### *Atomic Force Microscopy (AFM)*

Samples for the atomic force microscopy (AFM) study were prepared by drop casting 0.2  $\mu$ M of **5<sub>n=64</sub>** in 0.3 M citrate buffer onto silicon wafers. Control experiments in the absence of the dendrimer were performed as well. AFM images were recorded under ambient conditions using a Digital Instrument Multimode Nanoscope IIIA operating in the tapping mode regime. Microfabricated silicon cantilever tips (NSG01) with a resonance frequency of approximately 150 kHz and a spring constant of about 5.5 Nm<sup>-1</sup> were used. The set-point amplitude ratio ( $r_{sp} = A_{sp}/A_0$ , where  $A_{sp}$  is the amplitude set point, and  $A_0$  is the amplitude of the free oscillation) was adjusted to 0.9. The scan rate varied from 0.5 to 1.5 Hz. All AFM images shown here were subjected to a first-order plane-fitting procedure to compensate for sample tilt. AFM cross-sections analysis was done off-line.

#### *Cryogenic Transmission Electron Microscopy (cryo-TEM)*

Cryo-TEM measurements were performed on vitrified films of the fifth generation dendrimer **5<sub>n=64</sub>** in 0.3 M citric acid buffer at pH 5.8. Thin films of the solutions were prepared in a “Vitrobot” instrument.<sup>35</sup> In the preparation chamber of the Vitrobot a 3  $\mu$ L sample was applied on a Quantifoil grid (holey carbon film R2/2, Quantifoil Micro Tools GmbH; freshly glow discharged prior to use) at room temperature, excess of liquid was blotted away and the thin film thus formed was plunged into a reservoir of melting ethane. The vitrified film was transferred to a cryo-holder and observed in a Philips CM12 microscope at -170 °C (operating at 120 kV).

#### *Molecular dynamics simulations*

Molecular dynamics simulations were performed using NAMD 2.5.<sup>36</sup> The molecular models of the simulated Gd(III)DTPA-terminated poly(propylene imine) dendrimers were built using Accelrys Materials Studio 2.0 and software developed in house, and were converted into appropriate input files for NAMD using X-PLOR (online) 3.851.<sup>37</sup> Initial configurations of the molecular systems were generated by placing a dendrimer in an equilibrated water cube (TIPS3P water model), followed by removal of overlapping water molecules. To ensure an overall net charge of zero, sodium ions were added using VMD.<sup>38</sup> Periodic boundary conditions were applied and after minimization of the molecular systems, the resulting initial configurations

were then subjected to molecular dynamics simulations for time period of 10 ns (time step = 2 fs). The temperature was thermostatted at 300 K during the simulations using temperature rescaling, while pressure was maintained at 1 bar using the Berendsen pressure coupling.<sup>39</sup>

### Relaxivity Measurements

NMR relaxation measurements in 0.3 M citrate buffer were performed on a Gyroscan S15/ACS 1.5 T clinical MR system (Philips Medical Systems, Best, the Netherlands), using an 8 cm diameter surface coil. Solutions of dendritic MRI contrast agents were prepared in 0.3 M citrate buffer at pH 5.8 with a Gd(III) concentration ranging from 0.05–1.0 mM. For each measurement, one of the samples was positioned in the center of the coil. Standard spin-echo MR images were obtained for accurate localization. Localized <sup>1</sup>H-NMR spectra were recorded by using Point Resolved Spectroscopy (PRESS)<sup>40</sup> with 16 acquisitions and 16 phase-rotation steps. Voxel dimensions were 10 × 10 × 10 mm<sup>3</sup>. Longitudinal relaxation times (*T*<sub>1</sub>) were determined with an inversion recovery pulse sequence using 10 different inversion times. The echo time (TE) was set at 40 ms and the repetition time (TR) was at least 5 times larger than the estimated *T*<sub>1</sub> for each sample. Transverse relaxation times (*T*<sub>2</sub>) were determined by varying the PRESS echo time (10 measurements for each *T*<sub>2</sub> determination). In this case the TR was set at 1500 ms. NMR relaxation measurements in water at pH 6–7 were performed with a 2D-mixed dual-echo sequence (See Chapter 2). All relaxation measurements were performed for circular regions of interest of (area, 150 ± 10 mm<sup>2</sup>) positioned centrally each sample. The slopes of 1/*T*<sub>1</sub>, 1/*T*<sub>2</sub> versus the Gd(III) concentration were calculated (*r*<sub>1</sub>, *r*<sub>2</sub>), and the ratios *r*<sub>2</sub>/*r*<sub>1</sub> were determined for Gd(III)DTPA-terminated dendrimers. The Gd(III) concentration of the solutions used for the relaxivity measurements was determined by means of Inductively Coupled Plasma Atomic Emission (ICP-AES) analysis at 342.247 nm (Leeman Labs Echelle Unicam 701 emission spectrometer, TNO, Eindhoven, the Netherlands).

### Modification of poly(propylene imine) dendrimers with DTPA building blocks (tert-butyl ester protected) (3<sub>*n*</sub>)

**3<sub>*n*=4</sub> (G1).** A stirred solution of **1** (0.29 g, 0.40 mmol) in dry DCM (4 mL) was injected into a solution of di-*tert*-butyl tricarbonate (0.116 g, 0.44 mmol) in DCM (3.0 mL) under an argon atmosphere. The solution was stirred for 40 min and continuously purged with argon. IR spectroscopy of the colorless solution showed the appearance of the characteristic isocyanate vibration at 2272 cm<sup>-1</sup>. Residual di-*tert*-butyl tricarbonate was removed by adding two droplets of dry pyridine. The solution of **2** in DCM (4 mL) was slowly added to DAB-*dendr*-(NH<sub>2</sub>)<sub>4</sub> (29.4 mg, 0.093 mmol) in dry DCM (3 mL). The course of the reaction was monitored with IR spectroscopy, and the solution was vigorously stirred for 16 h. The solution was concentrated *in vacuo* and the residue was purified with preparative size exclusion chromatography (Biobeads S-X1 column). The fractions were collected and concentrated *in vacuo* to give **3<sub>*n*=4</sub>** (0.208 g, 0.061 mmol, 66%) as a very viscous yellow oil. Thin layer chromatography showed one spot (MeOH/DCM, 1/9, *v/v*). <sup>1</sup>H-NMR (CDCl<sub>3</sub>): δ 5.72 (br, 4H, NH), 5.37 (br, 4H, NH), 3.42 (s, 32H, NCH<sub>2</sub>COOC(CH<sub>3</sub>)<sub>3</sub>), 3.36–3.06 (m, 20H, CONH(CH<sub>2</sub>)<sub>4</sub>CHN {4H} + CH<sub>2</sub>CH<sub>2</sub>NHCO {8H} + CONHCH<sub>2</sub> {8H}), 2.86–2.50 (m, 32H, NCH<sub>2</sub>CH<sub>2</sub>N {16H} + NCH<sub>2</sub>CH<sub>2</sub>N {16H}), 2.39 (br, 8H, NCH<sub>2</sub>(CH<sub>2</sub>)<sub>2</sub>N), 2.30 (br, 4H, NCH<sub>2</sub>(CH<sub>2</sub>)<sub>2</sub>CH<sub>2</sub>N), 1.66–1.24 (m, 36 H, CONHCH<sub>2</sub>CH<sub>2</sub>(CH<sub>2</sub>)<sub>2</sub>CHN {24H} + NCH<sub>2</sub>CH<sub>2</sub>CH<sub>2</sub>N {8H} + NCH<sub>2</sub>(CH<sub>2</sub>)<sub>2</sub>CH<sub>2</sub>N {4H}; s, 180H, COOC(CH<sub>3</sub>)<sub>3</sub>). The assignment of the <sup>1</sup>H-NMR spectrum is confirmed by <sup>1</sup>H,<sup>1</sup>H-COSY. <sup>13</sup>C-NMR (CDCl<sub>3</sub>): δ = 172.9 (4C, C=O), 170.9 (16C, C=O), 159.3 (4C, NHCONH), 81.0 (20C, C(CH<sub>3</sub>)<sub>3</sub>), 64.7 (4C, CONH(CH<sub>2</sub>)<sub>4</sub>CHN), 56.2 (16C, NCH<sub>2</sub>COOC(CH<sub>3</sub>)<sub>3</sub>), 54.0 (8C, NCH<sub>2</sub>CH<sub>2</sub>N), 53.6 (2C, NCH<sub>2</sub>(CH<sub>2</sub>)<sub>2</sub>CH<sub>2</sub>N), 51.2 (4C, NCH<sub>2</sub>(CH<sub>2</sub>)<sub>2</sub>N), 50.5 (8C, NCH<sub>2</sub>CH<sub>2</sub>N), 40.2 (4C, CONHCH<sub>2</sub>(CH<sub>2</sub>)<sub>3</sub>), 38.5 (4C, N(CH<sub>2</sub>)<sub>2</sub>CH<sub>2</sub>N), 30.2–28.7 (10C, NHCOCH<sub>2</sub>CH<sub>2</sub>CH<sub>2</sub>CH<sub>2</sub> {8C} + NCH<sub>2</sub>(CH<sub>2</sub>)<sub>2</sub>CH<sub>2</sub>N {2C}), 28.4 (60C, C(CH<sub>3</sub>)<sub>3</sub>), 24.0 (4C,

CONH(CH<sub>2</sub>)<sub>2</sub>CH<sub>2</sub>). FT-IR (ATR):  $\nu$  (cm<sup>-1</sup>) 3360 (NH stretch), 2977, 2933, 1722 (C=O stretch), 1641 (C=O amide I stretch), 1563 (C=O amide II stretch), 1457, 1367, 1250, 1219, 1144 (C–O stretch). ESI-QTOF-MS:  $m/z$  [C<sub>172</sub>H<sub>320</sub>N<sub>22</sub>O<sub>44</sub> + H]<sup>+</sup> Calcd. 3400.5 Da; Obsd. 3400.0 Da; [C<sub>172</sub>H<sub>320</sub>N<sub>22</sub>O<sub>44</sub> + Na]<sup>+</sup> Calcd. 3422.34 Da; Obsd. 3422.0 Da; [C<sub>172</sub>H<sub>320</sub>N<sub>22</sub>O<sub>44</sub> + 2Na]<sup>+</sup> Calcd. 3444.3 Da; Obsd. 3444.0 Da.

**3<sub>n=16</sub> (G3)**. A stirred solution of **1** (0.776 g, 1.04 mmol) in dry DCM (8 mL) was injected into a solution of di-*tert*-butyl tricarboxylate (0.301 g, 1.15 mmol) in DCM (6.0 mL) under an argon atmosphere. The solution was stirred for 60 min and continuously purged with argon. IR spectroscopy of the colorless solution showed the appearance of the characteristic isocyanate vibration at 2272 cm<sup>-1</sup>. Residual di-*tert*-butyl tricarboxylate was removed by adding two droplets of dry pyridine. The solution of **2** in DCM (14 mL) was slowly added to DAB-*dendr*-(NH<sub>2</sub>)<sub>16</sub> (89.5 mg, 0.053 mmol) in dry DCM (3 mL). The course of the reaction was monitored with IR spectroscopy, and the solution was vigorously stirred for 16 h. The solution was concentrated *in vacuo* and the residue was purified with preparative size exclusion chromatography (Biobeads S-X1 column in DCM). The fractions were collected and concentrated *in vacuo* to give **3<sub>n=16</sub>** (55%, 0.407 g, 0.029 mmol) as a very viscous yellow oil. <sup>1</sup>H-NMR (CDCl<sub>3</sub>):  $\delta$  = 6.0–5.3 (br m, 32H, NHCONH), 3.38 (s, 128H, NCH<sub>2</sub>COOC(CH<sub>3</sub>)<sub>3</sub>), 3.16–3.05 (m, 80H, CONH(CH<sub>2</sub>)<sub>4</sub>CHN {16H} + CH<sub>2</sub>CH<sub>2</sub>NHCO {32H} + CONHCH<sub>2</sub> {32H}), 2.80–2.55 (m, 128H, NCH<sub>2</sub>CH<sub>2</sub>N {64H} + NCH<sub>2</sub>CH<sub>2</sub>N {64H}), 2.35–2.10 (br, 84H, NCH<sub>2</sub>(CH<sub>2</sub>)<sub>2</sub>CH<sub>2</sub>N {80H} + NCH<sub>2</sub>(CH<sub>2</sub>)<sub>2</sub>CH<sub>2</sub>N {4H}), 1.7–1.1 (m, 100 H, CONHCH<sub>2</sub>CH<sub>2</sub>(CH<sub>2</sub>)<sub>2</sub>CHN {72H} + NCH<sub>2</sub>CH<sub>2</sub>CH<sub>2</sub>N {24H} + NCH<sub>2</sub>(CH<sub>2</sub>)<sub>2</sub>CH<sub>2</sub>N {4H}); s, 720 H, COOC(CH<sub>3</sub>)<sub>3</sub>. FT-IR (ATR):  $\nu$  (cm<sup>-1</sup>) 3364 (NH stretch), 2977, 2934, 1726 (C=O stretch), 1647 (C=O amide I stretch), 1553 (C=O amide II stretch), 1457, 1367, 1253, 1220, and 1150 (C–O stretch).

**3<sub>n=64</sub> (G5)**. A stirred solution of **1** (0.783 g, 1.05 mmol) in dry DCM (6 mL) was injected into a solution of di-*tert*-butyl tricarboxylate (0.330 g, 1.26 mmol) in DCM (6.5 mL) under an argon atmosphere. The solution was stirred for 60 min and continuously purged with argon. IR spectroscopy of the colorless solution showed the appearance of the characteristic isocyanate vibration at 2272 cm<sup>-1</sup>. Residual di-*tert*-butyl tricarboxylate was removed by adding three droplets of dry pyridine. The solution of **2** in DCM (13 mL) was slowly added to DAB-*dendr*-(NH<sub>2</sub>)<sub>64</sub> (94.3 mg, 0.013 mmol) in dry DCM (5 mL). The course of the reaction was monitored with IR spectroscopy and the solution was vigorously stirred for 16 h. The solution was concentrated *in vacuo* and the residue was purified with preparative size exclusion chromatography (Biobeads S-X1 column in DCM). The fractions were collected and concentrated *in vacuo* to give **3<sub>n=64</sub>** (61%, 0.446 g, 7.89  $\mu$ mol) as a very viscous yellow oil. The <sup>1</sup>H-NMR spectrum showed considerable broadening of peaks. Typical absorptions in the <sup>1</sup>H-NMR spectrum are listed below. <sup>1</sup>H-NMR (CDCl<sub>3</sub>):  $\delta$  = 6.4–5.4 (NHCONH), 3.6–3.3 (NCH<sub>2</sub>COOC(CH<sub>3</sub>)<sub>3</sub>), 3.3–2.9 (CONH(CH<sub>2</sub>)<sub>4</sub>CHN + CH<sub>2</sub>CH<sub>2</sub>NHCO + CONHCH<sub>2</sub>), 2.9–2.6 (NCH<sub>2</sub>CH<sub>2</sub>N), 2.6–2.2 (NCH<sub>2</sub>(CH<sub>2</sub>)<sub>2</sub>CH<sub>2</sub>N + NCH<sub>2</sub>(CH<sub>2</sub>)<sub>2</sub>CH<sub>2</sub>N), 1.7–1.1 (COOC(CH<sub>3</sub>)<sub>3</sub> + CONHCH<sub>2</sub>CH<sub>2</sub>(CH<sub>2</sub>)<sub>2</sub>CHN + NCH<sub>2</sub>CH<sub>2</sub>CH<sub>2</sub>N + NCH<sub>2</sub>(CH<sub>2</sub>)<sub>2</sub>CH<sub>2</sub>N). FT-IR (ATR):  $\nu$  (cm<sup>-1</sup>) 3357 (NH stretch), 2978, 2934, 1725 (C=O stretch), 1642 (C=O amide I stretch), 1564 (C=O amide II stretch), 1457, 1367, 1250, 1220, and 1147 (C–O stretch).

#### Deprotection of poly(propylene imine) dendrimers with DTPA building blocks, giving **4<sub>n</sub>**

**4<sub>n=4</sub> (G1)** To a solution of **3<sub>n=4</sub>** (0.144 g, 0.042 mmol) in DCM (4 mL) was added TFA (2 mL), and the reaction mixture was stirred overnight at room temperature. After evaporation of the solvent a second portion of TFA (2 mL) and dry DCM (4 mL) were added, and stirring was continued overnight. The solution was concentrated *in vacuo* resulting in the TFA salt of **4<sub>n=4</sub>**. The crude product was dissolved in demineralized water and was extensively dialyzed with a 1 kDa MWCO membrane. The solution was lyophilized and a white solid (0.052 g, 22.8  $\mu$ mol, 54%) was obtained. <sup>19</sup>F-NMR spectroscopy confirmed the successful removal

of TFA by the absence of a signal at  $-75.6$  ppm.  $^1\text{H-NMR}$  ( $\text{D}_2\text{O}$ ):  $\delta = 3.99$  (s, 32H,  $\text{NCH}_2\text{COOH}$ ), 3.40–3.29 (m, 20H,  $\text{CONH}(\text{CH}_2)_4\text{CHN}$  {4H}+  $\text{NCH}_2\text{CH}_2\text{N}$  {16H}), 3.02–2.80 (m, 44H,  $\text{NCH}_2\text{CH}_2\text{N}$  {16H}+  $\text{CONHCH}_2(\text{CH}_2)_3$  {8H} +  $\text{N}(\text{CH}_2)_2\text{CH}_2\text{N}$  {8H} +  $\text{NCH}_2(\text{CH}_2)_2\text{N}$  {8H} +  $\text{NCH}_2(\text{CH}_2)_2\text{CH}_2\text{N}$  {4H}), 1.80–1.20 (m, 36 H,  $\text{CONHCH}_2\text{CH}_2(\text{CH}_2)_2\text{CHN}$  {24H} +  $\text{NCH}_2\text{CH}_2\text{CH}_2\text{N}$  {8H} +  $\text{NCH}_2(\text{CH}_2)_2\text{CH}_2\text{N}$  {4H}). The assignment of the  $^1\text{H-NMR}$  spectrum is confirmed by  $^1\text{H}, ^1\text{H-COSY}$ .  $^{13}\text{C-NMR}$  ( $\text{D}_2\text{O}$ ):  $\delta = 175.1$  (C=O), 169.8 (C=O), 169.1 (C=O), 160.6 (NHCONH), 63.5 ( $\text{CONH}(\text{CH}_2)_4\text{CHN}$ ), 55.28 ( $\text{NCH}_2\text{COOH}$ ), 53.3 ( $\text{NCH}_2\text{CH}_2\text{NCH}_2\text{COOH}$ ), 52.1 ( $\text{NCH}_2(\text{CH}_2)_2\text{CH}_2\text{N}$ ), 50.5 ( $\text{NCH}_2(\text{CH}_2)_2\text{N}$ ), 46.7 ( $\text{NCH}_2\text{CH}_2\text{N}$ ), 39.7 ( $\text{CONHCH}_2(\text{CH}_2)_3$ ), 36.8 ( $\text{N}(\text{CH}_2)_2\text{CH}_2\text{N}$ ), 29.2 ( $\text{NHCOCH}_2\text{CH}_2\text{CH}_2$ ), 27.8 ( $\text{NHCO}(\text{CH}_2)_3\text{CH}_2$ ), 24.3, ( $\text{NCH}_2\text{CH}_2\text{CH}_2\text{N}$  23.5 ( $\text{NHCO}(\text{CH}_2)_2\text{CH}_2$ ), 20.7 ( $\text{NCH}_2(\text{CH}_2)_2\text{CH}_2\text{N}$ ). FT-IR (ATR):  $\nu$  ( $\text{cm}^{-1}$ ) 3385 (NH stretch), 2961, 2546 (COOH stretch), 1727 (C=O stretch), 1660 (C=O stretch), 1582 (C=O stretch), 1427, 1147 (C–O stretch), 1135. ESI-QTOF-MS:  $m/z$  [ $\text{C}_{92}\text{H}_{160}\text{N}_{22}\text{O}_{44} + \text{H}$ ] $^+$  Calcd. 2278.1 Da; Obsd. 2278.0 Da.  $\mathbf{4}_{n=16}$  was prepared in a fashion similar to the preparation of  $\mathbf{4}_{n=4}$ .  $^1\text{H-NMR}$  ( $\text{D}_2\text{O}$ ): the spectrum exhibits extreme broadening of all signals, which can be ascribed to aggregation of dendrimers. FT-IR (ATR):  $\nu$  ( $\text{cm}^{-1}$ ) 3364 (NH stretch), 2960, 1622 (C=O), 1470, 1367, 1200, and 1127.  $\mathbf{4}_{n=64}$  was prepared in a fashion similar to the preparation of  $\mathbf{4}_{n=4}$ .  $^1\text{H-NMR}$  ( $\text{D}_2\text{O}$ ) spectrum exhibits extreme broadening off all signals, which might be attributed to aggregation of dendrimers. FT-IR (ATR):  $\nu$  ( $\text{cm}^{-1}$ ) 3361 (NH stretch), 2956, 2516 (COOH stretch), 1669 (C=O stretch), 1625 (C=O), 1472, 1370, 1179, and 1125.

#### Synthesis of Gd(III) complex ( $\mathbf{5}_{n=1}$ )

A detailed description of the synthesis of Gd(III)DTPA-based complex  $\mathbf{5}_{n=1}$  is described in Chapter 2.

#### Synthesis of the first generation Gd(III)DTPA-terminated dendrimer ( $\mathbf{5}_{n=4}$ )

DTPA-terminated poly(propylene imine) dendrimer  $\mathbf{4}_{n=4}$  (20.8 mg, 9.21  $\mu\text{mol}$ ) was dissolved in water (7 mL) and the pH was adjusted to 7 with 0.1 N NaOH solution. The solution was vigorously stirred and a stoichiometric amount of  $\text{GdCl}_3 \cdot 6 \text{H}_2\text{O}$  (13.7 mg, 36.9  $\mu\text{mol}$ ) dissolved in 4 mL of water was added. The pH was maintained at 7 with 0.1 N NaOH. The reaction was stirred for 2 h at roomtemperature. Subsequently the solution was extensively dialyzed with a 1 kDa MWCO membrane in water (1 L). The water was refreshed ( $3 \times 1$  L) and the dialyzed solution was lyophilized. A white powder of  $\mathbf{5}_{n=4}$  (22.1 mg, 7.20  $\mu\text{mol}$ ) was obtained in 78% yield. FT-IR (ATR):  $\nu$  ( $\text{cm}^{-1}$ ) 3332, 2946, 2934, 1583.1 (C=O stretch), 1389, 1218.  $^1\text{H-NMR}$  ( $\text{D}_2\text{O}$ ) the spectrum could not be recorded, due to the paramagnetic nature of Gd(III). ICP-AES (Gd): aqueous solution of  $\mathbf{5}_{n=4}$ , Calcd. 50.0  $\mu\text{M}$ ; Obsd. 35.5  $\mu\text{M}$ .

#### General procedure for the synthesis of higher generations Gd(III)DTPA-terminated dendrimers ( $\mathbf{5}_{n=16,64}$ )

A solution of DTPA-terminated fifth generation dendrimer  $\mathbf{4}_{n=64}$  (80.0 mg, 2.09  $\mu\text{mol}$ ) in 0.3 M citrate buffer pH 5.8 (12.5 mL), was added dropwise to a solution of  $\text{GdCl}_3 \cdot 6 \text{H}_2\text{O}$  (74.0 mg, 0.199 mmol) in 0.3 M citrate buffer (25 mL). The solution was stirred for 3 h at room temperature and was extensively dialyzed with a 1 kDa MWCO membrane in water ( $5 \times 1\text{L}$ ). The suspension was lyophilized and a yellowish powder,  $\mathbf{5}_{n=64}$ , was obtained. **Data for  $\mathbf{5}_{n=16}$ .** FT-IR (ATR):  $\nu$  ( $\text{cm}^{-1}$ ) 3363, 2931, 1586 (C=O stretch), 1440, 1407, 1322, 1088. ICP-AES (Gd): buffered solution of  $\mathbf{5}_{n=16}$ , Calcd. 50.0  $\mu\text{M}$ , Obsd. 37.0  $\mu\text{M}$ . **Data for  $\mathbf{5}_{n=64}$ .** FT-IR (ATR):  $\nu$  ( $\text{cm}^{-1}$ ) 3348, 2925, 1582 (C=O stretch), 1405, 1324, 1264, 1087. ICP-AES (Gd): buffered solution of  $\mathbf{5}_{n=64}$ , Calcd. 50.0  $\mu\text{M}$ , Obsd. 36.2  $\mu\text{M}$ .

**General procedure for the synthesis of combined Gd(III)DTPA- and Y(III)DTPA-terminated dendrimers**

To a solution of DTPA-terminated fifth generation dendrimer  $4_{n=64}$  in 0.3 M citrate buffer was added dropwise a solution of GdCl<sub>3</sub> and YCl<sub>3</sub> in citrate buffer (in total 1.7 equivalents of metal per DTPA end-group for G5-mixed-A and 1.5 equivalents of metal per DTPA end group for G5-mixed-B and G5-mixed-C). The buffered solution was stirred, and stirring was continued overnight at room temperature. The excess of (toxic) metal was removed via extensive dialysis with a 1 kDa MWCO membrane in water (3 × 1 L). The suspension was lyophilized, and a yellowish powder was obtained. The ratio between Gd(III) and Y(III) was determined with ICP-AES analysis. **Data for G5-mixed-A.** FT-IR (ATR):  $\nu$  (cm<sup>-1</sup>) 3342, 2946, 1583 (C=O stretch), 1409, 1324, 1262, 1087. ICP-AES: Y(III)/Gd(III) ratio Calcd. 3.98, Obsd. 1.98. **Data for G5-mixed-B.** FT-IR (ATR):  $\nu$  (cm<sup>-1</sup>) 3342, 2946, 1582 (C=O stretch), 1407, 1324, 1264, 1086. ICP-AES: Y(III)/Gd(III) ratio Calcd. 0.99, Obsd. 0.48. **Data for G5-mixed-C.** FT-IR (ATR):  $\nu$  (cm<sup>-1</sup>) 3343, 2946, 1583 (C=O stretch), 1408, 1325, 1265, 1087. ICP-AES: Y(III)/Gd(III) ratio Calcd. 0.25, Obsd. 0.083.

**Synthesis of dendrimer 7 (tert-butyl ester protected)**

A stirred solution of **1** (0.111 g, 0.142 mmol) in dry DCM (2 mL) was injected into a solution of di-*tert*-butyl tricarboxylate (0.043 g, 0.164 mmol) in DCM (3 mL) under an argon atmosphere. The solution was stirred for 35 min and continuously purged with argon. IR spectroscopy showed the appearance of the characteristic isocyanate vibration at 2272 cm<sup>-1</sup>. Residual di-*tert*-butyl tricarboxylate was removed by adding two droplets of dry pyridine. The solution of **2** (0.142 mmol) in DCM (5 mL) was slowly added to DAB-*dendr*-(NH<sub>2</sub>)<sub>16</sub> (0.126 g, 0.075 mmol, 8 equivalents excess) in dry DCM (3 mL). The reaction was completed within 5 min and concentrated under reduced pressure. The crude product **6** was dissolved in a solution of methanol (5 mL) and triethylamine (217  $\mu$ L, 1.53 mmol). To the ice-cooled solution of **6**, acetic anhydride (123  $\mu$ L, 1.30 mmol) was added dropwise. The reaction was stirred overnight at room temperature. The solvent was removed under reduced pressure. The crude mixture was dissolved in methanol (1 mL) and purified with a DOWEX 550 anion exchange column, to give **7** (0.181 g) as a clear liquid. <sup>1</sup>H-NMR (CDCl<sub>3</sub>):  $\delta$  = 7.7–7.3 (br, CH<sub>3</sub>CONHCH<sub>2</sub>) 5.9 (br, NHCONH), 5.6 (br, NHCONH), 3.42 (NCH<sub>2</sub>COOC(CH<sub>3</sub>)<sub>3</sub>), 3.3–3.1 (CH<sub>2</sub>NHCONHCH<sub>2</sub> + NHCONH(CH<sub>2</sub>)<sub>4</sub>CHN + CH<sub>3</sub>CONHCH<sub>2</sub>CH<sub>2</sub>), 2.9–2.6 (NCH<sub>2</sub>CH<sub>2</sub>N + NCH<sub>2</sub>CH<sub>2</sub>N), 2.5–2.2 (NCH<sub>2</sub>(CH<sub>2</sub>)<sub>2</sub>CH<sub>2</sub>N + NCH<sub>2</sub>CH<sub>2</sub>CH<sub>2</sub>N + NCH<sub>2</sub>CH<sub>2</sub>CH<sub>2</sub>NCOCH<sub>3</sub>), 2.0 (CH<sub>3</sub>CONH), 1.8–1.4 (CONHCH<sub>2</sub>CH<sub>2</sub>(CH<sub>2</sub>)<sub>2</sub>CHN + NCH<sub>2</sub>CH<sub>2</sub>CH<sub>2</sub>N + NCH<sub>2</sub>(CH<sub>2</sub>)<sub>2</sub>CH<sub>2</sub>N + NCH<sub>2</sub>CH<sub>2</sub>CH<sub>2</sub>NCOCH<sub>3</sub> + COOC(CH<sub>3</sub>)<sub>3</sub>). The assignment of the <sup>1</sup>H-NMR spectrum is confirmed by <sup>1</sup>H,<sup>1</sup>H-COSY. FT-IR (ATR):  $\nu$  (cm<sup>-1</sup>) 3286 (NH stretch), 2937, 1727 (C=O stretch), 1639 (C=O stretch), 1553 (C=O stretch), 1457, 1367, 1292, 1252, and 1150.

**Synthesis of dendrimer 8 (deprotected)**

To a solution of **7** (95.6 mg) in DCM (4 mL) was added TFA (2 mL), and the reaction mixture was stirred overnight at room temperature. After evaporation of the solvent a second portion of TFA (2 mL) and dry DCM (4 mL) were added, and stirring was continued overnight. The solution was concentrated *in vacuo* resulting in the TFA salt of **8**. The crude product was dissolved in demineralized water and extensively dialyzed with a 0.5 kDa MWCO membrane. The solution was lyophilized and a white solid (76 mg) was obtained. <sup>1</sup>H-NMR (D<sub>2</sub>O):  $\delta$  = 4.1–3.9 (s, NCH<sub>2</sub>COOH), 3.50 (NHCONH(CH<sub>2</sub>)<sub>4</sub>CHN), 3.40 (NCH<sub>2</sub>CH<sub>2</sub>N), 3.3–2.9 (CH<sub>2</sub>NCONHCH<sub>2</sub> + CH<sub>3</sub>CONHCH<sub>2</sub>CH<sub>2</sub>CH<sub>2</sub>N + NCH<sub>2</sub>CH<sub>2</sub>CH<sub>2</sub>N + NCH<sub>2</sub>(CH<sub>2</sub>)<sub>2</sub>CH<sub>2</sub>N), 2.2–2.0 (NCH<sub>2</sub>CH<sub>2</sub>CH<sub>2</sub>N + NCH<sub>2</sub>(CH<sub>2</sub>)<sub>2</sub>CH<sub>2</sub>N + NCH<sub>2</sub>CH<sub>2</sub>CH<sub>2</sub>NCOCH<sub>3</sub>), 1.9–1.2 (m, CH<sub>3</sub>CONH + CONHCH<sub>2</sub>CH<sub>2</sub>(CH<sub>2</sub>)<sub>2</sub>CHN + NCH<sub>2</sub>CH<sub>2</sub>CH<sub>2</sub>N + NCH<sub>2</sub>(CH<sub>2</sub>)<sub>2</sub>CH<sub>2</sub>N + NCH<sub>2</sub>CH<sub>2</sub>CH<sub>2</sub>NCOCH<sub>3</sub>). FT-IR (ATR):  $\nu$  (cm<sup>-1</sup>) 2535 (COOH stretch), 1742 (C=O stretch), 1652 (C=O stretch), 1439, and 1136 (C–O stretch).

**Synthesis of Gd(III) complex 9**

DTPA-terminated dendrimer **8** (35.5 mg) was dissolved in water (5 mL) and the pH was adjusted to 7 by adding aliquots of 0.1 N NaOH. The solution was vigorously stirred and GdCl<sub>3</sub>·6 H<sub>2</sub>O (15.3 mg, 41.2 μmol) dissolved in 4 mL of water was added. The pH was continuously monitored and maintained at 7 by adding aliquots of 0.1 N NaOH. The reaction was stirred for 2 h at 20°C. Subsequently the solution filtered and extensively dialyzed with a 0.5 kDa MWCO membrane in water (1 L). The water was refreshed (3×) and freeze drying provided **9** (31.4 mg). FT-IR (ATR):  $\nu$  (cm<sup>-1</sup>) 3261, 2955, 1575, 1440, 1412, 1373, 1136. ICP-AES (Gd): Calcd. 50.0 μM ; Obsd. 54.1 μM.

**3.7 REFERENCES**

- (1) Lauffer, R. B. *Chem. Rev.* **1987**, *87*, 901-927.
- (2) Caravan, P.; Ellison, J. J.; McMurry, T. J.; Lauffer, R. B. *Chem. Rev.* **1999**, *99*, 2293-2352.
- (3) Merbach, A. E.; Tóth, E. *The Chemistry of Contrast Agents in Medical Magnetic Resonance Imaging*; John Wiley & Sons: New York, 2001.
- (4) Aime, S.; Dastru, W.; Crich Simonetta, G.; Gianolio, E.; Mainero, V. *Biopolymers* **2002**, *66*, 419-428.
- (5) Lauffer, R. B.; Brady, T. J. *Magn. Res. Imaging* **1985**, *3*, 11-16.
- (6) Manabe, Y.; Longley, C.; Furmanski, P. *Biochimica et Biophysica Acta* **1986**, *883*, 460-467.
- (7) Armitage, F. E.; Richardson, D. E.; Li, K. C. P. *Bioconjugate Chem.* **1990**, *1*, 365-374.
- (8) Spanoghe, M.; Lanens, D.; Dommissse, R.; Van der Linden, A.; Alder Weireldt, F. *Magn. Res. Imaging* **1992**, *10*, 913-917.
- (9) Sieving, P. F.; Watson, A. D.; Rocklage, S. M. *Bioconjugate Chem.* **1990**, *1*, 65-71.
- (10) Caravan, P.; Cloutier, N. J.; Greenfield, M. T.; McDermid, S. A.; Dunham, S. U.; Bulte, J. W. M.; Amedio, J. C., Jr.; Looby, R. J.; Supkowski, R. M.; Horrocks, W. D., Jr.; McMurry, T. J.; Lauffer, R. B. *J. Am. Chem. Soc.* **2002**, *124*, 3152-3162.
- (11) Aime, S.; Frullano, L.; Geninatti Crich, S. *Angew. Chem. Int. Ed.* **2002**, *41*, 1017-1019.
- (12) Vexler, V. S.; Clement, O.; Schmitt-Willich, H.; Brasch, R. C. *J. Magn. Res. Imaging* **1994**, *4*, 381-388.
- (13) Desser, T. S.; Rubin, D. L.; Muller, H. H.; Qing, F.; Khodor, S.; Zanazzi, G.; Young, S. W.; Ladd, D. L.; Wellons, J. A.; Kellar, K. E. *J. Magn. Res. Imaging* **1994**, *4*, 467-472.
- (14) Fischer, M.; Vögtle, F. *Angew. Chem. Int. Ed.* **1999**, *38*, 885-905.
- (15) Bosman, A. W.; Janssen, H. M.; Meijer, E. W. *Chem. Rev.* **1999**, *99*, 1665-1688.
- (16) Wiener, E. C.; Brechbiel, M. W.; Brothers, H.; Magin, R. L.; Gansow, O. A.; Tomalia, D. A.; Lauterbur, P. C. *Magn. Reson. Med.* **1994**, *31*, 1-8.
- (17) Tóth, E.; Pubanz, D.; Vauthey, S.; Helm, L.; Merbach, A. E. *Chem. Eur. J.* **1996**, *2*, 1607-1615.
- (18) Kobayashi, H.; Kawamoto, S.; Jo, S.-K.; Bryant, H. L., Jr.; Brechbiel, M. W.; Star, R. A. *Bioconjugate Chem.* **2003**, *14*, 388-394.
- (19) Wiener, E. C.; Auteri, F. P.; Chen, J. W.; Brechbiel, M. W.; Gansow, O. A.; Schneider, D. S.; Belford, R. L.; Clarkson, R. B.; Lauterbur, P. C. *J. Am. Chem. Soc.* **1996**, *118*, 7774-7782.
- (20) Bryant Jr., L. H.; Brechbiel, M. W.; Wu, C.; Bulte, J. W.; Herynek, V.; Frank, J. A. *J. Magn. Res. Imaging* **1999**, *9*, 348-352.
- (21) Dong, Q.; Hurst, D. R.; Weinmann, H. J.; Chenevert, T. L.; Londy, F. J.; Prince, M. R. *Invest. Radiol.* **1998**, *33*, 699-708.

- (22) Nicolle, G. M.; Tóth, E.; Schmitt-Willich, H.; Raduchel, B.; Merbach, A. E. *Chem. Eur. J.* **2002**, *8*, 1040-1048.
- (23) Kobayashi, H.; Kawamoto, S.; Saga, T.; Sato, N.; Hiraga, A.; Ishimori, T.; Akita, Y.; Mamede, M. H.; Konishi, J.; Togashi, K.; Brechbiel, M. W. *Magn. Reson. Med.* **2001**, *46*, 795-802.
- (24) van Hest, J. C. M.; Delnoye, D. A. P.; Baars, M. W. P. L.; van Genderen, M. H. P.; Meijer, E. W. *Science* **1995**, *268*, 1592-1595.
- (25) van Hest, J. C. M.; Baars, M. W. P. L.; Elissen-Roman, C.; van Genderen, M. H. P.; Meijer, E. W. *Macromolecules* **1995**, *28*, 6689-6691.
- (26) Langereis, S.; de Lussanet, Q. G.; van Genderen, M. H. P.; Backes, W. H.; Meijer, E. W. *Macromolecules* **2004**, *37*, 3084-3091.
- (27) Hummelen, J. C.; Van Dongen, J. L. J.; Meijer, E. W. *Chem. Eur. J.* **1997**, *3*, 1489-1493.
- (28) Jansen, J. F. G. A.; De Brabander - Van Den Berg, E. M. M.; Meijer, E. W. *New Macromol. Archit. Funct., Proc. OUMS'95, 2nd, 1995* **1996**, 99-106.
- (29) Zhang, X.; Wilhelm, M.; Klein, J.; Pfaadt, M.; Meijer, E. W. *Langmuir* **2000**, *16*, 3884-3892.
- (30) Zhang, H.; Grim, P. C. M.; Foubert, P.; Vosch, T.; Vanoppen, P.; Wiesler, U. M.; Berresheim, A. J.; Müllen, K.; De Schryver, F. C. *Langmuir* **2000**, *16*, 9009-9014.
- (31) Li, J.; Tomalia, D. A. in *Dendrimers and Other Dendritic Polymers*, edited by J. M. J. Fréchet and D. A. Tomalia; Wiley-VCH: New York, 2001, 285-307.
- (32) Vold, R. L.; Waugh, J. S.; Klein, M. P.; Phelps, D. E. *J. Chem. Phys.* **1968**, *48*, 3831-3832.
- (33) Nicolle, G. M.; Yerly, F.; Imbert, D.; Boettger, U.; Buenzli, J.-C.; Merbach, A. E. *Chem. Eur. J.* **2003**, *9*, 5453-5467.
- (34) Peerlings, H. W. I.; Meijer, E. W. *Tetrahedron Letters* **1999**, *40*, 1021-1024.
- (35) Frederik, P. M.; Bomans, P. H. H.; Laeven, P. F. J.; Nijpels, F. J. T., Device for preparing specimens for a cryo-electron microscope. Netherlands Industrial Property Office (RO/NL), PCT/NL02/00189 (2002).
- (36) Kale, L.; Skeel, R.; Bhandarkar, M.; Brunner, R.; Gursoy, A.; Krawetz, N.; Phillips, J.; Shinozaki, A.; Varadarajan, K.; Schulten, K. *Journal of Computational Physics* **1999**, *151*, 283-312.
- (37) Brunger, A. T. *X-PLOR, version 3.1: A system for X-ray crystallography and NMR*; Yale University Press, 1992.
- (38) Humphrey, W.; Dalke, A.; Schulten, K. *Journal of Molecular Graphics* **1996**, *14*, 33.
- (39) Berendsen, H. J. C.; Postma, J. P. M.; Van Gunsteren, W. F.; DiNola, A.; Haak, J. R. *J. Chem. Phys.* **1984**, *81*, 3684-3690.
- (40) Bottomley, P. A. *U.S. Patent 4 480 228* **1984**.





---

## Chapter 4

### Evaluation of dendritic contrast agents for MR imaging\*

---

**ABSTRACT:** *Different generations of Gd(III)DTPA-terminated poly(propylene imine) dendrimers  $\mathbf{5}_{n=4}$  (G1),  $\mathbf{5}_{n=16}$  (G3) and  $\mathbf{5}_{n=64}$  (G5) and Gd(III)DTPA-based complex  $\mathbf{5}_{n=1}$  were evaluated in terms of (i) longitudinal ( $r_1$ ) and transverse ( $r_2$ ) relaxivities in mouse blood plasma, (ii) concentration detection limits in vitro, and (iii) in vivo contrast-enhanced MR imaging (CE-MRI) in mice. The ionic relaxivities non-linearly increased with molecular weight (from ionic  $r_1 = 8.1 \text{ mM}^{-1}\text{s}^{-1}$  and ionic  $r_2 = 8.6 \text{ mM}^{-1}\text{s}^{-1}$  for  $\mathbf{5}_{n=1}$  ( $\text{MW} = 0.7 \text{ kg}\cdot\text{mol}^{-1}$ ) to 19.3 and 25.0, respectively for  $\mathbf{5}_{n=64}$  ( $\text{MW} = 51 \text{ kg}\cdot\text{mol}^{-1}$ ). The lowest detectable dendrimer concentration was more than two orders of magnitude lower for  $\mathbf{5}_{n=64}$  ( $8.1 \times 10^{-8} \text{ M}$ ) than for  $\mathbf{5}_{n=1}$  ( $3.1 \times 10^{-5} \text{ M}$ ). Serial and dynamic CE-MRI were performed to monitor the distribution of MRI contrast agent in the heart, the arteries, the renal system, the liver, the spleen, the bladder, and the tumor periphery. Sub-millimeter-sized blood vessels were well visualized with serial CE-MRI with each of the (dendritic) MRI contrast agents. Dynamic CE-MRI showed timely renal clearance for all MRI contrast agents, but stronger and prolonged blood signal enhancement for  $\mathbf{5}_{n=16}$  and  $\mathbf{5}_{n=64}$ . Moreover, the low molecular weight contrast agents  $\mathbf{5}_{n=1}$  and  $\mathbf{5}_{n=4}$  showed a rapid tumor in-wash, whereas the higher generations of the dendritic contrast agents  $\mathbf{5}_{n=16}$  and  $\mathbf{5}_{n=64}$  showed a more gradual and prolonged tumor in-wash. It was also found that  $\mathbf{5}_{n=16}$  and  $\mathbf{5}_{n=64}$  monitor tumor vessel permeability and vascular volume more accurately than  $\mathbf{5}_{n=1}$  and  $\mathbf{5}_{n=4}$ . Therefore, higher molecular weight contrast agents may be preferred over low molecular weight MRI contrast agents for evaluating reductions in microvessel permeability and vascular volume. Lower molecular weight MRI contrast agents may be more applicable for evaluating therapeutic reductions in magnitude and heterogeneity of microcirculatory blood flow.*

---

\* Part of this work has been published: de Lussanet, Q.G.; Langereis, S.; Beets-Tan, R.G.H.; van Genderen, M.H.P.; van Engelshoven, J.M.A.; Backes, W.H. *Radiology* **2005**, *235*, 65-72; Langereis, S.; de Lussanet, Q.G.; van Genderen, M.H.P.; Meijer, E.W.; Beets-Tan, R.G.H.; Griffioen, A.W.; van Engelshoven, J.M.A.; Backes, W.H. *NMR in Biomedicine*, submitted for publication.

## 4.1 INTRODUCTION

Low molecular weight (MW) MRI contrast agents based on chelates of gadolinium(III) are currently the most widely applied contrast agents for general clinical MR imaging. These MRI contrast agents are appreciated for their predominant positive signal enhancement in  $T_1$ -weighted MR imaging, non-specific tissue distribution, and particular high safety profile.<sup>1-3</sup> For some MR imaging purposes, however, the properties of low MW contrast agents are not optimal.

First, the rapid extravasation of low MW contrast agents causes a fast decrease in their concentration in the bloodstream after administration (Figure 4.1a). This rapid decrease in the concentration of the MRI contrast agent in the bloodstream is unfavorable for MR angiography purposes, because it will not only result in a lower signal enhancement in the blood vessel, but also in a higher background signal from the surrounding tissue. An increase in the background signal may reduce the spatial resolution such that blood vessels can no longer be discriminated from their surrounding. Contrary to low MW contrast agents, high MW contrast agents remain in high concentrations in the bloodstream during longer periods of time (Figure 4.1b). Due to the fact that high MW contrast agents show little extravasation and long intravascular retention, they are commonly referred to as blood pool agents, while low MW contrast agents are referred to as extravascular agents.<sup>2,4</sup>

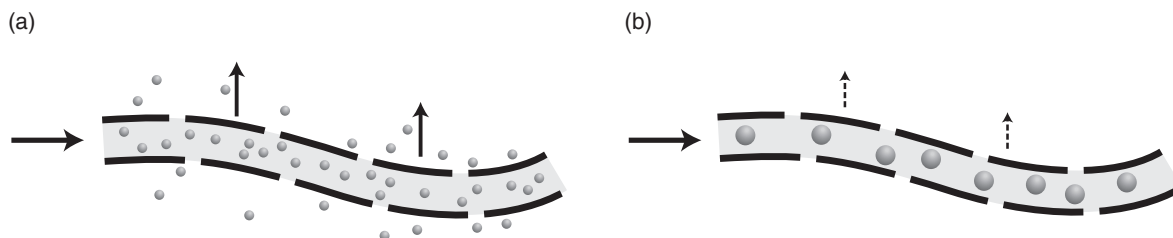


**Figure 4.1** Diffusion of MRI contrast agent from the blood through the vessel wall and the interstitial space in normal vessels. (a) Rapid extravasation of low MW contrast agents; (b) slow extravasation of high MW contrast agents.

Secondly, low MW contrast agents rapidly diffuse from the blood stream into the interstitial space, even in the case of healthy vessels. This relatively high permeability prevents their effective use in differentiating between benign lesions (normal vessels) and malignant tumors (hyperpermeable vessels) with contrast-enhanced MR imaging (CE-MRI) (Figure 4.1a and 4.2a). On the other hand differentiation between these two types of vessels is possible with high MW contrast agents (Figure 4.1b and 4.2b).<sup>5</sup>

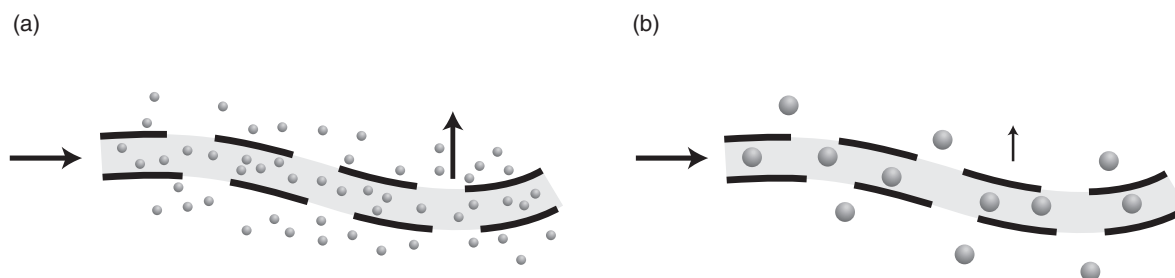


**Figure 4.2** Diffusion of MRI contrast agent from the blood through the vessel wall and the interstitial space in hyperpermeable vessels. (a) Low MW contrast agents; (b) high MW contrast agents.

Thirdly, low MW contrast agents, such as Gd(III) complexes of diethylenetriaminepentaacetic acid (DTPA), contain typically one Gd(III) ion per molecule. Consequently, the relatively low signal enhancing effect (or longitudinal relaxivity  $r_1$ ,  $\text{mM}^{-1}\text{s}^{-1}$ ) requires that high concentrations (*i.e.* high doses or injection rates) of MRI contrast agent must be administered to eventually obtain sufficient contrast between the blood vessel and its surrounding tissue. A straightforward approach to increase the loading of Gd(III) per molecule is to attach multiple Gd(III) chelates to a macromolecular scaffold. An additional advantage of (covalently) attaching multiple Gd(III)-based complexes to high MW structures is the strong increase in  $r_1$  per Gd(III) (*i.e.* ionic  $r_1$ ) as a result of the strong reduction in the molecular tumbling rate of the Gd(III) complex.<sup>1,2</sup>

In Chapter 3, a novel series of Gd(III)DTPA-terminated poly(propylene imine) dendrimers was synthesized ( $\mathbf{5}_{n=4,16,64}$ ) employing an isocyanate-activated lysine-based DTPA chelate.<sup>6</sup> Important aspects for the *in vivo* application of these dendritic MRI contrast agents involve their biodistribution and clearance, which are determined by the size of the MRI contrast agent, and their interactions with blood proteins. Non-covalent interactions with blood proteins are expected to affect the relaxivities of the MRI contrast agents.<sup>7-9</sup>

In this Chapter different generations of dendritic MRI contrast agents, ranging from  $\mathbf{5}_{n=4}$  ( $3.1 \text{ kg}\cdot\text{mol}^{-1}$ ) up to  $\mathbf{5}_{n=64}$  ( $51.2 \text{ kg}\cdot\text{mol}^{-1}$ ) (Figure 4.3) will be evaluated for MR imaging. In collaboration with Q.G. de Lussanet and dr. W.H. Backes (Maastricht University Hospital, the Netherlands) these MRI contrast agents were investigated and compared in terms of (i)  $T_1$ - and  $T_2$ -relaxivities in blood plasma, (ii) concentration detection limits *in vitro*, (iii) biodistribution and clearance in mice using a common  $T_1$ -weighted contrast-enhanced MR imaging (CE-MRI) protocol at 1.5 T. Furthermore, CE-MRI in mice with implanted colon cancers was performed with  $\mathbf{5}_{n=1,4,16,64}$  to study the effect of molecular size on the measurement of tumor angiogenesis.

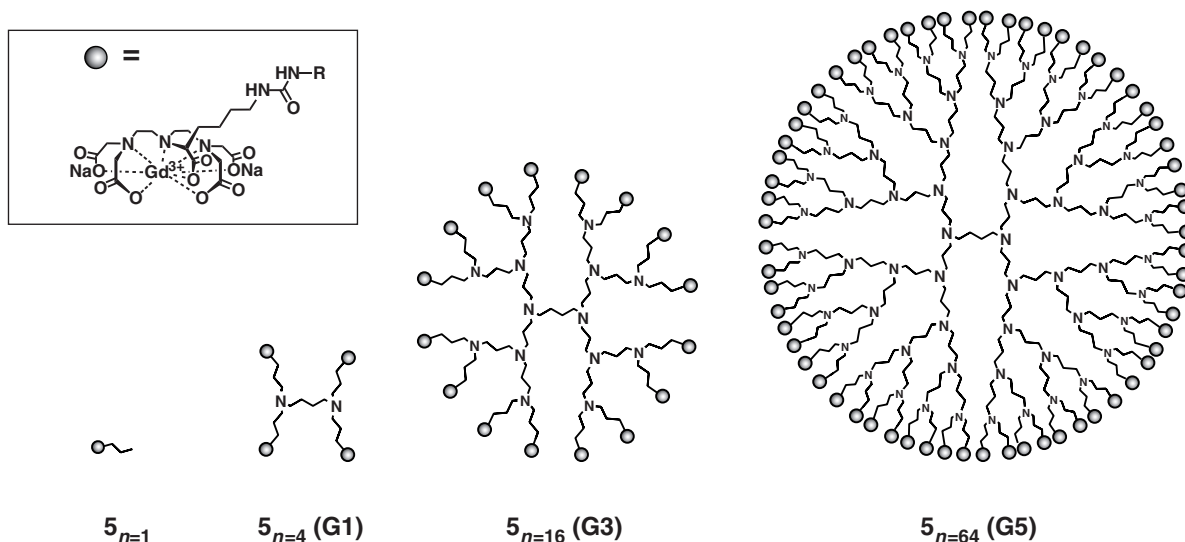


**Figure 4.3** Schematic representations of Gd(III)DTPA-based complex  $5_{n=1}$  and different generations of Gd(III)DTPA-terminated poly(propylene imine) dendrimers  $5_{n=4,16,64}$ .  $n$  denotes the number Gd(III)DTPA moieties per molecule and  $G$  represents the generation of the dendrimer.

## 4.2 IN VITRO MR IMAGING

### 4.2.1 Relaxivities in mouse plasma

To gain insight into the longitudinal ( $r_1$ ) and transverse ( $r_2$ ) relaxivities of dendritic MRI contrast agents in blood plasma and to exclude strong interactions of these MRI contrast agents with blood proteins, a dilution series was prepared for each generation in blood plasma. The  $r_1$  and  $r_2$  relaxivity measurements for Gd(III)DTPA, Gd(III)DTPA-based complex  $5_{n=1}$ , and different generations of dendritic contrast agents  $5_{n=4,16,64}$  in blood plasma are presented in Figure 4.4a and 4.4b. The corresponding  $r_1$  and  $r_2$  values are summarized in Table 4.1 (*vide infra*) and show an increase in  $r_1$  and  $r_2$  upon going to higher generations of the dendritic MRI contrast agent. The ionic relaxivities, *i.e.* the relaxivity per Gd(III) (ionic  $r_{1,2}$ ), increased as a function of dendrimer generation, such that the ionic  $r_1$  and ionic  $r_2$  for  $5_{n=64}$  were at least four times higher than of the parent Gd(III)DTPA complex (Table 4.1 and Figure 4.5a). The effect of increasing relaxivity upon going to higher generations of the dendrimer becomes more pronounced by expressing it in terms of molecular relaxivity, *i.e.* the relaxivity per molecule (mol.  $r_{1,2}$ ) (Table 4.1 and Figure 4.5b).

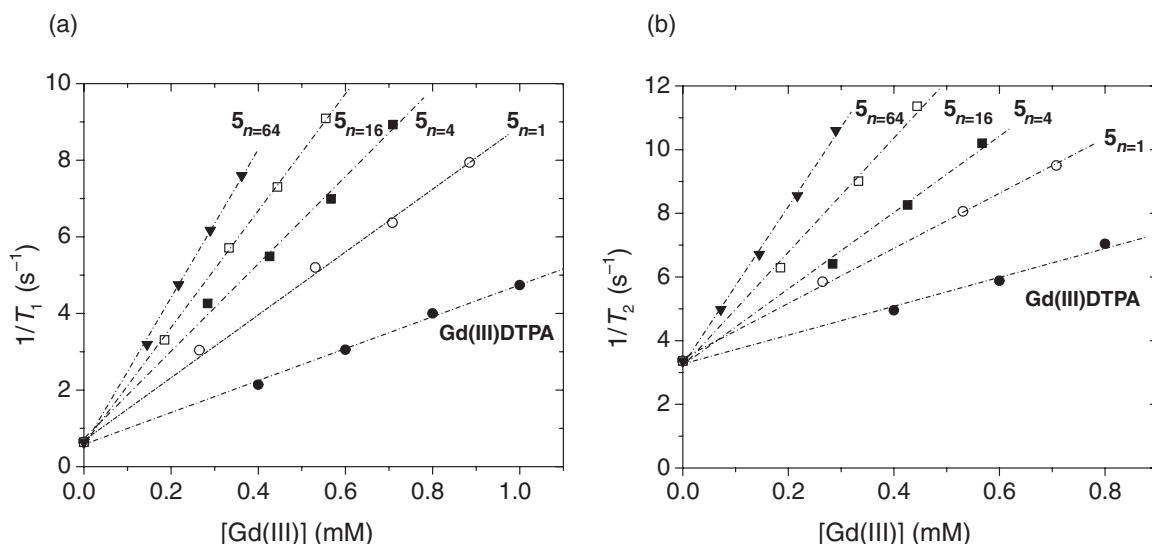


**Figure 4.4** *In vitro* relaxivities of different generations of the Gd(III)DTPA-terminated poly(propylene imine) dendrimer in blood plasma at 1.5 T and 20 °C. (a) Longitudinal relaxation rate ( $1/T_1$ ) versus the concentration of Gd(III); (b) transverse relaxation rate ( $1/T_2$ ) versus the concentration of Gd(III).

The  $r_1$  and  $r_2$  values of the different generations of the Gd(III)DTPA-terminated poly(propylene imine) dendrimer measured in blood plasma are slightly lower than those measured previously in citrate buffer (see Chapter 3, Section 3.2.4),<sup>6</sup> which may be assigned to the different nature of the medium (*e.g.* the pH, the ionic strength or the viscosity). This suggests that the dendritic MRI contrast agents have no or only extremely weak interactions with blood plasma proteins, since strong non-covalent interactions between the MRI contrast agent and blood plasma proteins will result in an increase in the relaxivities.<sup>2,7-9</sup>

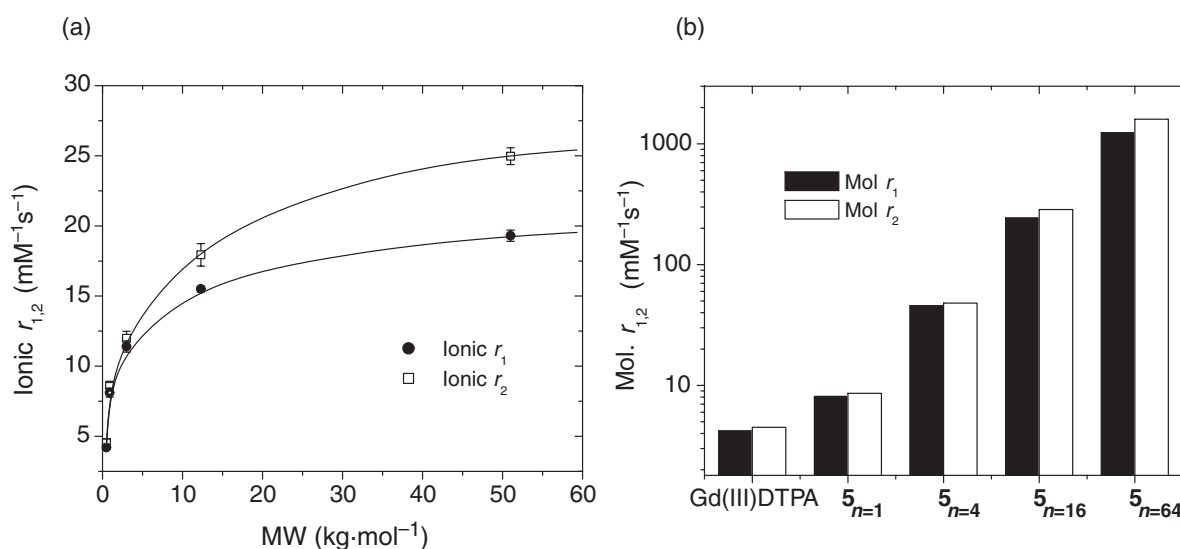


**Figure 4.5** (a) Ionic relaxivities (ionic  $r_{1,2}$ ), defined as the relaxivity per Gd(III) ion, versus the theoretical molecular weight (MW); (b) molecular relaxivities (mol.  $r_{1,2}$ ) of Gd(III)DTPA, Gd(III)DTPA-based complex  $5_{n=1}$ , and dendritic MRI contrast agents  $5_{n=4,16,64}$ .

**Table 4.1** Longitudinal ( $r_1$ ) and transverse ( $r_2$ ) relaxivities of Gd(III)DTPA, Gd(III)DTPA-based complex  $\mathbf{5}_{n=1}$  and different generations of Gd(III)DTPA-terminated poly(propylene imine) dendrimers  $\mathbf{5}_{n=4,16,64}$  in mouse plasma.<sup>a</sup>

	Ionic $r_1^b$ (mM <sup>-1</sup> s <sup>-1</sup> )	Ionic $r_2^b$ (mM <sup>-1</sup> s <sup>-1</sup> )	Ratio $r_2/r_1$	Theoretical no. Gd ions	Mol. $r_1$ (mM <sup>-1</sup> s <sup>-1</sup> ) <sup>c</sup>	Mol. $r_2$ (mM <sup>-1</sup> s <sup>-1</sup> ) <sup>c</sup>	MW (kg·mol <sup>-1</sup> )
Gd(III)DTPA	4.2 ± 0.1	4.5 ± 0.3	1.07	1	4.2	4.5	0.6
$\mathbf{5}_{n=1}$	8.1 ± 0.3	8.6 ± 0.2	1.06	1	8.1	8.6	0.7
$\mathbf{5}_{n=4}$ (G1)	11.4 ± 0.4	12.0 ± 0.5	1.05	4	45.6	48.0	3.1
$\mathbf{5}_{n=16}$ (G3)	15.2 ± 0.2	17.9 ± 0.8	1.18	16	243	286	12.7
$\mathbf{5}_{n=64}$ (G5)	19.3 ± 0.4	25.0 ± 0.6	1.30	64	1235	1600	51.2

<sup>a</sup> Measured with MR spectroscopy at 1.5 T and 20 °C (inversion recovery pulse sequence).<sup>10</sup>

<sup>b</sup> The ionic relaxivity is defined as the relaxivity per Gd(III).

<sup>c</sup> The maximum molecular relaxivity (mol.  $r_{1,2}$ ) is defined as the ionic relaxivity (ionic  $r_{1,2}$ ) multiplied with the theoretical number of Gd(III) moieties attached to a single molecule.

It was observed that the  $r_2/r_1$  ratio increased upon going to higher generations of the dendrimer, which may be attributed to the increase in local concentration of Gd(III) at the periphery of the dendrimer. Even in the case of  $T_1$ -weighted imaging it is important to account for  $r_2$ , because high  $r_2$  values imply the occurrence of stronger  $T_2$  and  $T_2^*$  effects. In theory,  $T_1$ -weighted images are not affected by  $T_2^*$  effects if the echo time (TE) is infinitely short. In practice, TE is limited by the sampling time necessary to acquire one echo signal. For high spatial resolution  $T_1$ -weighted imaging larger acquisition matrices are required. This implies that the TE will increase, which leads to significant  $T_2^*$  effects.

#### 4.2.2 Concentration detection limits of MRI contrast agents *in vitro*

In order to gain insight into concentration detection limits of dendritic MRI contrast agents  $\mathbf{5}_{n=4,16,64}$  and Gd(III)DTPA-based complex  $\mathbf{5}_{n=1}$ , high spatial resolution  $T_1$ -weighed MR imaging was performed on a series of Gd(III) concentrations in blood plasma (Figure 4.6a). The *in vitro*  $T_1$ -weighted measurements of the different concentrations of  $\mathbf{5}_{n=1,4,16,64}$  and Gd(III)DTPA in mouse plasma showed that the largest signal enhancement at low concentrations was obtained using the dendritic MRI contrast agents  $\mathbf{5}_{n=16}$  and  $\mathbf{5}_{n=64}$ , whereas with the lower MW contrast agents Gd(III)DTPA,  $\mathbf{5}_{n=1}$ , and  $\mathbf{5}_{n=4}$  the largest signal enhancement was obtained at higher concentrations; concentrations at which  $\mathbf{5}_{n=16}$  and  $\mathbf{5}_{n=64}$  already showed  $T_2^*$  susceptibility effects (Figure 4.6a). These  $T_2^*$  susceptibility effects caused a drop in the signal at the highest concentrations for each MRI contrast agent. Moreover, the  $T_1$ -weighted MR images showed that at a concentration of, for

example  $5.0 \times 10^{-5}$  M (Figure 4.6a, row indicated with an arrow), the signal increases going to higher generations of the dendritic contrast agent.

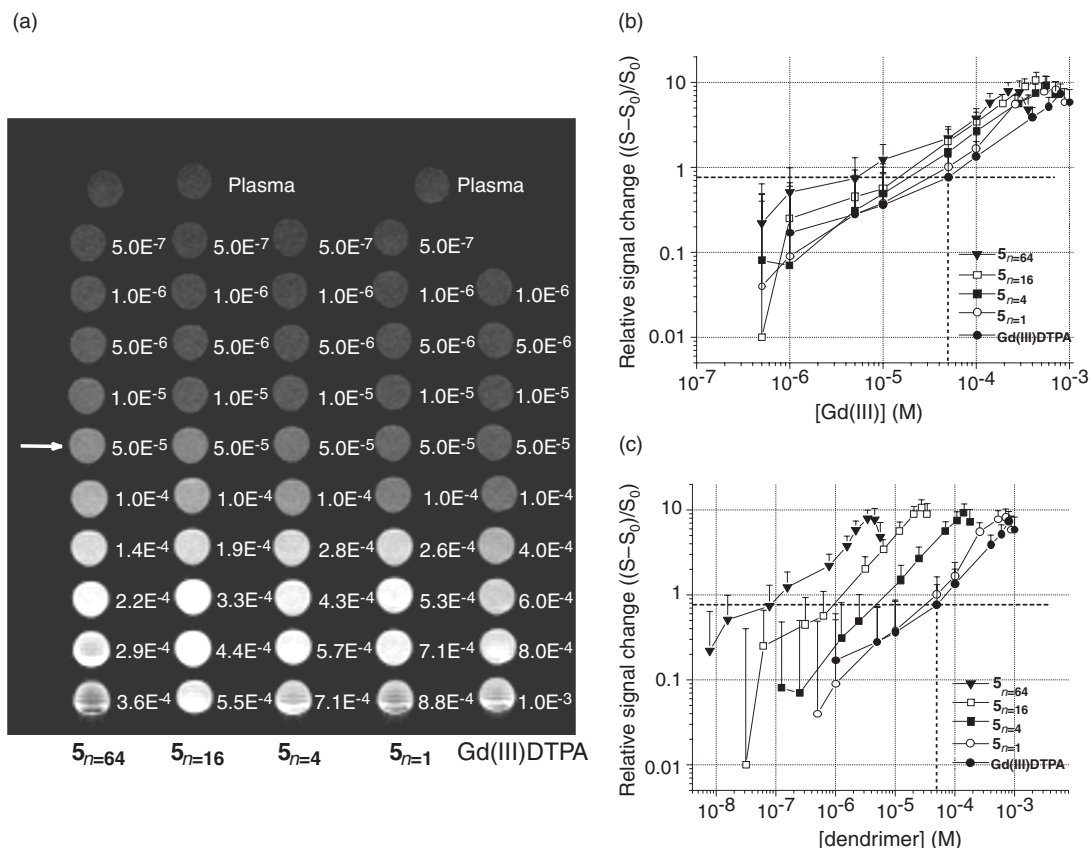


**Figure 4.6** (a) *In vitro*  $T_1$ -weighted MRI measurements for different concentrations of Gd(III) (M) of Gd(III)DTPA, complex  $5_{n=1}$ , and dendritic MRI contrast agents  $5_{n=4,16,64}$  in blood plasma at 1.5 T; (b) the log-log plot of the relative signal change versus the concentration of Gd(III); (c) the log-log plot of the relative signal change versus the concentration of the dendrimer. The detection limit of Gd(III)DTPA was set to  $5.0 \times 10^{-5}$  M (vertical dashed line) giving rise to a relative signal change  $((S - S_0)/S_0)$  of at least 0.76 (horizontal dashed line).

The relative signal change *versus* the Gd(III) concentration is shown in Figure 4.6b, which reflects the differences in ionic relaxivities (ionic  $r_{1,2}$ ). Figure 4.6c shows the relative signal change *versus* the dendrimer concentration reflecting the differences in molecular relaxivities (mol.  $r_{1,2}$ ). In correspondence with the literature value of  $5 \times 10^{-5}$  M for the lowest detectable concentration of Gd(III)DTPA,<sup>3,11</sup> a threshold relative signal change  $((S - S_0)/S_0)$  of 0.76 was used to derive the detectable concentrations for dendritic MRI contrast agents  $5_{n=4,16,64}$  and  $5_{n=1}$  (Figure 4.6b). The detection limits for  $5_{n=1}$  to  $5_{n=64}$  appear along this threshold at decreasing concentrations of Gd(III) (See Table 4.2). In a similar fashion, this analysis was carried out as a function of dendrimer concentration (Figure 4.6c). The detection limits expressed in terms of dendrimer concentration are related by the number of end groups and are listed in Table 4.2. The lowest detectable dendrimer



concentration was more than two orders of magnitude lower for  $\mathbf{5}_{n=64}$  ( $8.1 \times 10^{-8}$  M) than for  $\mathbf{5}_{n=1}$  ( $3.1 \times 10^{-5}$  M).

**Table 4.2** Minimally detectable concentrations for Gd(III)DTPA-based complex  $\mathbf{5}_{n=1}$  and dendritic MRI contrast agents  $\mathbf{5}_{n=4,16,64}$ , assuming a detection limit of  $5.0 \times 10^{-5}$  M for Gd(III)DTPA.<sup>3,11</sup>

	[Gd(III)] (M)	# Gd(III) ions	[dendrimer] (M)
$\mathbf{5}_{n=1}$	$3.1 \times 10^{-5}$	1	$3.1 \times 10^{-5}$
$\mathbf{5}_{n=4}$ (G1)	$1.9 \times 10^{-5}$	4	$4.8 \times 10^{-6}$
$\mathbf{5}_{n=16}$ (G3)	$1.5 \times 10^{-5}$	16	$9.3 \times 10^{-7}$
$\mathbf{5}_{n=64}$ (G5)	$5.2 \times 10^{-6}$	64	$8.1 \times 10^{-8}$

The finding that dendritic MRI contrast agent  $\mathbf{5}_{n=64}$  gives the lowest detection limit would make  $\mathbf{5}_{n=64}$  potentially the best candidate for future molecular imaging purposes (of the contrast agents evaluated in this study). In theory, the high  $T_1$ -relaxivity of  $\mathbf{5}_{n=64}$  makes it a particular good candidate for visualizing small blood vessels. Furthermore,  $\mathbf{5}_{n=64}$  has a longer blood circulation time compared to the lower generations dendritic MRI contrast agents. This is advantageous for MR angiography purposes.

A favorable characteristic of the low MW contrast agent is that only small  $T_2^*$  effects are observed with  $T_1$ -weighted imaging at high concentrations of MRI contrast agents. This characteristic may benefit CE-MR imaging with fast bolus injection of large contrast agent dosages, for example for first-pass MR arteriography of large vessels. The rapid diffusion of low MW contrast agents, *i.e.* rapid extravasation, may be used to their advantage, for example for evaluating microcirculation properties by CE-MRI.<sup>12</sup>

### 4.3 PHARMACOKINETICS OF DENDRITIC MRI CONTRAST AGENTS

The pharmacokinetics of dendritic MRI contrast agents  $\mathbf{5}_{n=4,16,64}$  and Gd(III)DTPA-based complex  $\mathbf{5}_{n=1}$  were studied with serial and dynamic CE-MRI in mice. Serial CE-MRI was used to determine the biodistribution of the MRI contrast agent over time in the whole body of the mouse. To this end, 3D whole body images, irregularly sampled over time, were recorded (Section 4.3.1). Dynamic CE-MRI specifically serves to obtain information on the speed of extravasation and rate of in- and outwash of the visceral organs. Therefore regularly time-sampled images were acquired to follow the distribution of the MRI contrast agent in the visceral organs (Section 4.3.2).

### 4.3.1 Serial CE-MRI

Serial CE-MRI was performed with MRI contrast agents  $\mathbf{5}_{n=1,4,16,64}$  in healthy mice at 1.5 T. The maximum intensity projections of the serial CE-MR measurements, which were digitally subtracted from the pre-contrast MR images, showed comparable images of the cardiovascular system directly (8 s) after the injection of contrast agent for  $\mathbf{5}_{n=1,4,16,64}$  (Figure 4.7). Thirty seconds after the injection of contrast agent the low MW Gd(III)DTPA-based complexes  $\mathbf{5}_{n=1}$  and  $\mathbf{5}_{n=4}$  showed clearance through the renal collecting system, while the higher MW contrast agents  $\mathbf{5}_{n=16}$  and  $\mathbf{5}_{n=64}$  showed some accumulation in the liver and the spleen. Eight minutes after injection of contrast agent the contrast enhancement of the cardiovascular system diminished, and all studied MRI contrast agents were to some extent cleared by the renal system, as indicated by the strong signal enhancement in the bladder (Figure 4.7).

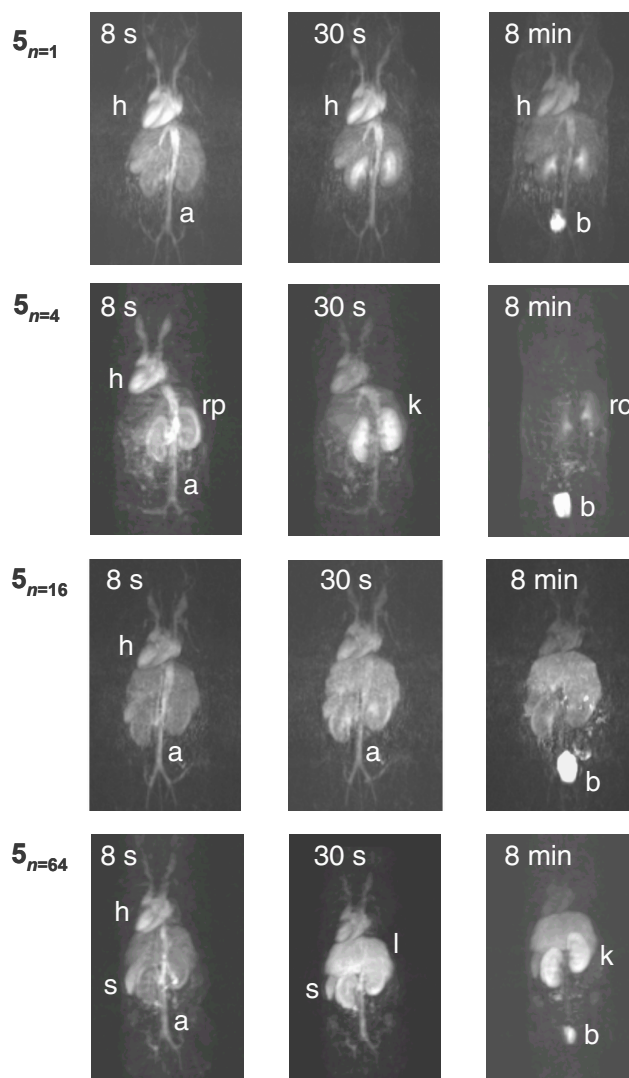


**Figure 4.7** Maximum intensity projections of digitally subtracted contrast-enhanced whole body MR images after 8 s, 30 s and 8 min for  $\mathbf{5}_{n=1,4,16,64}$  (a = aorta; b = bladder; h = heart; k = kidney; l = liver; rc = renal collecting system; rp = renal parenchyma kidney, and s = spleen).

The MRI protocol used here did not show the differences in visualization of small blood vessels using  $\mathbf{5}_{n=1}$  or  $\mathbf{5}_{n=64}$  that one may expect based on the large differences in relaxivities. All of the studied MRI contrast agents visualized small blood vessels, such as the vessels in the neck (these were likely both the carotid artery and jugular vein) and the hind-limbs, which typically have diameters of less than 0.4 mm. The relatively high volume of coverage with high spatial resolution served the purpose of serial CE-MRI to image the biodistribution of the MRI contrast agents.

### 4.3.2 Dynamic CE-MRI

Dynamic CE-MRI experiments were performed with  $\mathbf{5}_{n=1}$  and Gd(III)DTPA-terminated poly(propylene imine) dendrimers  $\mathbf{5}_{n=4,16,64}$  in mice with implanted colon cancers. Dynamic CE-MRI (semi-quantitatively) illustrated the differences in the circulation properties between the low and high MW weight MRI contrast agents. The dendritic MRI contrast agents  $\mathbf{5}_{n=4,16,64}$  and  $\mathbf{5}_{n=1}$  showed a typical bolus in the blood (strong signal increase) directly after injection of contrast agent, followed by a rapid distribution phase (fast signal decline) and later (approximately  $t = 5$  min) the clearance phase (slow signal decline) (Figure 4.8a). Furthermore, low MW contrast agents  $\mathbf{5}_{n=1}$  and  $\mathbf{5}_{n=4}$  were cleared from the blood at a higher rate than dendritic MRI contrast agents  $\mathbf{5}_{n=16}$  and  $\mathbf{5}_{n=64}$ . The low MW contrast agents showed a rapid tumor in-wash, whereas  $\mathbf{5}_{n=16}$  and  $\mathbf{5}_{n=64}$  showed a more gradual and prolonged tumor in-wash (Figure 4.8b). The relative signal intensity changes in the tumor periphery with  $\mathbf{5}_{n=1}$  and  $\mathbf{5}_{n=4}$  resembled the changes observed in the blood, whereas  $\mathbf{5}_{n=16}$  and  $\mathbf{5}_{n=64}$  showed a gradual increase in signal intensity in time.

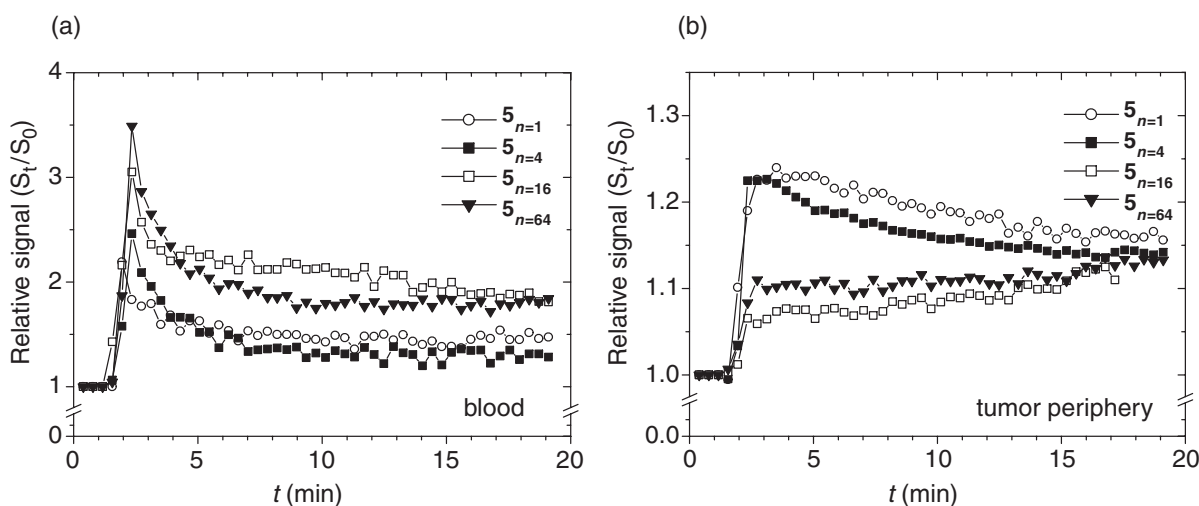


**Figure 4.8** Dynamic CE-MRI with different generations of dendritic contrast agent  $\mathbf{5}_{n=4,16,64}$  and Gd(III)DTPA-based complex  $\mathbf{5}_{n=1}$ . The relative signal over time (a) in the blood and (b) at the tumor periphery.

Gd(III)DTPA-based complex  $\mathbf{5}_{n=1}$  and all generations of the dendritic MRI contrast agent were cleared through the kidneys as observed by the signal intensity curves of the renal collecting system

(Figure 4.9a) and bladder (Figure 4.9b). However, the clearance of the higher generations proceeds slower, suggesting an inverse relationship between the rate of renal clearance and the generation of the dendritic MRI contrast agent.

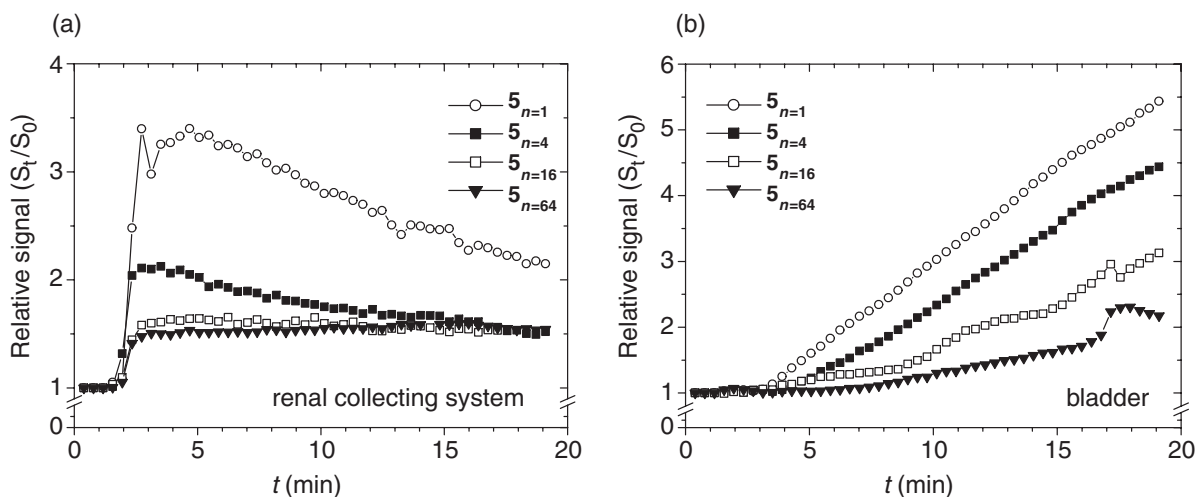


**Figure 4.9** Dynamic CE-MRI with different generations of dendritic contrast agents  $5_{n=4,16,64}$  and Gd(III)DTPA-based complex  $5_{n=1}$ . The relative signal over time in (a) the renal collecting system and (b) the bladder.

#### 4.4 MR IMAGING OF TUMOR ANGIOGENESIS

In this section, an interesting application of dendritic MRI contrast agents for the *in vivo* characterization of tumor angiogenesis is presented. Angiogenesis (the formation of new blood vessels) plays a key role in tumor growth and has become a target for new therapeutic agents, which inhibit the development of neovasculature.<sup>13-17</sup> A promising development is the *in vivo* characterization of tumor angiogenesis<sup>16</sup> and monitoring the effects of therapeutic agents by means of dynamic  $T_1$ -weighted CE-MRI.<sup>18</sup> A typical angiogenic property is an increased microvessel permeability, which may lead to increases in tumor blood volume and flow level. These properties are reflected in dynamic CE-MRI data.<sup>17,19,20</sup>

Dynamic CE-MRI data may be subjected to a pharmacokinetic analysis to derive quantitative parameters that reflect tumor microcirculation characteristics and the angiogenic activity.<sup>21,22</sup> MR imaging derived kinetic parameters include the endothelial transfer coefficient ( $K^{PS}$ ), which represents the rate of transfer of contrast medium from the blood to the interstitial space, and the fractional plasma volume ( $f^{PV}$ ), which represents the volumetric fraction of the (blood) plasma in the tissue. The  $K^{PS}$  has been shown to correlate with the histological microvessel density and the tumor grade and has been used to monitor the effect of anti-angiogenic treatments in different tumor models.<sup>18,23-27</sup>

An important discussion in the field of dynamic CE-MRI is the choice of the MRI contrast agent, particularly regarding the molecular weight or the particle size of the contrast agent. Previous literature studies have shown that higher molecular weight MRI contrast agents, such as Gd(III)DTPA conjugated to polymers or BSA, and iron oxide particles, are better for deconvoluting the vessel permeability and the vascular volume compared to the low molecular weight Gd(III) complexes.<sup>5,18,23-27</sup>

It is hypothesized that low MW contrast agents leak relatively easily from the blood through the interstitial matrix compared to higher MW contrast agents (Figure 4.10). If this is true, tumor  $K^{\text{PS}}$  and  $f^{\text{PV}}$  values measured using low MW contrast agents are affected by flow, because the rate of extravasation depends on the magnitude of the blood flow. In addition to hyperpermeability, flow heterogeneity is another intrinsic characteristic of tumor vascularization. Consequently, there will be a large distribution (*i.e.* a large standard deviation) in the  $K^{\text{PS}}$ , which is directly related to the blood flow. Moreover, the easy extravasation of low MW MRI contrast agents causes an overestimation of their  $f^{\text{PV}}$  values in comparison to intravascularly residing higher MW contrast agents.

Alternatively, when high MW contrast agents leak from the blood, they move through the interstitial matrix with relative difficulty (Figure 4.10b). The transfer through the interstitial matrix is limited by their relatively low intrinsic permeability and is less dependent on tumor flow (*i.e.* permeability limited region). In this situation the tumor  $K^{\text{PS}}$ -value approximates the microvessel permeability–surface area product (*i.e.*  $K^{\text{PS}} = PS$ ). Therefore, measures for the permeability (or  $PS$ ) and  $f^{\text{PV}}$  may best be obtained with high MW contrast agents. However, microvascular flow, or the degree of vascularization, which is indirectly related to flow, may best be measured using a low MW contrast agent since the rate of small molecules is determined by the blood supply (*i.e.* flow limited regime).

However, the high MW contrast agents that have been evaluated to date (*e.g.* Gd(III)DTPA complexes conjugated to polymers, and iron oxide particles), may have been too different in molecular composition and paramagnetic properties to make a fair comparison. Dendritic MRI contrast agents, which vary only in MW but are otherwise chemically identical, might be ideal structures to reveal the effect of molecular size on the measurement of tumor angiogenesis. Therefore, different generations of the Gd(III)DTPA-terminated poly(propylene imine) dendrimer, and Gd(III)DTPA-based complex  $\mathbf{5}_{n=1}$  were used to investigate the influence of molecular size on the measurement of  $K^{\text{PS}}$  and  $f^{\text{PV}}$  in a tumor model.<sup>12</sup>

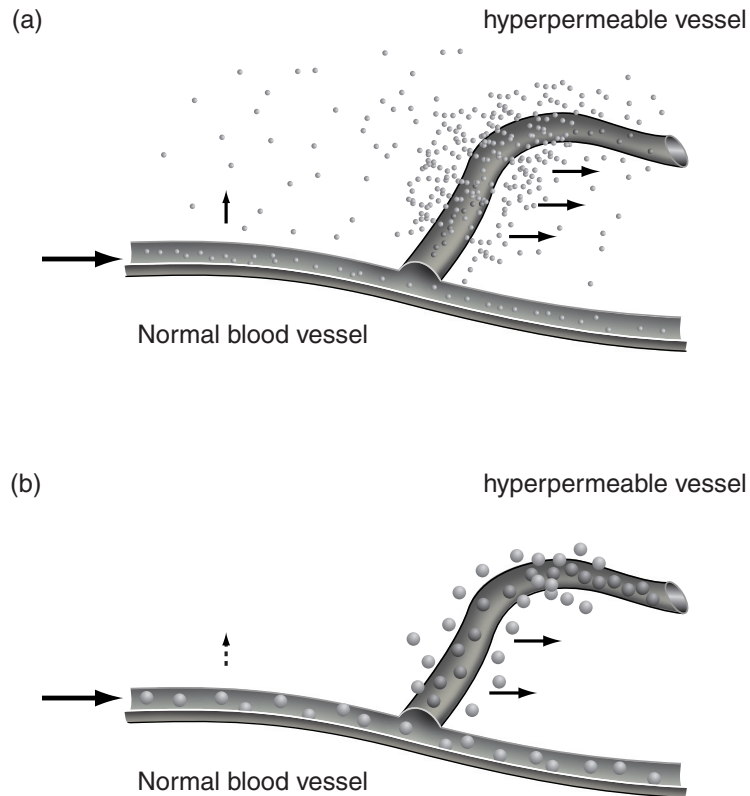


**Figure 4.10** A graphic depiction of the difference between low MW MRI contrast agents and high MW MRI contrast agents. (a) Low MW MRI contrast agents, e.g.  $Gd(III)DTPA$ , leak readily from the lumen of hyperpermeable vessels due to their small size; (b) high MW MRI contrast agents leak from hyperpermeable vessels at a lower rate and are more confined to the vascular space.

The endothelial transfer coefficient ( $K^{PS}$ ) and the fractional plasma volume ( $f^{PV}$ ) in the tumor were derived from the dynamic CE-MRI data applying a two-compartment pharmacokinetic model.<sup>12</sup> As shown in Figure 4.11, the  $K^{PS}$  values decreased as a function of the molecular weight of the MRI contrast agents. The  $f^{PV}$  values, in relation with the molecular weight of the MRI contrast agent, showed a stepwise pattern with a sudden decrease in  $f^{PV}$  between 3.0 and 12.0  $kg \cdot mol^{-1}$ . Moreover, it was observed that the average tumor  $K^{PS}$  and  $f^{PV}$  values decrease in spatial heterogeneity with increasing generation of the dendrimer (Figure 4.11). These observations support the notion that  $K^{PS}$  and  $f^{PV}$  values are more accurately measured using higher MW contrast agents.

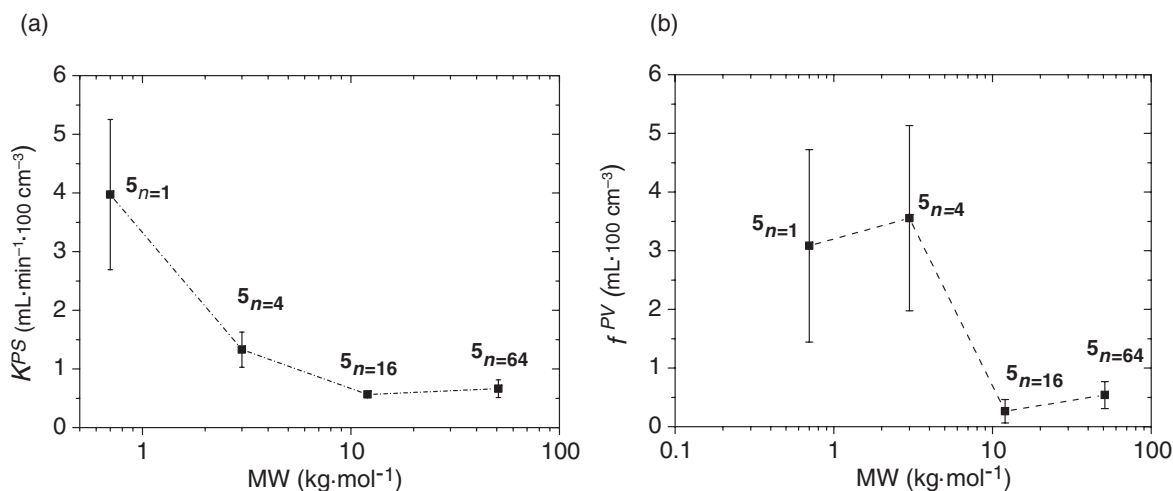


**Figure 4.11** Graphs of the average endothelial transfer coefficient ( $K^{PS}$ ) and the average fractional plasma volume ( $f^{PV}$ ) in the tumor versus the theoretical molecular weight ( $MW$ ) of Gd(III)DTPA-terminated poly(propylene imine) dendrimers  $5_{n=4,16,64}$  and Gd(III)DTPA-based complex  $5_{n=1}$ .

## 4.5 CONCLUSIONS

Gd(III)DTPA-terminated poly(propylene imine) dendrimers  $5_{n=4,16,64}$  show an increase of both the  $T_1$ - and  $T_2$ -relaxivities with increasing molecular weight. The relaxivity measurements in blood plasma as described here are slightly lower than those measured in citrate buffer (Chapter 3, Section 3.2.4); showing that these contrast agents have no or negligible interactions with blood plasma proteins. The dendritic MRI contrast agents  $5_{n=4,16,64}$  and Gd(III)DTPA-based complex  $5_{n=1}$  are well suited for imaging of sub-millimeter-sized blood vessels and evaluating tumor microcirculatory characteristics in mice. All presented contrast agents show renal clearance on CE-MRI. The higher generations of the dendritic MRI contrast agent display higher signal enhancement and lower concentration detection limits. Higher generations of Gd(III)DTPA-terminated poly(propylene imine) dendrimers  $5_{n=16,64}$  more accurately and independently monitor tumor vessel permeability and vascular volume than  $5_{n=1,4}$ . Higher molecular weight MRI contrast agents may be preferred over low molecular weight contrast agents for evaluating reductions in microvessel permeability and vascular volume. Lower molecular weight MRI contrast agents may be more applicable for evaluating therapeutic reductions in magnitude and heterogeneity of microcirculatory blood flow.

## 4.6 MATERIAL AND METHODS

### 4.6.1 Synthesis of Gd(III)DTPA-terminated poly(propylene imine) dendrimers

Different generations of the poly(propylene imine) dendrimer were obtained from SyMO-Chem BV (Eindhoven, the Netherlands). The primary amines of the first, the third and the fifth generation of the poly(propylene imine) dendrimer (DAB-*dendr*-(NH<sub>2</sub>)<sub>*n*</sub>) (with respectively 4, 16, and 64 end groups (*n*))<sup>28</sup> were reacted with an isocyanate-activated lysine-based DTPA pentaester in dichloromethane (DCM), deprotected with trifluoroacetic acid and complexated with GdCl<sub>3</sub> (See Chapter 3).<sup>6</sup>

### 4.6.2 *In vitro* MR imaging

MR imaging was performed on a 1.5 T system (Philips Medical Systems, Best, the Netherlands) with a maximum gradient strength of 30 mT/m and rise time of 200 μs.

#### *Relaxivities in mouse plasma*

For the relaxivity measurements, different concentrations of Gd(III) for Gd(III)DTPA and **5<sub>*n*=1,4,16,64</sub>** (range 0.05–1.0 mM) were prepared in mouse blood plasma (Harlan Sera-Lab, UK) with sodium citrate as anti-coagulant. Gd(III) concentrations used for the relaxivity measurements were determined by means of Inductively Coupled Plasma Atomic Emission Spectroscopy (ICP-AES). The MR measurements were performed using a circular surface coil (inner diameter, 8 cm). Localized <sup>1</sup>H-NMR spectra were recorded by using Point Resolved Spectroscopy (PRESS)<sup>29</sup> with 16 acquisitions and 16 phase-encoding steps (voxel dimensions 10 × 10 × 10 mm). Longitudinal relaxation times (*T*<sub>1</sub> in ms) were determined with an inversion recovery pulse-sequence using 10 different inversion times ranging from 9 ms to 2900 ms; the repetition times (TR) were at least 5 times longer than the estimated *T*<sub>1</sub> of each sample, and the TE was set at 40 ms. Transverse relaxation times (*T*<sub>2</sub> in ms) were determined by varying the PRESS echo time ranging from 30 to 700 ms (TR = 1500 ms, number of signal averages (NSA) 10).

#### *Concentration detection limits*

These experiments were performed in collaboration with Q.G. de Lussanet (University Maastricht Hospital, the Netherlands). Solutions of the MRI contrast agents in mouse blood plasma were prepared with a Gd(III) concentration in the range of 5.0 × 10<sup>-7</sup> to 1.0 × 10<sup>-3</sup> M, in vials with an inner diameter of 6 mm. All vials were measured simultaneously by using a quadrature volume coil (knee coil; inner diameter, 18 cm). *T*<sub>1</sub>-weighted measurements were performed (three-dimensional fast field echo (3D FFE); TR/TE 14/6 ms; flip angle (FA) 30°; NSA 2) with 30 coronal sections, 1.0 mm thick and subsequently interpolated to 0.5 mm thick sections during reconstruction. Matrix dimensions were 256 × 256, with a field of view of 168 × 134 mm, and reconstructed voxel sizes were 0.65 × 0.52 × 0.5 mm. The average signal intensity (± one standard deviation (SD)) was measured in each vial by selecting 60 (± 5) central voxels in circular regions of interest in the central section thus avoiding Gibbs ringing artefacts. The relative signal change, defined as (S – S<sub>0</sub>)/S<sub>0</sub> in which S represents the MRI signal at a specified concentration and S<sub>0</sub> the MRI signal at concentration zero, was then calculated.

### 4.6.3 *In vivo* MR imaging

#### *Animal Model*

The ethical review committee of the Maastricht University Hospital (the Netherlands) approved the animal studies. The maintenance and care of the experimental animals was in compliance with the guidelines set by the institutional animal care committee, accredited by the National Department of Health. These



experiments were performed in collaboration with Q.G. de Lussanet (University Maastricht Hospital). Four healthy male mice (C57 black 6, Charles River, Maastricht, the Netherlands) were used for serial CE-MR measurements with Gd(III)DTPA-based complex  $\mathbf{5}_{n=1}$  and different generations of dendritic contrast agents  $\mathbf{5}_{n=4,16,64}$  (dose 0.03 mmol Gd(III)/kg body weight). Twelve male nude mice (Swiss *nu/nu*, Charles River, Maastricht) (age 9 weeks) received an injection of  $10^6$  human colon carcinoma cells (LS 174T) subcutaneously in their left flank (QdL). On day 16 after tumor cell injection mice tumor ( $\pm$  SD) volume  $153 \pm 104 \text{ mm}^3$ , were used for dynamic CE-MRI. The mice were anaesthetized with subcutaneous injection of 100 mg of ketamine (Nimatek, Eurovet, Bladel, the Netherlands) per kilogram of body weight and 10 mg/kg of xylazine HCl (Sedamun, Eurovet). The mice were randomly assigned to Gd(III)DTPA-based complex  $\mathbf{5}_{n=1}$  or one of the dendritic MRI contrast agents that were injected (approximate injection rate,  $2 \mu\text{L/s}$ ) into the tail vein and flushed with  $15 \mu\text{L}$  of normal saline (NaCl 0.9 % Injection Fluid, Braun, Melsungen, Germany) ( $2 \mu\text{L/s}$ ). MR imaging was performed using a small circular surface coil (inner diameter, 5 cm). Warm water bags were placed near the mouse to keep the local temperature in the MR imaging unit bore near  $28^\circ\text{C}$ . After MR imaging the mice, while still under anesthesia, were sacrificed by means of cervical dislocation.

### **Serial CE-MRI**

These experiments were performed in collaboration with Q.G. de Lussanet (Maastricht University Hospital). The serial CE-MRI protocol included 6 MR acquisitions of 25 seconds each (one pre-contrast ‘mask’ acquisition, and five contrast-enhanced acquisitions were timed at 8 s, 30 s, 1 min, 3 min, and 8 min after the start of contrast agent injection) (3D FFE; TR/TE 12/3.2 ms; FA  $30^\circ$ ) with 30 coronal, 1.6 mm thick (interpolated to 0.8 mm) slices. Matrix dimensions were  $224 \times 224$ , with a field of view (FOV) of  $90 \times 90$  mm, and reconstructed voxel sizes were  $0.4 \times 0.4 \times 0.8$  mm. Images were evaluated on maximum intensity projections (anterior posterior direction) of subtraction images (*i.e.* each contrast-enhanced image data set minus the mask).

### **Dynamic CE-MRI**

The dynamic CE-MRI protocol included a  $T_1$ -weighted dynamic contrast-enhanced series (3D FFE; TR/TE, 50/7 ms; FA  $35^\circ$ ) with 30 dynamic volume acquisitions of 39 seconds each, sixteen 4.0 mm thick axial sections (interpolated to 2.0 mm). Matrix dimensions were  $128 \times 128$ , with a FOV of  $64 \times 64$  mm, and reconstructed voxel sizes were  $0.5 \times 0.5 \times 2.0$  mm. The MRI contrast agent was slowly injected ( $2 \mu\text{L/s}$ ) during the fifth dynamic volume acquisition. The average signal intensities (arbitrary units, AU) prior to contrast agent injection (*i.e.*  $S_0$ ) were recorded by defining regions of interest for the blood in the aorta, the tumor rim (*i.e.*, outer 1–2 mm margin of the tumor in the central section through the tumor), the renal collecting system, and the bladder. The tumor rim was selected because this area of the tumor is considered the leading edge of the tumor, in which processes such as tumor angiogenesis are most prominent.<sup>17</sup> The signal time course ( $S_t$ ) was averaged for the three mice for each of the contrast agents, and the relative signal over time was calculated ( $S_t/S_0$ ).

### **Analysis of the dynamic CE-MRI data**

Q.G. de Lussanet and dr. W.H. Backes (University Hospital Maastricht, the Netherlands) performed the (statistical) analysis of the dynamic CE-MRI data and the calculation of the fractional blood volume in the tumor (expressed as mL per  $100 \text{ cm}^3$  tissue) and the transfer coefficient (expressed as mL per minute per  $100 \text{ cm}^3$  of tissue). For more details the reader is referred to literature reference 12.

## 4.7 REFERENCES

- (1) Caravan, P.; Ellison, J. J.; McMurry, T. J.; Lauffer, R. B. *Chem. Rev.* **1999**, *99*, 2293-2352.
- (2) Merbach, A. E.; Tóth, E. *The Chemistry of Contrast Agents in Medical Magnetic Resonance Imaging*; John Wiley & Sons: New York, 2001.
- (3) Jacques, V.; Desreux, J. F. *Top. Curr. Chem.* **2002**, *221*, 123-164.
- (4) Clarkson, R. B. *Top. Curr. Chem.* **2002**, *221*, 201-235.
- (5) Daldrup, H.; Shames, D. M.; Wendland, M.; Okuhata, Y.; Link, T. M.; Rosenau, W.; Lu, Y.; Brasch, R. C. *Am. J. Roentgenol.* **1998**, *171*, 941-949.
- (6) Langereis, S.; de Lussanet, Q. G.; van Genderen, M. H. P.; Backes, W. H.; Meijer, E. W. *Macromolecules* **2004**, *37*, 3084-3091.
- (7) Caravan, P.; Cloutier, N. J.; Greenfield, M. T.; McDermid, S. A.; Dunham, S. U.; Bulte, J. W. M.; Amedio, J. C., Jr.; Looby, R. J.; Supkowski, R. M.; Horrocks, W. D., Jr.; McMurry, T. J.; Lauffer, R. B. *J. Am. Chem. Soc.* **2002**, *124*, 3152-3162.
- (8) Hovland, R.; Aasen, A. J.; Klaveness, J. *Org. Biomol. Chem.* **2003**, *1*, 1707-1710.
- (9) Aime, S.; Fasano, M.; Terreno, E. *Chem. Soc. Rev.* **1998**, *27*, 19-29.
- (10) Vold, R. L.; Waugh, J. S.; Klein, M. P.; Phelps, D. E. *J. Chem. Phys.* **1968**, *48*, 3831-3832.
- (11) Nunn, A. D.; Linder, K. E.; Tweedle, M. F. *Q J Nucl. Med.* **1997**, *41*, 155-162.
- (12) Lussanet, Q. G.; Langereis, S.; Beets-Tan, R. G. H.; van Genderen, M. H. P.; Griffioen, A. W.; van Engelshoven, J. M. A.; Backes, W. H. *Radiology* **2005**, *235*, 65-72.
- (13) Griffioen, A. W.; Molema, G. *Pharmacological Reviews* **2000**, *52*, 237-268.
- (14) Folkman, J. *Nature Med.* **1995**, *1*, 27-31.
- (15) Cristofanilli, M.; Charnsangavej, C.; Hortobagyi, G. N. *Nat. Rev. Drug Discovery* **2002**, *1*, 415-426.
- (16) McDonald, D. M.; Choyke, P. L. *Nature Med.* **2003**, *9*, 713-725.
- (17) Carmeliet, P.; Jain, R. K. *Nature* **2000**, *407*, 249-257.
- (18) Padhani Anwar, R. *J. Magn. Res. Imaging* **2002**, *16*, 407-422.
- (19) Patan, S.; Munn, L. L.; Jain, R. K. *Microvasc. Res.* **1996**, *51*, 260-272.
- (20) Hobbs, S. K.; Monsky, W. L.; Yuan, F.; Roberts, W. G.; Griffith, L.; Torchilin, V. P.; Jain, R. K. *Proc. Natl. Acad. Sci.* **1998**, *95*, 4607-4612.
- (21) van Dijke, C. F.; Brasch, R. C.; Roberts, T. P.; Weidner, N.; Mathur, A.; Shames, D. M.; Mann, J. S.; Demsar, F.; Lang, P.; Schwickert, H. C. *Radiology* **1996**, *198*, 813-818.
- (22) Tofts, P. S.; Brix, G.; Buckley, D. L.; Evelhoch, J. L.; Henderson, E.; Knopp, M. V.; Larsson, H. B.; Lee, T. Y.; Mayr, N. A.; Parker, G. J.; Port, R. E.; Taylor, J.; Weisskoff, R. M. *J. Magn. Res. Imaging* **1999**, *10*, 223-232.
- (23) Choyke, P. L.; Dwyer, A. J.; Knopp, M. V. *J. Magn. Res. Imaging* **2003**, *17*, 509-520.
- (24) Lussanet, Q. G.; Backes, W. H.; Griffioen, A. W.; van Engelshoven, J. M. A.; Beets-Tan, R. G. H. *Radiology* **2003**, *229*, 429-438.
- (25) Turetschek, K.; Huber, S.; Floyd, E.; Helbich, T.; Roberts, T. P.; Shames, D. M.; Tarlo, K. S.; Wendland, M. F.; Brasch, R. C. *Radiology* **2001**, *218*, 562-569.
- (26) Roberts, T. P. L.; Turetschek, K.; Preda, A.; Novikov, V.; Moeglich, M.; Shames, D. M.; Brasch, R. C.; Weinmann, H. J. *Acad Radiol* **2002**, *9 Suppl 2*, S511-513.
- (27) Bhujwalla, Z. M.; Artemov, D.; Natarajan, K.; Solaiyappan, M.; Kollars, P.; Kristjansen, P. E. G. *Clin Canc Res* **2003**, *9*, 355-362.
- (28) Bosman, A. W.; Janssen, H. M.; Meijer, E. W. *Chem. Rev.* **1999**, *99*, 1665-1688.
- (29) Bottomley, P. A. *U.S. Patent 4 480 228* **1984**.



---

## Chapter 5

### Probing the interaction of the biotin–avidin complex with the relaxivity of biotinylated MRI contrast agents\*

---

**ABSTRACT:** *The association between biotinylated Gd(III)-based complexes and avidin has been used to study the effect of binding on the ionic longitudinal relaxivity (per Gd(III), ionic  $r_1$ ). MR titration experiments have shown that the strong and specific interaction between biotin and avidin can be probed through the ionic  $r_1$  of biotinylated Gd(III)-based complexes. Furthermore, E-titrations with biotinylated MRI contrast agents, based on either Gd(III)DTPA or Gd(III)DO3A, show an increase in the ionic  $r_1$  by a factor 2.7 and 1.7, respectively, upon binding to avidin. The quantitative model that has been presented provides an elegant tool to study the formation of supramolecular assemblies in aqueous media. Furthermore, a new class of MRI contrast agents based on the self-assembly of DTPA-functionalized copolymer **11** and amphiphilic copolymer **12** into polymeric micelles has been developed. Cryo-TEM images revealed the presence of spherical particles with a core–corona structure (average diameter of the core 40–45 nm). The ionic  $r_1$  of the Gd(III)DTPA complex in the mixed polymeric aggregate was  $27.6 \text{ mM}^{-1}\text{s}^{-1}$ , almost 7-fold higher than parent Gd(III)DTPA.*

---

\* Part of this work has been published: Langereis, S.; Kooistra, H.A.T.; van Genderen, M.H.P.; Meijer, E.W. *Org. Biomol. Chem*, **2004**, 1271-1273.

## 5.1 INTRODUCTION

In the previous Chapters, it has been shown that the relaxivity of Gd(III)DTPA can be modulated through covalent attachment to poly(propylene imine) dendrimers.<sup>1</sup> The gain in relaxivity was attributed to a lower molecular tumbling rate of the Gd(III) complex, *i.e.* an increase in the rotational correlation time. An alternative strategy to increase the relaxivity by decreasing the molecular tumbling rate of a Gd(III) complex involves the non-covalent binding of the complex to a macromolecule, as in substrate–receptor interactions.<sup>2,3</sup> This phenomenon is known as receptor-induced magnetization enhancement (RIME).<sup>4,6</sup> In a pioneering study, Lauffer *et al.* reported the non-covalent, reversible binding of a low molecular weight RIME contrast agent (MS-325) to human serum albumin, a plasma protein (Figure 5.1).<sup>7-9</sup> The hydrophobic interaction between MS-325 and the plasma protein led to a 5-fold increase in the relaxivity over the native MS-325, at 1.5 T and 37 °C.<sup>8</sup> Furthermore, *in vivo* studies showed that the higher effective molecular weight of the supramolecular complex resulted in a prolonged retention time in the vascular system.<sup>10,11</sup>

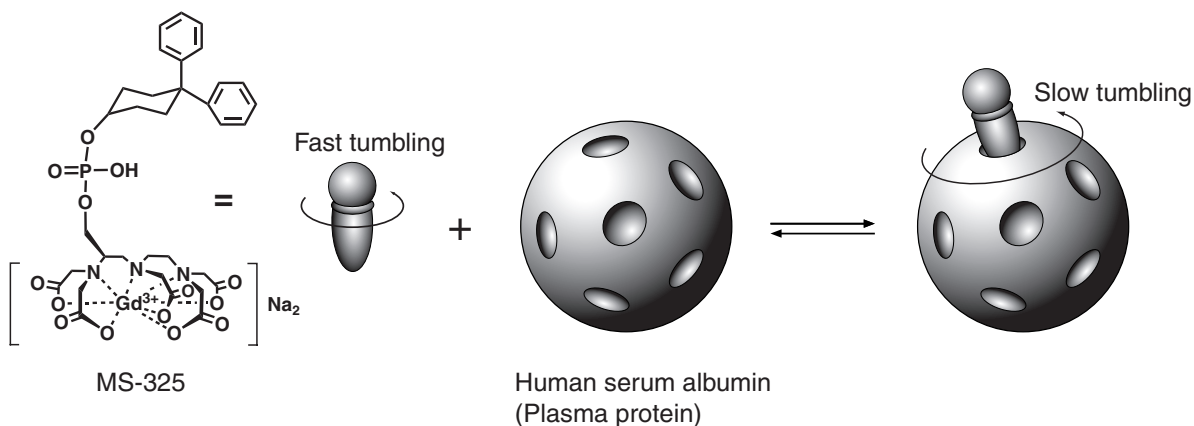


**Figure 5.1** Schematic representation of the receptor-induced magnetization enhancement (RIME) effect,<sup>4,6</sup> illustrated for the non-covalent interaction between MS-325 and human serum albumin.<sup>7,8</sup>

The binding between MS-325 and the plasma protein is rather weak ( $K_a \approx 1.1 \times 10^4 \text{ M}^{-1}$ ) and non-specific.<sup>8</sup> Under such conditions the association process is difficult to study due to the presence of multiple binding sites with different association constants. Lately, several exciting approaches in the development of MRI contrast agents with both higher binding selectivities and affinities have been reported, including enzyme-specific MRI contrast agents,<sup>12</sup> DNA-specific MRI contrast agents<sup>13</sup> and protein-specific MRI contrast agents.<sup>14</sup>

To study the RIME effect quantitatively in well-defined supramolecular systems, we synthesized a series of biotinylated MRI contrast agents that can bind to avidin (Figure 5.2). It has been well established that avidin (MW = 64 kDa), a tetrameric protein, is capable of binding four equivalents of biotin in a strong ( $K_a \approx 1.7 \times 10^{15} \text{ M}^{-1}$ ), specific, and non-cooperative fashion.<sup>15,16</sup> Both

compounds **1** and **2**, based on DTPA and an *N*-monosubstituted DO3A-derivative (DO3A = 1,4,7,10-tetraazacyclododecane-1,4,7-triacetic acid), were prepared as guest molecules for avidin. This allows a comparison between these two widely used Gd(III) chelates with respect to the RIME effect. Moreover, we can use these new Gd(III) complexes as a probe to study the biotin-avidin association.

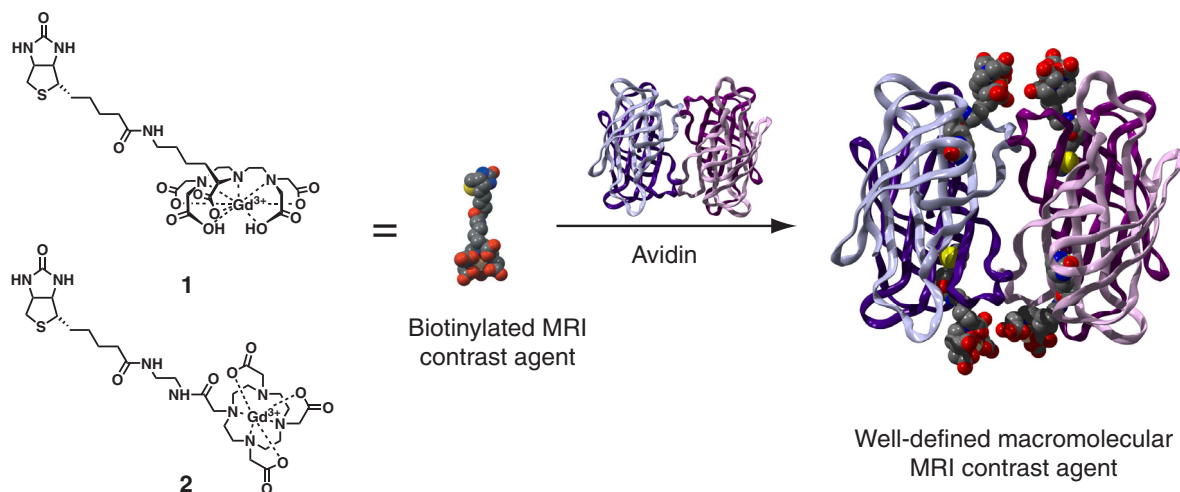
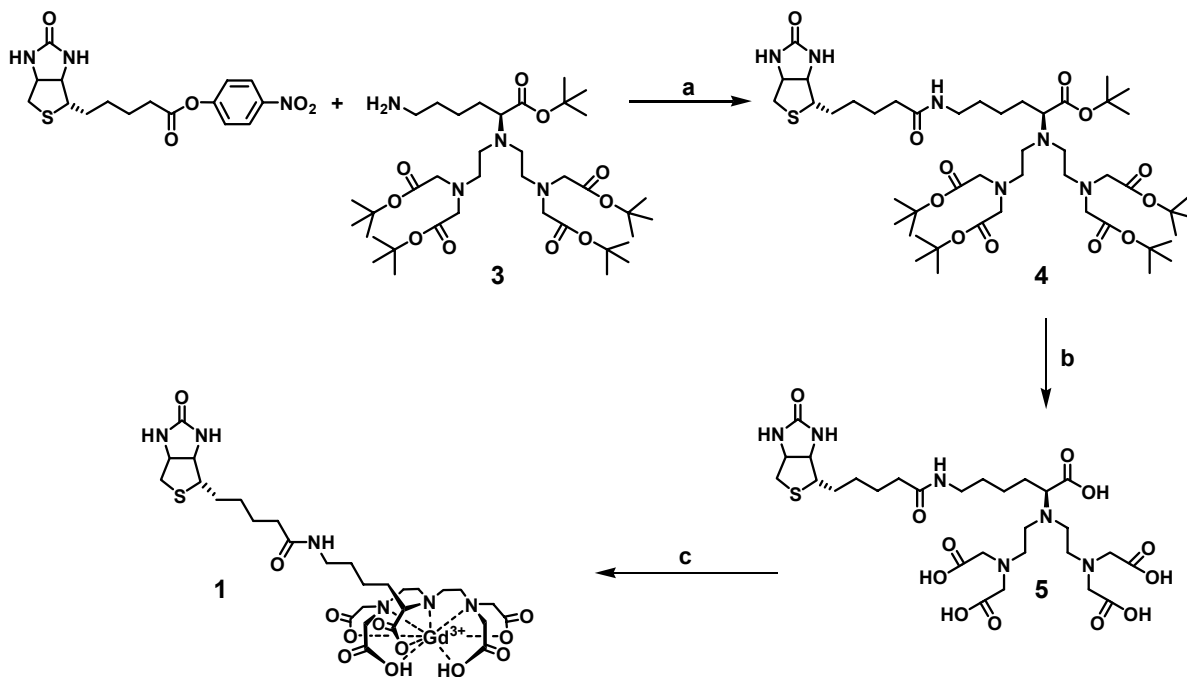


**Figure 5.2** A supramolecular approach for the synthesis of well-defined supramolecular MRI contrast agents based on either biotinylated Gd(III)DTPA (**1**) or biotinylated Gd(III)DO3A (**2**) and avidin.

## 5.2 BIOTINYLATED Gd(III)DTPA

### 5.2.1 Synthesis and characterization

The synthetic strategy to biotinylated Gd(III)DTPA complex **1** is depicted in Scheme 5.1. For the synthetic details on the lysine-based DTPA pentaester **3** the reader is referred to Chapter 2 (Section 2.2.1). The amidation reaction between **3** and (+)-biotin-4-nitrophenyl ester was carried out in *N,N*-dimethylformamide (DMF), to provide biotinylated DTPA analogue **4** in 76% yield after preparative size exclusion chromatography (Biobeads S-X8). The  $^1\text{H-NMR}$  spectrum of **4** featured a set of well-resolved signals in the region 4.0–7.0 ppm, which were ascribed to the biotin part of **4** (Figure 5.3). Cleavage of the *tert*-butyl ester moieties was accomplished with trifluoroacetic acid (TFA) in dichloromethane (DCM). Additional purification by dialysis and freeze-drying yielded **5**, as evidenced from  $^1\text{H-NMR}$  spectroscopy and ESI-MS. In the final step Gd(III) complex **1** was obtained through the addition of  $\text{GdCl}_3$  to a solution of **5** at pH 7. The solution was purified with dialysis and after freeze-drying the Gd(III) complex **1** was obtained in 67% yield.



**Scheme 5.1** Synthesis of biotinylated Gd(III)DTPA (**I**). (a) DMF; (b) 1:2 v/v TFA/DCM, 20 °C; (c) GdCl<sub>3</sub>·6 H<sub>2</sub>O, water, NH<sub>4</sub>OH, 20 °C at pH 7.

The formation of **1** was verified with IR spectroscopy and ESI-QTOF mass spectrometry, while the Gd(III) content was determined with inductively coupled plasma atomic emission spectroscopy (ICP-AES).

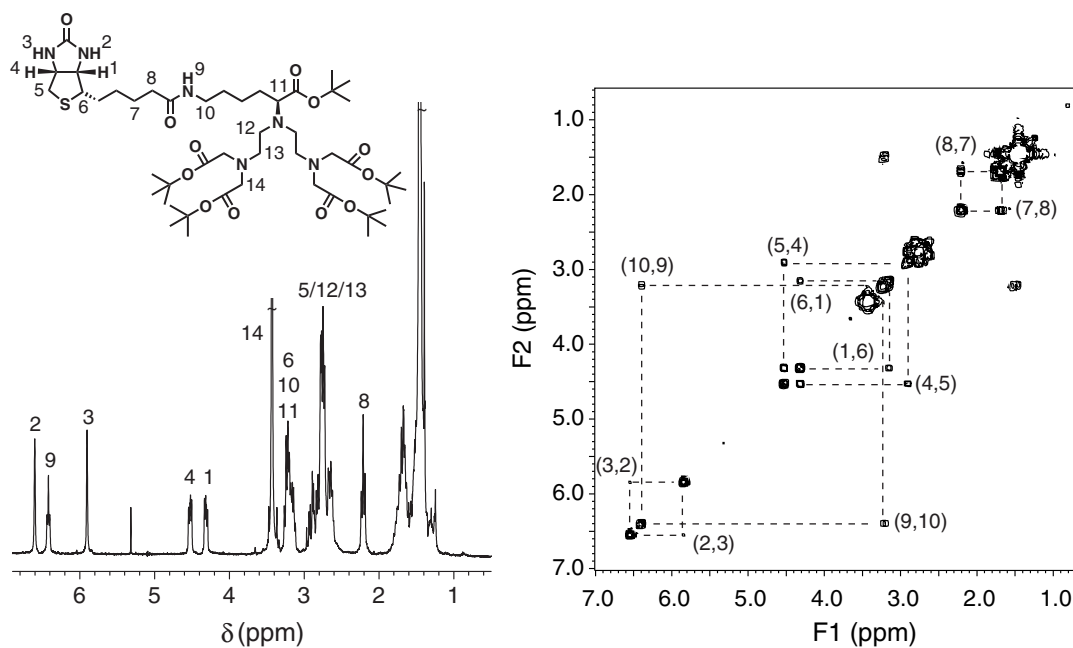


**Figure 5.3** <sup>1</sup>H-NMR and <sup>1</sup>H,<sup>1</sup>H-COSY spectra of **4** in CDCl<sub>3</sub>.

The IR spectra of DTPA analogue **5** and the corresponding Gd(III)DTPA complex **1** (Figure 5.4a) show the characteristic shifts of the carbonyl absorptions from 1700  $\text{cm}^{-1}$  and 1630  $\text{cm}^{-1}$  to 1586  $\text{cm}^{-1}$  upon complexation with Gd(III).

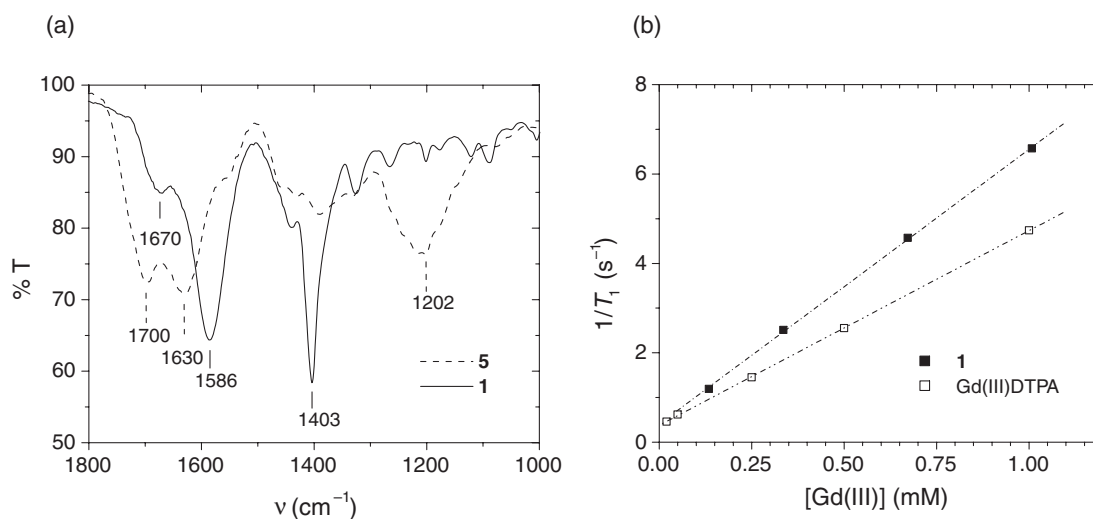


**Figure 5.4** (a) IR spectra of biotinylated DTPA (**5**) and biotinylated Gd(III)DTPA complex (**1**); (b) longitudinal relaxation rate ( $1/T_1$ ) versus the concentration of Gd(III) in PBS buffer at pH 7.4 and 20 °C. Biotinylated Gd(III)DTPA complex **1** (filled squares) and Gd(III)DTPA (open squares).

The longitudinal relaxivity ( $r_1$ ) of **1** was determined by measuring the concentration dependency of its longitudinal relaxation time ( $T_1$ ) at 1.5 T and 20 °C (Figure 5.4b). The data gave a good linear fit ( $R^2 > 0.999$ ) to the equation  $(1/T_1)_{\text{observed}} = (1/T_1)_{\text{diamagnetic}} + r_1[\text{Gd(III)}]$  and an  $r_1$  of  $6.1 \pm 0.2 \text{ mM}^{-1}\text{s}^{-1}$  was calculated. The  $r_1$  of **1** (MW = 0.8  $\text{kg}\cdot\text{mol}^{-1}$ ) is slightly lower than the relaxivities found for functionalized Gd(III)DTPA complexes presented in Chapter 2 (Figure 2.11, e.g. Gd(III) complex **19** (MW = 0.8  $\text{kg}\cdot\text{mol}^{-1}$ )  $r_1 = 8.4 \text{ mM}^{-1}\text{s}^{-1}$  and Gd(III) complex **23** (MW = 0.9  $\text{kg}\cdot\text{mol}^{-1}$ )  $r_1 = 8.5 \text{ mM}^{-1}\text{s}^{-1}$ ). This illustrates that not only the molecular weight of the Gd(III)DTPA complex but also other parameters determine the overall relaxivity (See Chapter 2, Section 2.3.1).

### 5.2.2 Binding studies

MR titration experiments with **1** and avidin were performed to investigate the effect of binding on the longitudinal ionic relaxivity (ionic  $r_1$ , i.e. relaxivity per Gd(III)). It was found that the addition of a concentrated stock solution of avidin to **1**, a so-called E-titration<sup>17</sup> in which the multivalent protein is added to the ligand, resulted in a linear increase in the ionic  $r_1$ , as shown in Figure 5.5. This is indicative of strong binding between **1** and the biotin-binding pocket of avidin (See Appendix). At higher ratios between avidin and **1** a plateau value for the ionic  $r_1$  was reached.



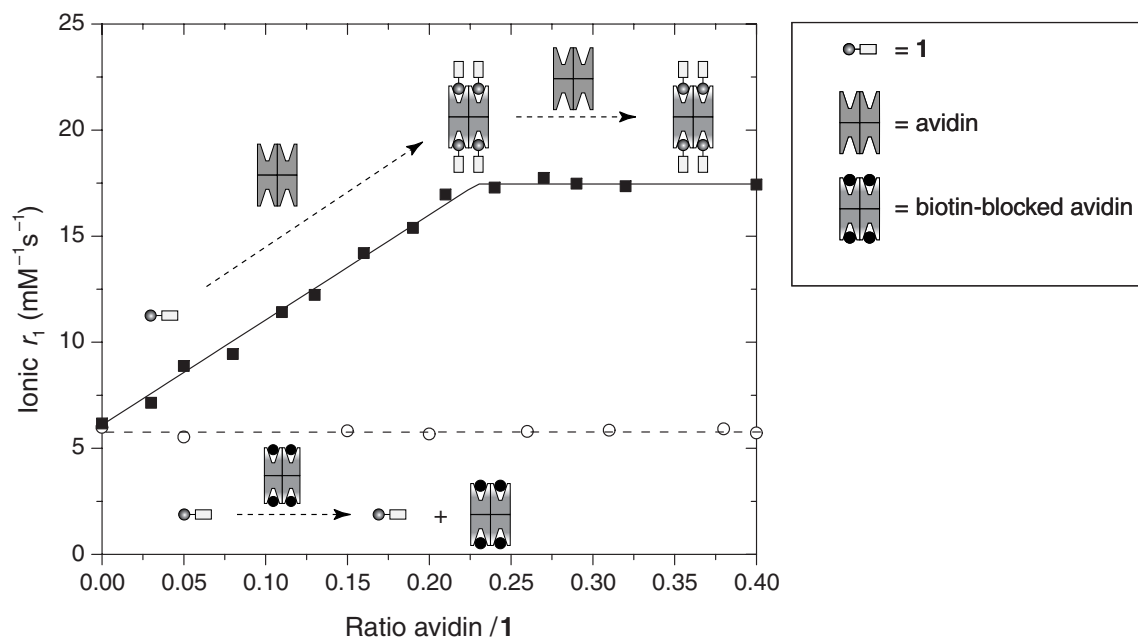


**Figure 5.5** E-titration<sup>17</sup> of a  $67 \mu\text{M}$  solution of biotinylated Gd(III)DTPA (**1**) with avidin (filled squares) at 1.5 T and 20 °C. The control experiment showing the titration of a solution of  $67 \mu\text{M}$  of biotinylated Gd(III)DTPA with (+)-biotin blocked avidin (open circles). All MR titration experiments were performed in 0.1 M PBS buffer at pH 7.4.

Both the ionic  $r_1$  of **1** bound to avidin (ionic  $r_{1,bound}$ ) and the binding stoichiometry between **1** and avidin ( $N$ ) were calculated with a mathematical model describing the binding of multiple ligands to a multivalent protein with  $N$  identical, independent binding sites (See Appendix).<sup>18</sup> Fitting the E-titration data to this model, taking into account that  $K_a = 1.7 \times 10^{15} \text{ M}^{-1}$  and  $r_{1,free} = 6.1 \text{ mM}^{-1}\text{s}^{-1}$ , resulted in an ionic  $r_{1,bound} = 17.5 \pm 0.3 \text{ mM}^{-1}\text{s}^{-1}$  and  $N = 4.4 \pm 0.2$  ( $R^2 > 0.995$ ). The ionic  $r_{1,bound}$  is a factor 2.7 higher than ionic  $r_{1,free}$ . This observed gain in the ionic  $r_1$  of **1** upon binding to avidin is related to a decrease in the molecular tumbling rate, *i.e.* an increase in the rotational correlation time. The calculated value for the binding stoichiometry between **1** and avidin is only slightly higher than the theoretical value. Non-specific binding (physical adsorption) of **1** to avidin was ruled out by performing a control experiment, wherein the biotin binding pockets of avidin are presaturated with (+)-biotin. In that case, no increase in the ionic  $r_1$  of **1** was observed (Figure 5.5). This implied also that ligand exchange between **1** and (+)-biotin was extremely slow on the MR timescale. Therefore, this exchange process can be disregarded under the applied experimental conditions.<sup>16</sup>

The MR titration experiment was also performed in the reversed way, a so-called M-titration<sup>17</sup> in which **1** is added to a solution of avidin (Figure 5.6). Upon addition of **1** to a solution of avidin in 0.1 M PBS buffer at pH 7.4 initially a minor increase in the ionic  $r_1$  of **1** was observed. Such a small increase may be attributed either to the increase in molecular weight upon complexation or to interactions between individual Gd(III) moieties bound to the same avidin molecule. The latter

effect was observed for higher generations of the Gd(III)DTPA-terminated poly(propylene imine) dendrimers (See Chapter 3, Section 3.3),<sup>1</sup> but is most likely not very pronounced in the case of **1** and avidin, since the distance between the Gd(III)DTPA units is much larger. The use of an excess of **1** resulted in a decrease of the average ionic  $r_1$  as a consequence of the increasing amount of unbound **1** in solution (Figure 5.6).

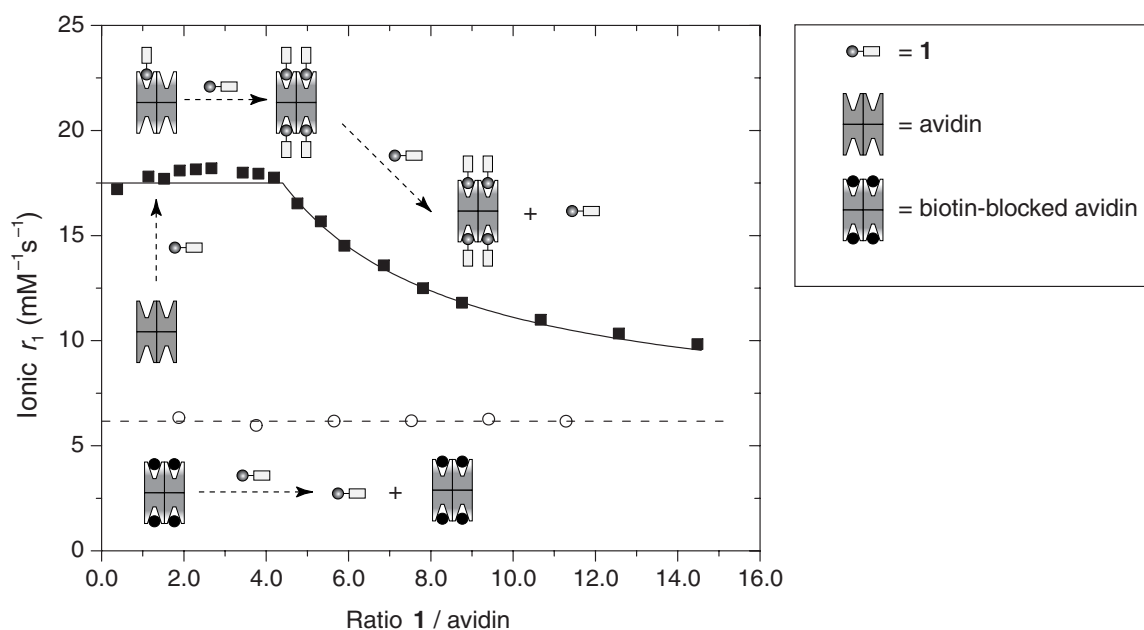


**Figure 5.6**  $M$ -titration<sup>17</sup> of a  $70 \mu\text{M}$  solution of avidin with biotinylated Gd(III)DTPA (filled squares) at 1.5 T and 20 °C. The solid line represents the expected average ionic relaxivity. The control experiments showing the titration of  $70 \mu\text{M}$  avidin with (+)-biotin blocked avidin and biotinylated Gd(III)DTPA (open circles) at 1.5 T and 20 °C. All MR titration experiments were performed in 0.1 M PBS buffer at pH 7.4.

Additionally, the binding stoichiometry between **1** and avidin was validated independently using the HABA assay (Figure 5.7).<sup>19-21</sup> In this titration experiment biotinylated Gd(III)DTPA is added to a solution of avidin in which the biotin binding sites are saturated with the organic dye 4'-hydroxyazobenzene-2-carboxylic acid (HABA,  $K_a \approx 1.7 \times 10^6 \text{ M}^{-1}$ ).<sup>16,20</sup>

Upon addition of **1** to a solution of avidin in 0.1 M PBS buffer at pH 7.4 containing 5 equivalents of HABA per biotin binding site, HABA is expelled from the biotin binding pocket of avidin, resulting in a decrease in the absorption at 500 nm of HABA bound to avidin (Figure 5.8). After the addition of 3.8 equivalents of **1**, the UV/vis absorption spectrum at 500 nm does not change any further, indicating that all binding sites of avidin are occupied with **1**. As a reference experiment, the HABA assay was conducted with native (+)-biotin and avidin. In that case, a binding stoichiometry of 3.9 (+)-biotin molecules per avidin was found.

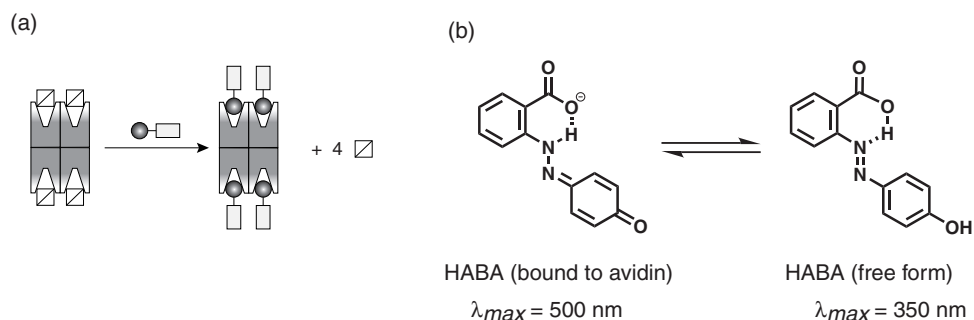


**Figure 5.7** Schematic representation of the HABA assay. (a) Displacement of HABA from the biotin binding pockets of avidin by **1**; (b) chemical structures of HABA in the bound and free form and their absorption maxima.<sup>19,21</sup>

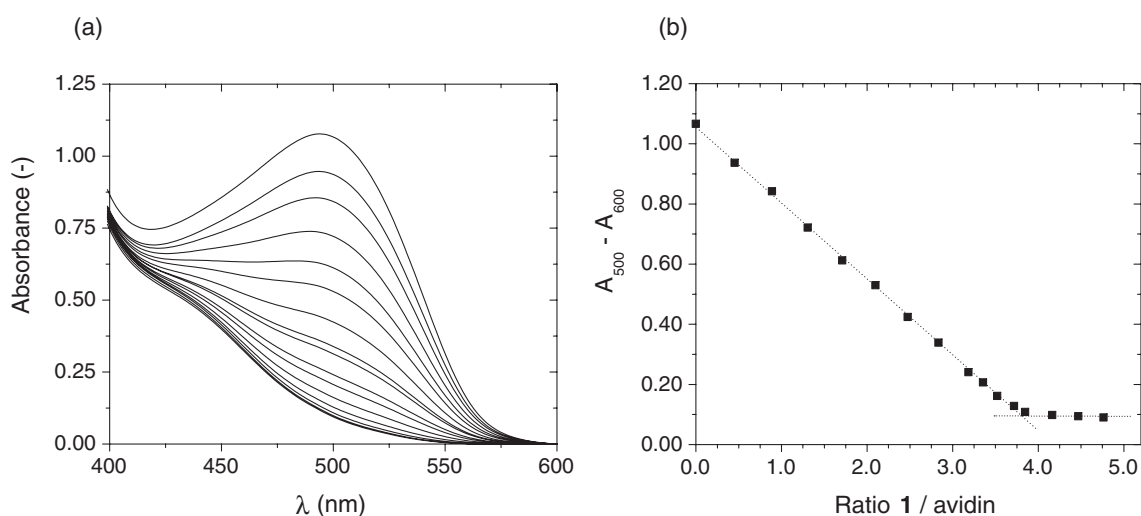
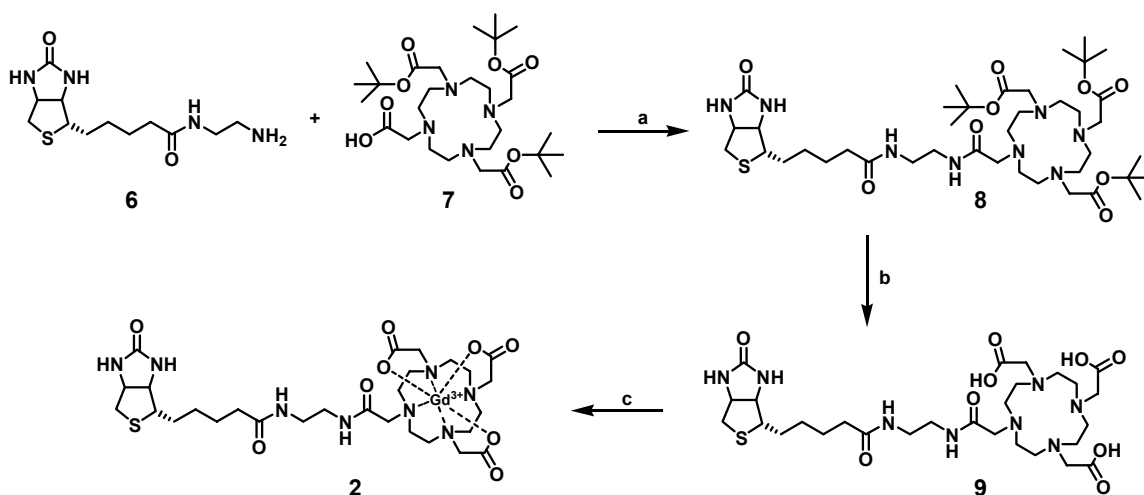


**Figure 5.8** HABA assay of **1** and avidin. (a) UV/vis titration of HABA-saturated avidin with **1** in 0.1 M PBS buffer at pH 7.4; (b) intensity of the UV/vis absorbance at 500 nm versus the ratio between **1** and avidin.

### 5.3 BIOTINYLATED Gd(III)DO3A

#### 5.3.1 Synthesis and characterization

The synthetic strategy to biotinylated Gd(III)DO3A complex **2** is illustrated in Scheme 5.2. Amine-functionalized biotin **6** was synthesized according to the literature procedure of Tolbert *et al.*<sup>24</sup> The DOTA-tris(*tert*-butyl ester) **7** was prepared in analogy to a four-step literature procedure.<sup>22,23</sup> In the first step amine-functionalized biotin **6** was reacted with **7** in DMF using a 2-(1*H*-benzotriazol-1-yl)-1,1,3,3-tetramethyl-uronium hexafluorophosphate (HBTU) activation procedure employing *N,N*-diisopropylethylamine (DiPEA) as a base.



**Scheme 5.2** Synthesis of biotinylated Gd(III)DO3A (**2**). (a) HBTU, DiPEA, DMF; (b) 1:10 v/v triethylsilane/TFA; (c)  $\text{GdCl}_3 \cdot 6 \text{H}_2\text{O}$ ,  $\text{NH}_4\text{OH}$ ,  $\text{H}_2\text{O}$ , pH 7.

Cleavage of the *tert*-butyl esters was accomplished with TFA using triethylsilane as a scavenger. Purification with semi-preparative reversed-phase HPLC using a C18 column afforded intermediate **9**. The corresponding Gd(III) complex was obtained by the addition of an equimolar amount of  $\text{GdCl}_3$  to an aqueous solution of **9** at pH 7. The Gd(III) complex was further purified by dialysis in demineralized water. After freeze-drying **2** was obtained in 89% yield. IR spectroscopy demonstrated that more than 90% of **9** was complexed with Gd(III), by the disappearance of the C–O stretching vibration at  $1187 \text{ cm}^{-1}$  and the shifts of the carbonyl stretching vibrations from  $1720 \text{ cm}^{-1}$  and  $1661 \text{ cm}^{-1}$  to  $1590 \text{ cm}^{-1}$  (Figure 5.9a). In the ESI-MS spectrum the molecular ion  $[\text{M} - \text{H}]^-$  of **2** could be observed at  $m/z$  828.3 amu (Figure 5.9b). The signal at  $m/z$  1655.3 is assigned to a non-covalent dimeric species, whereas the signal at 1241.3 corresponds to a non-covalent doubly charged trimeric species.

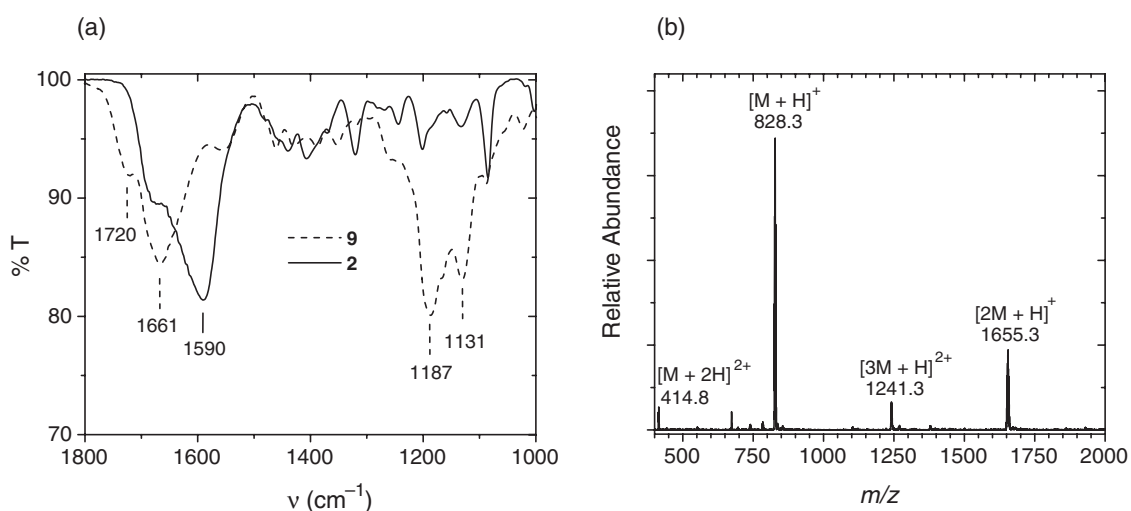


**Figure 5.9** (a) IR spectra of **9** and **2**; (b) ESI-MS spectrum of Gd(III) complex **2** (positive mode).

The longitudinal relaxivity ( $r_1$ ) of **2** in 0.1 M PBS buffer at pH 7.4 was determined by measuring the concentration dependency of its relaxation time at 1.5 T and 20 °C. The data gave a good linear fit ( $R^2 > 0.999$ ) to the equation  $(1/T_1)_{observed} = (1/T_1)_{diamagnetic} + r_1[Gd(III)]$ . The  $r_1$  of **2** is  $4.0 \text{ mM}^{-1}\text{s}^{-1}$  (normalized to ICP-AES data). This value is in good agreement with literature reports on Gd(III)DOTA-based complexes (e.g. Gd(III)DOTA  $r_1 = 4.0 \text{ mM}^{-1}\text{s}^{-1}$  and *N*-monosubstituted Gd(III)DO3A complexes  $r_1 \approx 4 \text{ mM}^{-1}\text{s}^{-1}$ ).<sup>6,25</sup> In contrast to Gd(III)DTPA complexes, substitution with low molecular weight functionalities, such as (+)-biotin, seems not to affect the  $r_1$  of Gd(III)DO3A complexes.

### 5.3.2 Binding studies

To verify the binding stoichiometry between biotinylated Gd(III)DO3A and avidin, the HABA assay was performed probing the UV/vis absorption at 500 nm. The binding of **2** to avidin was indicated by the decrease of the absorption at 500 nm as a result of the displacement of HABA from the biotin binding pockets (Figure 5.10a). From the corresponding titration curve it was found that 3.9 equivalents of **2** bind to one avidin molecule (Figure 5.10b).

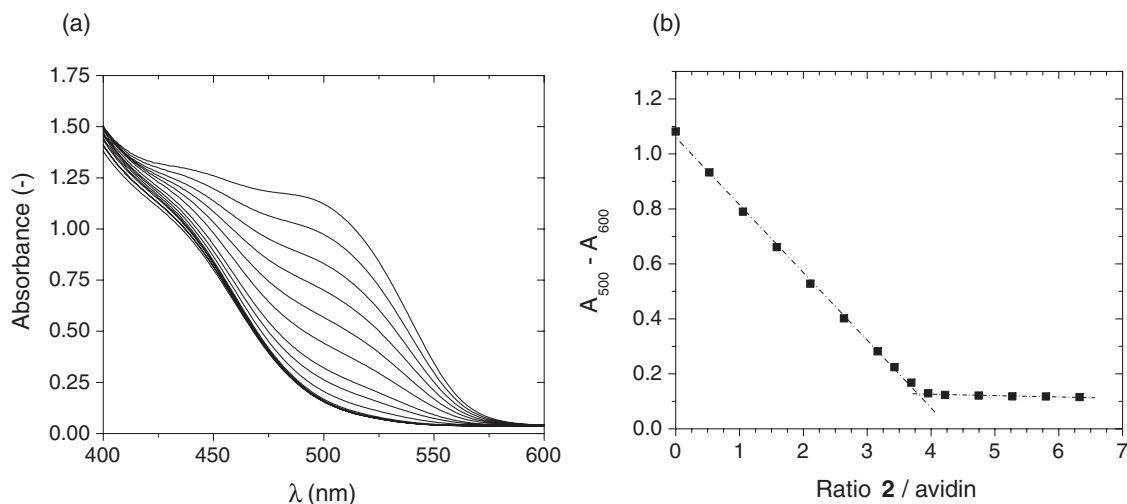


**Figure 5.10** HABA assay of biotinylated Gd(III)DO3A (**2**) and avidin. (a) UV/vis titration of HABA-saturated avidin with **2** in 0.1 M PBS buffer at pH 7.4; (b) UV/vis absorbance at 500 nm versus the ratio between **2** and avidin.

To gain insight into the effect of the binding of **2** to avidin on the ionic  $r_1$  of **2** an E-titration was performed at 1.5 T and 20 °C, by adding a solution of avidin in 0.1 M PBS buffer at pH 7.4 to a solution of **2** (Figure 5.11). A linear increase in the ionic  $r_1$  of **2** was observed indicative for strong binding between **2** and avidin. The addition of more than 0.23 equivalents of avidin did not result in any further changes in the ionic  $r_1$  of **2**, which rules out non-specific binding between **2** and avidin. By fitting the data of the E-titration<sup>17</sup> to a mathematical model describing the binding of multiple

ligands to a multivalent protein with  $N$  identical, independent binding sites, and by taking into account that  $K_a = 1.7 \times 10^{15} \text{ M}^{-1}$  and ionic  $r_{1,free} = 4.0 \text{ mM}^{-1}\text{s}^{-1}$ , an ionic  $r_{1,bound}$  of  $6.8 \pm 0.2 \text{ mM}^{-1}\text{s}^{-1}$  and an  $N$  of  $4.4 \pm 0.2$  ( $R^2 > 0.993$ ) were calculated (See Appendix). The calculated value for the binding stoichiometry between **2** and avidin is only slightly higher (ca. 10%) than the theoretical value.

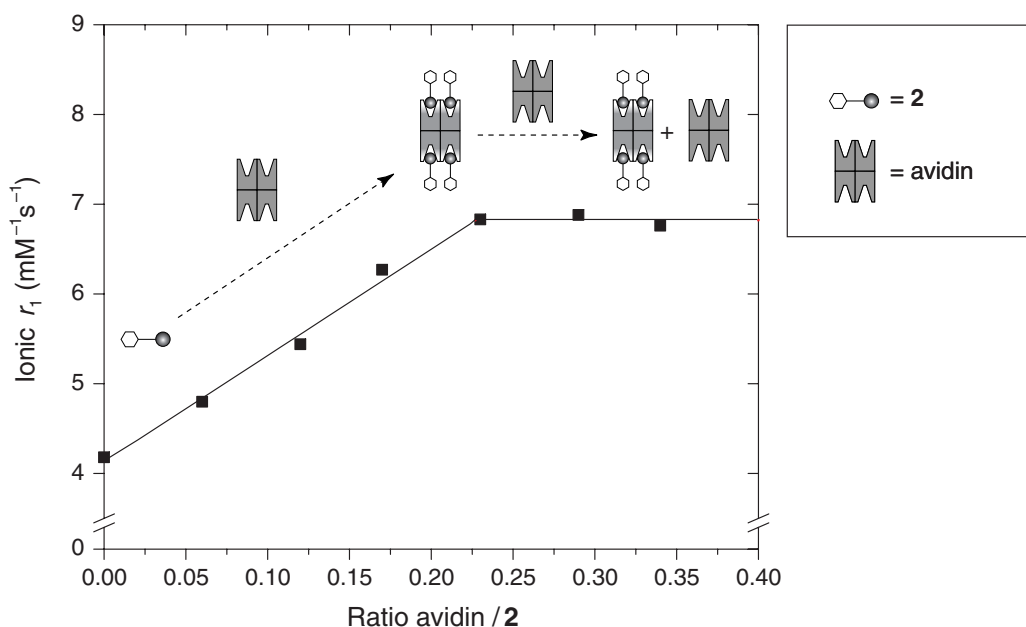


**Figure 5.11** E-titration<sup>17</sup> of a  $101 \mu\text{M}$  solution of biotinylated Gd(III)DO3A (**2**) with avidin (filled squares) at  $1.5 \text{ T}$  and  $20 \text{ }^\circ\text{C}$ . Fitted data with ionic  $r_{1,free} = 4.2 \text{ mM}^{-1}\text{s}^{-1}$ , yielding ionic  $r_{1,bound} = 6.8 \pm 0.2 \text{ mM}^{-1}\text{s}^{-1}$  and  $N = 4.4 \pm 0.2$  (solid line). The E-titration experiment was performed in  $0.1 \text{ M}$  PBS buffer at pH 7.4.

The observed increase in ionic  $r_1$  upon binding to avidin is approximately a factor 1.7. Interestingly, this effect is not as pronounced as in the case of biotinylated Gd(III)DTPA, where an increase in the ionic  $r_1$  with a factor of 2.7 was found, while the spacer length between the Gd(III) chelate and biotin is comparable. This is in agreement with the earlier observation that the molecular weight has less effect on the  $r_1$  for Gd(III)DO3A-based complexes. A fundamental difference between **1** and **2** is the overall charge of the Gd(III) complex (Gd(III) complex **1** is negatively charged at neutral conditions, whereas Gd(III) complex **2** is neutral at pH 7), which may affect the water-exchange rate.

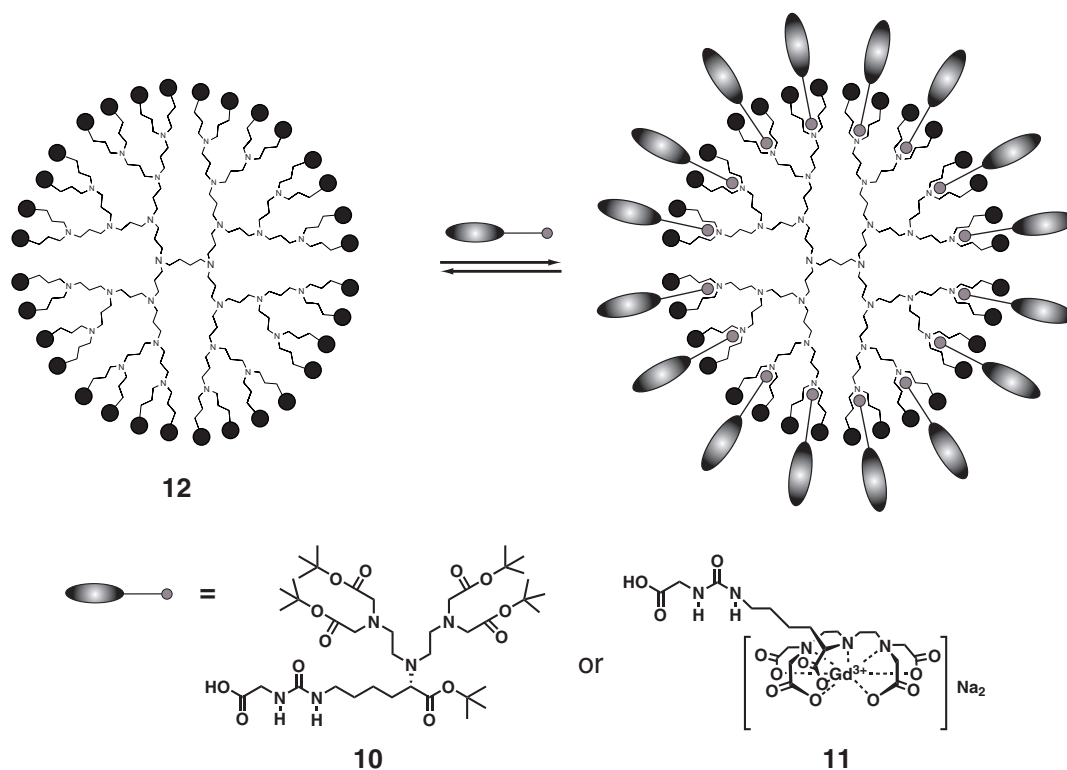
In conclusion, MR titration experiments demonstrated that the strong and specific interaction between biotin and avidin can be probed through the ionic  $r_1$  of biotinylated Gd(III)-based complexes **1** and **2** upon binding to this multivalent protein. The quantitative model presented in this study provides an elegant tool to study in detail the formation of supramolecular assemblies in water.

Currently, we are extending the RIME effect to probe the formation of supramolecular systems of higher complexity in aqueous media. Two systems, namely dendritic host-guest systems and polymeric micelles are under investigation. Initial results on these studies will be presented in the following sections.

## 5.4 Gd(III)DTPA-BASED COMPLEXES IN SUPRAMOLECULAR STRUCTURES

### 5.4.1 Dendritic host-guest complexes

Dendritic structures have shown to be excellent multivalent hosts for various guest molecules resulting in novel supramolecular architectures.<sup>26-39</sup> In our group a supramolecular host-guest system has been developed based on poly(propylene imine) dendrimers functionalized with urea–adamantyl groups, which are able to bind to glycinylurea guests through hydrogen bonding and electrostatic interactions.<sup>33-35,40</sup> The formation of these host–guest complexes has been studied in great detail in CDCl<sub>3</sub> with several NMR techniques, such as <sup>1</sup>H,<sup>1</sup>H-NOESY, <sup>1</sup>H-DOSY, <sup>1</sup>H-NMR, and <sup>13</sup>C-NMR spectroscopy.<sup>41-43</sup> In the previous section, it has been shown that the ionic  $r_1$  of Gd(III)DTPA-based complexes can be used to study the formation of supramolecular assemblies in aqueous media. Here, we explore the usage of glycinylurea-functionalized DTPA derivatives **10** and **11** as guest molecules for the construction of well-defined assemblies in respectively chloroform and aqueous media (Scheme 5.3).



**Scheme 5.3** Schematic representation of a host–guest complex consisting of an adamantylurea-functionalized poly(propylene imine) dendrimer (**12**) and glycinylurea-functionalized guest molecules **10** or **11**.

The formation of host–guest complexes between adamantylurea-functionalized dendrimer **12** and **10** was investigated with  $^1\text{H-NMR}$  spectroscopy in  $\text{CDCl}_3$ . Polar interactions between the host and guest are stabilized by the aprotic nature of this solvent, thereby enhancing the host–guest interaction. Significant shifts were observed in the  $^1\text{H-NMR}$  spectrum upon addition of 32 equivalents of **10** to a solution of **12**, indicative of the formation of the host–guest complex **13** (Figure 5.12). The methylene protons adjacent to the tertiary amines of the outermost shell of the dendrimer were shifted from 2.38 to 2.55 ppm as a result of protonation of the neighboring tertiary amine. In addition, downfield shifts for the urea NH protons of **10** and for the urea NH protons of the dendrimer were observed. These shifts are characteristic for the formation of a host–guest complex consisting of an adamantylurea-functionalized dendrimer and glycinylurea-functionalized guest molecules.<sup>33,42</sup>

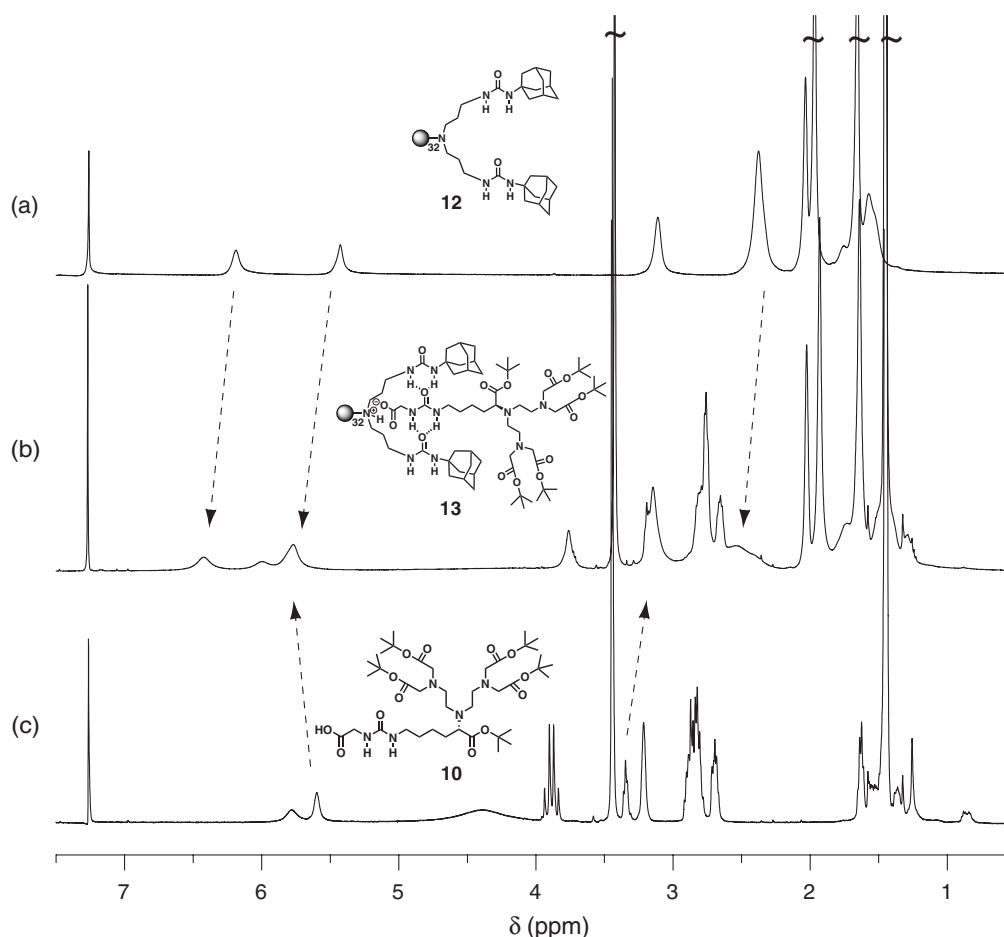
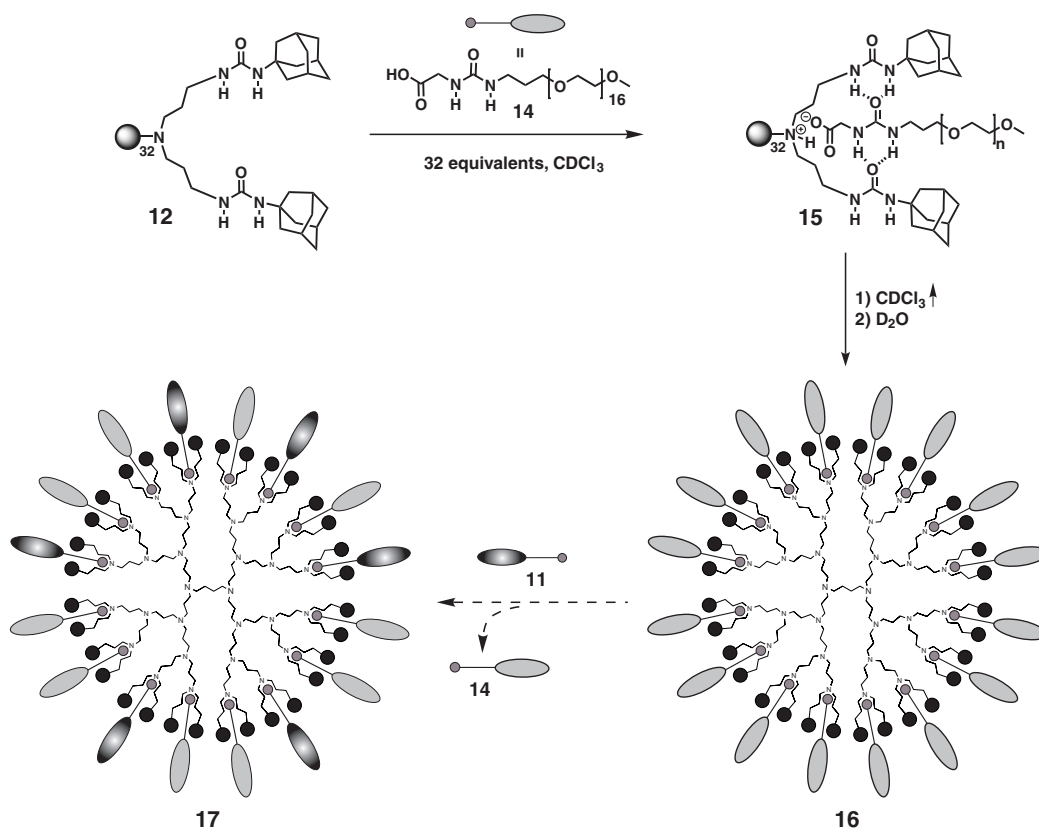


**Figure 5.12**  $^1\text{H-NMR}$  spectra recorded in  $\text{CDCl}_3$  at  $25^\circ\text{C}$ . (a) Adamantylurea-functionalized dendrimer **12**; (b) host-guest complex **13** consisting of dendrimer **12** and 32 equivalents of **10**; (c) glycinylurea-functionalized DTPA guest **10**.

Having established that **10** forms a host-guest complex with dendrimer **12** in  $\text{CDCl}_3$ , the next step is to introduce the  $\text{Gd(III)DTPA}$  complex **11** to the dendrimer. The glycinylurea-functionalized  $\text{Gd(III)DTPA}$  guest **11** is readily soluble in water, while the adamantylurea-functionalized



dendrimer is insoluble in aqueous media. It was not possible to draw the dendrimer into solution by adding a solution of **11** in H<sub>2</sub>O. Furthermore, when the periphery of the dendrimer is modified with hydrophilic groups (*e.g.* ethylene glycol moieties), no host–guest complex formation was observed. Apparently, hydrophobic interactions between the guest molecules and the dendrimer are required for the formation of host–guest complexes in aqueous media. Therefore, a stepwise approach as studied in great detail by ir. M.A.C. Broeren of our laboratories was attempted to gain dendrimer solubility as shown in Scheme 5.4.<sup>44</sup> First a PEG-modified glycinyurea guest **14** was complexed to dendrimer **12** in CHCl<sub>3</sub> to give **15**. Subsequently, the solvent was gently removed under an atmosphere of nitrogen and the obtained film was dispersed in demineralized water. Finally, 16 equivalents of **11** were added to guest–host complex **16**. This was followed by immediate precipitation of the dendrimer from solution precluding the formation of the desired complex **17**.



**Scheme 5.4** Strategy for the synthesis of water-soluble host–guest complex **17**.

Most likely, the concentration of charges at the periphery of the dendrimer has led to formation of insoluble aggregates. Future investigations will focus on the use of neutral Gd(III) chelates, such as glycinyurea-functionalized Gd(III)DO3A complexes to prevent precipitation upon complex formation.



**18** and  $\text{GdCl}_3$ . Purification was carried out by dialysis in demineralized water (0.5 kDa MWCO membrane), followed by freeze-drying and reconstitution in water. The opaque solutions of the mixed polymeric micelles as well as the control sample showed no tendency to phase separate upon standing for weeks at 4 °C. The solution morphology of both samples was investigated with cryogenic transmission electron microscopy (cryo-TEM) on vitrified aqueous solutions. A representative cryo-TEM image of diblock copolymer **18** in water revealed spherical particles with a core–corona structure (Figure 5.14a). Uniformly sized, dark spheres with an average diameter of 20–25 nm were observed, representing the self-assembled hydrophobic domains of amphiphilic diblock copolymer **18**. Around the dark spheres a slightly shaded corona could be detected, likely consisting of hydrated poly(ethylene glycol) chains. A comparable morphology has previously been observed by Bates *et al.* for self-assembled diblock copolymers of poly(ethylene glycol) and poly(butadiene).<sup>55-57</sup> A representative TEM micrograph of the mixture of **18** and **19** (after addition of  $\text{GdCl}_3$ ) is depicted in Figure 5.14b. Also in this case spherical polymeric micelles were found to be present. However, the average diameter for the core is now 40–45 nm, substantially larger than the hydrophobic core of the aggregates formed by **11** alone. The size distributions of the hydrophobic domain based on statistical analysis of 110 particles are shown in Figure 5.14c.

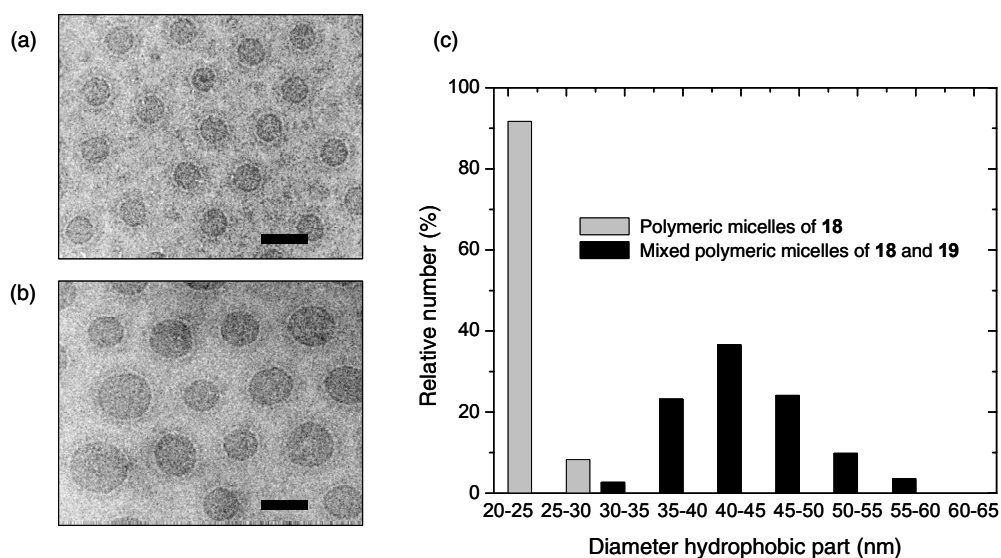


**Figure 5.14** (a) Cryo-TEM image of 1 wt-% aqueous solution of **18**; (b) cryo-TEM image of a mixture of 0.84 wt-% **18** and 0.16 wt-% **19** in the presence of  $\text{GdCl}_3$  in water (magnification of 29,500 $\times$ , without staining). The scale bar represents 40 nm. (c) Size distribution of the hydrophobic core for the (mixed) polymeric micelles.

The Gd(III) concentration of the samples was validated by means of ICP-AES. The Gd(III) content in the mixed polymeric micelles was unexpectedly low (by a factor of 9), even though a 10-fold excess of  $\text{GdCl}_3$  was used. This may be due to limited accessibility of DTPA moieties buried in the mixed aggregates for Gd(III). Another possibility is that the amount of DTPA-functionalized polymer **19** incorporated in the mixed polymeric micelles is overestimated. In case of the control

experiment, no Gd(III) was detected by ICP-AES, thereby excluding the possibility of non-specific binding of Gd(III) to polymer **18**. The ionic  $r_1$  of the Gd(III)DTPA complex in the mixed polymeric micelles was  $27.6 \text{ mM}^{-1}\text{s}^{-1}$  in water at pH 7. The ionic  $r_1$  of our system is significantly higher than ionic  $r_1$  values reported for both mixed micellar aggregates ( $r_1 = 20 \text{ mM}^{-1}\text{s}^{-1}$  at 1.5 T)<sup>47</sup> and self-organized micellar structures of lyophilic Gd(III)DOTA complexes ( $r_1 = 19 \text{ mM}^{-1}\text{s}^{-1}$  at 1.5 T).<sup>45</sup> The mixed micellar aggregates and the micellar structures reported in literature are composed of low molecular weight flexible amphiphiles, whereas in our case high molecular weight amphiphilic copolymers were used. Therefore, it is hypothesized that the local mobility of the Gd(III) complex in our system is lower, resulting in a higher ionic  $r_1$ .

In conclusion, a stepwise approach to MRI contrast agents through the self-assembly of amphiphilic copolymers **18** and **19** into mixed spherical polymeric micelles has been developed. Future studies will focus on the optimization of the synthesis of Gd(III)DTPA-containing polymeric micelles and the properties of this novel class of MRI contrast agents will be investigated in more detail.

## 5.5 OVERALL CONCLUSIONS

The synthesis of a series of biotinylated MRI contrast agents based on Gd(III)DTPA and Gd(III)DO3A has been performed successfully. The strong and specific interaction between biotin and avidin could be probed through the ionic  $r_1$  of these biotinylated MRI contrast agents. An increase in the ionic  $r_1$  by a factor of 1.7 and 2.7 was observed for Gd(III)DO3A and Gd(III)DTPA-based contrast agents, respectively, upon binding to this multivalent protein. This suggested that both the nature of the Gd(III) chelate and the spacer length are of great influence on the RIME effect. Future studies aim to further explore the work introduced in Section 5.4 to provide a general tool to study the formation of supramolecular assemblies in aqueous media, exploiting the RIME effect.

## 5.6. EXPERIMENTAL

### General procedures

Unless stated otherwise, all reagents and chemicals were obtained from commercial sources and used without further purification. Water was demineralized prior to use. DCM was obtained by distillation from P<sub>2</sub>O<sub>5</sub>. Avidin from egg-white (affinity purified) was purchased from Sigma-Aldrich. The overall concentration of avidin in PBS solution was determined by means of UV/vis experiments by measuring the intensity of the absorbance band at 282 nm. <sup>1</sup>H-NMR and <sup>19</sup>F-NMR spectra were recorded on a Varian Gemini-2000 300 MHz spectrometer at 298 K. Chemical shifts are given in ppm ( $\delta$ ). Infrared spectra were recorded on a Perkin-Elmer 1605 FT-IR spectrophotometer. ESI-QTOF-MS experiments were recorded on a Q-TOF Ultima GLOBAL mass spectrometer (Micromass, Manchester, UK). Analytical reversed phase high pressure liquid chromatography (RP HPLC) of the biotinylated DO3A (**2**) was performed on a Varian Prostar HPLC system with a Vydac<sup>TM</sup> protein peptide C18 column (0.5  $\times$  15 cm, flow 1 mL/min), eluted with a linear gradient of 0–60% CH<sub>3</sub>CN in 0.1% aqueous TFA in 30 minutes. The HPLC system was coupled to a UV/vis detector probing at 214 nm. Semi preparative HPLC was performed using a Vydac C18 column (2.5  $\times$  20 cm, 10 mL/min), eluted with a linear gradient of 0–30% CH<sub>3</sub>CN in 0.1% aqueous TFA in 90 minutes

### Relaxivity measurements

The longitudinal ionic relaxivity (ionic  $r_1$ ) was determined by a concentration dependent measurement of the longitudinal relaxation time ( $T_1$ ) via an inversion recovery pulse sequence as described in the experimental of Chapter 3. The Gd(III) content of the aqueous solutions used for the relaxivity measurements was determined by means ICP-AES analysis at 342.247 nm.

### HABA assay

Aliquots (5–10  $\mu$ L) of biotinylated Gd(III)DTPA **1** (253  $\mu$ M) were added cumulatively to a solution of avidin (10.39  $\mu$ M) and 4'-hydroxyazobenzene-2-carboxylic acid (200  $\mu$ M) in PBS buffer pH 7.4 at 1 min intervals. The binding of **1** to avidin was indicated by the decrease of the absorption at 500 nm as a result of the displacement of HABA from the biotin binding pockets of avidin.

### Gd(III) complex of biotinylated DTPA (**1**)

The Gd(III) complex of **5** was prepared by adding a stoichiometric amount of GdCl<sub>3</sub>·6 H<sub>2</sub>O (25.7 mg, 69  $\mu$ mol) in demineralized water (3 mL) to a solution of **5** (48.3 mg, 70  $\mu$ mol) in water (5 mL). The solution was vigorously stirred for 2 h at room temperature. The pH was continuously monitored and maintained at pH 7 with 0.1 N NH<sub>4</sub>OH (aq). The formation of the complex was monitored and confirmed with ESI-QTOF-MS. The aqueous solution was dialysed (100 Da MWCO membrane) and lyophilized. Gd(III) complex **1** was obtained as a white hygroscopic powder (39.2 mg, 46.3  $\mu$ mol, 67%). FT-IR (ATR):  $\nu$  (cm<sup>-1</sup>) = 3142, 3048, 1669 (C=O amide stretch), 1586 (antisym. COO stretch), 1403 (sym. COO stretch), 1326. ESI-QTOF-MS:  $m/z$  [M + H]<sup>+</sup> Calcd. 846.20 Da, Obsd. 846.15 Da; [M + Na]<sup>+</sup> Calcd. 868.18 Da, Obsd. 868.13 Da. ICP-AES (Gd(III)): Calcd. 50.0  $\mu$ M, Obsd. 33.6  $\mu$ M.

### Gd(III) complex of biotinylated DO3A (**2**)

Biotinylated DO3A **9** (23.7 mg, 35.2  $\mu$ mol) was dissolved in demineralized water (1.3 mL). The pH was adjusted to 7 by adding small aliquots of 2.5 wt-% NH<sub>4</sub>OH (aq). To this solution was added a stoichiometric amount of GdCl<sub>3</sub>·6 H<sub>2</sub>O (13.1 mg, 35.2  $\mu$ mol) in water (2.4 mL). The pH was maintained at 7 by adding aliquots of 2.5 wt-% NH<sub>4</sub>OH (aq). The solution was vigorously stirred overnight at room temperature. The aqueous solution was extensively dialysed (100 Da MWCO membrane) and lyophilized. The corresponding

Gd(III) complex **2** (26 mg, 31.4  $\mu\text{mol}$ ) was obtained in 89% yield as a fluffy white powder. FT-IR (ATR):  $\nu$  ( $\text{cm}^{-1}$ ) = 3253, 1676 (C=O amide stretch), 1590 (antisym. COO stretch), 1440, 1307, 1320, 1244, 1201, 1085. ESI-QTOF-MS:  $m/z$  [ $\text{C}_{28}\text{H}_{45}\text{N}_8\text{O}_9\text{S}_1\text{Gd} + \text{H}$ ]<sup>+</sup> Calcd. 828.2 Da, Obsd. 828.3 Da; [ $\text{M} + 2\text{H}$ ]<sup>2+</sup> Calcd. 414.6 Da, Obsd. 414.8 Da; [ $3\text{M} + \text{H}$ ]<sup>2+</sup> Calcd. 1241.3 Da, 1241.3 Da Obsd. ICP-AES (Gd(III)): Calcd. 72  $\mu\text{M}$ , Obsd. 73.4  $\mu\text{M}$ .

#### **Amine-functionalized DTPA-based building block (3)**

*tert*-Butyl ester-protected DTPA building block **3** was synthesized according to the previously described procedure (See Chapter 2, Section 2.2).

#### **Biotinylated DTPA (tert-butyl protected) (4)**

A solution of (+)-biotin-4-nitrophenyl ester (0.119 g, 0.33 mmol) was added dropwise to a colorless and ice cooled solution of DTPA synthon **3** (0.242 g, 0.32 mmol) in freshly dried DMF (4 mL). After 1 h of stirring at 0 °C, the reaction mixture was allowed to attain room temperature and stirring was proceeded overnight. The reaction mixture was concentrated under reduced pressure. Subsequently, DCM (20 mL) was added and the solution was washed with 5%  $\text{NaHCO}_3$  (aq) (5  $\times$  20 mL). The organic layer was washed with brine (10 mL), dried over  $\text{MgSO}_4$ , and concentrated under reduced pressure. The crude product was further purified by preparative size exclusion chromatography (Biobeads S-X8, DCM) and **4** was obtained as a colorless oil (0.24 g, 0.247 mmol, 76%). <sup>1</sup>H-NMR ( $\text{CDCl}_3$ ):  $\delta$  = 6.60 (s, 1H,  $\text{NHCONH}$ ), 6.42 (t, 1H,  $J$  = 5.64 Hz,  $\text{NHCO}$ ), 5.90 (s, 1H,  $\text{NHCONH}$ ), 4.51 (m, 1H, biotin- $\text{SCH}_2\text{CHNH}$ ), 4.32 (m, 1H, biotin- $\text{SCHCHNH}$ ), 3.43 (s, 8H,  $\text{NCH}_2\text{COOC}(\text{CH}_3)_3$ ), 3.3–3.1 (m, 4H, biotin- $\text{SCH}$  {1H} +  $\text{CONH}(\text{CH}_2)_4\text{CHN}$  {1H} +  $\text{CONHCH}_2(\text{CH}_2)_3$  {2H}), 3.0–2.6 (m, 10 H, biotin- $\text{CH}_2\text{S}$  {2H} +  $\text{NCH}_2\text{CH}_2\text{N}$  {4H} +  $\text{NCH}_2\text{CH}_2\text{N}$  {4H}), 2.21 (t, 2H,  $J$  = 7.56 Hz,  $(\text{CH}_2)_3\text{CH}_2\text{CONH}$ ), 1.8–1.2 (m, 12H,  $(\text{CH}_2)_3\text{CH}_2\text{CONH}$  {6H} +  $\text{CONHCH}_2(\text{CH}_2)_3$  {6H}; s, 45H,  $\text{COOC}(\text{CH}_3)_3$ ). The assignment of the <sup>1</sup>H-NMR spectrum is in complete agreement with earlier data<sup>59</sup> and is confirmed by <sup>1</sup>H,<sup>1</sup>H-COSY. FT-IR (ATR):  $\nu$  ( $\text{cm}^{-1}$ ) = 3299 (-NH stretch), 3223, 2977, 2932, 2862, 1707 (C=O ester), 1644 (C=O amide), 1550, 1458, 1393, 1367, 1250, 1217, 1136 (C–O stretch). MALDI-TOF:  $m/z$  [ $\text{M} + \text{H}$ ]<sup>+</sup> Calcd. 971.61 Da, Obsd. 971.64 Da; [ $\text{M} + \text{Na}$ ]<sup>+</sup> Calcd. 993.59 Da, Obsd. 993.62 Da.

#### **Biotinylated DTPA (5)**

To a stirred solution of **4** (0.211 g, 0.217 mmol) in DCM was added TFA (2 mL) and the reaction mixture was stirred overnight at room temperature. After evaporation of the solvent a second portion of TFA (2 mL) and DCM (4 mL) was added and stirring was continued overnight. The solution was concentrated *in vacuo* rendering the TFA salt of **5**. Additional purification by dialysis (100 Da MWCO membrane) and freeze-drying yielded **5** (0.062 g, 89.7  $\mu\text{mol}$  41%) as a white hygroscopic powder. <sup>1</sup>H-NMR ( $\text{D}_2\text{O}$ ):  $\delta$  4.17 (m, 1H, biotin- $\text{SCH}_2\text{CHNH}$ ), 3.98 (m, 1H, biotin- $\text{SCHCHNH}$ ), 3.84 (s, 8H,  $\text{NCH}_2\text{COOH}$ ), 3.2–3.1 (m, 5H,  $\text{NCH}_2\text{CH}_2\text{NCH}_2\text{COOH}$  {4H} +  $\text{CONH}(\text{CH}_2)_4\text{CHN}$  {1H}), 2.95–2.7 (m, 7H,  $\text{NCH}_2\text{CH}_2\text{N}$  {4H} + biotin- $\text{SCH}$  {1H} +  $\text{CONHCH}_2(\text{CH}_2)_3$  {2H}), 2.6–2.5 (dd, 1H,  $J_1$  = 12.9 Hz,  $J_2$  = 5.0 Hz, biotin- $\text{SCHH}_{\text{exo}}$ ), 2.4–2.3 (d, 1H,  $J$  = 12.9 Hz, biotin- $\text{SCHH}_{\text{endo}}$ ), 1.84 (t, 2H,  $J$  = 6.6 Hz,  $(\text{CH}_2)_3\text{CH}_2\text{CONH}$ ), 1.5–0.9 (m, 12 H,  $(\text{CH}_2)_3\text{CH}_2\text{CONH}$  {6H} +  $\text{CONHCH}_2(\text{CH}_2)_3$  {6H}). The assignment of the <sup>1</sup>H-NMR spectrum is in complete agreement with earlier literature data<sup>59</sup> and is confirmed by <sup>1</sup>H,<sup>1</sup>H-COSY. FT-IR (ATR):  $\nu$  ( $\text{cm}^{-1}$ ) = 3297, 2933, 2531 (COOH stretch), 1700 (C=O stretch), 1630 (C=O stretch), 1551, 1431, 1389, 1333, 1202 (C–O stretch). ESI-QTOF-MS:  $m/z$  [ $\text{M} + \text{H}$ ]<sup>+</sup> Calcd. 691.29 Da, Obsd. 691.17 Da; [ $\text{M} + \text{Na}$ ]<sup>+</sup> Calcd. 713.28 Da, Obsd. 713.17 Da; [ $\text{M} + 2\text{Na}$ ]<sup>+</sup> Calcd. 735.26 Da, Obsd. 735.18 Da.

***N-Biotinyl-1,2-ethanediamine (6)***

Compound **6** was synthesized by ir. B.F.M. de Waal according to the literature procedure of Garlick *et al.*<sup>60</sup>

***4,7,10-Tricarboxymethyl-tert-butyl ester 1,4,7,10-tetraazacyclododecane-1-acetate (7)***

Compound **7** was prepared by ir. B.F.M. de Waal and was obtained according to the literature procedure of Heppeler *et al.*<sup>23</sup>

***Biotinylated DO3A (tert-butyl ester protected) (8)***

Compound **8** was kindly provided by ir. B.F.M. de Waal. To a solution of DiPEA (0.39 g, 3.0 mmol), HBTU (0.265 g, 0.70 mmol) and **7** (0.40 g, 0.70 mmol) in DMF (2 mL) was added **6** (0.28 g, 0.69 mmol) under an atmosphere of nitrogen. After 14 h of stirring at room temperature, the solution was concentrated under reduced pressure. The residue was dissolved in DCM (100 mL) and washed with saturated NaHCO<sub>3</sub> (aq) (2 × 100 mL). The combined water phase was extracted with DCM (50 mL). The collected organic layers were washed with saturated NaHCO<sub>3</sub> (100 mL), water (100 mL), and saturated KCl (2 × 100 mL). The organic layer was concentrated under reduced pressure. The crude product (0.61 g) was purified by column chromatography (SiO<sub>2</sub>, DCM/MeOH 9:1 v/v). The title compound was obtained as a colorless oil (0.16 g, 0.19 mmol, 28%). <sup>1</sup>H-NMR (CDCl<sub>3</sub>): δ = 8.85 (t, 1H, NHCO), 8.49 (t, 1H, NHCO), 6.27 (s, 1H, NHCONH), 5.47 (s, 1H, NHCONH), 4.50 (m, 1H, biotin-SCH<sub>2</sub>CHNH), 4.39 (m, 1H, biotin-SCHCHNH), 3.47–3.33 (br, 8H, NCH<sub>2</sub>CO), 3.26–3.19 (m, 1H, biotin-SCH), 2.98–2.92 (dd, 1H, J<sub>1</sub> = 13 Hz, J<sub>2</sub> = 5.0 Hz, biotin-SCH<sub>endo</sub>), 2.83–2.78 (d, 1H, J = 13 Hz, biotin-SCH<sub>endo</sub>), 2.44 (t, 2H, J = 6.9 Hz, (CH<sub>2</sub>)<sub>3</sub>CH<sub>2</sub>CONH), 3.4–2.1 (16 H, br, ring NCH<sub>2</sub>CH<sub>2</sub>N), 1.9–1.38 (m, 33H, NHCOCH<sub>2</sub>(CH<sub>2</sub>)<sub>3</sub> + COOC(CH<sub>3</sub>)<sub>3</sub>).

***Biotinylated DO3A (9)***

Compound **9** was prepared by ir. B.F.M. de Waal. To a stirred solution of **8** (130 mg, 0.152 mmol) and triethylsilane (0.43 mL) in DCM was added TFA (4.3 mL). The reaction mixture was stirred for 3 h at room temperature. The solution was concentrated *in vacuo*. The obtained solid was triturated using cold diethyl ether (3 × 10 mL). The obtained white solid (83.8 mg) was further purified employing semi-preparative RP HPLC purification over a C18 column, eluted with a linear gradient of 0–30% CH<sub>3</sub>CN on 0.1% aqueous TFA in 90 minutes. Analytical RP HPLC: **9** eluting at 8.27 minutes. Freeze drying yielded **9** (55.6 mg, 0.083 mmol, 55%) as a fluffy white powder. <sup>1</sup>H-NMR (D<sub>2</sub>O): δ = 4.48 (m, 1H, biotin-SCH<sub>2</sub>CHNH), 4.29 (m, 1H, biotin-SCHCHNH), 4.0–3.5 (br, 8H, NCH<sub>2</sub>COOH {6H} + NHCOCH<sub>2</sub>N {2H}), 3.5–2.9 (br, 21 H, CONHCH<sub>2</sub>CH<sub>2</sub>NHCO {4H} + NCH<sub>2</sub>CH<sub>2</sub>N {16H} + biotin-SCH {1H}), 2.87–2.83 (dd, 1H, J<sub>1</sub> = 13.2 Hz, J<sub>2</sub> = 5.0 Hz, biotin-SCH<sub>exo</sub>), 2.65–2.63 (d, 1H, J = 13.2 Hz, biotin-SCH<sub>endo</sub>), 2.13 (t, 2H, J = 7.8 Hz, (CH<sub>2</sub>)<sub>3</sub>CH<sub>2</sub>CONH), 1.7–1.2 (m, 6H, (CH<sub>2</sub>)<sub>3</sub>CH<sub>2</sub>CONH). The assignment of the <sup>1</sup>H-NMR spectrum is in complete agreement with earlier literature data<sup>59</sup> and is confirmed by <sup>1</sup>H, <sup>1</sup>H-COSY. FT-IR (ATR): ν (cm<sup>-1</sup>) = 3288, 2927, 1720 (C=O stretch), 1661 (C=O stretch), 1551, 1460, 1429, 1384, 1351, 1187 (C–O stretch), 1131 cm<sup>-1</sup>. ESI-MS: *m/z* [C<sub>28</sub>H<sub>48</sub>N<sub>8</sub>O<sub>9</sub>S + H]<sup>+</sup> Calcd. 673.3 Da, Obsd. 673.2 Da.

***tert-Butyl 2-{{bis-{{2-[[bis-(tert-butoxycarbonylmethyl)amino]-ethyl]-amino}} 6-(carboxymethyl-3-ureido) hexanoate (10)***

In a Parr apparatus *tert*-butyl 6-(benzyloxycarbonylmethyl-3-ureido) 2-{{bis-{{2-[[bis-(*tert*-butoxycarbonyl-methyl)amino]-ethyl]-amino}} hexanoate (See Chapter 2 for the synthesis) (36 mg, 38.5 μmol) was catalytically hydrogenated in the presence of *tert*-BuOH (3 mL), water (1 mL) and 10 wt-% palladium on activated carbon (6.1 mg). After 3 h, the suspension was filtered over Celite and washed with THF,

concentrated under reduced pressure at 40°C, and the residue was coevaporated with toluene (3 × 10 mL). Compound **10** (26 mg, 30.7 μmol, 80%) was obtained as colorless oil. <sup>1</sup>H-NMR (DMSO-d<sub>6</sub>): δ = 6.08 (t, 1H, *J* = 5.4 Hz, NHCONH), 5.98 (t, 1H, *J* = 5.4 Hz, NHCONH), 3.66 (d, 2H, *J* = 5.4 Hz, NHCONHCH<sub>2</sub>CH<sub>2</sub>), 3.36 (s, 8H, NCH<sub>2</sub>COOC(CH<sub>3</sub>)<sub>3</sub>), 3.17 (m, 1H, NHCONH(CH<sub>2</sub>)<sub>4</sub>CHN), 2.94 (m, 2H, NHCONHCH<sub>2</sub>CH<sub>2</sub>), 2.75–2.5 (m, 8H, NCH<sub>2</sub>CH<sub>2</sub>N {4H} + NCH<sub>2</sub>CH<sub>2</sub>N {4H}), 1.60–1.12 (m, 6H, NHCONHCH<sub>2</sub>(CH<sub>2</sub>)<sub>3</sub>CHN; s, 45H, COOC(CH<sub>3</sub>)<sub>3</sub>) ppm. The assignment of the <sup>1</sup>H-NMR spectrum is confirmed by <sup>1</sup>H,<sup>1</sup>H-COSY. MALDI-TOF: *m/z* [C<sub>41</sub>H<sub>75</sub>N<sub>5</sub>O<sub>13</sub> + H]<sup>+</sup> Calcd. 846.54 Da, Obsd. 846.47 Da; [C<sub>41</sub>H<sub>75</sub>N<sub>5</sub>O<sub>13</sub> + Na]<sup>+</sup> Calcd. 868.53 Da, Obsd. 968.46 Da.

#### ***Glycylurea-functionalized Gd(III)DTPA complex (11)***

Gd(III) complex **11** was synthesized following previously described procedures that can be found in Chapter 2.

#### ***Adamantylurea-terminated poly(propylene imine) dendrimer (12)***

The fifth generation of the adamantylurea-modified dendrimer was kindly provided by ir. B.F.M. de Waal. Details on the synthetic procedures are given in the literature.<sup>33,61</sup> <sup>1</sup>H-NMR (CDCl<sub>3</sub>): δ = 6.19 (s, 64H, CH<sub>2</sub>NHCONH), 5.43 (s, 64H, CH<sub>2</sub>NHCONH), 3.11 (br., 128 H, NCH<sub>2</sub>CH<sub>2</sub>CH<sub>2</sub>NHCONH), 2.20–2.50 (m, 372H, NCH<sub>2</sub>(CH<sub>2</sub>)<sub>2</sub>CH<sub>2</sub>N {4H} + NCH<sub>2</sub>CH<sub>2</sub>CH<sub>2</sub>N {240H} + NCH<sub>2</sub>CH<sub>2</sub>CH<sub>2</sub>NHCO {128H}), 2.03 (s, 192 H, H-3), 1.97 (s, 384H, H-4), 1.65 (s, 384H, H-2), 1.58–1.40 (m, 252H, (NCH<sub>2</sub>(CH<sub>2</sub>)<sub>2</sub>CH<sub>2</sub>N {4H} + NCH<sub>2</sub>CH<sub>2</sub>CH<sub>2</sub>N {120H} + NCH<sub>2</sub>CH<sub>2</sub>CH<sub>2</sub>NHCO {128H})).

#### ***Synthesis of dendritic host–guest complex (13)***

To a solution of dendrimer **12** (10 mg, 0.54 μmol) in CDCl<sub>3</sub> (0.75 mL) was added **10** (14.6 mg, 17.3 μmol). The solution was stirred for 5 minutes at room temperature. Host–guest complex **13** was analyzed by NMR. <sup>1</sup>H-NMR (CDCl<sub>3</sub>): δ = 6.41, (broad s, NH urea, dendrimer), 6.0 (broad s, NH urea, guest), 5.9–5.6 (broad s, NH urea, guest + dendrimer), 3.75 (broad s, CH<sub>2</sub>, guest), 3.42 (s, NCH<sub>2</sub>COOC(CH<sub>3</sub>)<sub>3</sub>), 3.2–3.0 (broad m, CH<sub>2</sub>CH<sub>2</sub>NHCONH guest and dendrimer + NHCONH(CH<sub>2</sub>)<sub>4</sub>CHN guest), 3.0–2.2 (broad m, CH<sub>2</sub> dendrimer and guest), 2.02 (s, adamantyl dendrimer), 1.97 (s, adamantyl dendrimer), 1.75 (CH<sub>2</sub>, dendrimer), 1.64 (s, CH<sub>2</sub>, adamantyl dendrimer), 1.34–1.20 (s, COO(CH<sub>3</sub>)<sub>3</sub> guest; CH<sub>2</sub> guest and dendrimer).

#### ***Glycylurea-functionalized PEG guest (14)***

Compound **14** was kindly provided by ir. M.A.C. Broeren.

#### ***Synthesis of dendritic host–guest complex (16)***

To a solution of dendrimer **12** (10 mg, 0.54 μmol) in CHCl<sub>3</sub> (2 mL) was added **14** (15.4 mg, 17.2 μmol). The solution was stirred for 5 minutes at room temperature. The solvent was gently removed under a nitrogen flow. Subsequently, D<sub>2</sub>O (0.5 mL) was added and host–guest complex **16** was obtained.

#### ***Poly(ethylene butylene-block-ethyleneglycol) (18)***

Amphiphilic copolymer **18** was kindly provided by dr. N. Chebotareva and was prepared from commercially available amine-functionalized poly(ethylene oxide) (PEO-NH<sub>2</sub>, M<sub>n</sub> = 5 kg/mol) and α-hydroxy-poly(ethylene butylene) (M<sub>n</sub> = 3.8 kg/mol).

#### ***DTPA-functionalized polymer (19)***

Polymer **19** was synthesized following previously described procedures that can be found in Chapter 2.



### Preparation of mixed polymeric micelles

Copolymer **18** (42.3 mg) and DTPA-functionalized polymer **19** (8.3 mg, 2.1  $\mu\text{mol}$ ) were dissolved in 1:9 v/v TFA/DCM (0.42 mL). The solution was stirred for 20 minutes and concentrated under a flow of argon. After 3 h, the viscous oil was dried under reduced pressure at 50°C for 3 h. The obtained film was dispersed in demineralized water (4 mL), sonicated for 1 h, and diluted with 0.3 M citrate buffer pH 5.8 (3.78 mL). To the opaque solution was added a 10-fold excess of Gd(III)Cl<sub>3</sub>·6 H<sub>2</sub>O (7.52 mg, 20.2  $\mu\text{mol}$ ) in 0.3 M citrate buffer at pH 5.8 (1 mL). The opaque solution was stirred for 40 h at room temperature, purified by dialysis with a 1 kDa MWCO membrane. The sample was lyophilized and reconstituted in demineralized water for ICP-AES and relaxivity measurements. ICP-AES (Gd(III)): Calcd. 64  $\mu\text{M}$ , Obsd. 7.1  $\mu\text{M}$ .

## 5.7 APPENDIX

### 5.7.1 Fitting the E-titration data

There is a mathematical model describing the binding of multiple ligands (L), *e.g.* biotin, to a multivalent protein (P), *e.g.* avidin, with  $N$  identical, independent binding sites, as for instance can be found in reference 18. From this model the longitudinal relaxivity of the ligand bound to the protein ( $r_{1,bound}$ ), and the binding stoichiometry between ligand and protein ( $N$ ) were determined, according to the equation

$$r_1 = r_{1,bound} + (r_{1,free} - r_{1,bound}) \times \left( \frac{1}{2} + \frac{1}{2K_a[L]} - N \times \frac{[P]}{2[L]} + \sqrt{\left( \frac{1}{2K_a[L]} - \frac{1}{2} + N \times \frac{[P]}{2[L]} \right)^2 + \frac{1}{K_a[L]}} \right)$$

in which  $r_1$  represents the longitudinal relaxivity ( $\text{mM}^{-1}\text{s}^{-1}$ ),  $r_{1,free}$  the relaxivity of the free ligand ( $\text{mM}^{-1}\text{s}^{-1}$ ),  $r_{1,bound}$  the longitudinal relaxivity of the ligand bound to the protein ( $\text{mM}^{-1}\text{s}^{-1}$ ),  $K_a$  the association constant ( $\text{M}^{-1}$ ), and  $[P]$  and  $[L]$  the concentration of the protein and the ligand (M), respectively.

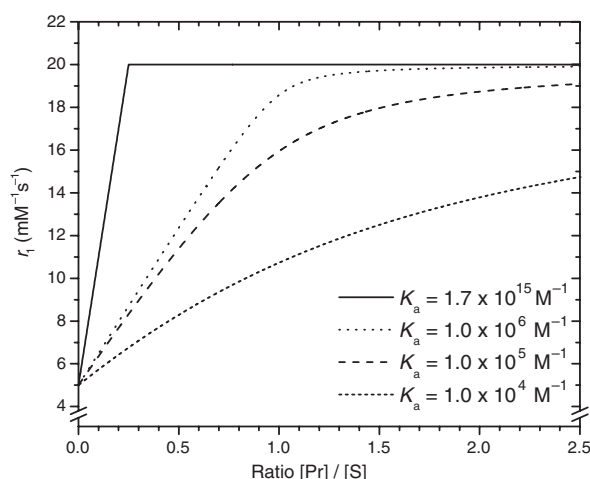


**Figure 5.15** Theoretical curves illustrating the relationship between the observed longitudinal relaxivity and protein (P) to ligand (L) ratios for association constants ranging from  $1.0 \times 10^4$  to  $1.7 \times 10^{15} \text{ M}^{-1}$ , with  $r_{1,free} = 5 \text{ mM}^{-1}\text{s}^{-1}$ ,  $r_{1,bound} = 20 \text{ mM}^{-1}\text{s}^{-1}$ , and  $N = 4$ .

### 5.7.2 Fitting the M-titration data

The average longitudinal relaxivity ( $r_1$ ) can be described according to the equation

$$r_1 = \frac{r_{1,bound} [L]_{bound} + r_{1,free} [L]_{free}}{[L]_t}$$

in which  $r_{1,free}$  represents the longitudinal relaxivity of the free ligand ( $\text{mM}^{-1}\text{s}^{-1}$ ),  $r_{1,bound}$  the longitudinal relaxivity of ligand bound to the protein ( $\text{mM}^{-1}\text{s}^{-1}$ ), the total concentration of ligand  $[L]_t$  (M), the concentration of unbound ligand  $[L]_{free}$ , and the concentration of ligand bound to the protein  $[L]_{bound}$ .

Plotting the average longitudinal relaxivity versus the ratio between  $[L]_t$  and  $[P]$ , where  $[P]$  is the concentration of protein, gives theoretically for the biotin-avidin system

$[L]_t/[P] < 4.0$ , then  $[L]_t = [L]_{bound}$  and  $[L]_{free} = 0$ , leading to  $r_1 = r_{1,bound}$  and for

$[L]_t/[P] > 4.0$ , then  $[L]_{bound} = 4.0[P]$  and  $[L]_{free} = [L]_t - [L]_{bound}$ , so that

$$r_1 = r_{1,free} + \left( \frac{4.0 (r_{1,bound} - r_{1,free}) [L]}{[L]_t} \right)$$

## 5.8 REFERENCES

- (1) Langereis, S.; de Lussanet, Q. G.; van Genderen, M. H. P.; Backes, W. H.; Meijer, E. W. *Macromolecules* **2004**, *37*, 3084-3091.
- (2) Merbach, A. E.; Tóth, E. *The Chemistry of Contrast Agents in Medical Magnetic Resonance Imaging*; John Wiley & Sons: New York, 2001.
- (3) Jacques, V.; Desreux, J. F. *Top. Curr. Chem.* **2002**, *221*, 123-164.
- (4) Jenkins, B. G.; Armstrong, E.; Lauffer, R. B. *Magn. Reson. Med.* **1991**, *17*, 164-178.
- (5) Lauffer, R. B. *Magn. Reson. Med.* **1991**, *22*, 339-342.
- (6) Caravan, P.; Ellison, J. J.; McMurry, T. J.; Lauffer, R. B. *Chem. Rev.* **1999**, *99*, 2293-2352.
- (7) Lauffer, R. B.; Parmelee, D. J.; Dunham, S. U.; Ouellet, H. S.; Dolan, R. P.; Witte, S.; McMurry, T. J.; Walovitch, R. C. *Radiology* **1998**, *207*, 529-538.
- (8) Caravan, P.; Cloutier, N. J.; Greenfield, M. T.; McDermid, S. A.; Dunham, S. U.; Bulte, J. W. M.; Amedio, J. C., Jr.; Looby, R. J.; Supkowski, R. M.; Horrocks, W. D., Jr.; McMurry, T. J.; Lauffer, R. B. *J. Am. Chem. Soc.* **2002**, *124*, 3152-3162.
- (9) Zhou, X.; Caravan, P.; Clarkson, R. B.; Westlund, P.-O. *Journal of Magnetic Resonance* **2004**, *167*, 147-160.
- (10) Parmelee, D. J.; Walovitch, R. C.; Ouellet, H. S.; Lauffer, R. B. *Invest. Radiol.* **1997**, *32*, 741-747.
- (11) Corot, C.; Violas, X.; Robert, P.; Gagneur, G.; Port, M. *Invest. Radiol.* **2003**, *38*, 311-319.
- (12) Anelli, P. L.; Bertini, I.; Fragai, M.; Lattuada, L.; Luchinat, C.; Parigi, G. *Eur. J. Inorg. Chem.* **2000**, 625-630.
- (13) Caravan, P.; Greenwood, J. M.; Welch, J. T.; Franklin, S. J. *Chem. Commun.* **2003**, 2574-2575.
- (14) De Leon-Rodriguez, L. M.; Ortiz, A.; Weiner, A. L.; Zhang, S.; Kovacs, Z.; Kodadek, T.; Sherry, A. D. *J. Am. Chem. Soc.* **2002**, *124*, 3514-3515.
- (15) Green, N. M. *Advances in Protein Chemistry* **1975**, *29*, 85-133.
- (16) Green, N. M. *Methods Enzymol.* **1990**, *184*, 51-67.
- (17) Dwek, R. A. *Nuclear Magnetic Resonance in Biochemistry. Applications to Enzyme Systems*; Clarendon Press: Oxford, 1973.
- (18) Tinoco, I., Jr.; Sauer, K.; Wang, J. C. *Physical Chemistry: Principles and Applications in Biological Sciences, 3rd Edition, Chapter 11*, 1995.
- (19) Green, N. M. *Biochem. J.* **1965**, *94*, 23c-24c.
- (20) Livnah, O.; Bayer, E. A.; Wilchek, M.; Sussman, J. L. *FEBS Letters* **1993**, *328*, 165-168.
- (21) Hofstetter, H.; Morpurgo, M.; Hofstetter, O.; Bayer, E. A.; Wilchek, M. *Anal. Biochem.* **2000**, *284*, 354-366.
- (22) Kimura, E.; Aoki, S.; Koike, T.; Shiro, M. *J. Am. Chem. Soc.* **1997**, *119*, 3068-3076.
- (23) Heppeler, A.; Froidevaux, S.; Macke, H. R.; Jermann, E.; Behe, M.; Powell, P.; Hennig, M. *Chem. Eur. J.* **1999**, *5*, 1974-1981.
- (24) Tolbert, T. J.; Wong, C.-H. *J. Am. Chem. Soc.* **2000**, *122*, 5421-5428.
- (25) Woods, M.; Kiefer, G. E.; Bott, S.; Castillo-Muzquiz, A.; Eshelbrenner, C.; Michaudet, L.; McMillan, K.; Mudigunda, S. D. K.; Ogrin, D.; Tircso, G.; Zhang, S.; Zhao, P.; Sherry, A. D. *J. Am. Chem. Soc.* **2004**, *126*, 9248-9256.
- (26) Zeng, F.; Zimmerman, S. C. *Chem. Rev.* **1997**, *97*, 1681-1712.
- (27) Alonso, E.; Valerio, C.; Ruiz, J.; Astruc, D. *New J. Chem.* **1997**, *21*, 1139-1141.
- (28) Valerio, C.; Fillaut, J.-L.; Ruiz, J.; Guittard, J.; Blais, J.-C.; Astruc, D. *J. Am. Chem. Soc.* **1997**, *119*, 2588-2589.
- (29) Narayanan, V. V.; Newkome, G. R. *Top. Curr. Chem.* **1998**, *197*, 19-77.

- (30) Bosman, A. W.; Janssen, H. M.; Meijer, E. W. *Chem. Rev.* **1999**, *99*, 1665-1688.
- (31) Chechik, V.; Zhao, M.; Crooks, R. M. *J. Am. Chem. Soc.* **1999**, *121*, 4910-4911.
- (32) Baars, M. W. P. L.; Meijer, E. W. *Top. Curr. Chem.* **2000**, *210*, 131-182.
- (33) Baars, M. W. P. L.; Karlsson, A. J.; Sorokin, V.; de Waal, B. F. M.; Meijer, E. W. *Angew. Chem. Int. Ed.* **2000**, *39*, 4262-4265.
- (34) Boas, U.; Karlsson, A. J.; de Waal, B. F. M.; Meijer, E. W. *J. Org. Chem.* **2001**, *66*, 2136-2145.
- (35) Boas, U.; Söntjens, S. H. M.; Jensen, K. J.; Christensen, J. B.; Meijer, E. W. *ChemBioChem* **2002**, *3*, 433-439.
- (36) Boas, U.; Heegaard, P. M. H. *Chem. Soc. Rev.* **2004**, *33*, 43-63.
- (37) Zimmerman, S. C.; Lawless, L. J. *Top. Curr. Chem.* **2001**, *217*, 95-120.
- (38) Dirksen, A.; Hahn, U.; Schwanke, F.; Nieger, M.; Reek, J. N. H.; Vögtle, F.; De Cola, L. *Chem. Eur. J.* **2004**, *10*, 2036-2047.
- (39) Gillies, E. R.; Fréchet, J. M. J. *J. Org. Chem.* **2004**, *69*, 46-53.
- (40) Tomalia, D. A.; Majoros, I. *J. of Macromolecular Science - Polymer Reviews* **2003**, *C43*, 411-477.
- (41) Broeren, M. A. C.; van Dongen, J. L. J.; Pittelkow, M.; Christensen, J. B.; van Genderen, M. H. P.; Meijer, E. W. *Angew. Chem. Int. Ed.* **2004**, *43*, 3557-3562.
- (42) Banerjee, D.; Broeren, M. A. C.; Van Genderen, M. H. P.; Meijer, E. W.; Rinaldi, P. L. *Macromolecules* **2004**, *37*, 8313-8318.
- (43) Broeren, M. A. C.; de Waal, B. F. M.; van Dongen, J. L. J.; van Genderen, M. H. P.; Meijer, E. W. *Org. Biomol. Chem.* **2005**, *3*, 281-285.
- (44) Broeren, M. A. C. *PhD thesis in preparation*; Eindhoven University of Technology, 2005.
- (45) Andre, J. P.; Tóth, E.; Fischer, H.; Seelig, A.; Macke, H. R.; Merbach, A. E. *Chem. Eur. J.* **1999**, *5*, 2977-2983.
- (46) Nicolle, G. M.; Tóth, E.; Eisenwiener, K.-P.; Macke, H. R.; Merbach, A. E. *JBIC* **2002**, *7*, 757-769.
- (47) Accardo, A.; Tesaro, D.; Roscigno, P.; Gianolio, E.; Paduano, L.; D'Errico, G.; Pedone, C.; Morelli, G. *J. Am. Chem. Soc.* **2004**, *126*, 3097-3107.
- (48) Anelli, P. L.; Lattuada, L.; Lorusso, V.; Schneider, M.; Tournier, H.; Uggeri, F. *MAGMA* **2001**, *12*, 114-120.
- (49) Glogard, C.; Stensrud, G.; Hovland, R.; Fossheim, S. L.; Klaveness, J. *International Journal of Pharmaceutics* **2002**, *233*, 131-140.
- (50) Lokling, K.-E.; Skurtveit, R.; Fossheim, S. L.; Smistad, G.; Henriksen, I.; Klaveness, J. *Magn. Res. Imaging* **2003**, *21*, 531-540.
- (51) Mulder, W. J. M.; Strijkers, G. J.; Griffioen, A. W.; van Bloois, L.; Molema, G.; Storm, G.; Koning, G. A.; Nicolay, K. *Bioconjugate Chem.* **2004**, *15* (4), 799-806.
- (52) Bull, S. R.; Guler, M. O.; Bras, R. E.; Meade, T. J.; Stupp, S. I. *Nano Letters* **2005**, *5*, 1-4.
- (53) Morel, S.; Terreno, E.; Ugazio, E.; Aime, S.; Gasco, M. R. *Eur. J. Pharm. Biopharm.* **1998**, *45*, 157-163.
- (54) Morawski, A. M.; Winter, P. M.; Crowder, K. C.; Caruthers, S. D.; Fuhrhop, R. W.; Scott, M. J.; Robertson, J. D.; Abendschein, D. R.; Lanza, G. M.; Wickline, S. A. *Magn. Reson. Med.* **2004**, *51*, 480-486.
- (55) Zheng, Y.; Won, Y.-Y.; Bates, F. S.; Davis, H. T.; Scriven, L. E.; Talmon, Y. *J. Phys. Chem. B* **1999**, *103*, 10331-10334.
- (56) Jain, S.; Bates, F. S. *Science* **2003**, *300*, 460-464.
- (57) Won, Y.-Y.; Brannan, A. K.; Davis, H. T.; Bates, F. S. *J. Phys. Chem. B* **2002**, *106*, 3354-3364.
- (58) Opsteen, J. A.; Cornelissen, J. J. L. M.; van Hest, J. C. M. *Pure App. Chem.* **2004**, *76*, 1309-1319.

- (59) Ikura, M.; Hikichi, K. *Organic Magnetic Resonance* **1982**, *20*, 266-273.
- (60) Garlick, R. K.; Giese, R. W. *J. Biol. Chem.* **1988**, *263*, 210-215.
- (61) Schenning, A. P. H. J.; Elissen-Roman, C.; Weener, J.-W.; Baars, M. W. P. L.; van der Gaast, S. J.; Meijer, E. W. *J. Am. Chem. Soc.* **1998**, *120*, 8199-8208.

---

## Chapter 6

### Synthetic strategies for targeting and bimodality\*

---

**ABSTRACT:** *Novel strategies for the synthesis of Gd(III)DTPA complexes composed of a target-specific oligopeptide for angiogenesis (i.e. cyclic CNGRC (cNGR)) and/or Oregon Green 488 (OG488) as a fluorescent label have successfully been developed. First, cNGR-functionalized Gd(III)DTPA was synthesized employing solid phase peptide synthesis using an isocyanate-functionalized DTPA pentaester. Secondly, Gd(III)DTPA was labeled with OG488 to give a bimodal contrast agent for MRI and optical imaging. Finally, a bimodal target-specific contrast agent composed of cNGR, OG488, and Gd(III)DTPA was prepared using a sequence of highly efficient, chemoselective reactions, such as native chemical ligation. In a pilot study, the efficacy of cNGR-Gd(III)DTPA for MR imaging of angiogenesis has been studied using a murine myocardial model. Serial contrast-enhanced MRI with cNGR-Gd(III)DTPA showed a local increase in signal intensity in the suspected infarcted region of the ventricle wall. The large difference in sensitivity between MRI and optical imaging has been demonstrated with a fluorescently labeled Gd(III)DTPA-based complex in the CAM model. For validation of the targeting process with cNGR, a bimodal target-specific MRI contrast agents composed of Gd(III)DTPA, cNGR and OG488 has been synthesized.*

---

\* Part of this work has been published: Langereis, S.; de Lussanet, Q.G.; van Genderen, M.H.P.; Backes, W.H.; Hackeng, T.M.; van Engelshoven, J.M.A.; Meijer, E.W. *Polym. Mater. Sci. Eng.* **2004**, *91*, 56-57. Dirksen, A.; Langereis, S.; de Waal, B.F.M.; van Genderen, M.H.P.; Meijer, E.W.; de Lussanet, Q.G.; Hackeng, T.M. *Org. Lett.* **2004**, *6*, 4857-4860. Langereis, S.; Dirksen, A.; de Waal, B.F.M.; van Genderen, M.H.P.; de Lussanet, Q.G.; Hackeng, T.M.; Meijer, E.W. *Eur. J. Org. Chem.*, *accepted for publication.*

## 6.1 INTRODUCTION

Magnetic Resonance Imaging (MRI) contrast agents based on the gadolinium(III) complex of diethylenetriaminepentaacetic acid (Gd(III)DTPA) are generally employed as diagnostic agents in medical imaging.<sup>1,2</sup> A low toxicity combined with an excellent solubility in water is a major advantage of Gd(III)DTPA-based complexes.<sup>1,2</sup> One of the drawbacks, however, is their non-specificity, which necessitates the use of relatively high concentrations of MRI contrast agent. An improvement of the effectiveness of Gd(III)DTPA-based MRI contrast agents can be accomplished by incorporating target-specific oligopeptides to induce accumulation of MRI probes at regions of interest.<sup>3</sup>

In recent years, target-specific oligopeptides for angiogenesis, *i.e.* the formation of new blood vessels,<sup>4,6</sup> have been identified by differential phage display experiments in tumor models.<sup>7</sup> Among the various target-specific peptides, the cyclic Cys-Asn-Gly-Arg-Cys (CNGRC) peptide with a disulfide bridge between the cysteine residues (cNGR) has proven to be suitable for delivering doxorubicin, pro-apoptotic peptides, and tumor necrosis factor- $\alpha$  (TNF) to tumor vessels (Figure 6.1).<sup>7-11</sup> It has been established that cNGR homes specifically to CD13, a glycoprotein that is overexpressed on endothelial cells during angiogenesis.<sup>8,11-13</sup> Colombo *et al.* have shown that the targeting efficacy of cNGR-TNF is more than 10-fold higher compared to linear GNGRG-TNF, implying that the folded conformation with a disulfide bridge is critical for targeting.<sup>14</sup> Buehler *et al.* have studied the potential of cNGR for optical imaging of cardiac angiogenesis in a murine myocardial model. *In vivo* optical imaging with cNGR, that was functionalized with Oregon Green 488 (OG488) as a fluorescent label, showed that cNGR homes specifically to angiogenic areas in the ischemic heart.<sup>15</sup>

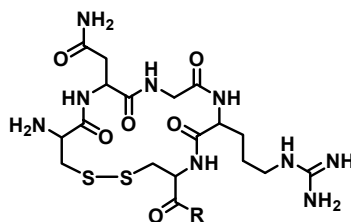


**Figure 6.1** Chemical structure of the cyclic Cys-Asn-Gly-Arg-Cys (CNGRC) peptide residue with a disulfide bridge between the cysteine residues (cNGR).  $R = -G(TNF)$ .

In this Chapter, a series of Gd(III)DTPA-based complexes composed of cNGR as a homing domain and/or OG488 as a fluorescent label is synthesized (Figure 6.2). Firstly, a convenient methodology for the solid phase peptide synthesis of cNGR-functionalized Gd(III)DTPA (**1**) is discussed. In our design, the targeting peptide motif and the Gd(III)DTPA complex are connected with a glycylglycine spacer to enhance peptide flexibility and to minimize potential steric interactions that may hamper binding,<sup>9</sup> and the Gd(III)DTPA moiety is attached to the lysine side-

chain. Moreover, *in vivo* studies using a murine myocardial model are performed to validate the efficacy of **1** as a contrast agent for target-specific MR imaging of angiogenesis. Secondly, Gd(III)DTPA-based complexes with OG488 as a fluorescent label (**2**) are synthesized. The combination of MRI and fluorescent labels in a single molecule may allow for bimodality in imaging, thereby integrating the advantages of MRI (a non-invasive technique with a high spatial resolution) and optical imaging (a high sensitivity). Finally, a bimodal target-specific contrast agent (**3**), based on OG488, Gd(III)DTPA, and cNGR is synthesized, which may allow for the verification of the targeting process with both MRI and optical imaging.

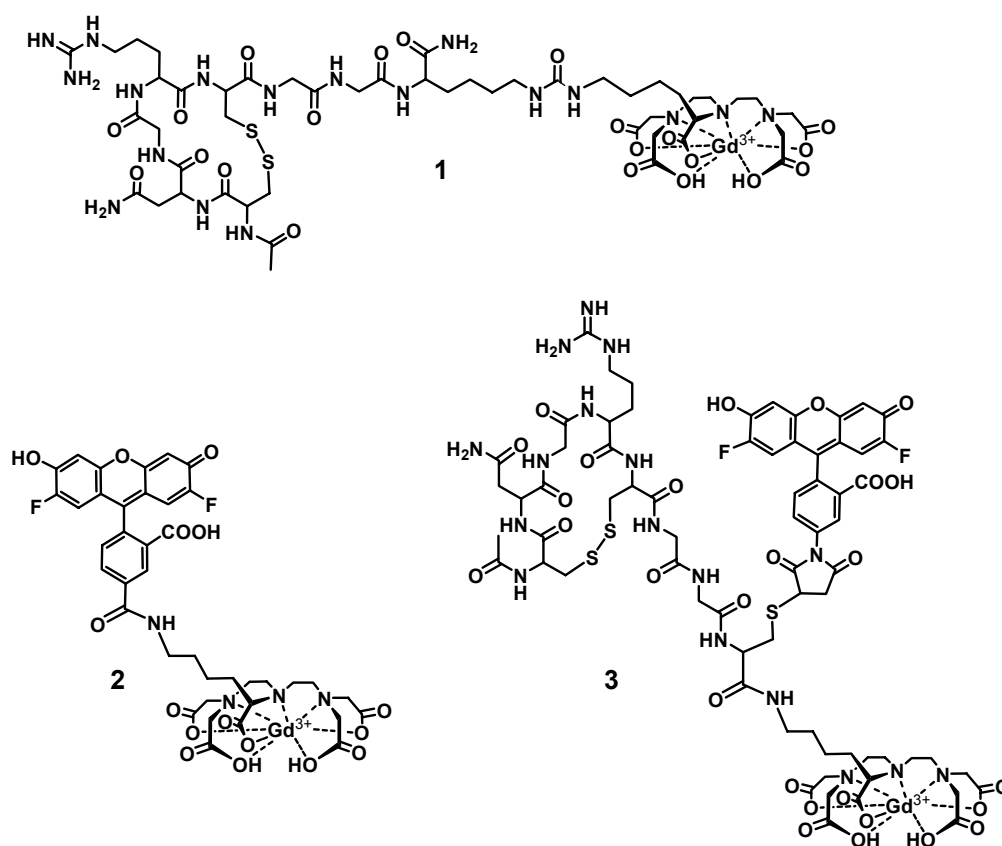


**Figure 6.2** Chemical structures of cNGR-functionalized Gd(III)DTPA (**1**), OG488-labeled Gd(III)DTPA (**2**), and bimodal target-specific contrast agent (**3**) containing the cNGR sequence, Gd(III)DTPA, and OG488.

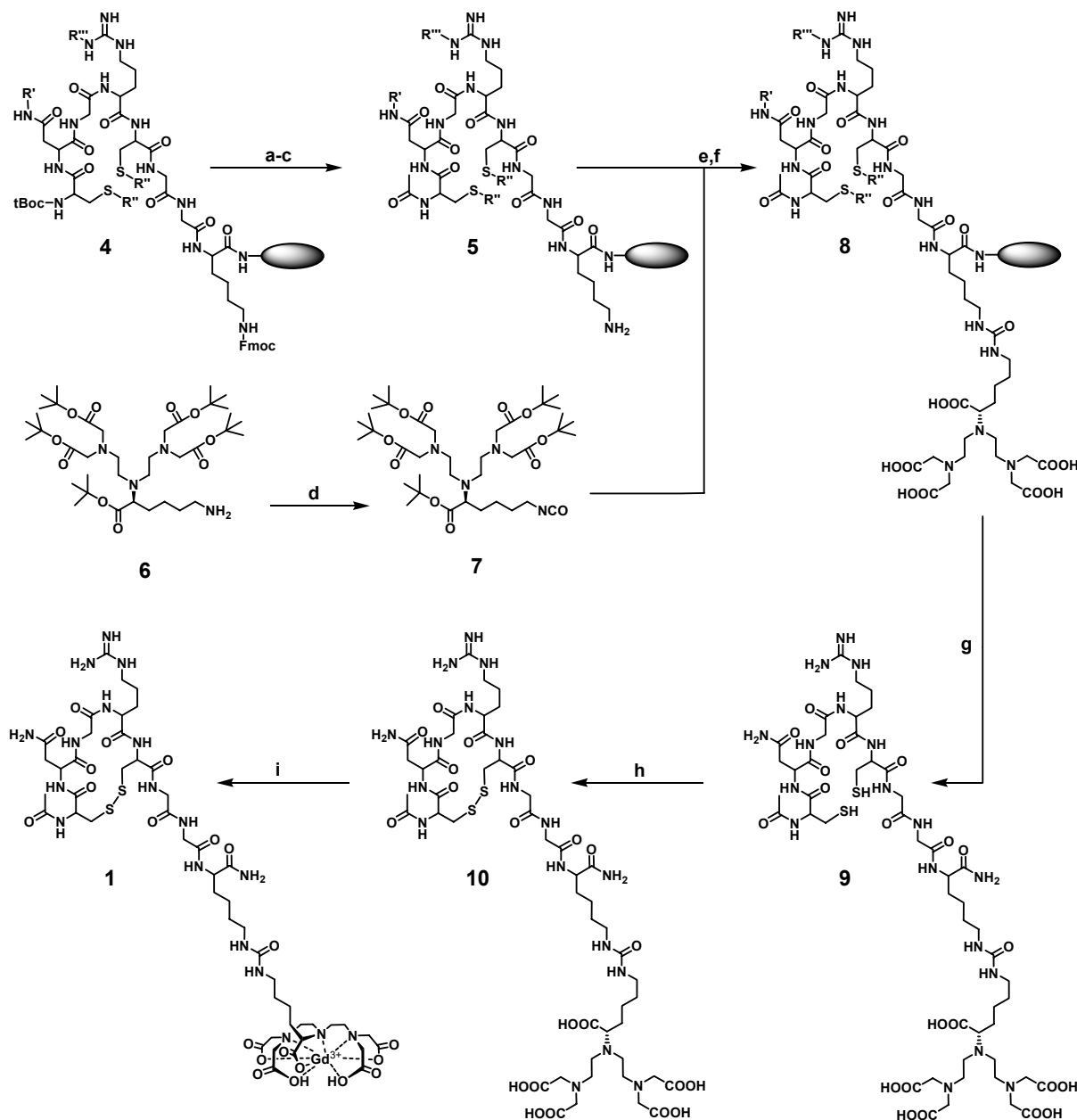
## 6.2 CYCLIC NGR-FUNCTIONALIZED Gd(III)DTPA

### 6.2.1 Solid phase peptide synthesis

Solid phase peptide synthesis (SPPS) using the *in-situ* neutralization/ 2-(1*H*-benzotriazol-1-yl)-1,1,3,3-tetramethyluronium hexafluorophosphate (HBTU) activation procedure for *tert*-butoxy-carbonyl (Boc) chemistry on a MBHA resin<sup>16</sup> was applied to synthesize side chain-protected BocCNGRCGGK(Fmoc)-MBHA (**4**) containing the target-specific CNGRC sequence (Scheme 6.1).



The  $N^{\alpha}$ -Boc group of **4** was removed with trifluoroacetic acid (TFA) and the corresponding primary amine was acetylated with acetic anhydride and pyridine. Subsequently, the Fmoc protective group of the lysine side chain was removed with 20% piperidine in DMF, to give partially side chain-protected NAcCNGRCGGK(NH<sub>2</sub>)-MBHA (**5**).



**Scheme 6.1** Synthesis of *c*NGR-Gd(III)DTPA (**1**).  $R'$ – $R'''$  represent the protective groups of the amino acids, with  $R'$  = xanthyl,  $R''$  = 4-methylbenzyl and  $R'''$  = *p*-toluenesulfonyl. (a) TFA; (b) acetic anhydride (0.25 M), pyridine (0.25 M) in DMF; (c) 20% piperidine in DMF; (d) di-tert-butyl-tricarbonate in DCM, 2 h, argon atmosphere; (e) isocyanate-functionalized DTPA pentaester **7** (7 eq) in DMF; (f) TFA; (g) cleavage of the peptide from MBHA resin with anhydrous HF; (h) 1 M guanidine in 0.1 M Tris buffer pH 8; (i)  $GdCl_3 \cdot 6 H_2O$  (0.9 eq),  $NH_4OH$ ,  $H_2O$ , pH 6.5–7.

To enable the coupling of **6** to the  $\epsilon$ -amino group of the lysine residue, the primary amine of lysine-based DTPA pentaester **6** was converted into the corresponding isocyanate with di-*tert*-butyl-tricarbonate in dichloromethane (DCM) (See Chapter 2, Section 2.2.3), yielding isocyanate-functionalized DTPA synthon **7** (Scheme 6.1).<sup>17</sup> This reaction was performed in DCM since this procedure cannot be performed in DMF (the preferred solvent for solid phase peptide synthesis) due to decomposition of di-*tert*-butyl-tricarbonate. A droplet of pyridine was added to quench the excess of di-*tert*-butyl-tricarbonate and DCM was removed under an argon flow. The crude mixture was redissolved in DMF and directly used in 7-fold excess for the reaction with  $\epsilon$ -amine-group of the lysine side chain of the peptide on the solid phase. The excess of **7** was easily removed by washing with DMF. Subsequently, cleavage of the *tert*-butyl esters with TFA in DCM yielded side chain-protected NAcNGRCGGK(DTPA)-MBHA (**8**). The coupling efficiency between the isocyanate-functionalized DTPA pentaester and the primary  $\epsilon$ -amine of the lysine side chain of **5** was ca. 67% based on the mass increase of MBHA resin. The DTPA-functionalized oligopeptide was cleaved from the resin with anhydrous HF and lyophilized to give NAcNGRCGGK-DTPA (**9**).

The coupling efficiency of ca. 67% between **7** and the primary  $\epsilon$ -amine of the lysine side chain was confirmed by analytical reversed phase high pressure liquid chromatography (RP HPLC) on the crude mixture. The reaction mixture containing **9** was used for the next reaction without further purification, avoiding additional product loss due to HPLC purification procedures. The oxidation of the sulfhydryl (-SH) functionalities of the cysteine residues was performed in 1 M of guanidine in 0.1 M Tris buffer at pH 8 and was monitored with analytical RP HPLC and electrospray ionization mass spectrometry (ESI-MS). Quantitative formation of the disulfide bridge was accomplished after 3 h (Figure 6.2, note the mass difference between **9** and cNGR-DTPA (**10**) in the ESI-MS spectra below is only 1 amu, due to the doubly charged nature of **9** and **10**). Semi-preparative RP HPLC purification and subsequent lyophilization yielded **10** in an overall isolated yield of 19%. The Gd(III) complex (**1**) was prepared by adding 0.9 equivalents of GdCl<sub>3</sub> to a solution of **10** in water. The pH was maintained at 6.5–7 by adding 0.25% NH<sub>4</sub>OH (aq). A slight excess of **10** was used to ensure the absence of free Gd(III), which is highly toxic. Gd(III) complex **1** was characterized with IR spectroscopy and ESI-MS, while the Gd(III) content was determined by inductively coupled plasma atomic emission spectroscopy (ICP-AES). The value for the observed Gd(III) content was found to be 94% of the theoretical value.

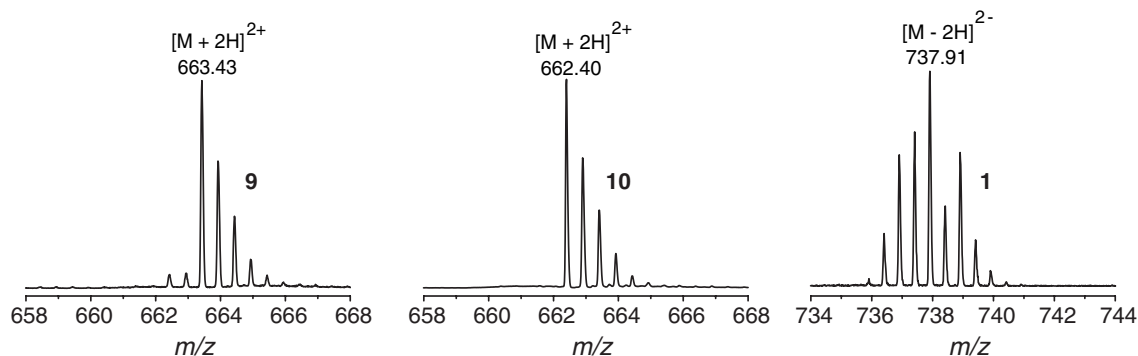


**Figure 6.3** ESI-QTOF-MS spectra of **9** (left), **10** (middle), and cNGR-functionalized Gd(III)DTPA (**1**) (right). The  $m/z$  region of interest shows the doubly charged state of the constructs.

The longitudinal relaxivity ( $r_1$ ) of cNGR-Gd(III)DTPA (**1**), which is an intrinsic property of an MRI contrast agent, was determined by measuring the concentration dependency of its longitudinal relaxation time ( $T_1$ ) at 1.5 T and 20 °C.<sup>2</sup> The data gave a good linear fit ( $R^2 > 0.999$ ) to the equation  $(1/T_1)_{\text{observed}} = (1/T_1)_{\text{diamagnetic}} + r_1[\text{Gd(III)}]$  and an  $r_1$  of 9.8  $\text{mM}^{-1}\text{s}^{-1}$  was calculated. Gd(III) complex **1** has a higher  $r_1$  compared to biotinylated Gd(III)DTPA (Chapter 5,  $r_1 = 6.1 \text{ mM}^{-1}\text{s}^{-1}$ ,  $\text{MW} = 0.8 \text{ kg}\cdot\text{mol}^{-1}$ ) and the functionalized Gd(III)DTPA-based complexes presented in Chapter 2 ( $r_1$  values: 8–8.5 and  $\text{MW} 0.7\text{--}0.9 \text{ kg}\cdot\text{mol}^{-1}$ ). So in this case the higher  $r_1$  of **1** ( $\text{MW} = 1.5 \text{ kg}\cdot\text{mol}^{-1}$ ) may be explained in terms of molecular weight.

### 6.2.2 Serial contrast-enhanced MRI

In a pilot study, the efficacy of **1** for MR imaging of angiogenesis was validated using a murine myocardial model. Seven days after the induction of a myocardial infarct, mice were injected intravenously with either **1** (0.03 mmol Gd(III)/kg) or Gd(III)DTPA (0.07 mmol Gd(III)/kg) as a negative control. Serial contrast-enhanced MRI studies were performed on a 1.5 T clinical scanner.  $T_1$ -weighted digitally subtracted MR images of **1** and Gd(III)DTPA show a rapid renal excretion and accumulation of the contrast agent in the bladder (Figure 6.4). These features are characteristic for low molecular weight MRI contrast agents (See Chapter 4, Section 4.3.1). As shown in Figure 6.4, the left ventricle is enlarged due to a massive infarction. Moreover, a local increase in signal intensity at the suspected infarct region is observed after 8 minutes with **1**. The determination that targeting is solely responsible for this increase in signal intensity cannot be concluded from these experiments. Most likely, the non-specific diffusion of MRI contrast agent into the interstitial space also contributes to the signal observed. To validate the targeting of cardiac angiogenesis using the cNGR motif, more sensitive methods such as optical imaging techniques are required.

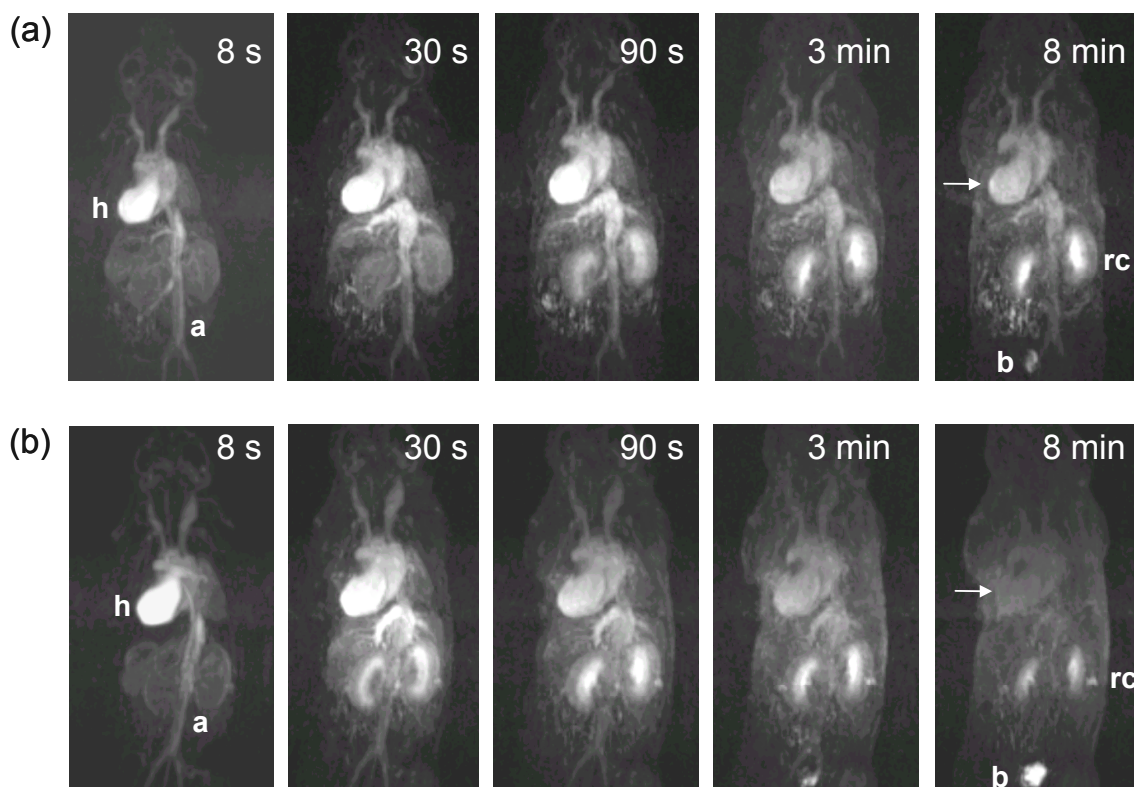
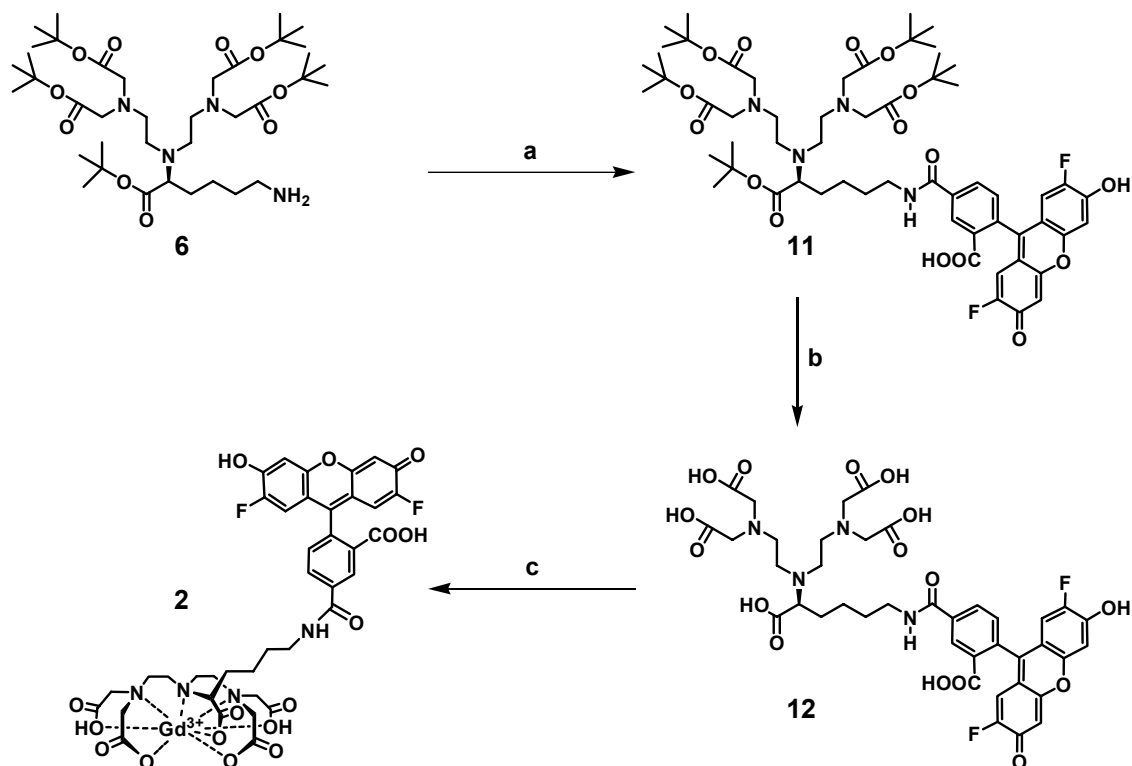


**Figure 6.4** Serial contrast-enhanced MRI in mice at 1.5 T. (a)  $T_1$ -weighted maximum intensity projections digitally subtracted with cNGR-Gd(III)DTPA **1** (0.03 mmol Gd(III)/kg body weight); (b)  $T_1$ -weighted maximum intensity projections digitally subtracted with Gd(III)DTPA (0.07 mmol Gd(III)/kg body weight). The MR images show the cardiovascular system (h = heart; a = aorta), the renal collecting system (rc) and the bladder (b). The arrows indicate the suspected infarct region.

### 6.3 FLUORESCENTLY LABELED Gd(III)DTPA COMPLEX: A BIMODAL CONTRAST AGENT

To illustrate the difference in sensitivity between MRI and optical imaging, Gd(III)DTPA was functionalized with OG488 (Scheme 6.2). The synthesis of this bimodal contrast agent started with the reaction of amine-functionalized DTPA synthon (**6**) and *N*-succinimidyl activated ester of OG488 in the presence of triethylamine in DMF. Cleavage of the *tert*-butyl esters was accomplished with TFA in DCM. Further purification with dialysis afforded water-soluble intermediate **12**. In the final step, the Gd(III) complex was obtained by the addition of a stoichiometric amount of GdCl<sub>3</sub> to an aqueous solution **12** under neutral conditions. Gd(III) complex **2** was characterized with FT-IR spectroscopy, ESI-QTOF mass spectrometry, and ICP-AES.



**Scheme 6.2** Synthesis of bimodal contrast agent **2** containing Gd(III)DTPA as an MRI label and OG488 as a fluorescent label. (a) *N*-succinimidyl activated ester of OG488,  $\text{NEt}_3$  and DMF; (b) TFA; (c)  $\text{GdCl}_3 \cdot 6 \text{H}_2\text{O}$ ,  $\text{NH}_4\text{OH}$ ,  $\text{H}_2\text{O}$ , pH 7.

The  $r_1$  for **2** of  $6.6 \text{ mM}^{-1}\text{s}^{-1}$  was determined in a 0.1 M PBS buffer at pH 7.4. This value is in the same range as the  $r_1$  of biotinylated Gd(III)DTPA complex ( $r_1 = 6.1 \text{ mM}^{-1}\text{s}^{-1}$ , See Chapter 5). The photoluminescence (PL) detection limit of **2** was determined by analyzing the photoluminescence intensity upon varying the concentration of **2** in Tris buffer at pH 8. As illustrated in Figure 6.5a, the detected PL intensity follows a linear relation with the concentration upon dilution until a concentration of  $2 \times 10^{-10} \text{ M}$  was reached. Upon further dilution of the solution, the PL intensity at 518 nm levels off and became almost invariant on concentration.

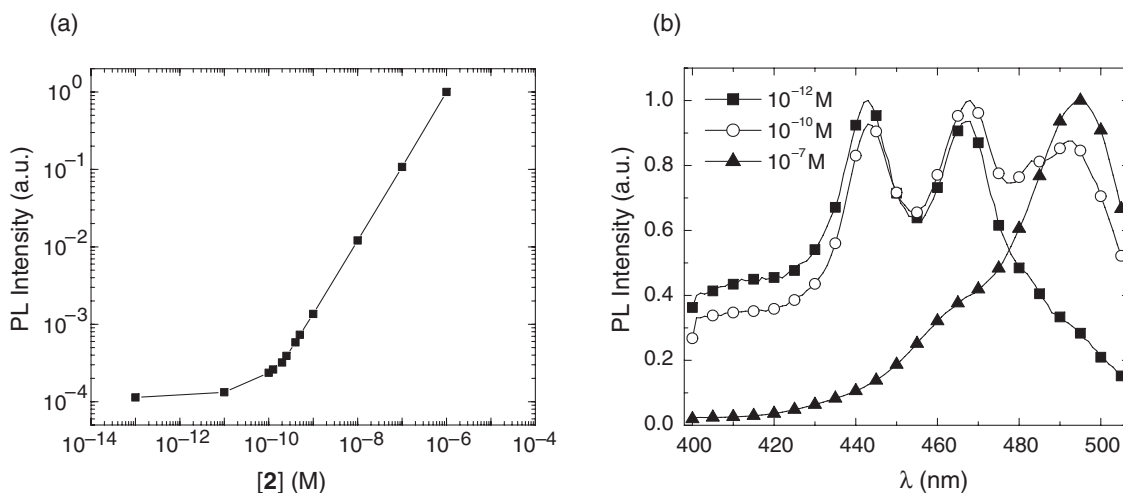


**Figure 6.5** (a) Photoluminescence (PL) intensity versus the concentration of **2** in Tris buffer at pH 8 detecting at 518 nm ( $\lambda_{exc} = 488$  nm); (b) normalized excitation spectra of different concentrations of **2** ( $\lambda_{det} = 518$  nm).

In addition to the PL intensity dependence the excitation spectra recorded at a detection wavelength of 518 nm also gave information on the detection limit of **2** (Figure 6.5b). At concentrations where the dependence of the PL was linear, the excitation spectrum was identical to the absorption spectrum of the measured solution with a distinct maximum at 495 nm (Figure 6.5b). However, at a concentration of  $10^{-10}$  M additional peaks at 445 and 465 nm appeared and at a concentration of  $10^{-12}$  M only the latter two peaks were observed. Thus, these peaks originate from the TRIS buffer and not from compound **2**. Therefore, it was concluded that the detection limit for **2** with PL techniques is around  $10^{-10}$  M.

In collaboration with several departments at the University of Maastricht and the Maastricht University Hospital, the potential of combined MR imaging and optical imaging was shown for **2** employing the chick chorioallantoic membrane (CAM) model (Figure 6.6). The CAM is commonly used as a model for *in vivo* research on angiogenesis and is an attractive alternative model to traditional mammalian models.<sup>18-21</sup>  $T_1$ -weighted post-contrast MR images showed the microcirculatory characteristics of the CAM of the chick embryo (Figure 6.6b and 6.6c). Fluorescence microscopy images of the CAM, directly after contrast agent injection, allowed the visualization of much smaller blood vessels (Figure 6.6d). This illustrates the large difference in sensitivity between MRI and optical imaging techniques.

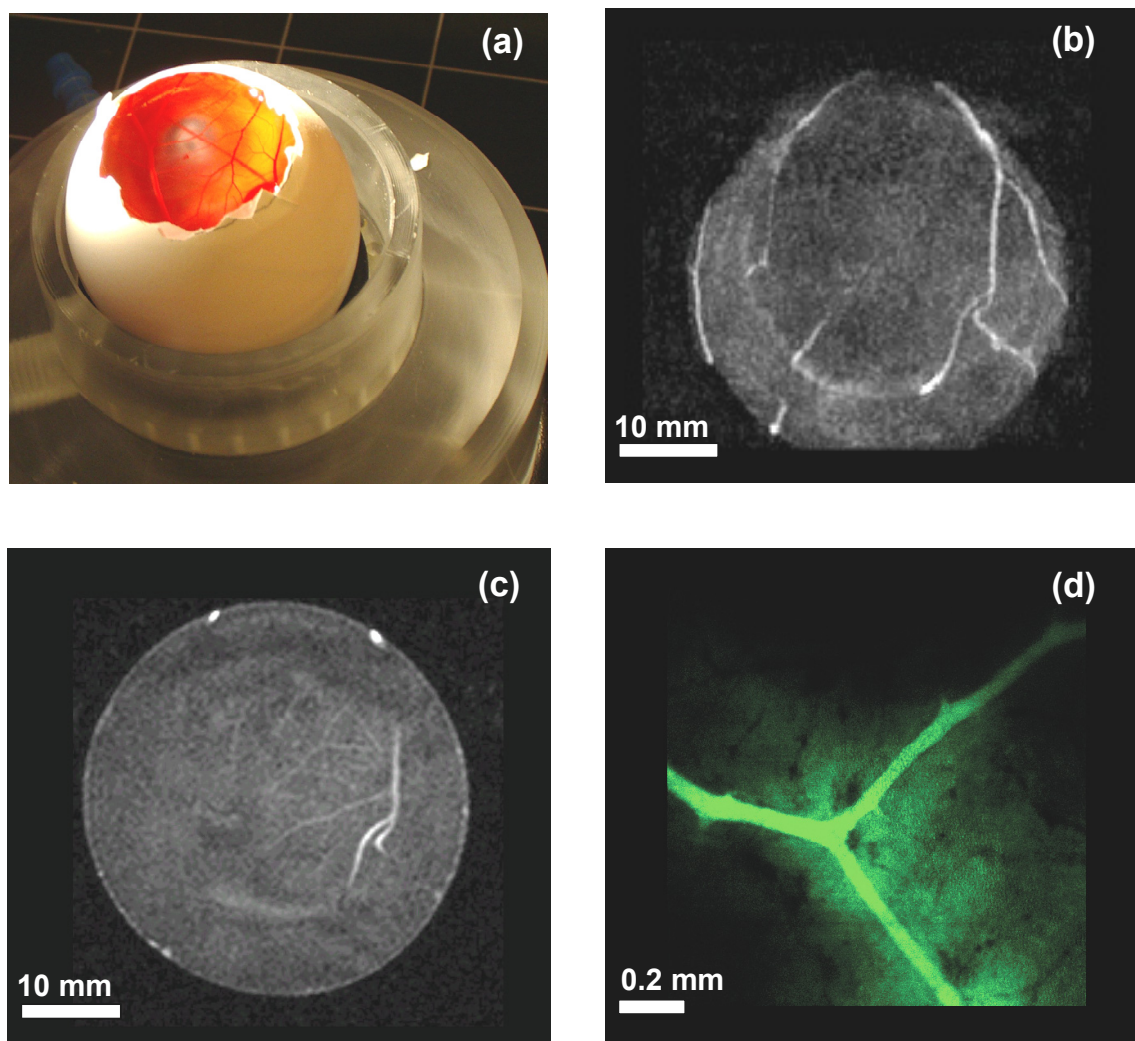


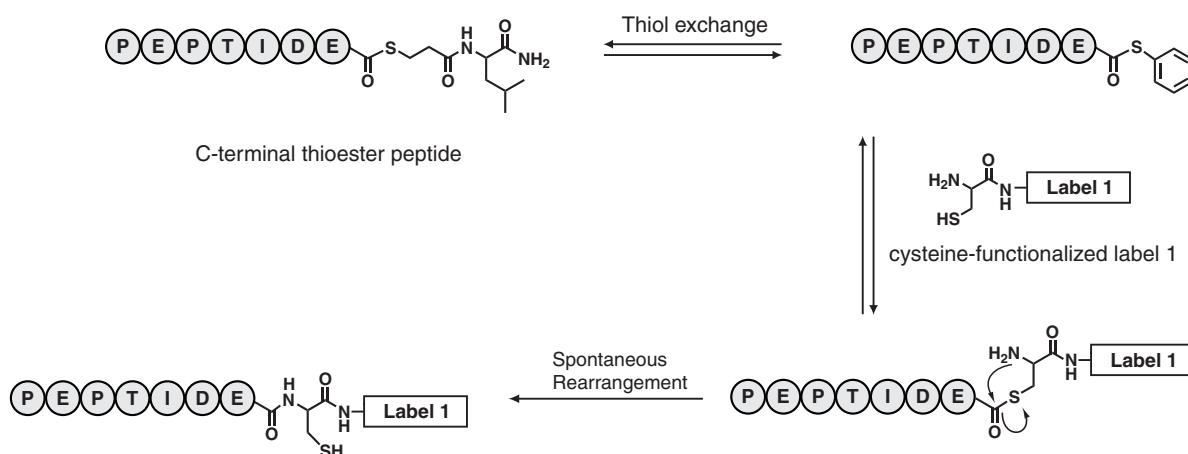
**Figure 6.6** Visualization of the chick chorioallantoic membrane (CAM) by MRI and fluorescence microscopy using bimodal contrast agent **2**. (a) Photograph of the CAM of the chick embryo; (b) and (c) T<sub>1</sub>-weighted post-contrast MR images of the CAM with 0.015 mmol Gd(III) of **2**/kg at 1.5 T; (d) fluorescence microscope image of the CAM immediately after injection of 3.3  $\mu$ mol of **2**/kg.

#### 6.4 GENERAL STRATEGY FOR THE DOUBLE LABELING OF OLIGOPEPTIDES

In collaboration with dr. A. Dirksen of our laboratories and dr. T. M. Hackeng (University of Maastricht), a novel synthetic strategy for the double labeling of oligopeptides in solution utilizing highly efficient and chemoselective reactions, such as native chemical ligation was developed. This approach allows for the synthesis of target-specific peptides with both an MRI as well as a fluorescent label.

### 6.4.1 Introduction

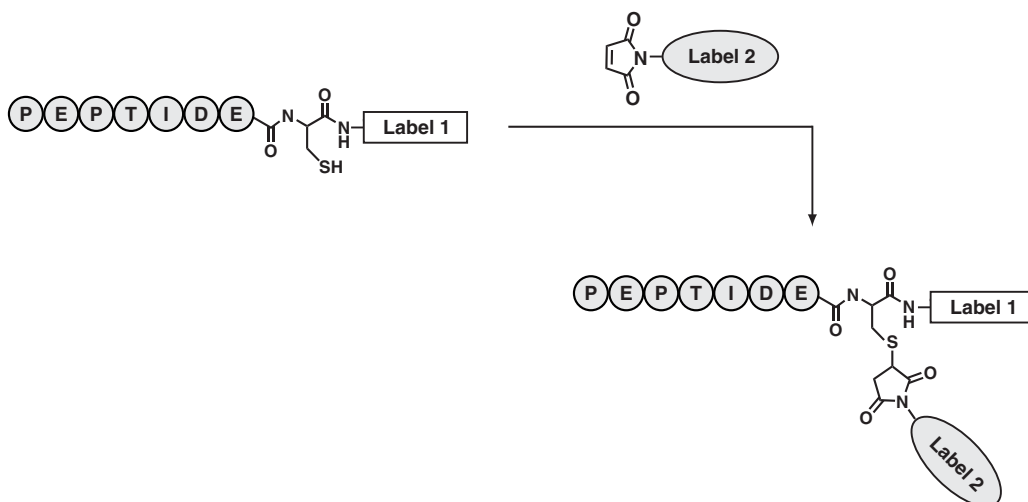
In 1994, Dawson *et al.* introduced native chemical ligation as a synthetic tool to facilitate the synthesis of proteins of moderate size.<sup>22-30</sup> The ligation process involves the chemoselective reaction between a C-terminal thioester peptide and an *N*-terminal cysteine residue in solution, resulting in a native peptide bond at the site of ligation. Recently, Tolbert *et al.* exploited this approach to incorporate labels to proteins by reacting a cysteine-functionalized label with a thioester-functionalized protein.<sup>31,32</sup> In a similar fashion, we used this synthetic methodology for the labeling of oligopeptides. The principle of native chemical ligation is illustrated in Scheme 6.3. The native chemical ligation reaction consists of a two reaction sequence: a transthioesterification and an intramolecular acyl rearrangement.<sup>22,33</sup> The transthioesterification between the C-terminal thioester of peptide and the sulfhydryl group from the cysteine-functionalized label yields a thioester intermediate.<sup>33</sup> This reaction is reversible under ligation conditions, *i.e.* in the presence of benzylmercaptan and thiophenol for exchange while the pH is maintained at 7.0–7.5. The rapid irreversible intramolecular rearrangement of the thioester intermediate eventually leads to the formation of a peptide functionalized with label 1.



**Scheme 6.3** General strategy for the labeling of peptides using native chemical ligation.<sup>33</sup>

Subsequently, the free sulfhydryl group of the peptide involved in native chemical ligation reaction can be used for the introduction of a second label. For instance, the sulfhydryl moiety can be reacted with a maleimide-functionalized label (Scheme 6.4).



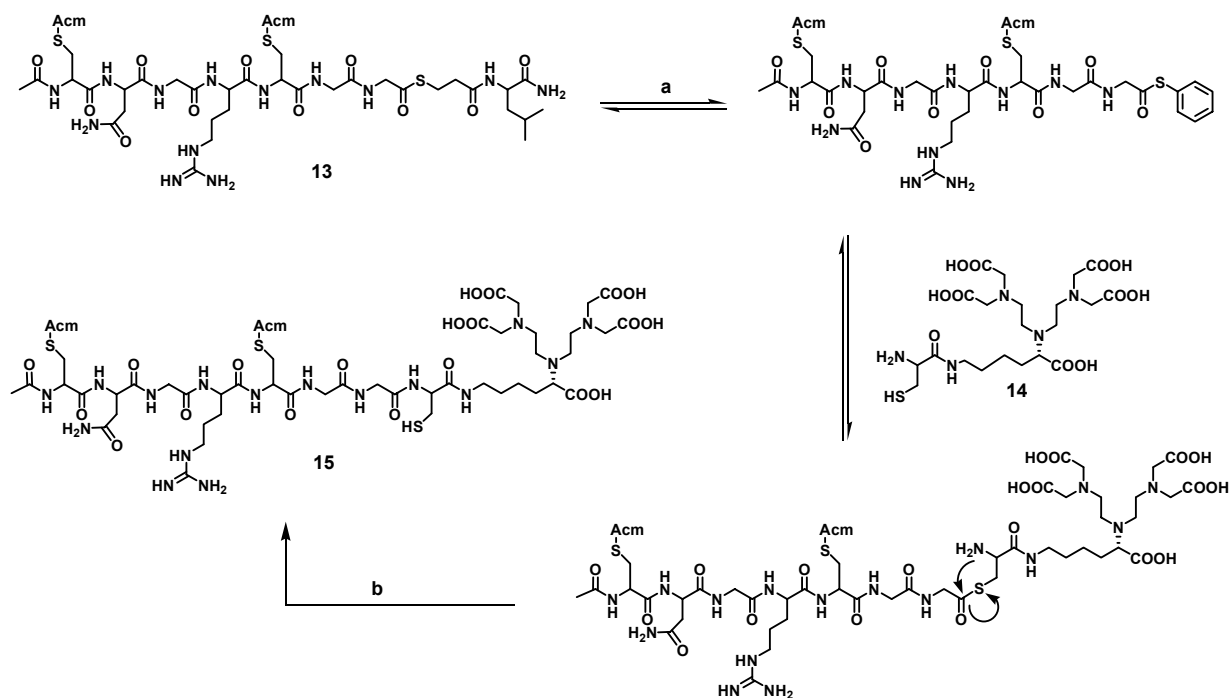


**Scheme 6.4** Incorporation of the second label via the maleimide-sulfhydryl coupling to give a doubly labeled oligopeptide.

In the following section two examples of target-specific MRI contrast agents will be given, which were synthesized according to this strategy. Moreover, this versatile strategy will be applied for the synthesis of target-specific MRI contrast agents functionalized with biotin (See Chapter 7, Section 7.2) and the synthesis of GRGDS-DTPA-functionalized dendrimers (See Chapter 7, Section 7.3).

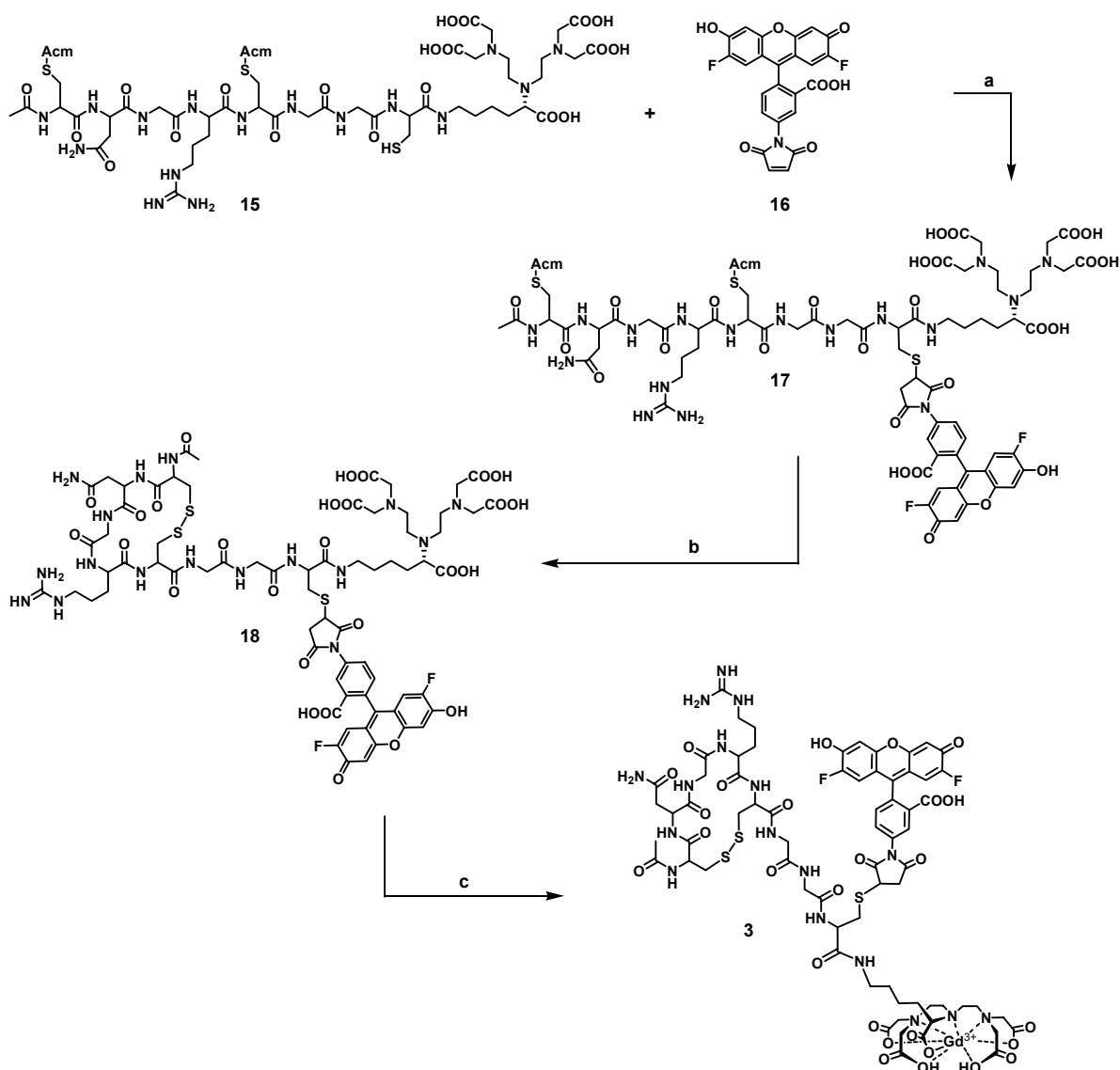
#### 6.4.2 Synthesis of bimodal target-specific MRI contrast agents

A target-specific bimodal contrast agent (**3**) based on a cyclic oligopeptide containing the CNGRC sequence (cNGR), Gd(III)DTPA, and OG488 was designed to allow the combination of MRI and optical imaging (Figure 6.2).<sup>34</sup> For this, manual SPPS using the *in situ* neutralization/HBTU activation procedure Boc chemistry on an MBHA resin was applied to synthesize C-terminal thioester peptide **13** containing the CNGRC sequence (Scheme 6.5).<sup>16,35,36</sup> At this point it is important to notice that the sulfhydryl groups of the two cysteine residues of CNGRC peptide **13** are protected with acetamidomethyl (Acm) groups. This will ensure the correct “folding” of the peptide into its cyclic form later on. The ligation reaction was monitored employing analytical RP HPLC using a C18 column for separation coupled to an UV/vis detector ( $\lambda_{\text{probe}} = 214 \text{ nm}$ ). After 2 hours the ligation reaction was completed and the thioester-functionalized peptide **13** reacted quantitatively with cysteine-functionalized DTPA **14** to yield **15**.



**Scheme 6.5** Strategy for site-specific labeling of C-terminal thioester-peptide **13**—containing the target specific CNGRC sequence—with cysteine-functionalized DTPA (**14**) using native chemical ligation. The sulfhydryl moieties of the two cysteine residues of **13** are protected with acetamidomethyl (Acm =  $-\text{CH}_2\text{CONHCH}_3$ ) groups. (a) 2 v-% thiophenol, 2 v-% benzylmercaptan, 6 M guanidine in 0.1 M Tris buffer, 1 h, pH 7.0–7.5 at 37 °C; (b) spontaneous rearrangement.

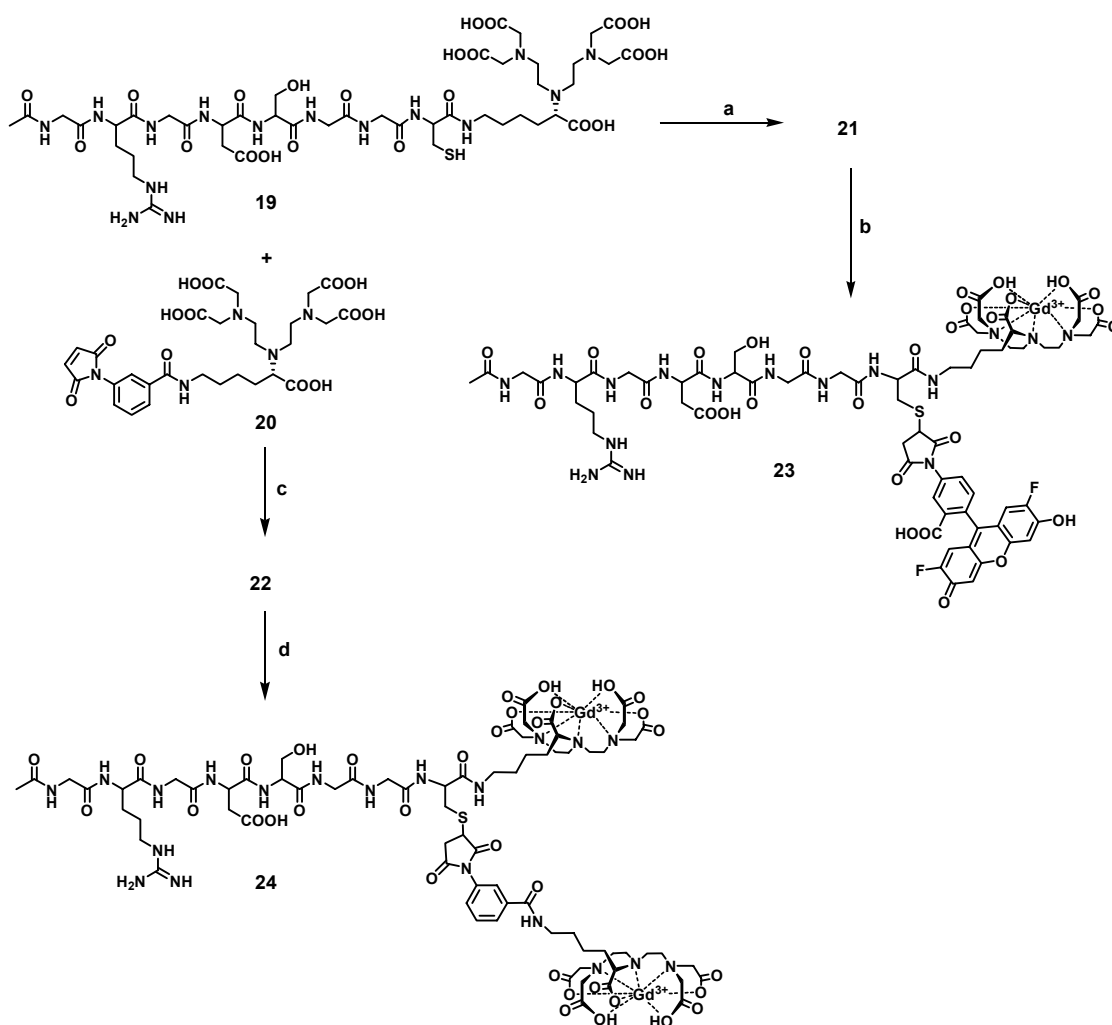
The free sulfhydryl group of the cysteine residue of **15**, which took part in the ligation reaction, was used to introduce OG488 as the fluorescent label. This was achieved through the reaction of **15** with maleimide-functionalized OG488 (**16**) (Scheme 6.6). Again the reaction was monitored employing analytical RP HPLC coupled to UV/vis. Once the reaction went to completion, the reaction mixture was diluted approximately 30 times with 0.1 M Tris buffer containing 10 v-% of acetic acid. Under these conditions the Acm protecting groups of **17** were removed through the addition of 1.2 equivalents of  $\text{I}_2$  to give **18**. The removal of the Acm groups resulted instantaneously in the correct “folding” of the peptide unit into its cyclic form (Scheme 6.6) as confirmed with ESI-MS, which shows a loss in molecular weight of 144 corresponding to the weight of the two Acm groups. Purification with RP HPLC using a C18 column gave **18** in 71% isolated yield. Upon addition of one equivalent of  $\text{GdCl}_3$  to **18**, the desired Gd(III) complex **3** was obtained in a nearly quantitative yield (> 95%) as an orange powder.



**Scheme 6.6** Bimodal target-specific MRI contrast agent (**3**) containing the cNGR moiety, Gd(III)DTPA, and OG488. (a) 0.1 M Tris buffer at pH 6.5, 1 h, 20 °C; (b) 1.2 eq  $I_2$  (5 mM in MeOH), 0.1 M Tris, 10 v-% acetic acid, 1 h, pH 4–4.5, 20 °C; (c) 1 eq  $GdCl_3 \cdot 6 H_2O$  at pH 7, 20 °C (Acm =  $-CH_2CONHCH_3$ ).

Concentration dependent measurements of the longitudinal ( $T_1$ ) and transverse ( $T_2$ ) relaxation times were performed with **3** in water, giving an  $r_1$  of  $7.5 \text{ mM}^{-1}\text{s}^{-1}$  and an  $r_2$  of  $8.3 \text{ mM}^{-1}\text{s}^{-1}$ . Surprisingly, the  $r_1$  of **3** is in between the values of **1** ( $r_1 = 9.8 \text{ mM}^{-1}\text{s}^{-1}$ , MW =  $1.5 \text{ kg}\cdot\text{mol}^{-1}$ ) and **2** ( $r_1 = 6.6 \text{ mM}^{-1}\text{s}^{-1}$ , MW =  $1.0 \text{ kg}\cdot\text{mol}^{-1}$ ), which are combined in this molecule with a molecular weight of  $1.9 \text{ kg}\cdot\text{mol}^{-1}$ . Although the molecular weight of **3** is significantly higher than of **1** and **2**, the  $r_1$  seems to be rather low. Apparently, other factors dominate the  $r_1$  of **3**, e.g. the spacer length between the Gd(III) complex and the other two functionalities is much longer.

The general applicability of this synthetic approach was further explored to prepare a series of doubly labeled GRGDS-based contrast agents. The GRGDS sequence has been shown to bind to cell surface integrins, such as  $\alpha_v\beta_3$ , which are expressed during angiogenesis.<sup>37-41</sup> In analogy to the synthesis of **15**, DTPA-functionalized peptide (**19**) containing the target-specific GRGDS sequence was prepared. The free sulfhydryl moiety of **19** was reacted with maleimide-functionalized OG488 (**16**) or maleimide-functionalized DTPA (**20**) to give **21** and **22**, respectively. Complexation of **21** with  $\text{GdCl}_3$  provided a bimodal contrast agent composed of the GRGDS targeting domain,  $\text{Gd(III)DTPA}$  and OG488. Upon addition of two equivalents of  $\text{GdCl}_3$  to **22**,  $\text{Gd(III)}$  complex **24** with multiple MRI labels and the GRGDS targeting domain was obtained. The ESI-MS spectra of **23** and **24** are shown in Figure 6.7.



**Scheme 6.7** Bimodal target-specific contrast agent (**23**) containing the GRGDS sequence,  $\text{Gd(III)DTPA}$ , and OG488. GRGDS-based MRI contrast agent (**24**) composed of multiple  $\text{Gd(III)}$  moieties. (a) 1 eq of **16**, 0.1 M Tris buffer at pH 6.5, 1 h, 20 °C; (b) 1 eq  $\text{GdCl}_3 \cdot 6 \text{H}_2\text{O}$ , 0.1 M Tris buffer at pH 6.5, 20 °C; (c) 0.1 M Tris buffer at pH 6.5, 1 h, 20 °C; (d) 2 eq  $\text{GdCl}_3 \cdot 6 \text{H}_2\text{O}$ , 0.1 M Tris buffer at pH 6.5, 20 °C.

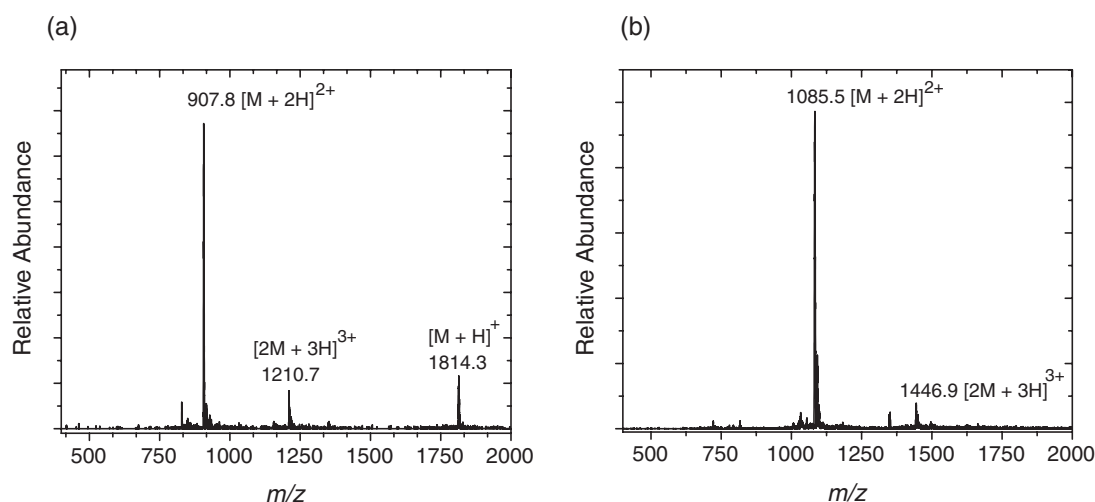


**Figure 6.7** LC-ESI-MS spectra of (a) **23** and (b) **24**.

All intermediates **19**, **21**, **22** and the Gd(III) complexes **23**, **24** were characterized with LC-ESI-MS analysis. In the ESI-MS spectra the  $[M + 2H]^{2+}$  ion was registered as the most abundant molecular ion.

**Table 6.1** LC-ESI-MS data of GRGDS-based structures **19–24**.

Comp.	Label 1	Label 2	Molecular Formula	Mol. Ion	Calcd.	Obsd.
<b>19</b>	–	–	$C_{44}H_{73}N_{15}O_{22}S_1$	$[M + 2H]^{2+}$	598.8	598.8
<b>21</b>	DTPA	OG488	$C_{68}H_{84}F_2N_{16}O_{29}S_1$	$[M + 2H]^{2+}$	830.3	830.4
<b>22</b>	DTPA	DTPA	$C_{73}H_{110}N_{20}O_{35}S_1$	$[M + 2H]^{2+}$	930.4	930.5
<b>23</b>	Gd(III)DTPA	OG488	$C_{68}H_{81}F_2N_{16}O_{29}S_1Gd_1$	$[M + 2H]^{2+}$	907.7	907.8
<b>24</b>	Gd(III)DTPA	Gd(III)DTPA	$C_{73}H_{104}N_{20}O_{35}S_1Gd_2$	$[M + 2H]^{2+}$	1085.3	1085.5

In conclusion, a straightforward methodology for the double labeling oligopeptides, such as cNGR and GRGDS has been developed. This synthetic approach can be regarded as a general strategy for the multilabeling of oligopeptides. Bimodal contrast agent **3** will be investigated *in vivo* and *ex vivo* with MRI and optical imaging methods to gain more insight in the targeting of cardiac angiogenesis with cNGR.

## **6.5 OVERALL CONCLUSIONS**

Strategies for the synthesis of Gd(III)DTPA complexes equipped with either OG488 as a fluorescent label and/or cNGR as a target-specific oligopeptide for angiogenesis have been developed. MR imaging of angiogenesis with cNGR-Gd(III)DTPA in a myocardial model was not conclusive; only a small increase in the MR signal was observed in the infarcted region. From this experiment we can assess that a higher local concentration of MRI probe is needed for sufficient contrast. In addition, it could not be concluded whether the targeting process was responsible for the observed contrast. Therefore, a more sensitive technique, such as optical imaging, is required for the validation of the targeting process. The CAM experiment with a fluorescently labeled Gd(III)DTPA-based complex illustrates the large difference in sensitivity between MRI and optical imaging. This implies that a large number of MRI labels is required with respect to the number of fluorescent labels to compensate for the inherently low sensitivity of MRI. Furthermore, a stronger accumulation of contrast agent may be achieved by the attachment of multiple targeting units to a single scaffold (See Chapter 1, Section 1.4). The strategy for the double labeling of peptides provides an elegant tool to establish this as will be demonstrated in Chapter 7.

## 6.6 EXPERIMENTAL

### General

Unless stated otherwise, all reagents and chemicals were obtained from commercial sources and used without further purification. 2-(1*H*-benzotriazol-1-yl)-1,1,3,3-tetramethyluronium hexafluorophosphate (HBTU) and Boc-amino acids were obtained from NovaBiochem (USA). Boc-Arg (*p*-toluenesulfonyl)-OH and Boc-Asn(xanthyl)-OH were purchased from Midwest Biotech (Fischers, USA). 4-Methylbenzhydrylamine (MBHA) resin was obtained from AnaSpec (USA). Trifluoroacetic acid (TFA) was obtained from Halocarbon (USA). *N,N*-diisopropylethylamine (*D*iPEA) was obtained from Applied Biosystems (USA). Peptide synthesis grade *N,N*-dimethylformamide (DMF) and HPLC grade acetonitrile (CH<sub>3</sub>CN) were purchased from Biosolve. HF was purchased from Matheson Gas (USA). Dichloromethane (DCM) was obtained by distillation from P<sub>2</sub>O<sub>5</sub>. Water was demineralized prior to use. DCM was obtained by distillation from P<sub>2</sub>O<sub>5</sub>. The *N*-succinimidyl activated ester of OG488 (**16**) was obtained from Molecular Probes (the Netherlands). <sup>1</sup>H-NMR spectra were recorded on a Varian Mercury Vx 400 MHz spectrometer at 298 K. Chemical shifts are given in ppm (δ) values. Infrared spectra were recorded at 298 K on a Perkin-Elmer 1605 FT-IR spectrophotometer. Steady-state fluorescence spectra were recorded on an Edinburgh Instruments FS920 double-monochromator spectrometer with a Peltier-cooled red-sensitive photomultiplier. Analytical RP HPLC was performed on a Varian Prostar HPLC system with a Vydac<sup>TM</sup> protein peptide C18 column (0.5 × 15 cm, flow 1 mL/min), eluted with a linear gradient of 0–60% CH<sub>3</sub>CN in 0.1% TFA in H<sub>2</sub>O in 30 minutes. The HPLC system was coupled to an UV/vis detector probing at 214 nm. Semi-preparative HPLC was performed using a Vydac C18 column (2.5 × 20 cm, 10 mL/min), eluted with a linear gradient of 0–20% CH<sub>3</sub>CN in 0.1% aqueous TFA in 90 minutes. ESI-QTOF-MS experiments were recorded on a Q-TOF Ultima GLOBAL mass spectrometer (Micromass, Manchester, U.K.). ESI-MS measurements were performed on a Perkin Elmer API-150 SCIEX. LC-ESI-MS measurements were performed on a Finnigan LCQ Deca XP Max ion trap mass spectrometer (Thermo Electron Corporation, San Jose, USA). The experimental details of the *r*<sub>1</sub> and *r*<sub>2</sub> measurements are described in Chapter 2. Aqueous solutions of MRI contrast agents **1-3** (2 mL) were prepared with a Gd(III) concentration ranging from 0.05–1.00 mM. Gd(III) concentrations in the aqueous solutions used for the *T*<sub>1</sub>-relaxivity measurements were determined by means of ICP-AES at 342.247 nm (Leeman Labs Echelle Unicam701 emission spectrometer, TNO, Eindhoven, the Netherlands).

### Murine myocardial model

The ethical review committee of the Maastricht University Hospital (the Netherlands) approved the animal studies. The maintenance and care of the experimental animals was in compliance with the guidelines set by the institutional animal care committee, accredited by the National Department of Health. These experiments were performed by dr. A. Buehler (University of Maastricht, the Netherlands) and Q.G. de Lussanet (Maastricht University Hospital, the Netherlands). Myocardial infarctions were induced in 10–12 week old male mice (Swiss *nu/nu*, Charles River) by ligation of the left coronary artery, as previously described in the literature.<sup>42</sup> The mice were anesthetized with subcutaneous injection of 100 mg of ketamine (Nimatek; Eurovet, Bladel, the Netherlands) per kilogram of body weight and 10 mg/kg of xylazine-HCl (Sedamun; Eurovet, Bladel, the Netherlands). The mice were randomly assigned to either **1** (dose, 0.03 mmol/kg body weight) or Gd(III)DTPA (dose, 0.07 mmol/kg body weight) that were injected slowly into the tail vein and flushed with 15 μL of normal saline (NaCl 0.9% Injection Fluid, Braun, Melsungen, Germany). After MR imaging the mice, while still under anesthesia, were sacrificed by means of cervical dislocation.

**Serial contrast-enhanced MRI**

These experiments were performed in collaboration with dr. A. Buehler (University of Maastricht, the Netherlands) and Q.G. de Lussanet (Maastricht University Hospital, the Netherlands). MR imaging was performed as described previously using a small surface coil (diameter, 5 centimeters) and a 1.5 T system (Intera, release 9.1.2, Philips Medical Systems) with a maximum gradient strength of 30 mT/m and rise time of 200  $\mu$ s.<sup>43</sup> Warm water bags were placed near the mouse to keep the local temperature in the MR imaging unit bore near 28 °C. Serial contrast-enhanced MRI was performed 7 days after myocardial infarction. Since renal clearance of **1** occurs within 24 h, the same mice were subsequently subjected to Gd(III)DTPA on the next day and *vice versa*. The MRI protocol included 6 dynamic MR acquisitions of 25 s each (one pre-contrast ‘mask’ acquisition), and five acquisitions were timed at 8 s, 30 s, 90 s, 3 min and 8 min after contrast injection (3D FFE; TR/TE 12/3.2; FA 30°; NSA 1) with 30 coronal sections, 1.6 mm thick (interpolated to 0.8 mm). Matrix dimensions were 224  $\times$  224, with a field of view of 90  $\times$  90 mm, and reconstructed voxel sizes were 0.4  $\times$  0.4  $\times$  0.8 mm. Contrast-enhanced MRI measurements were reconstructed as anterior-posterior view digitally subtracted maximum intensity projections.

**CAM model**

These experiments were performed in collaboration with dr. J.M.C.G. van Golde (University of Maastricht, the Netherlands), Q.G. de Lussanet (Maastricht University Hospital, the Netherlands) and dr. M.A.M.J. van Zandvoort (University of Maastricht, the Netherlands). A microtube was connected to one of the main vessels of the CAM of the chick-embryo for the injection of bimodal contrast agent **2**. A thin layer of NaCl (aq) was carefully drizzled on top of the CAM to prevent susceptibility artifacts near the air–tissue interface. For MR imaging, the egg was placed in a knee coil to facilitate convenient handling for the injection of **2** (0.015 mmol/kg body weight). The CAM of the chick-embryo was located with a 3D  $T_1$ -weighted MR protocol of the entire chick-embryo. High spatial resolution,  $T_1$ -weighted, post-contrast MR images of the CAM were recorded using a 3D fast field echo protocol (TR/TE = 22/10.9 msec; NSA = 2; 40 slices, voxel size 0.31  $\times$  0.23  $\times$  0.3 mm (FOV 64  $\times$  48  $\times$  12 mm, matrix 208  $\times$  208, FOV 64  $\times$  48 mm in plane). Fluorescence microscopy experiments of the CAM were performed with 3.3  $\mu$ mol of **2**/kg body weight.

**Gd(III) complex of cNGR-DTPA (1)**

Compound **10** (8.8 mg, 6.7  $\mu$ mol) was dissolved in demineralized water (9 mL). The pH of the aqueous solution was adjusted to 6.5–7.0 by adding small aliquots of 0.25% NH<sub>4</sub>OH (aq). Subsequently, a solution of GdCl<sub>3</sub>·6 H<sub>2</sub>O (2.2 mg, 5.9  $\mu$ mol, 0.9 eq.) in water (0.4 mL) was added while maintaining the pH at 6.5–7 with a 0.25% NH<sub>4</sub>OH (aq) solution. The solution was vigorously stirred for 2 h at room temperature. The formation of the Gd(III) complex was confirmed with ESI-MS. After freeze drying the desired Gd(III) complex **10** was obtained as a white hygroscopic powder (9.7 mg). ESI-MS:  $m/z$  [C<sub>49</sub>H<sub>79</sub>N<sub>18</sub>O<sub>21</sub>S<sub>2</sub>Gd – H]<sup>–</sup> Calcd. 1476.43 Da, Obsd. 1476.83 Da; [M – 2H]<sup>2–</sup> Calcd. 737.71 Da, Obsd. 737.91 Da. ICP-AES (Gd(III)): aqueous solution of **7** Calcd. 12.5  $\mu$ M, Obsd. 11.7  $\mu$ M. FT-IR (ATR):  $\nu$  (cm<sup>–1</sup>) = 3252, 1634, 1577, 1447, 1413, 1202, and 1141.

**Gd(III) complex of OG488-labeled DTPA (2)**

Gd(III) complex **2** was prepared by adding a solution of GdCl<sub>3</sub>·6 H<sub>2</sub>O (2.0 mg, 5.0  $\mu$ mol) in water (2 mL) dropwise to a solution of **12** (4.6 mg, 5.4  $\mu$ mol) in water (20 mL). The pH was continuously monitored and maintained at pH 7 with 0.1 N NH<sub>4</sub>OH (aq). The solution was vigorously stirred for 6 h at room temperature. The solution was dialyzed with a 100 Da MWCO membrane and lyophilized. Gd(III) complex **2** was obtained as an orange powder (5.5 mg, quantitative yield). FT-IR (ATR):  $\nu$  (cm<sup>–1</sup>) = 3142, 3049, 1669, 1646, 1586,



1486, 1439, 1404, 1322, 1301, 1184, 1130. ESI-QTOF-MS:  $m/z$   $[\text{C}_{39}\text{H}_{37}\text{N}_4\text{O}_{16}\text{F}_2\text{Gd}_1 - \text{H}]^-$  Calcd. 1012.1 Da, Obsd. 1012.2 Da;  $[\text{M} - 2\text{H}]^{2-}$  Calcd. 506.1 Da, Obsd. 505.6 Da. ICP (Gd(III)) Calcd. 25  $\mu\text{M}$ , Obsd. 17.5  $\mu\text{M}$ .

### **Synthesis of cNGR-GGC(OG488)-Gd(III)DTPA (3)**

Compounds **3** was synthesized by dr. A. Dirksen according to reference 34.

### **Solid phase peptide synthesis (NACNGRCGGK(NH<sub>2</sub>)-MBHA) (5)**

Manual solid phase peptide synthesis (SPPS) was employed on a 0.4 mmol scale using the *in situ* neutralization/ HBTU activation procedure for Boc chemistry as previously described by Schnölzer *et al.*<sup>16</sup> Each synthetic cycle consisted of *N*<sup>t</sup>-Boc-removal by a 1–2 minute treatment with neat TFA, a 1 min DMF flow wash, a 10 to 20 min coupling time with 2.0 mmol activated Boc-*N*<sup>t</sup>-protected amino acid in the presence of an excess of DiPEA, followed by a second DMF flow wash. *N*<sup>t</sup>-Boc amino acids (2.2 mmol) were preactivated for 3 min with 2.0 mmol HBTU (0.5 M in DMF) in the presence of excess DiPEA (3 mmol). Side chain-protected amino acids were: Boc-Arg(*p*-toluenesulfonyl)-OH, Boc-Asn(xanthyl)-OH, Boc-Cys(4-methylbenzyl)-OH, and Boc-Lys(Fmoc)-OH. After each coupling step, the yields (> 99%) were determined by measuring residual free amine with the quantitative ninhydrin assay.<sup>44</sup> The peptide on MBHA resin was washed with DMF, DCM, and 1:1 *v/v* DCM/MeOH, to give side chain-protected BocCNGRCGGK(Fmoc)-MBHA **4** (1.46 g, 99%). The removal of the Boc group at the *N*-terminus of **4** (0.363 g, 0.10 mmol) was achieved by a 1–2 min treatment with neat TFA, a 2 min DMF flow wash, followed by neutralization with 10% DiPEA in DMF. The acetylation reaction was carried out with a solution of acetic anhydride (0.25 M) and pyridine (0.25 M) in DMF for 2 min (2 times), followed by a DMF flow wash. The Fmoc group was removed with 20% piperidine in DMF for 4 min (3 times), followed by a DMF flow wash, giving partially side chain-protected NACNGRCGGK(NH<sub>2</sub>)-MBHA **5** (0.35 g, 96%).

### **Isocyanate-functionalized DTPA synthon (7)**

Amine-functionalized DTPA pentaester **7** was synthesized following previously described procedures that can be found in Chapter 2. A solution of **6** (0.516 g, 0.69 mmol) in DCM (5 mL) was injected into a stirred solution of di-*tert*-butyl-tricarbonate<sup>17</sup> (0.21 g, 0.80 mmol) in DCM (5 mL) under an argon atmosphere. The colorless solution was vigorously stirred for 1 h at room temperature. FT-IR spectroscopy revealed the presence of the characteristic isocyanate absorption at 2272  $\text{cm}^{-1}$ . The excess of di-*tert*-butyl-tricarbonate was quenched by the addition of three droplets of dry pyridine. DCM was removed under an argon flow and the crude mixture was redissolved in DMF (10 mL) and directly used for the reaction with the peptide on the solid phase.

### **DTPA-functionalization of the peptide on solid phase**

A solution of **7** (0.69 mmol) in DMF (10 mL) was added to **5** (0.347 g peptide on resin, 0.10 mmol peptide). The reaction mixture was incubated overnight at 200 rpm under an argon atmosphere, followed by a DMF flow wash, a 10 min treatment with neat TFA (2 times), a second DMF flow wash, a DCM flow wash, an 1:1 *v/v* DCM/MeOH flow wash, and then dried overnight, yielding crude peptide-resin **8** (0.380 g, 0.10 mmol). The gain in weight of 33 mg corresponds to a coupling efficiency of ca. 67%.

### **Cleavage of the peptide from the resin**

The crude peptide on resin **8** (0.25 g, 0.066 mmol peptide) was cleaved from the MBHA resin by treatment with anhydrous HF for 1 h at 0 °C with 4% *p*-cresol as a scavenger. Subsequently, the deprotected free peptide was precipitated in cold Et<sub>2</sub>O, collected on a filter and subsequently dissolved in 0.1% aqueous

TFA and lyophilized, yielding crude peptide **9** (80 mg, nearly quantitative yield of HF cleavage) as a white powder. Analytical RP HPLC (linear gradient of 0–60% CH<sub>3</sub>CN in 0.1% TFA in H<sub>2</sub>O in 30 minutes): product **9** eluting at 10.9 min. ESI-QTOF-MS:  $m/z$  Calcd. for [C<sub>49</sub>H<sub>84</sub>N<sub>18</sub>O<sub>21</sub>S<sub>2</sub> + H]<sup>+</sup> Calcd. 1325.56 Da, Obsd. 1325.86 Da; [M + 2H]<sup>2+</sup> Calcd. 663.28 Da, Obsd. 663.43 Da.

#### Formation of the disulfide bridge (10)

The intramolecular disulfide bond formation between the two cysteine residues was performed by dissolving the crude peptide **5** (80 mg) in 0.1 M Tris, pH 8.0 (200 mL), containing 1 M guanidine. The reaction was monitored with analytical RP HPLC. Stirring for 3 h while exposed to air at 4 °C yielded quantitative formation of the disulfide bridge. Semi-preparative RP HPLC purification and freeze-drying yielded **10** (17 mg, 0.013 mmol, isolated yield of ca. 29%) as a white powder. The peptide was stored at –20 °C until further use. Analytical RP HPLC (linear gradient of 0–60% CH<sub>3</sub>CN in 0.1% TFA in H<sub>2</sub>O in 30 minutes): **10** eluting at 8.8 min. ESI-MS:  $m/z$  [C<sub>49</sub>H<sub>82</sub>N<sub>18</sub>O<sub>21</sub>S<sub>2</sub> + H]<sup>+</sup> Calcd. 1323.54 Da, Obsd. 1323.80 Da; [M + 2H]<sup>2+</sup> Calcd. 662.27 Da, Obsd. 662.40 Da. FT-IR (ATR):  $\nu$  (cm<sup>-1</sup>) = 3281, 1628, 1541, 1406, 1376, 1200, 1178, and 1132.

#### OG488-labeled DTPA (tert-butyl ester protected) (11)

To a solution of the amine-functionalized DTPA pentaester **6** (36.5 mg, 0.049 mmol) in dry DMF (6 mL) were sequentially added *N*-succinimidyl activated ester of OG488 (25 mg, 0.049 mmol) and NEt<sub>3</sub> (15  $\mu$ L, 0.11 mmol). The reaction was continued overnight at room temperature. The solution was concentrated under reduced pressure. The crude product was dissolved in diethyl ether (15 mL) and washed with water (2  $\times$  15 mL). The collected organic layer was concentrated under reduced pressure. Compound **11** was obtained as an orange solid (42 mg, 0.037 mmol, 75%). <sup>1</sup>H-NMR (CD<sub>3</sub>OD):  $\delta$  = 8.22–8.14 (m, 2H, H-5' {1H} + H6' {1H}), 7.69 (s, 1H, H-3'), 6.9–6.82 (d,  $J_{HF}$  = 7.3 Hz, 2H, H-2 {1H} + H-10 {1H}), 6.68–6.58 (d,  $J_{HF}$  = 11.8 Hz, 2H, H-5 {1H} + H-7 {1H}), 3.55–2.90 (m, 3H, CONHCH<sub>2</sub>(CH<sub>2</sub>)<sub>3</sub>CHN {2H} + CONHCH<sub>2</sub>(CH<sub>2</sub>)<sub>3</sub>CHN {1H}); s, 8H, NCH<sub>2</sub>COOC(CH<sub>3</sub>)<sub>3</sub>; m, 8H, NCH<sub>2</sub>CH<sub>2</sub>N {4H} + NCH<sub>2</sub>CH<sub>2</sub>N {4H}), 1.90–1.20 (m, 6H, CONHCH<sub>2</sub>(CH<sub>2</sub>)<sub>3</sub>CHN; s, 45H, COOC(CH<sub>3</sub>)<sub>3</sub>). FT-IR (ATR):  $\nu$  (cm<sup>-1</sup>) = 2977, 2934, 1729 (C=O stretch), 1646, 1614, 1537, 1511, 1480, 1454, 1393, 1367, 1337, 1277, 1255, 1223, 1147, and 1102. ESI-QTOF-MS:  $m/z$  [C<sub>59</sub>H<sub>80</sub>N<sub>4</sub>O<sub>16</sub>F<sub>2</sub> – H]<sup>-</sup> Calcd. 1137.5 Da, Obsd. 1137.4 Da.

#### OG488-labeled DTPA (12)

A solution of **11** (38.5 mg, 0.034 mmol) in TFA (10 mL) was stirred overnight at room temperature. The solution was concentrated *in vacuo*. The crude product was dissolved in demineralized water (8 mL) and the pH was adjusted to 7 with 0.1 N NH<sub>4</sub>OH (aq). This solution was dialyzed with a 100 Da MWCO membrane. The solution was lyophilized and compound **12** was obtained in near quantitative yield. <sup>1</sup>H-NMR (D<sub>2</sub>O):  $\delta$  = 7.94 (dd,  $J$  = 1.5 Hz and  $J$  = 7.8 Hz, 1H, H-5'), 7.86 (d,  $J$  = 7.8 Hz, 1H, H-6'), 7.60 (d,  $J$  = 1.7 Hz, 1H, H-3'), 6.90–6.84 (dd,  $J$  = 2.0 Hz and  $J_{HF}$  = 11.8 Hz, 2H, H-5 {1H} + H-7 {1H}), 6.78–6.74 (d,  $J_{HF}$  = 7.3 Hz, 2H, H-2 {1H} + H-10 {1H}), 3.71 (s, 8H, NCH<sub>2</sub>COOH), 3.40–3.20 (m, 6H, CONHCH<sub>2</sub>(CH<sub>2</sub>)<sub>3</sub>CHN {2H} + NCH<sub>2</sub>CH<sub>2</sub>N {4H}), 3.16 (m, 1H, CONHCH<sub>2</sub>(CH<sub>2</sub>)<sub>3</sub>CHN), 3.10–3.00 (m, 2H, NCH<sub>2</sub>CH<sub>2</sub>N), 2.85–2.75 (m, NCH<sub>2</sub>CH<sub>2</sub>N), 1.70–1.30 (m, 6H, CONHCH<sub>2</sub>(CH<sub>2</sub>)<sub>3</sub>CHN). FT-IR (ATR):  $\nu$  (cm<sup>-1</sup>) = 3183, 3024, 2857, 1644, 1599, 1472, 1435, 1395, 1372, 1313, 1174, and 1124. ESI-TOF-MS:  $m/z$  [C<sub>39</sub>H<sub>40</sub>N<sub>4</sub>O<sub>16</sub>F<sub>2</sub> – H]<sup>-</sup> Calcd. 857.2 Da, Obsd. 857.2 Da; [M – 2H]<sup>2-</sup> Calcd. 428.6 Da, Obsd. 428.1 Da.

#### Synthesis of 13

This compound was synthesized by dr. A. Dirksen according to reference 34.

**Cysteine-functionalized DTPA synthon (14)**

Compound **14** was synthesized according to a previously described literature procedure.<sup>31</sup>

**Synthesis of 15,17, and 18**

These compounds were synthesized by dr. A. Dirksen according to reference 34.

**NAcGRGDSGGC-DTPA (19)**

A manual SPPS using the *in situ* neutralization/HBTU activation procedure for Boc chemistry on an MBHA resin was applied to synthesize NAcGRGDSGG-MPAL. ESI-MS:  $m/z$   $[\text{C}_{32}\text{H}_{54}\text{N}_{12}\text{O}_{13}\text{S}_1 + \text{H}]^+$  Calcd. 847.4 Da, Obsd. 847.3 Da. NAcGRGDSGG-MPAL (30 mg, 0.035 mmol) and 1.5 equivalents of **4** (30.2 mg, 0.053 mmol) were dissolved in 1 mL of 6 M guanidine, 0.07 M Tris (aq) pH 8. To this solution 20  $\mu\text{L}$  (2 v-%) of thiophenol and 20  $\mu\text{L}$  (2 v-%) of benzyl mercaptan were added. The pH was adjusted to 7.5 by the addition of small aliquots of 0.5 M NaOH (aq). The reaction was continued for 90 min at 37 °C. The reaction mixture was filtered and the product was purified employing semi-preparative RP HPLC over a C18 column (gradient: 0–22% MeCN in H<sub>2</sub>O, 0.1% TFA in 90 minutes). Freeze drying yielded **19** (29.3 mg, 0.025 mmol, 71%) as a fluffy white powder. ESI-MS:  $m/z$   $[\text{C}_{44}\text{H}_{73}\text{N}_{15}\text{O}_{22}\text{S}_1 + \text{H}]^+$  Calcd. 1196.5 Da, Obsd. 1196.5 Da;  $[\text{M} + \text{H}]^{2+}$  Calcd. 598.8 Da, Obsd. 598.8 Da.

**Maleimide-functionalized DTPA (20)**

This compound was kindly provided by dr. A. Dirksen.

**NAcGRGDSGGC(OG488)-DTPA (21)**

Compound **21** was synthesized on an analytical scale to test the synthetic feasibility. NAcGRGDSGGC-DTPA (1.2 mg, 1.0  $\mu\text{mol}$ ) was dissolved in 120  $\mu\text{L}$  0.1 M Tris buffer (aq, pH 6.9). The pH of the solution was adjusted to 6.5 by the addition of small aliquots of 0.5 M NaOH (aq). Subsequently, the solution was added to maleimide-functionalized OG488 (0.4 mg, 0.9  $\mu\text{mol}$ ). The reaction mixture was shaken until all maleimide-functionalized OG488 dissolved and the reaction was continued for 1 h at room temperature. The reaction was monitored employing RP HPLC over a C18 column (gradient: 0–60% MeCN in H<sub>2</sub>O, 0.1% TFA in 30 minutes). Analytical RP HPLC: **21** eluting at 14.7 min. The reaction mixture was used for the next reaction step without any purification. ESI-MS:  $m/z$   $[\text{C}_{68}\text{H}_{84}\text{F}_2\text{N}_{16}\text{O}_{29}\text{S}_1 + \text{H}]^+$  Calcd. 1659.5 Da, Obsd. 1659.5 Da;  $[\text{M} + 2\text{H}]^{2+}$  Calcd. 830.3 Da, Obsd. 830.4 Da.

**NAcGRGDSGGC(DTPA)-DTPA (22)**

This compound was prepared on an analytical scale to test the synthetic feasibility. NAcGRGDSGGC-DTPA **19** (0.49 mg, 0.41  $\mu\text{mol}$ ) was dissolved in 74  $\mu\text{L}$  0.1 M Tris buffer (aq, pH 6.9). The pH of the solution was adjusted to 6.5 by the addition of small aliquots of 0.5 M NaOH (aq). Subsequently, the solution was added to **20** (0.25 mg, 0.38  $\mu\text{mol}$ ). The reaction was completed within 1 h at room temperature. LC-ESI-MS:  $m/z$   $[\text{C}_{73}\text{H}_{110}\text{N}_{20}\text{O}_{35}\text{S}_1 + 2\text{H}]^{2+}$  Calcd. 930.4 Da, Obsd. 930.5 Da;  $[\text{M} + 3\text{H}]^{3+}$  Calcd. 620.6 Da, Obsd. 620.7 Da.

**NAcGRGDSGGC(OG488)-Gd(III)DTPA (23)**

To the crude mixture of **21** was added 1 equivalent of GdCl<sub>3</sub>·6 H<sub>2</sub>O. The pH was adjusted to 7 by adding small aliquots of 0.5 M NaOH (aq). The reaction was completed within 1 h at room temperature LC-ESI-MS  $m/z$   $[\text{C}_{68}\text{H}_{81}\text{F}_2\text{N}_{16}\text{O}_{29}\text{S}_1\text{Gd}_1 + \text{H}]^+$  Calcd. 1814.4 Da, Obsd. 1814.4 Da;  $[\text{M} + 2\text{H}]^{2+}$  Calcd. 907.7 Da, Obsd. 907.8 Da.

**NAcGRGDSGGC(Gd(III)DTPA)-Gd(III)DTPA (24)**

To the crude mixture of **22** were added 2 equivalents of GdCl<sub>3</sub>·6 H<sub>2</sub>O. The pH was adjusted to 7 by adding small aliquots of 0.5 M NaOH (aq). The reaction was completed within 1 h at room temperature. LC-ESI-MS *m/z* [C<sub>73</sub>H<sub>104</sub>N<sub>20</sub>O<sub>35</sub>S<sub>1</sub>Gd<sub>2</sub> + 2H]<sup>2+</sup> Calcd. 1085.3 Da, Obsd. 1085.5 Da.

**6.7 REFERENCES**

- (1) Caravan, P.; Ellison, J. J.; McMurry, T. J.; Lauffer, R. B. *Chem. Rev.* **1999**, *99*, 2293-2352.
- (2) Merbach, A. E.; Toth, E. *The Chemistry of Contrast Agents in Medical Magnetic Resonance Imaging*; John Wiley & Sons: New York, 2001.
- (3) Jacques, V.; Desreux, J. F. *Top. Curr. Chem.* **2002**, *221*, 123-164.
- (4) Griffioen, A. W.; Molema, G. *Pharmacological Reviews* **2000**, *52*, 237-268.
- (5) Cristofanilli, M.; Charnsangavej, C.; Hortobagyi, G. N. *Nat. Rev. Drug Discovery* **2002**, *1*, 415-426.
- (6) Carmeliet, P.; Jain, R. K. *Nature* **2000**, *407*, 249-257.
- (7) Arap, W.; Kolonin, M. G.; Trepel, M.; Lahdenranta, J.; Cardo-Vila, M.; Giordano, R. J.; Mintz, P. J.; Ardelt, P. U.; Yao, V. J.; Vidal, C. I.; Chen, L.; Flamm, A.; Valtanen, H.; Weavind, L. M.; Hicks, M. E.; Pollock, R. E.; Botz, G. H.; Koivunen, E.; Cahill, D.; Troncoso, P.; Baggerly, K. A.; Pentz, R. D.; Do, K.-A.; Logothetis, C. J.; Pasqualini, R. *Nature Med.* **2000**, *8*, 121-127.
- (8) Arap, W.; Pasqualini, R.; Ruoslahti, E. *Science* **1998**, *279*, 377-380.
- (9) Ellerby, H. M.; Arap, W.; Ellerby, L. M.; Kain, R.; Andrusiak, R.; Rio, G. D.; Krajewski, S.; Lombardo, C. R.; Rao, R.; Ruoslahti, E.; Bredesen, D. E.; Pasqualini, R. *Nature Med.* **1999**, *5*, 1032-1038.
- (10) Curnis, F.; Sacchi, A.; Borgna, L.; Magni, F.; Gasparri, A.; Corti, A. *Nature Biotechnol.* **2000**, *18*, 1185-1190.
- (11) Pasqualini, R.; Koivunen, E.; Kain, R.; Lahdenranta, J.; Sakamoto, M.; Stryhn, A.; Ashmun, R. A.; Shapiro, L. H.; Arap, W.; Ruoslahti, E. *Cancer Res.* **2000**, *60*, 722-727.
- (12) Riemann, D.; Kehlen, A.; Langner, J. *Immunology Today* **1999**, *20*, 83-88.
- (13) Bhagwat, S. V.; Lahdenranta, J.; Giordano, R.; Arap, W.; Pasqualini, R.; Shapiro, L. H. *Blood* **2001**, *97*, 652-659.
- (14) Colombo, G.; Curnis, F.; De Mori, G. M. S.; Gasparri, A.; Longoni, C.; Sacchi, A.; Longhi, R.; Corti, A. *J. Biol. Chem.* **2002**, *277*, 47891-47897.
- (15) Buehler, A.; van Zandvoort, M. A. M. J.; Hackeng, T. M.; Schrans-Stassen, B. H. G. J.; Bennaghmouch, A.; Hofstra, L.; Cleutjens, J. P. M.; Duijvestijn, A.; Smeets, M. B.; de Kleijn, D. P. V.; Post, M. J.; de Muinck, E. D. *submitted for publication*.
- (16) Schnölzer, M.; Alewood, P.; Jones, A.; Alewood, D.; Kent, S. B. H. *Int. J. Peptide Protein Res.* **1992**, *40*, 180-193.
- (17) Peerlings, H. W. I.; Meijer, E. W. *Tetrahedron Letters* **1999**, *40*, 1021-1024.
- (18) Maas, J. W.; Le Noble, F. A.; Dunselman, G. A.; de Goeij, A. F.; Struyker Boudier, H. A.; Evers, J. L. *Gynecologic and obstetric investigation* **1999**, *48*, 108-112.
- (19) Richardson, M.; Singh, G. *Curr. Drug Targets Cardiovasc. Haematol. Disord.* **2003**, *3*, 155-185.
- (20) Brooks, P. C.; Clark, R. A. F.; Cheresch, D. A. *Science* **1994**, *264*, 569-571.
- (21) van Golde, J. M. C. G. *PhD thesis: Chick embryo as a model in fetal physiology*; University of Maastricht, 1999.
- (22) Dawson, P. E.; Muir, T. W.; Clark-Lewis, I.; Kent, S. B. H. *Science* **1994**, *266*, 776-779.
- (23) Beligere, G. S.; Dawson, P. E. *J. Am. Chem. Soc.* **1999**, *121*, 6332-6333.

- (24) Dawson, P. E.; Kent, S. B. H. *Annu. Rev. Biochem.* **2000**, *69*, 923-960.
- (25) Kochendoerfer, G. G. *Current Opinion in Drug Discovery & Development* **2001**, *4*, 205-214.
- (26) Yan, L. Z.; Dawson, P. E. *Angew. Chem. Int. Ed.* **2001**, *40*, 3625-3627.
- (27) Tam, J. P.; Xu, J.; Eom, K. D. *Biopolymers* **2001**, *60*, 194-205.
- (28) Bang, D.; Chopra, N.; Kent, S. B. H. *J. Am. Chem. Soc.* **2004**, *126*, 1377-1383.
- (29) Bang, D.; Kent, S. B. H. *Angew. Chem. Int. Ed.* **2004**, *43*, 2534-2538.
- (30) Yeo, D. S. Y.; Srinivasan, R.; Chen, G. Y. J.; Yao, S. Q. *Chem. Eur. J.* **2004**, *10*, 4664-4672.
- (31) Tolbert, T. J.; Wong, C.-H. *J. Am. Chem. Soc.* **2000**, *122*, 5421-5428.
- (32) Tolbert, T. J.; Wong, C.-H. *Angew. Chem. Int. Ed.* **2002**, *41*, 2171-2174.
- (33) Dawson, P. E.; Churchill, M.; Ghadiri, M. R.; Kent, S. B. H. *J. Am. Chem. Soc.* **1997**, *119*, 4325-4329.
- (34) Dirksen, A.; Langereis, S.; de Waal, B. F. M.; van Genderen, M. H. P.; Meijer, E. W.; de Lussanet, Q. G.; Hackeng, T. M. *Org. Lett.* **2004**, *6*, 4857-4860.
- (35) Canne, L. E.; Walker, S. M.; Kent, S. B. H. *Tetrahedron Letters* **1995**, *36*, 1217-1220.
- (36) Hackeng, T. M.; Griffin, J. H.; Dawson, P. E. *Proc. Natl. Acad. Sci.* **1999**, *96*, 10068-10073.
- (37) Pierschbacher, M. D.; Ruoslahti, E. *Nature* **1984**, *309*, 30-33.
- (38) Ruoslahti, E.; Pierschbacher, M. D. *Science* **1987**, *238*, 491-497.
- (39) Ruoslahti, E. *Nature reviews* **2002**, *2*, 83-90.
- (40) Brooks, P. C.; Montgomery, A. M. P.; Rosenfeld, M.; Reisfeld, R. A.; Hu, T.; Klier, G.; Cheresch, D. A. *Cell* **1994**, *79*, 1157-1164.
- (41) Hersel, U.; Dahmen, C.; Kessler, H. *Biomaterials* **2003**, *24*, 4385-4415.
- (42) Lutgens, E.; Daemen, M. J.; de Muinck, E. D.; Debets, J.; Leenders, P.; Smits, J. F. *Cardiovasc. Res.* **1999**, *41*, 586-593.
- (43) Lussanet, Q. G.; Backes, W. H.; Griffioen, A. W.; van Engelshoven, J. M. A.; Beets-Tan, R. G. H. *Radiology* **2003**, *229*, 429-438.
- (44) Sarin, V. K.; Kent, S. B. H.; Tam, J. P.; Merrifield, R. B. *Anal. Biochem.* **1981**, *117*, 147-157.

---

## Chapter 7

### Design and synthesis of multivalent target-specific MRI contrast agents\*

---

**ABSTRACT:** *In this Chapter, two different approaches for the synthesis of multivalent target-specific MRI contrast agents are described. In the supramolecular approach, the self-assembly of monovalent biotinylated cNGR-functionalized Gd(III)DTPA complexes (**1**) to avidin yielded a well-defined multivalent MRI contrast agent. MR titration experiments showed that the ionic  $r_1$  of **1** increases with a factor of 1.7 upon binding to avidin. From MR titrations and the HABA assay a binding stoichiometry between **1** and avidin was determined to be 4:1 in PBS buffer at pH 7.4. In the covalent approach, poly(propylene imine) dendrimers were used as a multivalent scaffold for the construction of multivalent target-specific MRI contrast agents. Multiple GRGDS-based oligopeptides were introduced at the periphery of cysteine-functionalized poly(propylene imine) dendrimers using native chemical ligation. Subsequently, the sulfhydryl (-SH) group of the cysteine residues involved in ligation reaction was utilized to introduce the DTPA moiety through the reaction with maleimide-functionalized DTPA. The corresponding Gd(III)DTPA-functionalized dendrimer composed of four GRGDS moieties was prepared from GdCl<sub>3</sub> in PBS buffer and characterized with ESI-MS.*

---

\* Part of this work has been accepted for publication: Dirksen, A.; Langereis, S.; de Waal, B.F.M.; van Genderen, M.H.P.; Hackeng, T.M.; Meijer E.W. *Chem. Commun.*

## 7.1 Introduction

Magnetic Resonance Imaging (MRI) is a powerful, non-invasive technique, which plays an important role in clinical diagnosis. To enhance the contrast in  $T_1$ -weighted MR images, gadolinium(III) chelates are commonly used as MRI contrast agents.<sup>1-3</sup> Despite the efforts to improve contrast in MR images, some processes of interest, such as angiogenesis (the formation of new blood vessels),<sup>4-6</sup> are difficult to visualize with MRI. Target-specific MRI contrast agents designed to bind to proteins expressed by the cells involved in angiogenesis could improve the imaging of this process drastically due to the *in situ* accumulation of MRI contrast agent.<sup>7-9</sup> Recently, a cyclic oligopeptide containing the asparagine-glycine-arginine (NGR) sequence (cNGR)<sup>10-13</sup> and a linear oligopeptide containing the glycine-arginine-glycine-aspartic acid-serine sequence (GRGDS)<sup>14-18</sup> were identified as target-specific peptides for angiogenesis. By immobilizing multiple target-specific oligopeptides and MRI labels on one single scaffold, the binding of the oligopeptide to its receptor may be improved through cooperative binding (multivalency),<sup>19-22</sup> resulting in a stronger accumulation of MRI contrast agent around regions of angiogenesis. Next to targeting, sensitivity is the other major challenge for molecular MR imaging.<sup>23,24</sup> One way to increase the contrast is the connection of multiple Gd(III) chelates to a well-defined macromolecular scaffold. High local concentrations of Gd(III) can be reached, while due to a higher molecular weight the  $T_1$  of water molecules is more effectively reduced as compared to their monovalent low molecular weight analogues.

In this Chapter, two synthetic strategies to multivalent target-specific MRI contrast agents are presented. The first approach comprises the self-assembly of monovalent target-specific MRI contrast agent based on the biotin–avidin system (Figure 7.1).

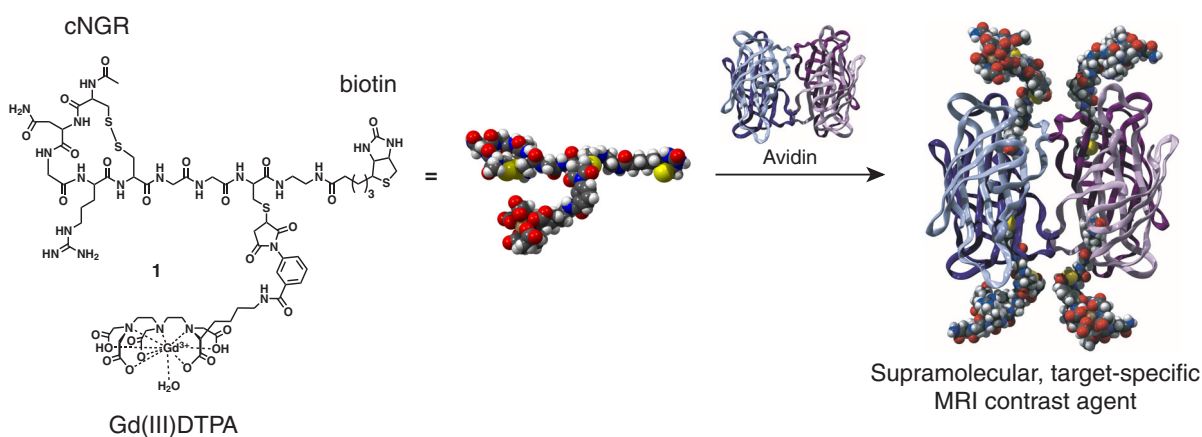


**Figure 7.1** Supramolecular approach to multivalent target-specific MRI contrast agents based on biotinylated cNGR equipped with Gd(III)DTPA (**1**) and avidin.

Avidin, a tetrameric protein, is capable of binding four equivalents of biotin in a strong, non-cooperative fashion and has been successfully employed as a versatile supramolecular scaffold for the synthesis of large well-defined structures.<sup>25-29</sup> For multivalent target-specific MRI contrast agent based on the biotin–avidin system, cNGR was functionalized with both Gd(III)DTPA and biotin (**1**).

The second approach comprises the synthesis of target-specific MRI contrast agents based on dendrimers. Recently, it was demonstrated that multiple oligopeptides could be introduced at the periphery of cysteine-functionalized poly(propylene imine) dendrimers using native chemical ligation.<sup>30</sup> Moreover, a general strategy for the double labeling of oligopeptides using a sequence of highly efficient, chemoselective reactions was described in Chapter 6.<sup>24,31</sup> Here, we demonstrate how these strategies can be combined for the synthesis of target-specific dendritic MRI contrast agents (Figure 7.2). The target-specific GRGDS sequence, which binds to  $\alpha_v\beta_3$  integrins expressed at the surface of cells involved in angiogenesis, was utilized as a model peptide.<sup>14-18</sup>

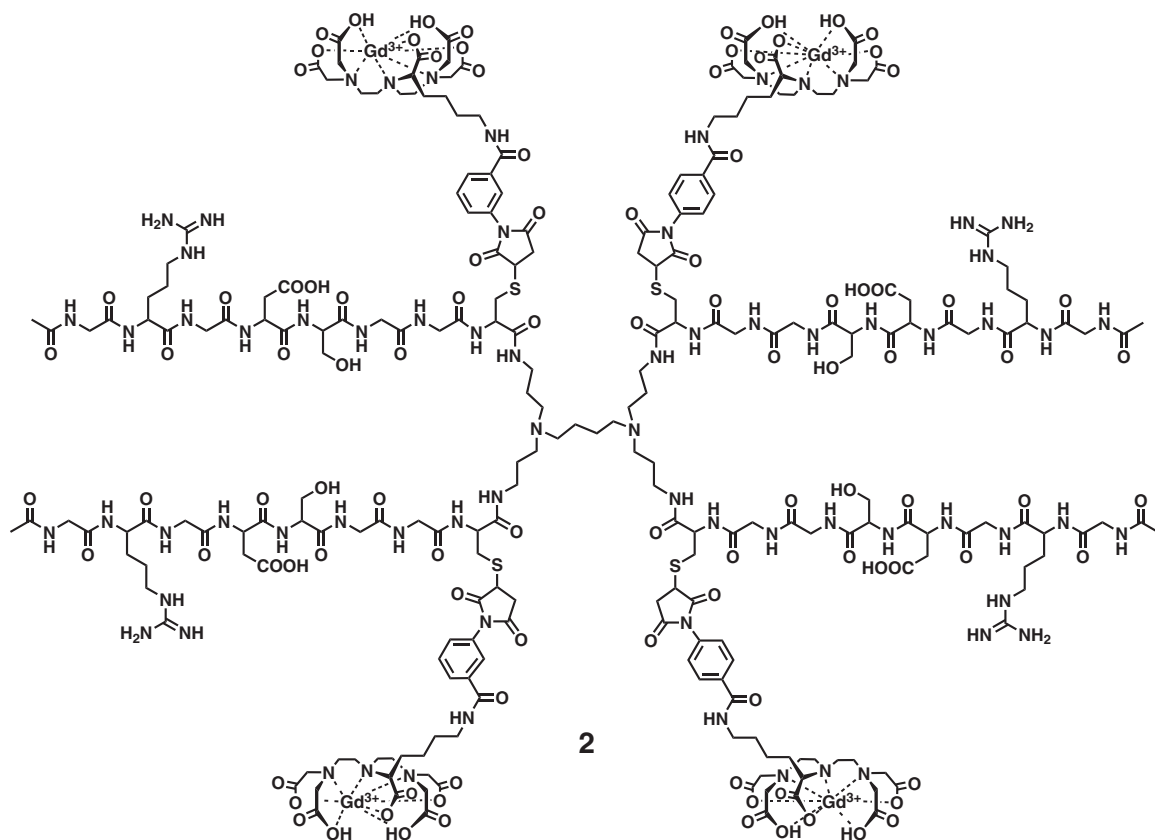


**Figure 7.2** Multivalent target-specific dendritic MRI contrast agent **2** composed of Gd(III)DTPA and GRGDS.

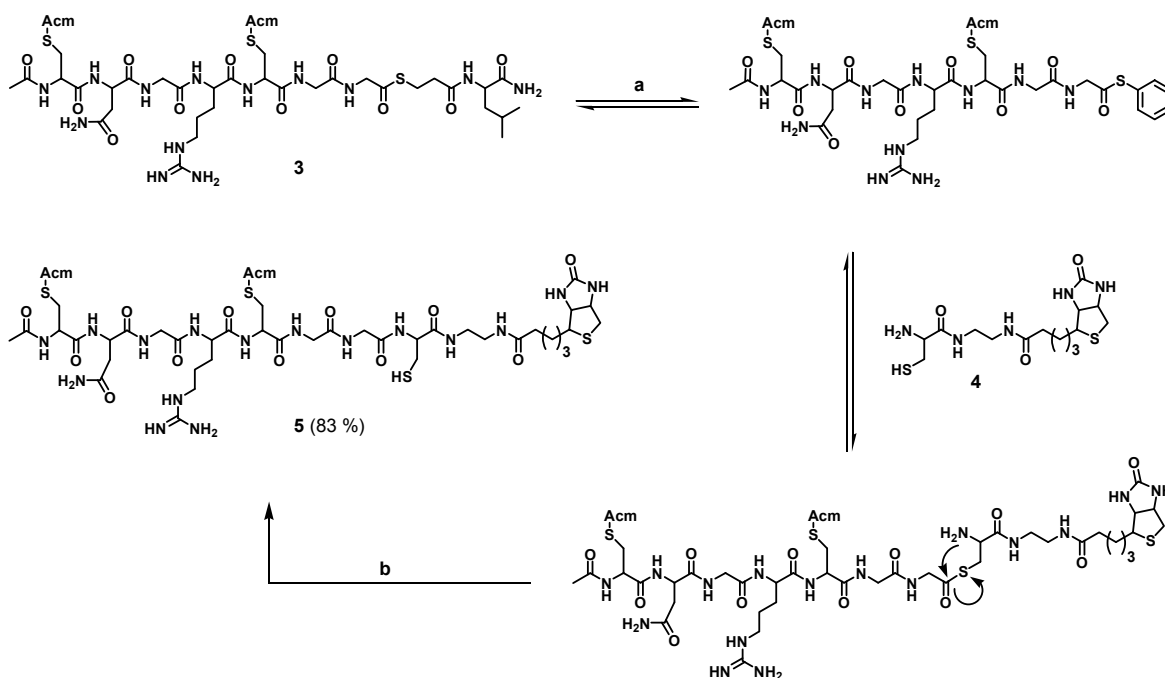


## 7.2 A SUPRAMOLECULAR APPROACH TO MULTIVALENT TARGET-SPECIFIC MRI CONTRAST AGENTS

In collaboration with dr. A. Dirksen of our laboratories and dr. T.M. Hackeng (University of Maastricht), a synthetic strategy for the functionalization of cNGR with Gd(III)DTPA and biotin (**1**) was developed. The synthesis of **1** comprises a sequence of highly efficient and chemoselective reactions, which was recently introduced as a general strategy for the double labeling of peptides (See Chapter 6).<sup>8</sup>

### 7.2.1 Synthesis

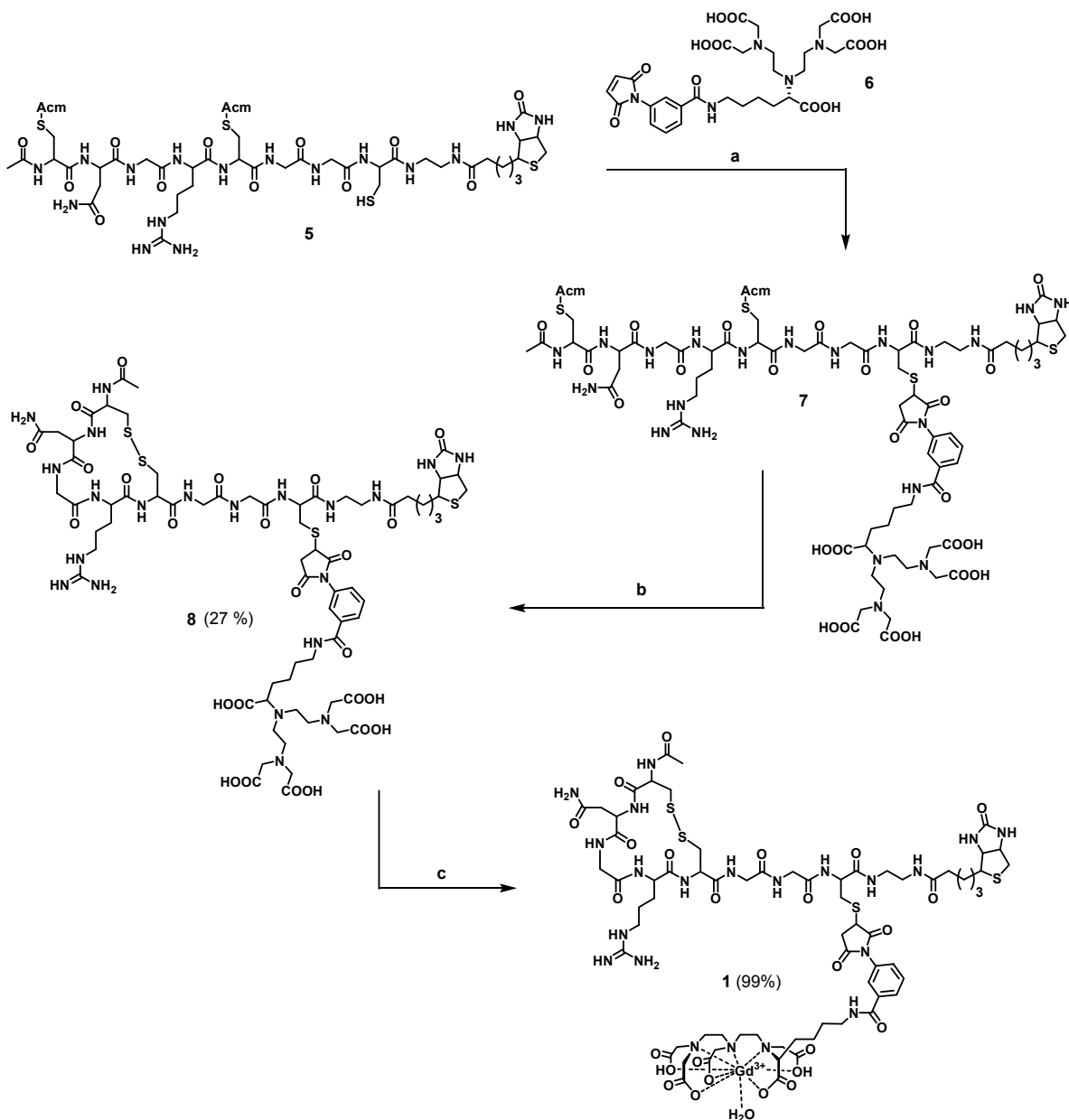
The C-terminal thioester of peptide **3** containing the target-specific NGR sequence was reacted with biotinylated cysteine (**4**) under native chemical ligation conditions (Scheme 7.1).<sup>32-34</sup>



**Scheme 7.1** Strategy for site-specific labeling of C-terminal thioester **3**—containing the target specific CNGRC sequence— with biotinylated cysteine (**4**) using native chemical ligation. The sulfhydryl moieties of the two cysteine residues are protected with acetoamidomethyl (Acm) groups. (a) 2 v-% thiophenol, 2 v-% benzylmercaptan, 6 M guanidine in 0.1 M Tris, 1 h, pH = 7.0–7.5, 37 °C; (b) spontaneous rearrangement.

At this point both the cysteine residues of peptide **3** are protected with acetamidomethyl (Acm) groups to ensure a correct “folding” of the peptide later on. The ligation reaction between **3** and **4** was monitored employing analytical reversed-phase HPLC (RP HPLC) using a C18 column for separation coupled to UV/vis ( $\lambda_{\text{probe}} = 214 \text{ nm}$ ). Within 2 hours the thioester-functionalized peptide **3** reacted quantitatively with **4**. The crude ligation product was purified using semi-preparative RP

HPLC on a C18 column and lyophilization to afford **5** in 83% isolated yield. Subsequently, the sulfhydryl group of the cysteine residue that was involved in the ligation reaction was utilized to introduce the DTPA moiety through the reaction of **5** with maleimide-functionalized DTPA (**6**) (Scheme 7.2).



**Scheme 7.2** The synthesis of biotinylated target-specific MRI contrast agent **1**. (a) 0.1 M Tris, 1 h, pH 6.5, 20 °C; (b) 1.75 eq  $I_2$ , 10 v-% acetic acid, 1 h, 20 °C; (c) 1 eq  $GdCl_3$ , pH 6.5–7 (Acm =  $-CH_2CONHCH_3$ ).

Again the reaction was monitored employing analytical RP HPLC coupled to UV/vis ( $\lambda_{probe} = 214$  nm). Once the reaction went to completion the reaction mixture was diluted ca. 30 times with 0.1 M Tris at pH 6.5 after which 10 v-% of acetic acid was added. Then 1.75 equivalents of  $I_2$  were added to remove the Acm protecting groups of **7**. The removal of the Acm groups resulted

instantaneously in the correct “folding” of the peptide unit into its cyclic conformation (Scheme 7.2). Purification using semi-preparative RP HPLC and subsequent lyophilization gave **8** in 27% isolated yield. The corresponding Gd(III) complex **1** was obtained in quantitative yield through the addition of 1 equivalent of GdCl<sub>3</sub> to **8** under neutral conditions. The formation of Gd(III) complex **1** was confirmed with electrospray ionization mass spectrometry (ESI-MS).

### 7.2.2 Binding studies

To verify the binding stoichiometry between **1** and avidin, the HABA (4'-hydroxyazobenzene-2-carboxylic acid) assay was performed probing the UV/vis absorption at 500 nm (See Chapter 5, Section 5.2.2).<sup>11</sup> Upon addition of **1** to a solution of avidin in PBS buffer containing 5 equivalents of HABA per biotin binding site, HABA was expelled from the biotin binding pocket of avidin. This resulted in a decrease in the absorption at 500 nm of HABA bound to avidin (Figure 7.3). After the addition of 3.8 equivalents of **1** the absorption spectrum at 500 nm did not change any further, which indicated that all binding sites of avidin were occupied with **1**.

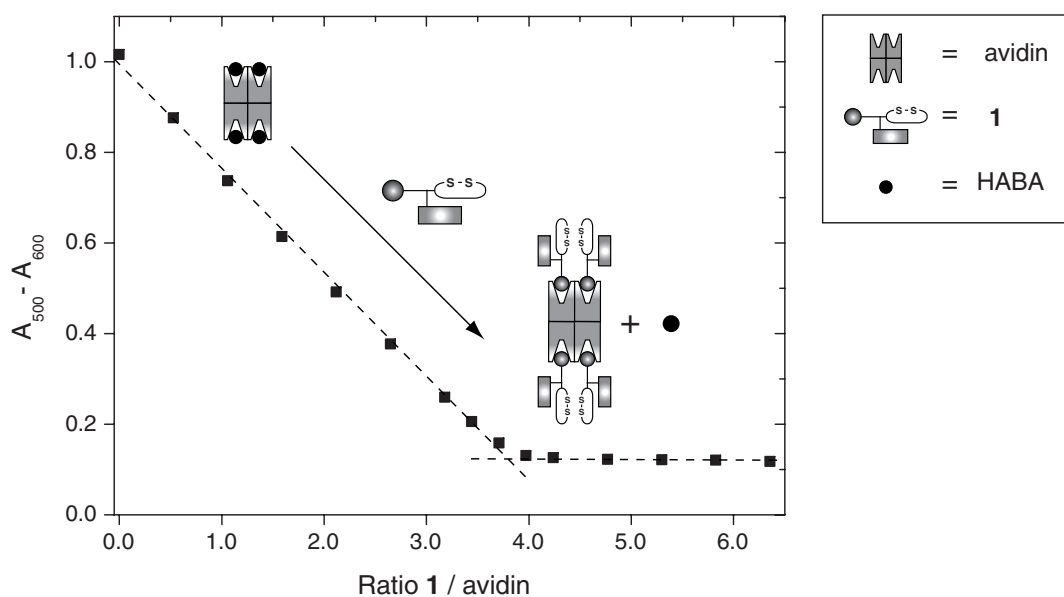


**Figure 7.3** HABA assay showing the decrease in UV/vis absorption at 500 nm upon the addition of **1** (0.26 mM in PBS buffer, pH 7.4) to a solution of avidin (10  $\mu$ M in PBS buffer, pH 7.4) containing 5 eq of HABA per binding site.

The longitudinal ionic relaxivity (ionic  $r_1$ , defined as the longitudinal relaxivity per Gd(III)), which is an intrinsic property of the MRI contrast agent, was determined from concentration dependent measurements of the longitudinal relaxation time ( $T_1$ ) of **1** at 1.5 T at 20 °C. The data gave a good linear fit to the equation  $(1/T_1)_{\text{observed}} = (1/T_1)_{\text{diamagnetic}} + r_1[\text{Gd(III)}]$  ( $R^2 > 0.999$ ) and an ionic  $r_1$  of

$8.1 \text{ mM}^{-1}\text{s}^{-1}$  was calculated. This value is comparable to the  $r_1$  of the Gd(III)DTPA complex composed of both the cNGR sequence and Oregon Green 488 (See Chapter 6,  $r_1 = 7.5 \text{ mM}^{-1}\text{s}^{-1}$ ), which has a similar molecular weight and molecular structure. To gain insight into the effect of binding of **1** to avidin on the ionic  $r_1$  of **1** an E-titration<sup>12</sup> was performed, adding a 0.12 mM solution of avidin in PBS buffer to a 0.08 mM solution of **1** in PBS buffer. This resulted in a linear increase in the ionic  $r_1$  of **1** (Figure 7.4). The addition of more than 0.24 equivalents of avidin did not result in any further changes in the ionic  $r_1$  of **1** (Figure 7.4). This behavior rules out non-specific binding between **1** and avidin and demonstrates that all the biotin-binding pockets of avidin were occupied with **1**.

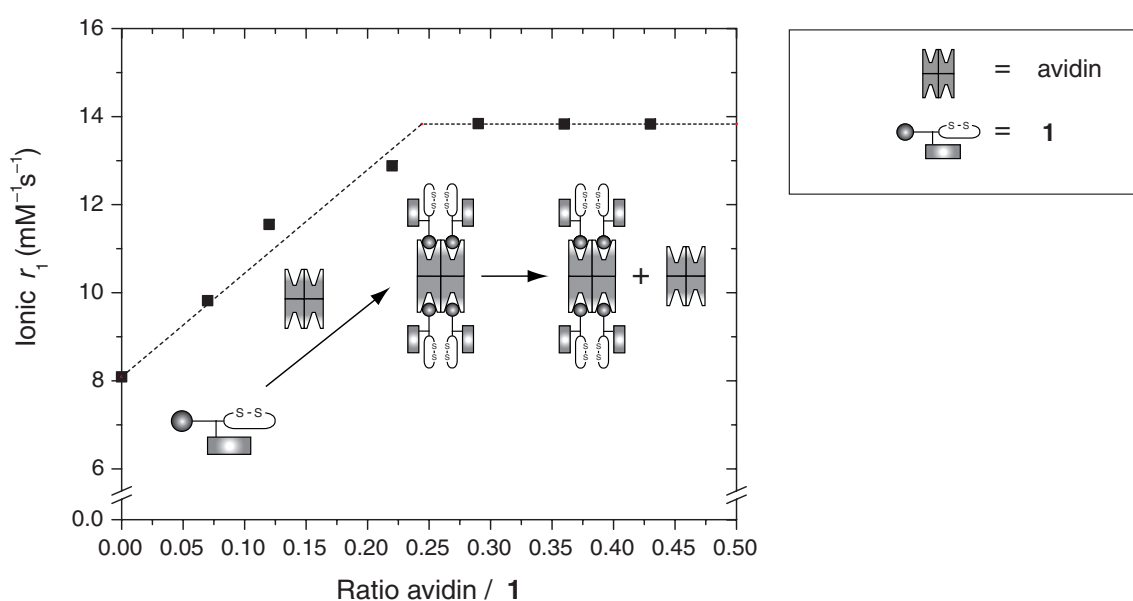


**Figure 7.4** E-titration<sup>35</sup> showing the ionic  $r_1$  of **1** (0.08 mM in PBS buffer, pH 7.4) in the presence of increasing amounts of avidin at 1.5 T and 20 °C (dotted line: fitted data with  $K_a = 1.7 \times 10^{15} \text{ M}^{-1}$  and ionic  $r_{1,free} = 8.1 \text{ mM}^{-1}\text{s}^{-1}$ , yielding ionic  $r_{1,bound} = 13.8 \pm 0.5 \text{ mM}^{-1}\text{s}^{-1}$  and  $N = 4.1 \pm 0.3$ ).

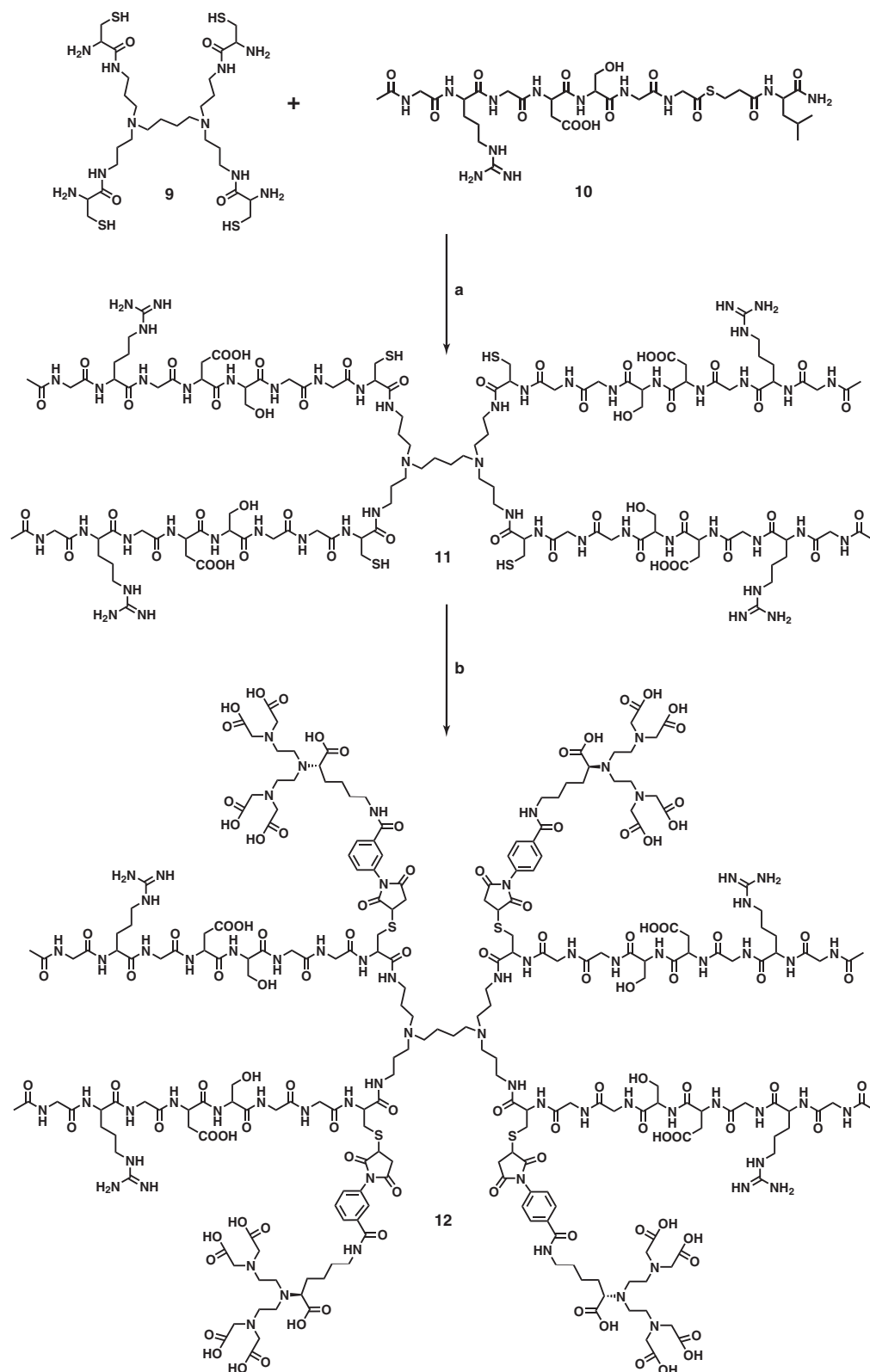
Previously, we described that the ionic  $r_1$  of biotinylated Gd(III)DTPA increases by a factor 2.7 from ionic  $r_{1,free} = 6.1 \text{ mM}^{-1}\text{s}^{-1}$  to ionic  $r_{1,bound} = 17.5 \text{ mM}^{-1}\text{s}^{-1}$  upon binding to avidin (See Chapter 5).<sup>36</sup> This result was assigned to a strong reduction in the molecular tumbling rate of the Gd(III)DTPA moiety once the contrast agent was bound to avidin (molecular weight of 64 kDa). By fitting the data of the E-titration to a mathematical model describing the binding of multiple substrates to a multivalent protein with  $N$  identical, independent binding sites (See Chapter 6, Appendix),<sup>36</sup> and by taking into account that  $K_a = 1.7 \times 10^{15} \text{ M}^{-1}$  and ionic  $r_{1,free} = 8.1 \text{ mM}^{-1}\text{s}^{-1}$ , an ionic  $r_{1,bound}$  of  $13.8 \pm 0.5 \text{ mM}^{-1}\text{s}^{-1}$  and an  $N$  of  $4.1 \pm 0.3$  ( $R^2 > 0.98$ ) were calculated. Interestingly, the increase in  $r_1$  of **1** by a factor of 1.7 is not as pronounced as in the case of biotinylated Gd(III)DTPA, where a 2.7-fold increase was observed. This may be attributed to the longer spacer between the Gd(III)DTPA moiety

and the biotin unit in the case of **1**, which leads to a higher degree of flexibility for the Gd(III)DTPA moiety.

In conclusion, by exploiting the strong and specific binding of biotin to avidin, a multivalent target-specific MRI contrast agent based on avidin and **1** was synthesized. The advantages of multiple of Gd(III)DTPA moieties on one single scaffold as well as the presence of target-specific peptides on this scaffold will be investigated *in vitro* and *in vivo* to assess its efficacy as a multivalent target-specific MRI contrast agent for imaging of angiogenesis.

### 7.3 MULTIVALENT TARGET-SPECIFIC DENDRITIC MRI CONTRAST AGENTS

In collaboration with dr. A. Dirksen, drs. H. Malda, and dr. T.M. Hackeng (University of Maastricht), a convenient methodology for the synthesis of a target-specific MRI contrast agent based on poly(propylene imine) dendrimers was developed.<sup>37</sup> The synthesis started with the reaction of cysteine-functionalized poly(propylene imine) dendrimer **9** with 4 equivalents of the C-terminal thioester of GRGDS-based peptide (**10**) under native chemical ligation conditions. The coupling reaction was monitored employing analytical RP HPLC coupled to UV/vis ( $\lambda_{\text{probe}} = 214 \text{ nm}$ ) and showed that the ligation reaction was completed within one hour. The ESI-MS spectrum of **11** showed a repetition of different clusters of peaks, corresponding to dendrimers with 2–6 positive charges ( $m/z$  with  $z = 2\text{--}6$ ) (Figure 7.5a). Deconvolution by standard methods yielded a spectrum with a single peak at 3243 amu, which is in excellent agreement with the theoretical molecular weight of **11**. Purification using semi-preparative RP HPLC on a C18 column followed by lyophilization provided dendrimer **11** in 51% isolated yield. In the next step, the sulfhydryl groups of the cysteine residues—involved in the ligation reaction—were utilized to introduce the DTPA moiety through the reaction of **11** with 4 equivalents of maleimide-functionalized DTPA (Scheme 7.3). The reaction between dendrimer **11** and maleimide-functionalized DTPA proceeded within 1 hour as evidenced from analytical RP HPLC and ESI-MS.



**Scheme 7.3.** Synthesis of multivalent GRGDS-DTPA-functionalized dendrimer **12** using native chemical ligation and the sulfhydryl-maleimide coupling. (a) 2 v-% thiophenol, 2 v-% benzylmercaptan, 6 M guanidine in 0.1 M Tris, 1 h, pH = 7.0–7.5, 37 °C; (b) **6**, 0.1 M Tris, 1 h, pH 6.5, 20 °C.

Purification by semi-preparative RP HPLC and subsequent lyophilization provided dendrimer **12** in 31% isolated yield. The ESI-MS spectrum of **12** shows a repetition of different clusters of peaks, corresponding to dendrimers with 4–7 positive charges per dendrimer ( $m/z$  with  $z = 4-7$ ). After deconvolution of the ESI-MS spectrum a molecular weight of 5897.9 amu for **12** was calculated, which proved the addition of four DTPA units ( $4 \times 663.63$  amu) to **11** (MW = 3243.2 amu).

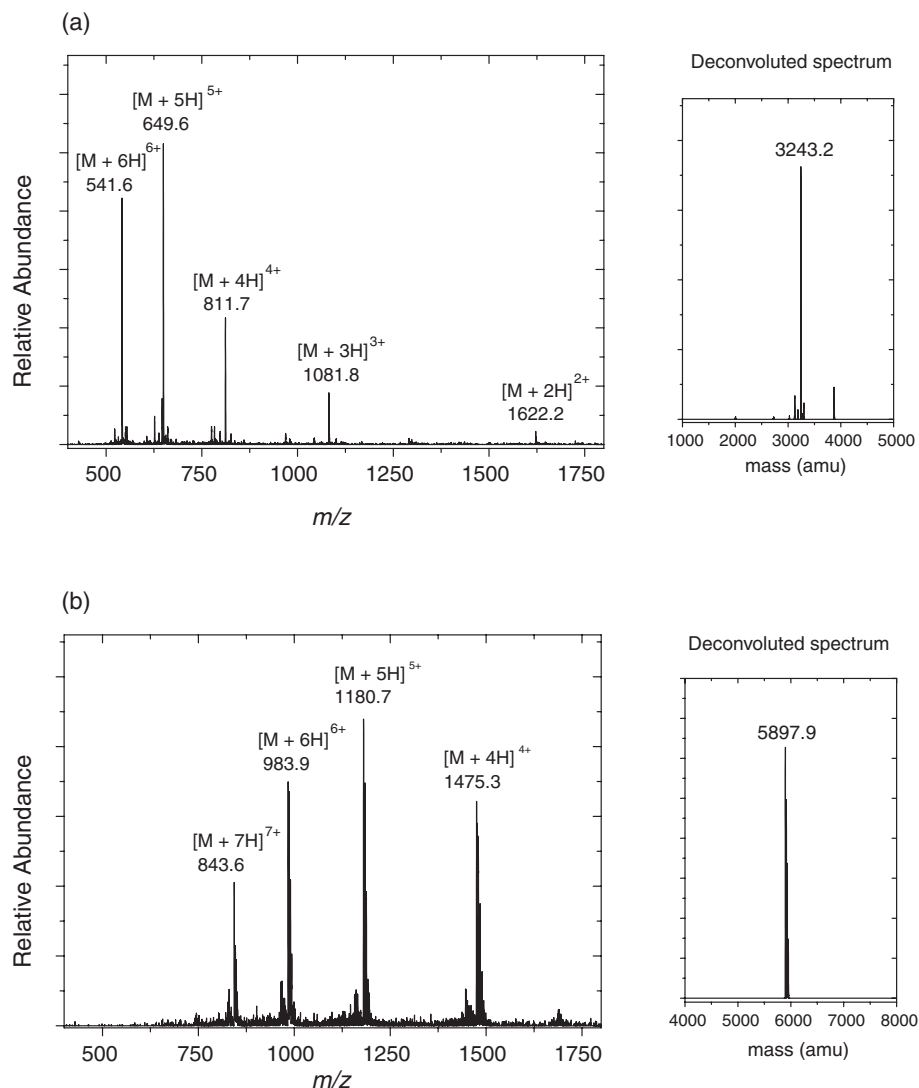


**Figure 7.5** LC-ESI-MS and deconvoluted spectra of (a) RGDSGGC-terminated dendrimer **11** and (b) RGDSGGC(DTPA)-terminated dendrimer **12**.

In the final step Gd(III) complex **2** was prepared through the addition of 4 equivalents of  $GdCl_3$  to an aqueous solution of **12**. The desired Gd(III) complex was formed instantaneously in quantitative yield. As shown in Figure 7.6b, the largest peak in the spectrum was assigned to the  $[M + 5H]^{5+}$  molecular ion of **2**, whereas the signals at 1086.7 and 1629.9, respectively, corresponds to  $[M + 6H]^{6+}$  and  $[M + 4H]^{4+}$ . From the ESI-MS spectrum a molecular weight of 6514.7 amu was calculated. This value is good agreement with the calculated mass of **2** (6514.9 amu).

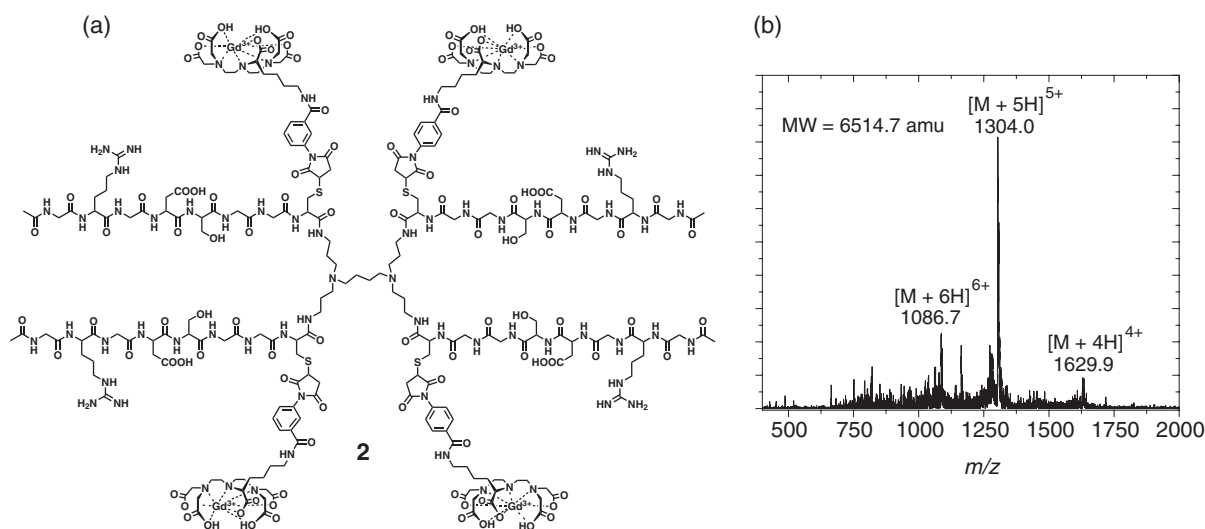


**Figure 7.6** (a) Multivalent target-specific dendritic MRI contrast agent **2**; (b) LC-ESI-MS spectrum of **2**.

In conclusion, a multivalent target-specific dendritic MRI contrast agent **2** was synthesized using the combination of native chemical ligation and the maleimide–thiol coupling. This methodology can be considered a general approach for the construction of dendritic MRI contrast agents composed of multiple oligopeptides and maleimide-functionalized labels.

## 7.4 OVERALL CONCLUSIONS

In this Chapter two different novel approaches are presented for the synthesis of multivalent target-specific MRI contrast agents based on oligopeptides. The supramolecular approach shows how monovalent target-specific contrast agents can be assembled to form well-defined multivalent structures. In the covalent approach dendrimers have shown to be excellent scaffolds for the synthesis of multivalent MRI contrast agents. In both cases the strategy for the double labeling of peptides (Chapter 6) demonstrates its versatility as a synthetic tool for the multifunctionalization of oligopeptides. All contrast agents presented in this Chapter contain oligopeptides and MRI labels in a 1:1 ratio. Future studies will focus on the synthesis of multivalent contrast agents in which the ratio between targeting units and labels can be tuned.



## 7.5 EXPERIMENTAL

### General

Unless stated otherwise, all reagents and chemicals were obtained from commercial sources and used without further purification. Trifluoroacetic acid (TFA) was obtained from Halocarbon (USA). *N,N*-diisopropylethylamine (DiPEA) was obtained from Applied Biosystems (USA). Peptide synthesis grade *N,N*-dimethylformamide (DMF) and HPLC grade acetonitrile (CH<sub>3</sub>CN) were purchased from Biosolve. Analytical RP HPLC was performed on a Varian Prostar HPLC system with a Vydac<sup>TM</sup> protein peptide C18 column (0.5 × 15 cm, flow 1 mL/min), eluted with a linear gradient of 0–60% CH<sub>3</sub>CN in 0.1% TFA in H<sub>2</sub>O in 30 minutes. Semi-preparative HPLC was performed using a Vydac C18 column (2.5 × 20 cm, 10 mL/min), eluted with a linear gradient of 0–20% CH<sub>3</sub>CN in 0.1% aqueous TFA in 90 minutes. LC-ESI-MS measurements were performed on a Finnigan LCQ Deca XP Max ion trap mass spectrometer (Thermo Electron Corporation, San Jose, USA). Deconvolution of the mass-to-charge ESI-MS spectra was performed with MagTran 1.02 software.<sup>38</sup>

### HABA assay

166 μL of a 30 μM solution of avidin in PBS buffer (pH 7.4), 20 μL of a 5 mM solution of 4'-hydroxy-azobenzene-2-carboxylic acid (HABA), and 314 μL of PBS buffer (pH 7.4) were mixed in a quartz cuvette (*l* = 1 cm). To this solution was added in aliquots of 10 μL a 0.26 mM solution of **1** at a 1 min interval. The UV/vis absorption was probed at 500 nm, which is in the absorption maximum of HABA bound to avidin. The binding of **1** to avidin was indicated by the decrease of the absorption at 500 nm as a result of the displacement of HABA from the biotin binding pockets of avidin.

### MR titration experiment

To 0.5 mL of a 0.08 mM solution of **1** in PBS buffer (pH 7.4) was added stepwise in aliquots of 25 μL a 0.12 mM solution of avidin in PBS buffer (pH 7.4). The *T*<sub>1</sub> was measured after each addition using an inversion recovery pulse sequence at 1.5 T and 20 °C.

### Synthesis of *cNGR-GGC(Gd(III)DTPA)-biotin (1)*

Compound **1** was synthesized by dr. A. Dirksen according to reference 39.

### *NAcGRGDSGGC(Gd(III)DTPA)-terminated poly(propylene imine) dendrimer (2)*

Dendrimer **12** (1 mg, 0.17 μmol) was dissolved in demineralized water (0.1 mL). The pH of the aqueous solution was adjusted to 6.5–7.0 by adding small aliquots of 0.25% NH<sub>4</sub>OH (aq). Subsequently, a solution of GdCl<sub>3</sub>·6 H<sub>2</sub>O (0.25 mg, 0.68 μmol) in water (0.1 mL) was added while maintaining the pH at 7 with a 0.25% NH<sub>4</sub>OH (aq) solution. The solution was vigorously stirred for 2 h at room temperature. The formation of the complex was confirmed with LC-ESI-MS (ProSphere column). After freeze drying the Gd(III) complex **2** was obtained as a white powder in quantitative yield. LC-ESI-MS: *m/z* [C<sub>236</sub>H<sub>340</sub>N<sub>70</sub>O<sub>100</sub>S<sub>4</sub>Gd<sub>4</sub> + 6H]<sup>6+</sup> Calcd. 1086.8 Da, Obsd. 1086.7 Da; [M + 5H]<sup>5+</sup> Calcd. Da, 1304.0 Obsd. 1304.0 Da; [M + 4H]<sup>4+</sup> Calcd. 1629.7 Da, Obsd. 1629.9 Da; MW Calcd. 6514.9 Da, Obsd. 6514.7 Da.

### Synthesis of *NAc(Acm)NGRC(Acm)GGMPAL (3)*

This compound was synthesized by dr. A. Dirksen according to reference 39.

### Cysteine-functionalized biotin (4)

Compound **4** was synthesized according to a previously described literature procedure of Tolbert *et al.*<sup>34</sup>

**CNGRC-based structures 5, 7, and 8**

More details on the synthesis of these compounds can be found in reference 39.

**Cysteine-terminated poly(propylene imine) dendrimer (9)**

The first generation cysteine-terminated poly(propylene imine) dendrimer **9** was synthesized by drs. H. Malda.<sup>30</sup>

**NAcGRGDSGG-MPAL (10)**

The peptide containing the GRGDS sequence with a thioester at its C-terminal has been synthesized as described in Chapter 6.

**NAcGRGDSGGC-terminated poly(propylene imine) dendrimer (11)**

Oligopeptide **10** (22.7 mg, 27  $\mu\text{mol}$ ) and **9** (4.9 mg, 6.7  $\mu\text{mol}$ ) were dissolved in 1 mL of 6 M guanidine, 0.07 M Tris (aq) pH 8. To this solution 20  $\mu\text{L}$  (2 v-%) of thiophenol and 20  $\mu\text{L}$  (2 v-%) of benzyl mercaptan were added. The pH was adjusted to 7.5 by the addition of small aliquots of 1.0 M NaOH (aq). The reaction was continued for 1 h at 37 °C. The reaction mixture was filtered and the product was purified employing semi-preparative RP HPLC over a C18 column (gradient: 5–25% MeCN in H<sub>2</sub>O, 0.1% TFA in 90 minutes). Freeze drying yielded **11** (11 mg, 3.4  $\mu\text{mol}$ , 51%) as a fluffy white powder. ESI-MS:  $m/z$  [C<sub>120</sub>H<sub>204</sub>N<sub>50</sub>O<sub>48</sub>S<sub>4</sub> + 6H]<sup>6+</sup> Calcd. 541.6 Da, Obsd. 541.6 Da; [M + 5H]<sup>5+</sup> Calcd. 649.7 Da, Obsd. 649.6 Da; [M + 4H]<sup>4+</sup> Calcd. 811.9 Da, Obsd. 811.7 Da; [M + 3H]<sup>3+</sup> Calcd. 1082.2 Da, Obsd. 1081.8 Da; [M + 2H]<sup>2+</sup> Calcd. 1622.8 Da, Obsd. 1622.2 Da; MW Calcd. 3243.5 Da, Obsd. 3243.2 Da.

**NAcGRGDSGGC(DTPA)-terminated poly(propylene imine) dendrimer (12)**

Dendrimer **11** (11 mg, 3.4  $\mu\text{mol}$ ) was dissolved in 500  $\mu\text{L}$  0.1 M Tris (aq, pH 6.9). The pH of the solution was adjusted to 6.5 by the addition of small aliquots of 1.0 M NaOH (aq). Subsequently, the solution was added to maleimide-functionalized DTPA (9 mg, 13  $\mu\text{mol}$ ). The reaction was monitored employing analytical RP HPLC over a C18 column (gradient: 0–60% MeCN in H<sub>2</sub>O, 0.1% TFA in 30 minutes). The reaction was completed within 1 h at room temperature at pH 6.5. Analytical RP HPLC: **12** eluting at 11.2 min. The reaction mixture was filtered and the crude product was purified employing semi-preparative RP HPLC over a C18 column (gradient: 9–27% MeCN in H<sub>2</sub>O, 0.1% TFA in 90 minutes). Freeze drying yielded **12** (6.3 mg, 1.1  $\mu\text{mol}$ , 31%) as a fluffy white powder. ESI-MS:  $m/z$  [C<sub>236</sub>H<sub>352</sub>N<sub>70</sub>O<sub>100</sub>S<sub>4</sub> + 7H]<sup>7+</sup> Calcd. 843.5 Da, Obsd. 843.6 Da; [M + 6H]<sup>6+</sup> Calcd. 983.9 Da, Obsd. 983.9 Da; [M + 5H]<sup>5+</sup> Calcd. 1180.5 Da, Obsd. 1180.7 Da; [M + 4H]<sup>4+</sup> Calcd. 1475.4 Da, Obsd. 1475.3 Da; MW Calcd. 5897.8 Da, Obsd. 5897.9 Da.

**7.6 REFERENCES**

- (1) Lauffer, R. B. *Chem. Rev.* **1987**, *87*, 901-927.
- (2) Caravan, P.; Ellison, J. J.; McMurry, T. J.; Lauffer, R. B. *Chem. Rev.* **1999**, *99*, 2293-2352.
- (3) Merbach, A. E.; Tóth, E. *The Chemistry of Contrast Agents in Medical Magnetic Resonance Imaging*; John Wiley & Sons: New York, 2001.
- (4) Griffioen, A. W.; Molema, G. *Pharmacological Reviews* **2000**, *52*, 237-268.
- (5) Cristofanilli, M.; Charnsangavej, C.; Hortobagyi, G. N. *Nat. Rev. Drug Discovery* **2002**, *1*, 415-426.
- (6) Carmeliet, P.; Jain, R. K. *Nature* **2000**, *407*, 249-257.
- (7) McDonald, D. M.; Choyke, P. L. *Nature Med.* **2003**, *9*, 713-725.
- (8) Jacques, V.; Desreux, J. F. *Top. Curr. Chem.* **2002**, *221*, 123-164.

- (9) Artemov, D. *Journal of Cellular Biochemistry* **2003**, *90*, 518-524.
- (10) Arap, W.; Pasqualini, R.; Ruoslahti, E. *Science* **1998**, *279*, 377-380.
- (11) Pasqualini, R.; Koivunen, E.; Kain, R.; Lahdenranta, J.; Sakamoto, M.; Stryhn, A.; Ashmun, R. A.; Shapiro, L. H.; Arap, W.; Ruoslahti, E. *Cancer Res.* **2000**, *60*, 722-727.
- (12) Riemann, D.; Kehlen, A.; Langner, J. *Immunology Today* **1999**, *20*, 83-88.
- (13) Bhagwat, S. V.; Lahdenranta, J.; Giordano, R.; Arap, W.; Pasqualini, R.; Shapiro, L. H. *Blood* **2001**, *97*, 652-659.
- (14) Pierschbacher, M. D.; Ruoslahti, E. *Nature* **1984**, *309*, 30-33.
- (15) Ruoslahti, E.; Pierschbacher, M. D. *Science* **1987**, *238*, 491-497.
- (16) Ruoslahti, E. *Nature reviews* **2002**, *2*, 83-90.
- (17) Brooks, P. C.; Montgomery, A. M. P.; Rosenfeld, M.; Reisfeld, R. A.; Hu, T.; Klier, G.; Cheresch, D. A. *Cell* **1994**, *79*, 1157-1164.
- (18) Hersel, U.; Dahmen, C.; Kessler, H. *Biomaterials* **2003**, *24*, 4385-4415.
- (19) Mammen, M.; Chio, S.-K.; Whitesides, G. M. *Angew. Chem. Int. Ed.* **1998**, *37*, 2755-2794.
- (20) Gestwicki, J. E.; Cairo, C. W.; Strong, L. E.; Oetjen, K. A.; Kiessling, L. L. *J. Am. Chem. Soc.* **2002**, *124*, 14922-14933.
- (21) Cairo, C. W.; Gestwicki, J. E.; Kanai, M.; Kiessling, L. L. *J. Am. Chem. Soc.* **2002**, *124*, 1615-1619.
- (22) Huskens, J.; Mulder, A.; Auletta, T.; Nijhuis, C. A.; Ludden, M. J. W.; Reinhoudt, D. N. *J. Am. Chem. Soc.* **2004**, *126*, 6784-6797.
- (23) Weissleder, R.; Mahmood, U. *Radiology* **2001**, *219*, 316-333.
- (24) Weissleder, R. *Nat. Rev. Cancer* **2002**, *2*, 11-19.
- (25) Green, N. M. *Methods Enzymol.* **1990**, *184*, 51-67.
- (26) Muller, W.; Ringsdorf, H.; Rump, E.; Wildburg, G.; Zhang, X.; Angermaier, L.; Knoll, W.; Liley, M.; Spinke, J. *Science* **1993**, *262*, 1706-1708.
- (27) Ringsdorf, H.; Simon, J. *Nature* **1994**, *371*, 284.
- (28) Niemeyer, C. M.; Adler, M.; Pignataro, B.; Lenhert, S.; Gao, S.; Chi, L.; Fuchs, H.; Blohm, D. *Nucleic Acids Res.* **1999**, *27*, 4553-4561.
- (29) Niemeyer, C. M.; Burger, W.; Peplies, J. *Angew. Chem. Int. Ed.* **1998**, *37*, 2265-2268.
- (30) van Baal, I.; Malda, H.; Synowsky, S. A.; Van Dongen, J. L. J.; Hackeng, T. M.; Merkx, M.; Meijer, E. W. *Angew. Chem.*, submitted for publication.
- (31) Dirksen, A.; Langereis, S.; de Waal, B. F. M.; van Genderen, M. H. P.; Meijer, E. W.; de Lussanet, Q. G.; Hackeng, T. M. *Org. Lett.* **2004**, *6*, 4857-4860.
- (32) Dawson, P. E.; Muir, T. W.; Clark-Lewis, I.; Kent, S. B. H. *Science* **1994**, *266*, 776-779.
- (33) Hackeng, T. M.; Griffin, J. H.; Dawson, P. E. *Proc. Natl. Acad. Sci.* **1999**, *96*, 10068-10073.
- (34) Tolbert, T. J.; Wong, C.-H. *J. Am. Chem. Soc.* **2000**, *122*, 5421-5428.
- (35) Dwek, R. A. *Nuclear Magnetic Resonance in Biochemistry. Applications to Enzyme Systems*; Clarendon Press: Oxford, 1973.
- (36) Langereis, S.; Kooistra, H. A. T.; van Genderen, M. H. P.; Backes, W. H.; Meijer, E. W. *Org. Biomol. Chem.* **2004**, *2*, 1271-1273.
- (37) In the thesis of drs. H. Malda more details will be presented on the synthesis of oligopeptide-functionalized poly(propylene imine) dendrimers using native chemical ligation.
- (38) Zhang, Z.; Marshall, A. G. *J. Am. Soc. Mass Spectrom.* **1998**, *9*, 225-233.
- (39) Dirksen, A.; Langereis, S.; de Waal, B. F. M.; van Genderen, M. H. P.; Hackeng, T. M.; Meijer, E. W. *Chem. Commun.* **2005**, accepted for publication.

showed that the first generation of the dendritic MRI contrast agent was rapidly cleared by the renal system, while higher generations of dendritic MRI contrast agents were cleared at significantly slower rates. Furthermore, dendritic MRI contrast agents allow for the *in vivo* characterization of tumor angiogenesis. It has been established that higher generations of the dendritic MRI contrast agent monitor tumor vessel permeability and vascular volume more accurately than lower generations of the dendrimer.

In Chapter 5, the ionic  $r_1$  of biotinylated MRI contrast agents has been used to probe the strong and specific binding of biotin to avidin. MR titration experiments with biotinylated Gd(III)-based complexes show a strong increase in the ionic  $r_1$  upon binding to avidin. The quantitative model provides an elegant tool to investigate the formation of supramolecular complexes in water.

Novel synthetic strategies for the preparation of Gd(III)DTPA complexes equipped with either a fluorescent label and/or a target-specific oligopeptide for angiogenesis (*e.g.* cNGR) are presented in Chapter 6. Unfortunately, MR imaging of angiogenesis with cNGR-functionalized Gd(III)DTPA in a myocardial model was not conclusive; only a small increase in the MR signal was observed in the infarcted region. From this result it was concluded that a higher local concentration of Gd(III) is required for sufficient contrast. The potential of bimodal imaging has been shown for Gd(III)DTPA functionalized with Oregon Green 488 (a fluorescent label) employing the chick chorioallantoic membrane (CAM). The CAM experiment illustrated the large difference in sensitivity between MRI and optical imaging. For the validation of the targeting process with cNGR, a bimodal target-specific MRI contrast agent bearing both Gd(III)DTPA and Oregon Green 488 was prepared using native chemical ligation, followed by the reaction of the sulfhydryl moiety with maleimide-functionalized DTPA. This strategy can be regarded as a general approach for the double labeling of oligopeptides.

Finally, in Chapter 7, two approaches for the synthesis of multivalent target-specific MRI contrast agents have been developed: (*i*) a supramolecular approach based on the self-assembly of biotinylated target-specific MRI contrast agents, containing the cNGR oligopeptide and Gd(III)DTPA, and avidin, (*ii*) a covalent approach, whereby multiple GRGDS-based oligopeptides are introduced at the periphery of cysteine-terminated poly(propylene imine) dendrimers. In both cases the strategy for the double labeling of oligopeptides demonstrates its versatility as a synthetic tool for the multifunctionalization of oligopeptides. The synthetic strategies for targeting and multivalency may contribute to the development of target-specific dendritic contrast agents for molecular MR imaging in the near future.

## Summary

Magnetic Resonance Imaging (MRI) is one of the most important non-invasive diagnostic techniques for the visualization of soft tissue anatomy and disease, such as tumors, which in part can be attributed to the development of MRI contrast agents. Gadolinium(III) complexes of diethylenetriaminepentaacetic acid (Gd(III)DTPA) are currently the most widely applied MRI contrast agents for general clinical MR imaging. Drawbacks of these low molecular weight MRI contrast agents are their relatively low contrast efficiency, their rapid renal excretion and extravasation, and their non-specific tissue distribution. Dendrimers, with their multivalent character and highly branched structure, are uniquely qualified to address all of these points. By modifying the periphery of dendrimers with multiple Gd(III) chelates, the contrast efficiency can be improved considerably. In addition, a prolonged vascular retention time is obtained due to their larger size. An improvement of the specificity of Gd(III)DTPA-based contrast agents can be accomplished by incorporating target-specific moieties to induce accumulation of MRI labels at regions of interest. Moreover, the combination of MRI labels and fluorescent labels on a single molecular scaffold allows for bimodality in imaging, thereby integrating the advantages of MRI (a non-invasive technique with a high spatial resolution) and optical imaging (a high sensitivity). In this thesis, new synthetic strategies for the construction of multivalent MRI contrast agents have been developed.

A general introduction into the synthesis and intriguing properties of dendritic structures is described in Chapter 1. Furthermore, the potential applications of dendrimers in biomedical imaging are emphasized in this Chapter.

In Chapter 2, a modular approach for the preparation of several functional Gd(III)DTPA complexes is introduced, which employs an amine-functionalized DTPA synthon. Through the use of orthogonal chemistries, novel methodologies have been developed in order to arrive at a series of low molecular weight Gd(III)DTPA-based complexes. The characterization and intrinsic properties of these functionalized Gd(III)DTPA-based complexes are discussed and a general introduction is given into the basic principles of MRI contrast agents.

Chapter 3 describes a convenient methodology for the synthesis of different generations of Gd(III)DTPA-terminated poly(propylene imine) dendrimers employing an isocyanate-functionalized DTPA synthon. The contrast efficiency of these MRI contrast agents, expressed in terms of longitudinal ( $r_1$ ) and transverse ( $r_2$ ) relaxivities, increases considerably as a function of dendrimer generation, such that the ionic relaxivities, *i.e.* the relaxivity per Gd(III) ion (ionic  $r_{1,2}$ ), are at least three times higher than of the parent Gd(III) complex. The effect of the Gd(III) density on the ionic  $r_1$  has been studied by varying the Gd(III) to Y(III) ratio at the periphery of the fifth generation DTPA-terminated poly(propylene imine) dendrimer. It has been shown that the ionic  $r_1$  increases for higher fractions of Gd(III). This effect is attributed to magnetic interactions between Gd(III) moieties and is a direct result of a high local concentration of Gd(III)DTPA end groups on a single dendrimer, giving rise to a *dendritic effect*.

In Chapter 4, different generations of Gd(III)DTPA-terminated poly(propylene imine) dendrimers are evaluated for MR imaging. Contrast-enhanced MR imaging (CE-MRI) in mice

# Samenvatting

Magnetic Resonance Imaging (MRI) is één van de belangrijkste niet-invasieve diagnostische technieken voor het visualiseren van zacht weefsel en tumoren. De toepasbaarheid van MRI is mede te danken aan de ontwikkeling van MRI contrastmiddelen. Momenteel worden vooral gadolinium(III) complexen van diethyleentriaminepenta-azijnzuur (Gd(III)DTPA) toegepast als contrastmiddel in ziekenhuizen. Nadelen van deze conventionele, laagmoleculaire MRI contrastmiddelen zijn hun lage gevoeligheid, een snelle uitscheiding door de nieren, een snelle extravasatie en een aspecifieke verdeling over weefsel. Dendrimeren zijn bij uitstek geschikt om MRI contrastmiddelen op deze punten te verbeteren door hun goed gedefinieerde structuur en hoge concentratie aan functionele eindgroepen. Het koppelen van meerdere Gd(III)DTPA complexen aan een dendrimeer leidt tot een verhoogd contrast. Daarnaast zullen deze macromoleculaire MRI contrastmiddelen langer in de bloedbaan blijven circuleren. Een verbetering van de specificiteit van Gd(III)DTPA-gebaseerde contrastmiddelen kan worden bereikt door receptor-specifieke eenheden in te bouwen, waardoor de accumulatie van contrastmiddel alleen op specifieke plekken zal plaatsvinden. De combinatie van MRI labels en fluorescerende groepen aan hetzelfde molecuul maakt bimodaliteit in beeldvorming mogelijk, waarbij de voordelen van MRI (een niet-invasieve techniek met een hoge ruimtelijke resolutie) en fluorescentie-microscopie (een hoge gevoeligheid) worden geïntegreerd. In dit onderzoek ligt de nadruk op het ontwikkelen van nieuwe methodes voor de synthese van multivalente MRI contrastmiddelen, zowel receptor-specifiek als aspecifiek.

Een algemene inleiding omtrent de synthese en de intrigerende eigenschappen van dendrimeren wordt beschreven in Hoofdstuk 1. Tevens worden de potentiële toepassingen van dendritische structuren voor biomedische beeldvorming besproken.

In Hoofdstuk 2 wordt een modulaire aanpak voor de synthese van verschillende gefunctionaliseerde Gd(III)DTPA complexen beschreven, waarbij gebruik gemaakt wordt van een amine-gefunctionaliseerde DTPA bouwsteen. De karakterisering, de intrinsieke eigenschappen van deze Gd(III)DTPA complexen en enkele basisprincipes met betrekking tot de werking van MRI contrastmiddelen worden in dit hoofdstuk behandeld.

Hoofdstuk 3 beschrijft een nieuwe methode om de buitenkant van poly(propyleen imine) dendrimeren te modificeren met Gd(III)DTPA. De werkzaamheid van deze MRI contrastmiddelen, uitgedrukt in longitudinale ( $r_1$ ) en transversale relaxiviteit ( $r_2$ ), neemt sterkt toe voor hogere generaties van het dendritische contrastmiddel. De ionische relaxiviteit (de relaxiviteit per Gd(III) ion (ionische  $r_{1,2}$ )) is voor de vijfde generatie van het Gd(III)DTPA-gefunctionaliseerde poly(propyleen imine) dendrimeer tenminste driemaal hoger dan voor het Gd(III)DTPA complex. Het effect van de dichtheid van Gd(III) op de ionische  $r_1$  is bestudeerd door de ratio Gd(III) over Y(III) te variëren. Hierbij is gevonden dat de ionische  $r_1$  voor een vijfde generatie dendrimeer toeneemt naarmate de fractie aan Gd(III) hoger wordt. Dit effect wordt toegeschreven aan magnetische interacties tussen Gd(III) eenheden en is direct het resultaat van een hoge lokale concentratie aan Gd(III)DTPA eindgroepen.

In Hoofdstuk 4 zijn de eigenschappen van dendritische MRI contrastmiddelen *in vivo* bestudeerd. Contrast-enhanced MR imaging (CE-MRI) toont aan dat de lagere generaties van de dendritische contrastmiddelen snel door de nieren worden uitgescheiden, terwijl de hogere generaties langer in de bloedbaan blijven circuleren. Daarnaast zijn dendritische contrastmiddelen gebruikt voor de *in vivo* karakterisering van tumor angiogenese. Hogere generaties dendritische contrastmiddelen geven een nauwkeurigere meting van de tumor permeabiliteit en het vasculair volume dan laagmoleculaire MRI contrastmiddelen.

In Hoofdstuk 5 wordt de ionische  $r_1$  van gebiotinyleerde MRI contrastmiddelen gebruikt om de sterke en specifieke interactie van biotine met avidine te onderzoeken. MR titratie-experimenten lieten een sterke toename van de ionische  $r_1$  van het gebiotinyleerde contrastmiddel zien na binding met avidine. Het ontwikkelde kwantitatieve model illustreert de kracht van deze benadering en levert een elegante methode om de vorming van supramoleculaire complexen in water te bestuderen.

Nieuwe strategieën voor de synthese van Gd(III)DTPA complexen bestaande uit een fluorescerend label en/of target-specifieke oligopeptiden voor angiogenese (zoals bijvoorbeeld cNGR), worden beschreven in Hoofdstuk 6. MRI van angiogenese met cNGR-gefunctionaliseerd Gd(III)DTPA *in vivo* was niet eenduidig; enkel een kleine toename van de MR signaalintensiteit in het geïnfarcteerd gebied werd waargenomen. Aan de hand van dit resultaat werd geconcludeerd dat een hogere concentratie aan Gd(III) nodig is voor het verkrijgen van voldoende contrast. Het potentieel van bimodaliteit in beeldvorming is aangetoond met MRI contrastmiddelen voorzien van Oregon Green 488 (een fluorescerend label) in het chorio-allantoïsch membraan van een kippenembryo (CAM model). Het CAM experiment toonde het grote verschil in gevoeligheid tussen MRI en fluorescentie microscopie. Daarnaast werd het Gd(III)DTPA complex gekoppeld aan cNGR en Oregon Green door gebruik te maken van “*native chemical ligation*”, gevolgd door de reactie van de thiol groep met maleïmide-gefunctionaliseerd DTPA. Deze synthetische strategie is algemeen toepasbaar voor het dubbel labelen van oligopeptiden.

In Hoofdstuk 7 worden twee methodes voor de synthese van multivalente receptor-specifieke MRI contrastmiddelen beschreven: (i) een supramoleculaire aanpak gebaseerd op de zelf-assemblage van biotine-gefunctionaliseerde contrastmiddelen bestaande uit cNGR oligopeptide en Gd(III)DTPA, en avidine; (ii) een covalente aanpak waarbij meerdere GRGDS-gebaseerde oligopeptiden zijn gekoppeld aan de buitenkant van cysteïne-gefunctionaliseerde poly(propyleenimine) dendrimeren, gevolgd door de reactie met maleïmide-gefunctionaliseerd DTPA. De ontwikkelde strategieën voor het inbouwen van receptor-specifieke eenheden en multivalentie kunnen een belangrijke bijdrage leveren aan de ontwikkeling van receptor-specifieke dendritische contrastmiddelen voor moleculaire MR beeldvorming.

## Curriculum Vitae



Sander Langereis werd geboren op 17 juli 1975 te Geldrop. Na het voltooien van de HAVO opleiding aan het Strabrecht College te Geldrop, werd in 1993 begonnen aan de studie Hoger Laboratorium Onderwijs aan de Hogeschool van Eindhoven. Tijdens zijn studie liep hij vier maanden stage bij ATO-DLO te Wageningen. Deze studie werd in 1997 afgerond met onderzoek naar de synthese en karakterisering van vertakte polymeren bij DSM Research te Geleen. Aansluitend trad de auteur in dienst bij DSM Research te Geleen, waarbij hij zich specialiseerde in dendrimeren, nanocomposieten en gecontroleerde radicaalpolymerisaties. In maart 2001 werd hij assistent in opleiding binnen de capaciteitsgroep ‘Macromoleculaire en Organische Chemie’ aan de faculteit Scheikundige Technologie van de Technische Universiteit Eindhoven. Onder leiding van prof.dr. E.W. Meijer en dr. M.H.P. van Genderen werkte hij tot maart 2005 aan zijn promotieonderzoek, waarvan de belangrijkste resultaten staan beschreven in dit proefschrift. Vanaf 1 april 2005 is de auteur werkzaam bij SyMo-Chem BV ([www.symo-chem.nl](http://www.symo-chem.nl)) te Eindhoven.

Sander Langereis was born in Geldrop, the Netherlands, on 17 July 1975. He completed the higher general secondary education (HAVO) in 1993 at the Strabrecht College in Geldrop. In the same year, he started studying chemistry at the Hogeschool Eindhoven. His external traineeship was performed at ATO-DLO in Wageningen. He obtained his Bachelor degree in 1997 with a graduation project at DSM Research in Geleen. From September 1997 to February 2001 he worked as a research scientist at DSM Research in Geleen. During this period he specialized in dendrimers, nanocomposites, and controlled radical polymerizations. From March 2001 to March 2005 the author worked as a PhD student in the group ‘Macromolecular and Organic Chemistry’ in the Department of Chemical Engineering at the Eindhoven University of Technology. Under the supervision of prof.dr. E.W. Meijer and dr. M.H.P. van Genderen he investigated the synthesis of multivalent MRI contrast agents for Magnetic Resonance Imaging. The most important results of his research are described in this thesis. As of April 2005 he works at SyMo-Chem BV ([www.symo-chem.nl](http://www.symo-chem.nl)) in Eindhoven.



## List of Publications

Probing the interaction of the biotin-avidin complex with the relaxivity of biotinylated Gd(III)DTPA

Langereis, S.; Kooistra, H. A. T.; van Genderen, M. H. P.; Backes, W. H.; Meijer, E. W. *Org.*

*Biomol. Chem.* **2004**, *2*, 1271-1273.

Multivalent contrast agents based on Gd(III)DTPA-terminated poly(propylene imine) dendrimers for Magnetic Resonance Imaging

Langereis, S.; de Lussanet, Q. G.; van Genderen, M. H. P.; Backes, W. H.; Meijer, E. W.

*Macromolecules* **2004**, *37*, 3084 -3091.

Towards target-specific molecular imaging of angiogenesis with Gd(III)DTPA-based dendritic architectures

Langereis, S.; de Lussanet, Q. G.; van Genderen, M. H. P.; Backes, W. H.; Hackeng, T. M.; van

Engelshoven, J.M.A.; Meijer, E. W. *Polym. Mater. Sci. Eng.* **2004**, *91*, 56-57.

Design and synthesis of a bimodal target-specific contrast agent for angiogenesis

Dirksen, A.; Langereis, S.; de Waal, B. F. M.; van Genderen, M. H. P.; Meijer, E. W.; de Lussanet,

Q. G.; Hackeng, T. M. *Org. Lett.* **2004**, *6*, 4857-4860.

A supramolecular approach to multivalent target-specific MRI contrast agents for angiogenesis

Dirksen, A.; Langereis, S.; de Waal, B. F. M.; van Genderen, M. H. P.; Hackeng, T. M.; Meijer, E.

W. *Chem. Commun.* **2005**, *accepted for publication.*

Dynamic contrast-enhanced MR Imaging kinetic parameters and molecular weight of dendritic contrast agents in tumor angiogenesis in mice

Lussanet, Q. G.; Langereis, S.; Beets-Tan, R. G. H.; van Genderen, M. H. P.; Griffioen, A. W.; van

Engelshoven, J. M. A.; Backes, W. H. *Radiology* **2005**, *235*, 65-72.

Solid-phase synthesis of a cyclic NGR-functionalized Gd(III)DTPA complex

Langereis, S.; Dirksen, A.; de Waal, B.F.M.; van Genderen, M.H.P.; de Lussanet, Q.G.; Hackeng,

T.M.; Meijer, E.W. *Eur. J. Org. Chem.*, *accepted for publication.*

Evaluation of Gd(III)DTPA-terminated poly(propylene imine) dendrimers as multivalent contrast agents for MR imaging

Langereis, S.; Lussanet, Q.G.; van Genderen M. H. P.; Meijer, E. W.; Beets-Tan, R.G.H.; Griffioen,

A. W.; van Engelshoven, J.M.A.; Backes, W.H. *NMR in Biomedicine*, *submitted for publication.*

# Dankwoord

Na vier jaar hard werken is het einde van een bijzonder leerzame en plezierige periode in zicht. Graag maak ik van deze gelegenheid gebruik om iedereen te bedanken die heeft bijgedragen aan het onderzoek. Toch zou ik een aantal mensen in het bijzonder willen bedanken.

Allereerst ben ik mijn promotor Bert Meijer zeer dankbaar voor zijn stimulerende begeleiding. Bert, jouw passie voor de wetenschap en jouw creativiteit in het onderzoek hebben een diepe indruk op me gemaakt. Ik heb zowel vakinhoudelijk als op het persoonlijke vlak erg veel van je geleerd. Ik zou Marcel van Genderen graag willen bedanken voor de talloze waardevolle discussies en zijn opbouwende kritiek. Marcel, jouw heldere analytische kijk op de wetenschap en jouw enorme kennis op het gebied van NMR spectroscopie hebben een positieve uitwerking gehad op het onderzoek. Bedankt voor de razendsnelle en nauwgezette correcties van de vele hoofdstukken en manuscripten.

Dank aan prof. Jos van Engelshoven, prof. Klaas Nicolay en prof. Jan van Hest voor de deelname aan de kerncommissie en het kritisch corrigeren van mijn proefschrift. I would like to thank prof. D.A. Tomalia for reading my manuscript and for his suggestions and improvements. Naast de leden van de leescommissie gaat mijn dank natuurlijk uit naar de totale promotiecommissie, gecompleteerd door prof. René Janssen en dr. Jef Vekemans.

Anouk Dirksen, als post-doc heb je het onderzoek een enorme stimulans gegeven. Onze prettige samenwerking heb ik enorm gewaardeerd en mede dankzij jouw waardevolle bijdrage zijn de laatste twee hoofdstukken tot stand gekomen. Samen met Henk Janssen en Oren Scherman heb je de leesbaarheid van mijn boekje aanzienlijk weten te verbeteren.

De samenwerking met verschillende onderzoeksgroepen in Maastricht en Eindhoven hebben een belangrijke bijdrage geleverd aan mijn promotieonderzoek. Ik ben veel dank verschuldigd aan de afdeling Radiologie van het Academisch Ziekenhuis in Maastricht, met name aan Quido de Lussanet en dr. Walter Backes, die me erg veel geleerd hebben over MRI. Quido, ik zal de MRI metingen, vaak tot diep in de nacht, niet snel vergeten. De eerste prijs voor onze poster tijdens de BMT onderzoeksdag bevestigde onze unieke samenwerking. Ik ben erg trots op onze gezamenlijke publicaties. Quido, ik wens je vanuit deze positie veel succes met je eigen promotie. Tilman Hackeng, op jouw lab kon ik altijd terecht voor de synthese van oligopeptiden en je expertise op dit gebied was onmisbaar voor mijn onderzoek. De samenwerking met jou en Wencke Adriaens is voor mij zeer plezierig en leerzaam geweest. Willem Mulder, Gustav Strijkers, Jeanine Prompers, Henk de Feyter en Larry de Graaf wil ik bedanken voor de nuttige discussies en de hulp bij de vele MRI metingen. Alhoewel MRI bekend staat als een niet-invasieve techniek, heb ik toch het nodige weten te slopen. Peter Frederik en Paul Bomans ben ik veel dank verschuldigd voor de cryo-TEM metingen.

Als promovendus heb ik de eer gehad om een groot aantal studenten te begeleiden. De stagiaires Judith Borsboom, Eva Wisse en Homme-Auke Kooistra wil ik bedanken voor hun bijdrage aan het initiële onderzoek. Addison Raymond, dankzij je doorzettingsvermogen heb je

enkele zeer lastige macrocyclische structuren weten te bereiden. Kelly van den Hout, je had het onderzoek razendsnel onder de knie. Bedankt voor het vele werk.

Joost van Dongen, Ralf Bovee en Xianwen Lou ben ik zeer erkentelijk voor hun hulp op analytisch gebied. Joost, hopelijk verloopt de verdediging van mijn proefschrift een stuk soepeler dan mijn eerste mondelinge tentamen ESI-MS. Verder wil ik Jef Vekemans bedanken voor zijn synthetische tips. Bas de Waal, bedankt voor je essentiële synthetische bijdrage. Nu snap ik volledig wat je met “goed, beter, best,..... Bas de Waal” bedoelt. Koen Pieterse ben ik zeer erkentelijk voor de vele gelikte prenten en de simulaties aan de dendrimeren. Edwin Beckers, bedankt voor je assistentie met de PL metingen.

Hannie van der Lee, bedankt voor de goede zorgen en het heerlijke kerstpakket. Ik zal onze eerste ontmoeting op het toilet niet snel vergeten (!). Henk Eding (“opa SMO”), bedankt voor het zetten van de dagelijkse koffie. Eén spatelpuntje van dit sterke brouwsel was vaak al voldoende om me de hele nacht wakker te houden. Henk, je bent deze zomer van harte uitgenodigd voor een barbecue. Dankzij de inspanningen van Hanneke Veldhoen, Joke Rediker, Ingrid Dirks, Carine van der Vaart en Hans Damen was alles tot in de puntjes geregeld.

Maarten Broeren (mijn onafscheidelijke “chemical brother”), onze gezamenlijke interesses voor de wetenschap en eten (“veel voor weinig”) hebben geleid tot een hechte vriendschap. Door onze instelling (“een normaal mens was al driemaal dood geweest”) hebben we menig dieptepunt weten te overwinnen. Maarten, bedankt voor de gezellige tijd. Verder wil ik Edwin Beckers, Patricia Dankers, Jack Donners, Tessa ten Cate, Michel Fransen, Judith van Gorp, Jeroen van Herrikhuizen, Henk Keizer, Hinke Malda, Ton Offermans, Serge Söntjens, René Sinkeldam, Jolanda Spiering en Martin Struijk bedanken voor de gezellige etentjes en/of de sportieve uitjes.

Joeri en Erik, jullie zijn fantastische broers en ik ben erg blij dat jullie mijn paranimfen willen zijn. Het zal voor jullie alleen niet meevallen om één uur stil te zitten. Verder wil ik Mandy, Esther, Tiny, Jeanne en Edwin bedanken voor de nodige ontspanning en de gezellige uurtjes. Frank, Ine en Dick (“Hoe doet een leeuw?”), bedankt voor de gezellige avonden en de hulp bij het grafische werk. Mijn ouders wil ik in het bijzonder bedanken voor hun onvoorwaardelijke steun, de relativerende gesprekken en de heerlijke weekendjes zeilen. Muriël, bedankt voor al je steun en liefde. Het viel niet altijd mee als ik weer eens in het weekend naar de universiteit ging. Het nummer “Eenzame kerst” van André Hazes was dit jaar wel heel toepasselijk. Muriël, je bent heel bijzonder.

*Sander*